IMPACT OF INCREASING AMOUNTS OF DISTRIBUTED GENERATION ON TRANSIENT BEHAVIOR OF THE DISTRIBUTION SYSTEM

A Thesis
Presented to
The Academic Faculty

by

Raeey A. Regassa

In Partial Fulfillment
of the Requirements for the Degree
Doctor of Philosophy in the
School of Electrical and Computer Engineering

Georgia Institute of Technology
May 2017

IMPACT OF INCREASING AMOUNTS OF DISTRIBUTED GENERATION ON TRANSIENT BEHAVIOR OF THE DISTRIBUTION SYSTEM

Approved by:

Dr. Ronald G. Harley, Advisor
School of Electrical and Computer Engineering
Georgia Institute of Technology

Dr. Lukas Graber
School of Electrical and Computer Engineering
Georgia Institute of Technology

Dr. Maryam Saeedifard
School of Electrical and Computer Engineering

Dr. Rhett Mayor
School of Mechanical Engineering
Georgia Institute of Technology

Dr. Thomas G. Habetler
School of Electrical and Computer Engineering
Georgia Institute of Technology

Date Approved: March 27, 2017

ACKNOWLEDGEMENTS

I would like to thank my advisor, Professor Ron Harley, for his guidance and support throughout my educational career at Georgia Tech. From my first energy conversion course in my undergraduate studies all the way up to this research, I have learned invaluable lessons from him. I would also like to thank Professor Tom Habetler, Professor Maryam Saeedifard, Professor Lukas Graber, and Professor Rhett Mayor for taking the time to review my dissertation and provide valuable feedback.

I want to express my gratitude to National Electric Testing Research and Application Center (NEETRAC) for sponsoring this research. The guidance, expertise, and support provided by Mr. Frank Lambert and Dr. Yamille Del Valle at NEETRAC in forming the scope of this research proved invaluable.

I am eternally thankful for my family's unconditional love and support. I missed quite a few holidays and birthday celebrations but their love and support kept me going. I would like to thank Josh Baughcum for editing my dissertation.

Most importantly, I would like to thank God Almighty for giving me the strength, knowledge, ability and opportunity to undertake this research. Without his blessings, this achievement would not have been possible.

TABLE OF CONTENTS

Page

LIST OF TABLES

Page

LIST OF FIGURES

Page

LIST OF SYMBOLS AND ABBREVIATIONS

DG	Distributed Generation
EMT	Electromagnetic Transient
EPRI	Electric Power Research Institute
IGBT	Insulated-Gate Bipolar Transistor
MPPT	Maximum Power Point Tracking
PCC	Point of Common Coupling
PF	Power Factor
PI	Proportional-Integral
PLL	Phase-Locked Loop
PWM	Pulse Width Modulation
PU	Per-Unit
RMS	Root-Mean-Square
STC	Standard Test Conditions
SG	Synchronous generator
SVM	Space Vector Modulation
THD	Total Harmonic Distortion

SUMMARY

The main objective of this research is to investigate the transient behavior of distribution feeders with high PV penetration levels and under different external conditions. The different external conditions include variable solar irradiance, different kinds of faults, sudden changes in type and amount of load, and changes in characteristics of the distribution system.

In order to achieve the main objective of the research, two actual feeder models and the IEEE 13 Node Test Feeder are investigated. The two actual feeder models are obtained from the National Electric Energy Testing and Application Center (NEETRAC, Project No. 13-257).

Feeder models and their data obtained from NEETRAC were created by others using OpenDSS software. OpenDSS is a steady state analysis software and it is not suitable for the purpose of this research into transient behavior [1]. DIgSILENT PowerFactory is an alternative power system simulation software, suitable for large systems and is able to perform a steady state as well as a transient analysis; it is therefore chosen for this research [2].

However, DIgSILENT PowerFactory does not allow importing OpenDSS models directly. Different methods and procedures are used to import the data of two NEETRAC member feeders from OpenDSS into DIgSILENT PowerFactory software. Part of the research objective focuses on the automation process used to extract data from OpenDSS models and importing into DIgSILENT PowerFactory.

DIgSILENT PowerFactory has a PV system as a template. Per recommendation from DIgSILENT PowerFactory helpdesk, this PV system is suitable for RMS mode of simulation and not valid for EMT mode of simulation [3]. In RMS mode of simulation, DIgSILENT PowerFactory uses symmetrical components to represent models, and in

EMT mode of simulation, it uses dynamic equations. This does not allow the transient switching and dynamic behavior of inverter controls to be studied. Therefore, a detailed model of a smart inverter with dynamic control is modeled in Matlab/Simulink software. It is the secondary objective of this research to develop a grid-tied smart inverter model.

Using the IEEE 13 Node Test Feeder, which is a smaller network, the behavior of the smart inverter is evaluated. PV systems with smart inverters and with a total penetration level of 120% are installed in the feeder along with a battery management system. The battery management system provides virtual inertia to the power system and helps the PV systems in the feeder to ride through frequency deviations while continuing to supply power to the loads in the feeder.

.

CHAPTER 1: INTRODUCTION

1.1. Problem Statement

Distributed Generation (DG) is fast becoming a preferred solution for many states in the U.S. searching for a way to connect new clean energy sources (PV and wind) to the grid. Prior to 2010 in the state of Washington, San Diego Gas and Electric (SDG&E) had less than 10% PV penetration on its feeders. Currently its feeders have more than 35% PV penetration [4]. SDG&E PV penetration level by circuit is shown in Figure 1.1. The state of Massachusetts is another example. Its Department of Energy Resources requested the National Grid to add 1,200 MW of PV to its system [5].

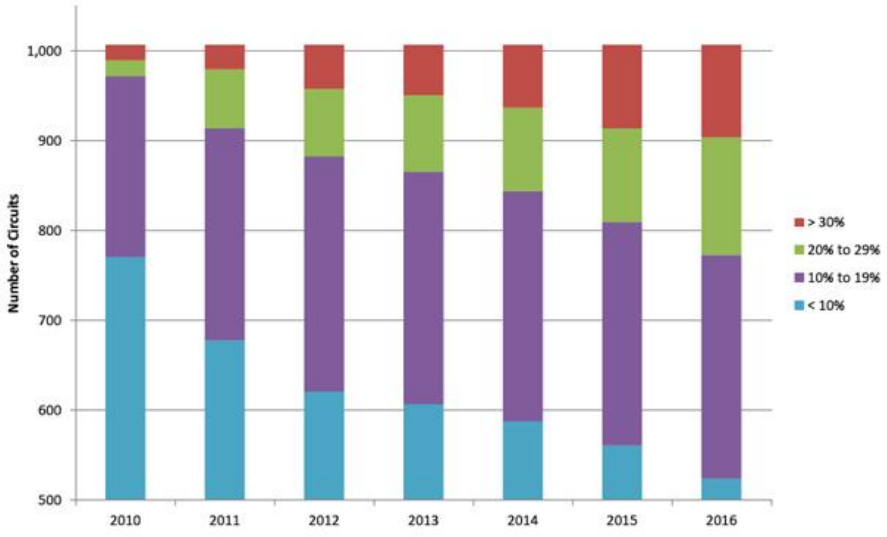

Figure 1.1: SDG&E PV penetration by circuit

As more and more distributed generations are added to the feeders, utilities need to understand:

- How the instantaneous changes in the DG output can create quality of service issues
- How much DG can safely be added to the existing radial feeder designs

- What technologies are available to mitigate any negative effects of DG

Answering the above questions requires an understanding of both steady state and transient phenomena. The Electric Power Research Institute (EPRI) has performed substantial research on the steady-state impacts of distributed generation on the distribution system in the past few years [6-21]. This research is a continuation of EPRI's work and is sponsored by the National Electric Energy Testing, Research and Application Center (NEETRAC, Project No. 13-257).

1.2. Research Scope and Objectives

The objective of this research is to investigate transient instability that could arise from increased penetration of PV on the distribution system under different external conditions. Two large feeders and one smaller feeder are evaluated.

1.2.1. NEETRAC Member Feeders

Two large (typically 1500 buses) NEETRAC member feeders that are located in the Northeast and Southeast parts of the United States are subjected to the following conditions and their transient responses are investigated:

- Fluctuating and out of phase cloud covering different PV sites in the feeders
- Switching ON/OFF of a capacitor bank while PVs are operating at their rated outputs
- Temporary short-circuit faults on the external grid (at the substation) that result in 10% voltage drop in the feeders and the faults are cleared after 150 ms

- The PV inverter's Volt-Var control capability to control local voltage is investigated as a means of mitigating effects of high PV penetration levels in feeders

The NEETRAC member feeder models were created by others using OpenDSS software (Distribution Simulation Software). OpenDSS is a steady state analysis software and it is not suitable for the purpose of this research. DIgSILENT PowerFactory, a power simulation software capable of performing transient analysis is chosen.

The feeder models received from NEETRAC in OpenDSS file format are imported into DIgSILENT PowerFactory software. Since DIgSILENT PowerFactory does not allow directly importing models created in OpenDSS software, different methods and procedures are followed to convert data in these models into DIgSILENT PowerFactory. The different methods and procedures followed along with Matlab scripts created are discussed in Appendix A.

The PV system that comes with DIgSILENT PowerFactory as a template is valid for RMS mode of Simulation [3]. To investigate whether valuable information is lost by using RMS instead of EMT in the study of transient behaviors of NEETRAC member feeder models, a similar PV system is created in PSCAD software. The EMT simulation results of PSCAD are converted to RMS and compared with results of DIgSILENT. RMS converted EMT simulation results of PSCAD show similar behavior to that of DIgSILENTs' RMS simulation results with acceptable tolerance. In chapter 3, comparison results of DIgSILENT and PSCAD are discussed.

1.2.2. **IEEE 13 Node Test Feeder**

A smaller network, the IEEE 13 Node Test Feeder is used to evaluate the behavior of a smart inverter where the control dynamics are modeled in detail in Matlab/Simulink. In order to investigate a scenario when PV generation is higher than consumption by loads in the feeder, PV systems with smart inverters and with a total

penetration level of 120% are installed in the feeder. A battery management system is also modeled in Matlab/Simulink and installed in the feeder. The frequency ride through capability of the battery management system is investigated when the grid frequency deviates from its nominal value of 60 Hz.

1.3. Outline of Chapters

Chapter 1: The background and motivation behind the research are discussed, and the scope and objectives of the research are outlined.

Chapter 2: Background information regarding PV system and interconnection requirements of IEEE 1547 are introduced. PV intermittency issues and adverse effects of increased PV penetration in distribution feeders are discussed in this chapter.

Chapter 3: Two NEETRAC member feeder models are imported from OpenDSS into DIgSILENT PowerFactory software. The methods and procedures used to import these models are described in Appendix A. Their validation and verification results are described in this chapter.

Chapter 4: Transient performance validation of DIgSILENT PowerFactory software is discussed in this chapter. Simple test circuits with PV systems, constant P-type loads, and induction motors are constructed in both PSCAD and DIgSILENT PowerFactory software and their results are compared.

Chapter 5: Transient simulation results of NEETRAC member Feeder B are discussed in this chapter. The feeder's transient behaviors under different external conditions are investigated.

Chapter 6: The dynamic equations of a current-controlled grid-tied inverter are discussed. Based on these equations, a smart inverter is modeled in Matlab/Simulink. The model is validated and verified under different grid voltages and frequency conditions.

Chapter 7: The IEEE 13 node feeder circuit, a voltage regulator, a PV system, and a battery management system are constructed in Matlab/Simulink software. The PV system

and battery management system models use the smart inverter model developed in Chapter 6. Seven nodes in the IEEE 13 node feeder circuit are selected, and seven PVs with a total of 4.2 MW (120% PV penetration) are added. The frequency fluctuation ride-through capability of the battery management system is investigated in this chapter.

Chapter 8: The conclusions that can be drawn from the work presented in this dissertation are discussed, as well as the new contributions of this work and recommendations for future work.

CHAPTER 2: BACKGROUND AND LITERATURE SURVEY

2.1. Introduction

In order to investigate the transient behaviors of a NEETRAC member feeder under high PV penetration level and different external conditions, a detailed understanding of a PV system is needed. Figure 2.1 shows a typical grid connected PV system. Sections 2.2 and 2.3 discuss the PV power generation and the inverter components respectively. Section 2.4 discusses interconnection requirements of IEEE 1547 rules. Section 2.5 describes the intermittency issues of PV systems and adverse effects of high penetration levels of PV systems on distribution feeders.

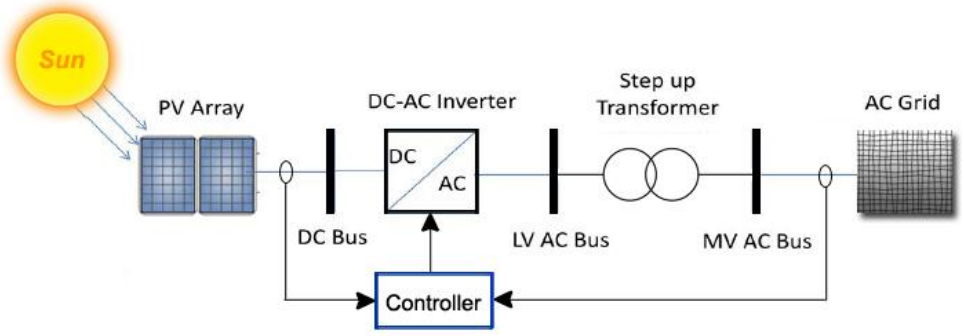

Figure 2.1: Grid-tied PV system components

2.2. PV Power Generation Component

PV cells are sunlight-into-electricity converting semiconductor devices. They are manufactured using different materials, but Silicon based PV cells share 90% of the market [22]. When sunlight is absorbed by a PV cell, photons in the sunlight excite electrons from its n-junction and the electrons start to flow through metal contacts installed in the cell. Figure 2.2 illustrates the sunlight-into-electricity conversion process by a PV panel [23].

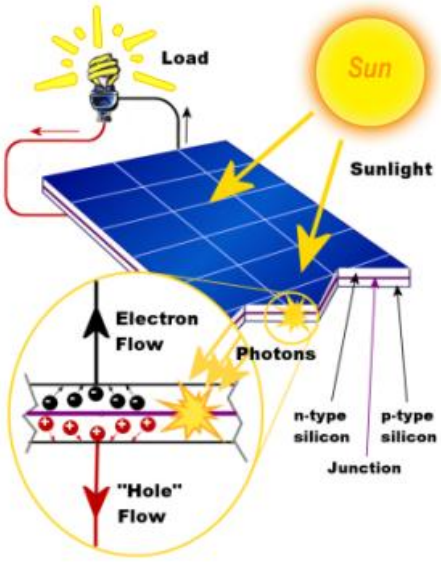

Figure 2.2: Solar panel diagram [23]

2.2.1. **Electrical Model of a PV Cell**

There are two widely accepted models for a PV cell [24-30]: Single-Diode Model (or Five Parameter Model) and Two-Diode Model. The Single-Diode Model uses one diode to represent the p-n junction of a PV cell while the Two-Diode Model uses two diodes to represent the p-n junction and the recombination that occurs in the p-n junction. Both models exhibit similar results under Standard Test Conditions (STC). However, the Two-Diode Model is a more accurate representation of a PV cell at low solar irradiation and temperature values. STC is an industry-wide standard set by IEC 60904 [31] to indicate the performance of PV arrays at cell temperature of 25°C, solar irradiation of 1000 $\frac{W}{m^2}$, and an air mass of 1.5 $\frac{Kg}{m^3}$. Since there are two diodes in the Two-Diode Model, two non-ideality or diode quality factors are unknown and the number of equations increases making calculations more complex compared to the Single-Diode Model. In this research, the Five Parameter Diode Model is used to represent a PV cell. Figure 2.3 shows the two widely accepted electrical models of a PV cell.

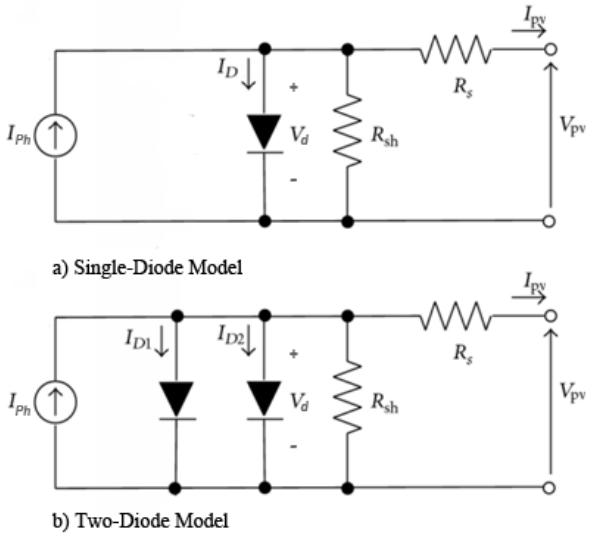

Figure 2.3: Two electrical models of a PV cell

From Figure 2.3(a), $I_{PV} = I_{Ph} - I_D - I_{Sh}$

$$= I_{Ph} - I_o\left(e^{\frac{q(V_{PV}+R_S I_{PV})}{nKT}} - 1\right) - \frac{(V_{PV}+R_S I_{PV})}{R_{Sh}} \quad (2.1)$$

where I_{Ph} = Photocurrent [A]

V_{PV} = PV voltage [V]

I_D = Diode current [A]

I_o = Diode saturation current [A]

I_{Sh} = Shunt current [A] through R_{Sh}

n = Diode ideality factor ($1 \leq n \leq 2$)

q = Electron charge, $1.6021 * 10^{-19}$ C

k = Boltzmann's constant, $1.3865 * 10^{-23}\ \frac{J}{K}$

T = Junction temperature [K]

R_S = Series resistance [Ω]

R_{Sh} = Shunt resistance [Ω

In Figure 2.3, defects in the PV cell and other leakage current mechanisms are represented by a shunt resistor (R_{Sh}) while contact resistance and other series resistances are represented by a series resistor (R_S).

2.2.2. **Characteristics of a PV Cell**

Solar irradiation and temperature affect the I-V characteristic of a PV cell. Figure 2.4 shows voltage and current dependency of a general PV cell on solar irradiation and junction temperature [32]. The figure shows that cell voltage has higher temperature dependence whereas current has higher dependence on solar irradiation.

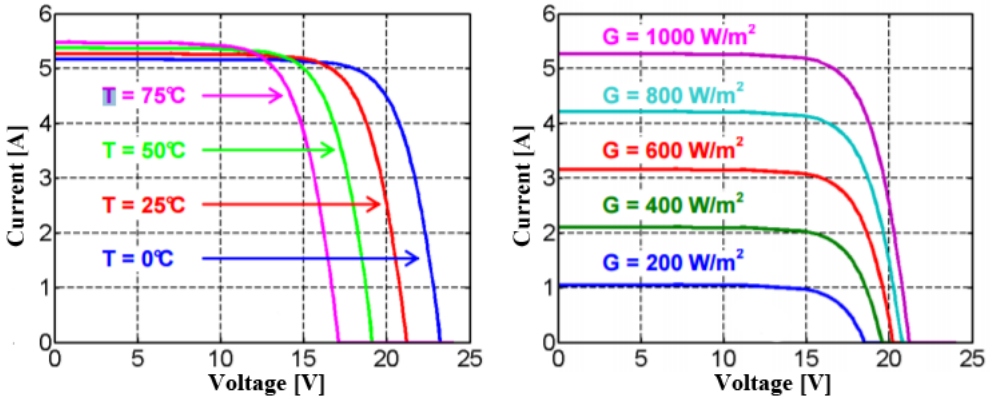

a) Effect of temperature **b) Effect of solar irradiation**

Figure 2.4: Effects of temperature and solar irradiation on the I-V characteristic curve of a PV cell [32]

The maximum current that can be extracted from a PV cell is its short-circuit current (I_{SC}) and the maximum voltage across the terminals of a PV cell is its open-circuit voltage (V_{OC}). Short-circuit current and open-circuit voltage dependence on temperature and solar irradiation can be approximated as follows [30]:

$$I_{SC}(T) = I_{SC_{STC}}(1 + \alpha.\Delta T) \tag{2.2}$$

$$I_{SC}(G) = I_{SC_{STC}}\left(\frac{G}{G_{STC}}\right) \tag{2.3}$$

$$V_{OC}(T) = V_{OC_{STC}}(1 + \beta.\Delta T) \tag{2.4}$$

$$V_{OC}(G) = V_{OC_{STC}}\left(\frac{\ln(G)}{\ln(G_{STC})}\right) \tag{2.5}$$

where $I_{SC}(T)$ = Short-circuit current at given temperature [A]

$I_{SC_{STC}}$ = Short-circuit current at STC [A]

α = Temperature correction factor for current $[\frac{\%}{°C}]$

ΔT = T-T_{ref}, T_{ref} is considered as 25°C at STC

$I_{SC}(G)$ = Short-circuit current at given irradiance [A]

G_{STC} = Solar irradiation at STC, 1000 $\frac{W}{m^2}$

$V_{OC}(T)$ = Open-circuit current at given temperature [V]

$V_{OC}(G)$ = Open-circuit current at given irradiation [V]

β = Temperature correction factor for voltage $[\frac{\%}{°C}]$

The theoretical maximum power that can be extracted from a PV cell at a given cell temperature and solar irradiation of 1000 $\frac{W}{m^2}$ $(i.e. G_{STC})$ is

$$P_{max} = I_{SC}.V_{OC}$$
$$= I_{SC_{STC}}(1+\alpha.\Delta T).V_{OC_{STC}}(1+\beta.\Delta T)$$
$$= I_{SC_{STC}}.V_{OC_{STC}}(1+(\alpha+\beta)\Delta T+\alpha\beta.\Delta T^2)$$

Ignoring the quadratic term,

$$P_{max} = P_{STC}.(1+(\alpha+\beta)\Delta T) \quad (2.6)$$

The theoretical maximum power that can be extracted from a PV cell at a given solar irradiation and cell temperature of 25°C $(i.e. T_{STC})$ is

$$P_{max} = I_{SC}.V_{OC}$$
$$= I_{SC_{STC}}\left(\frac{G}{G_{STC}}\right).V_{OC_{STC}}\left(\frac{ln(G)}{ln(G_{STC})}\right)$$
$$P_{max} = P_{STC}.\left(\frac{G}{G_{STC}}\right)\left(\frac{ln(G)}{ln(G_{STC})}\right) \quad (2.7)$$

Figure 2.5 shows dependency of power extracted from a general PV cell on solar irradiation and temperature [32].

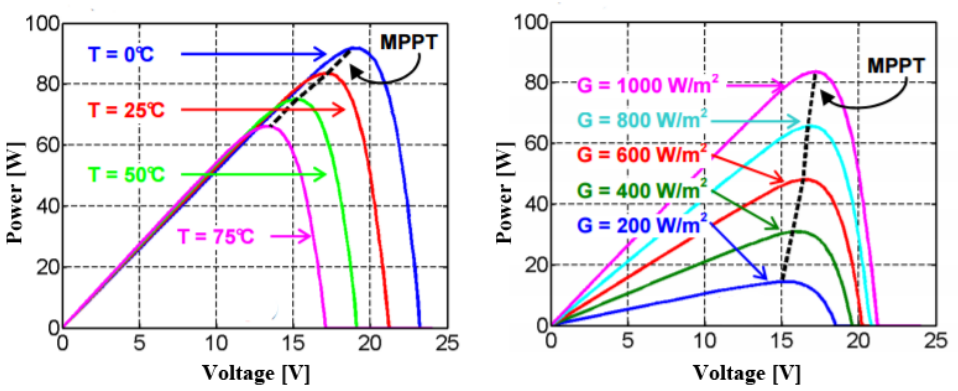

a) Effect of temperature on power output **b) Effect of solar irradiation on power output**

Figure 2.5: Effects of temperature and solar irradiance on power output of a PV cell [32]

Figure 2.5 shows that maximum power output of a PV cell is a function of temperature and solar irradiance. In order to extract maximum power from a PV cell at a given temperature and solar irradiance operating conditions, a maximum power point tracking (MPPT) system is necessary. For a grid-tied PV system, a maximum power point tracking system adjusts the voltage across the terminals of a PV array so that maximum current can be drawn at the given operating conditions. The most two common maximum power point tracking algorithms are: Perturb and Observe (P&O) and Incremental Conductance (IC).

2.2.2.1. Perturb and Observe Maximum Power Point Tracking Method

P&O is one of the simplest and most widely used MPPT methods [33-38]. As shown in Figure 2.6, the maximum power point is located at the knee of the P-V curve. In this method, voltage and current are measured at time t_k and t_{k-1}. Power is calculated at time t_k and $t_{k-1}(i.e.\ P_{k-1} = V_{k-1} * i_{k-1}\ \&\ P_k = V_k * i_k)$.

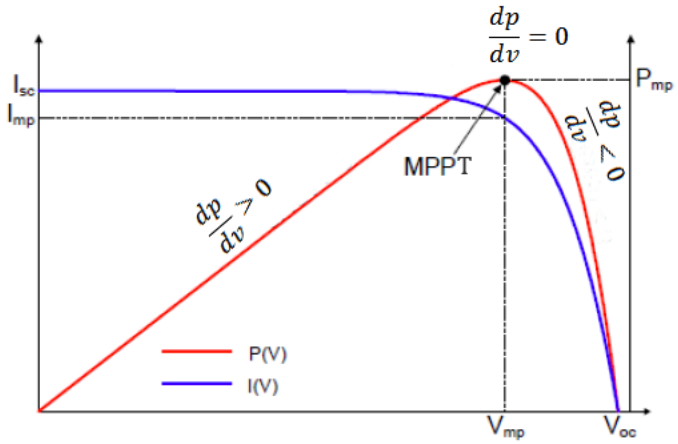

Figure 2.6: Perturb and Observe Method [34]

In Figure 2.6, I_{SC} = short-circuit current [A]

I_{mp} = current at maximum power point [A]

V_{OC} = open-circuit voltage [V]

V_{mp} = voltage at maximum power point [V]

There are three regions in Figure 2.6:

1 $\frac{dp}{dv} = 0$ (at MPPT)

2 $\frac{dp}{dv} > 0$ (left hand side of MPPT)

3 $\frac{dp}{dv} < 0$ (right hand side of MPPT)

If $\frac{dp}{dv} > 0$, then the maximum power point is to the right of the measured voltage at t_k and further perturbation is needed. If $\frac{dp}{dv} < 0$, then the maximum power point is to the left of the measured voltage at t_k and a negative perturbation is needed. If $\frac{dp}{dv} = 0$, the maximum power point is reached and no further purterbation is needed. Figure 2.7 shows the flow chart of Perturb and Observe (P&O) method.

One of the disadvantages of this method is that it hovers around the maximum power point and has a slow convergence rate.

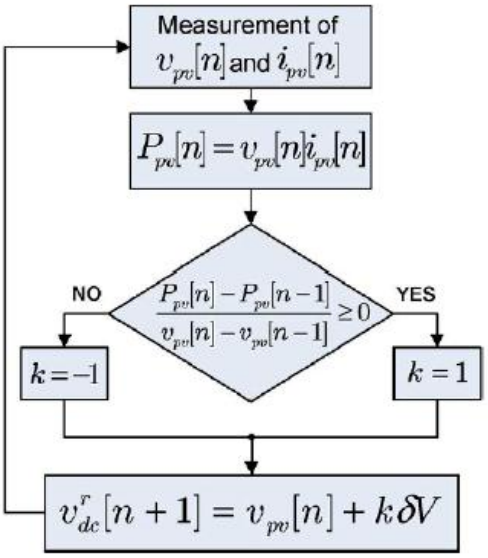

Figure 2.7: Flow chart of P&O method [34]

In Figure 2.7, $\delta V = \frac{(V_{mpo})(T_{delay})}{step} = \frac{V_{mpo}}{(freq)(step)}$ (2.8)

Where V_{mpo} = PV voltage at maximum power point at STC

T_{delay} = time delay between two measurements [s]

$freq$ = frequency of MPPT algorithm [Hz] (typically between 10-20 Hz)

$step$ = design parameter [s]

δV = increase or decrease in voltage per iteration [s]

Care must be given in selecting δV value. If δV is too small, the method is slow to converge and if δV is too large, there is ripple in the output voltage [7].

2.2.2.2. Incremental Conductance Maximum Power Point Tracking Method

This method uses conductance ($\frac{I}{V}$) to find the maximum power point.

$$P = V*I$$

$$\frac{dp}{dV} = \frac{d(V*I)}{dV} = I + V\frac{dI}{dV} \quad (2.9)$$

At maximum power point, $\frac{dp}{dV} = I + V\frac{dI}{dV} = 0$

$$\frac{dI}{dV} = -\frac{I}{V}$$

Therefore, at maximum power point, $\frac{dI}{dV} = -\frac{I}{V}$. Figure 2.8 shows the different zones of the Incremental Conductance method. $(\frac{I}{V})$.

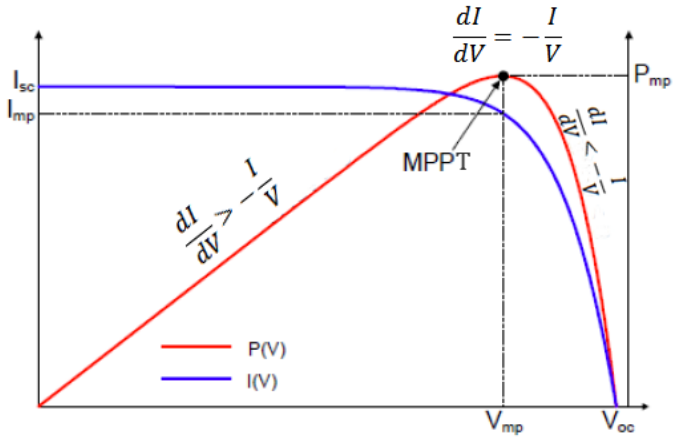

Figure 2.8: Incremental Conductance Method [34]

There are three regions in Figure 2.8:

1 $\frac{dI}{dV} = -\frac{I}{V}$ (at MPPT)

2 $\frac{dI}{dV} > -\frac{I}{V}$ (left hand side of MPPT)

3 $\frac{dI}{dV} < -\frac{I}{V}$ (right hand side of MPPT)

If $\frac{dI}{dV} > -\frac{I}{V}$, then the maximum power point is to the right of the measured voltage at t_k and further perturbation is needed. If $\frac{dI}{dV} < -\frac{I}{V}$, then the maximum power point is to the left of the measured voltage at t_k and a negative perturbation is needed. If $\frac{dI}{dV} = -\frac{I}{V}$, the maximum power point is reached and no further perturbation is needed. Figure 2.9 show the flow chart of Incremental Conductance (IncCond) method.

Unlike the Perturb and Observe method, this method does not hover around the maximum power point but it needs more hardware to implement it.

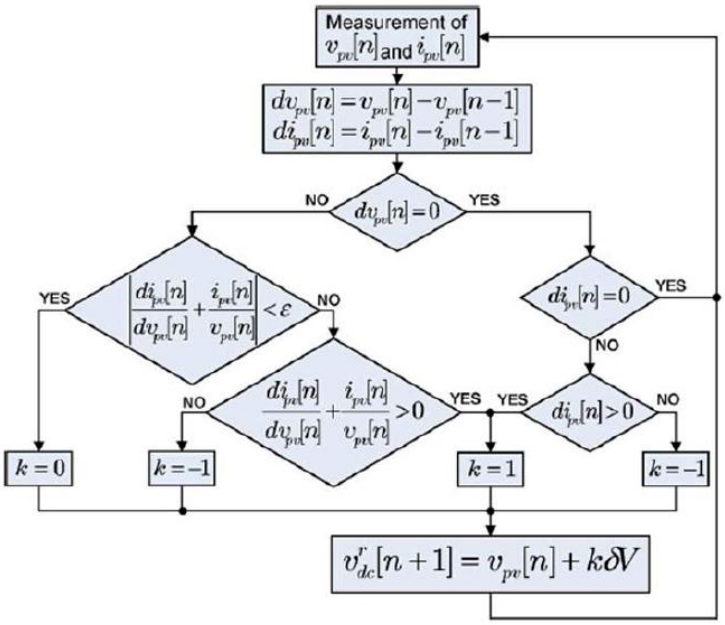

Figure 2.9: Flow chart of Incremental Conductance method [34]

2.2.3. **PV Cell Interconnection**

PV cells are connected in series to form a module and in turn, modules are connected in series and in parallel to form an array. Series connected modules are sometimes referred as a string. The voltage across the terminals of an array is the number of PV cells in a module times the number of modules connected in series [23]. Figure 2.10 shows the interconnection of PV cells to form an array.

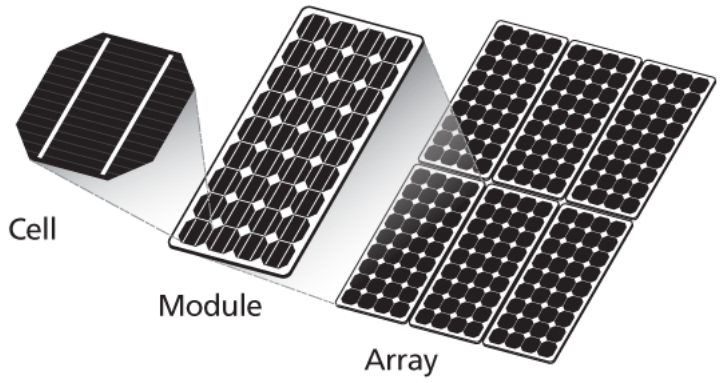

Figure 2.10: PV cells interconnection

2.2.3.1. Identical PV Cells

In theory, if identical PV cells are connected in series and in parallel to form an array, the PV array's I-V characteristic curve resembles that of a single PV cell except its current and voltage outputs are shifted by the number of cells connected in parallel and in series respectively [39-40]. Figure 2.11 shows I-V characteristics of identical PV cells connected in series and in parallel.

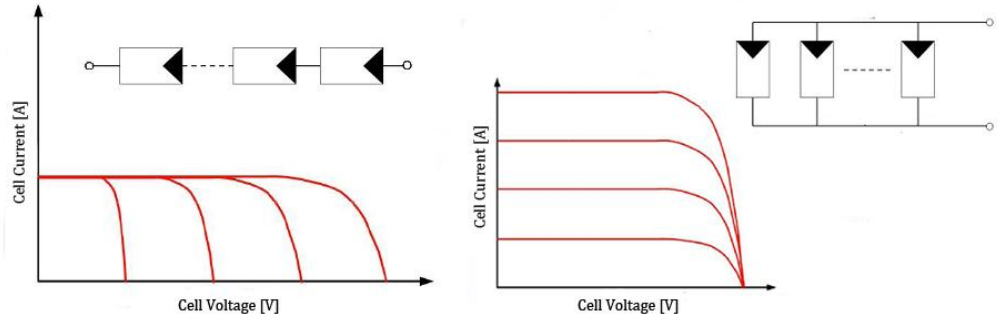

Figure 2.11: Ideal I-V Characteristics of series and parallel connected PV cells [39]

2.2.3.2. Non-Identical PV Cells

In practice, when PV cells are connected in series and parallel, a mismatch occurs because each PV cell has unique characteristics. Mismatch loss is defined as the difference between the actual output of the connected PV cells and the output of the component cells [39-40]. Mismatch is caused by:

- Manufacturing defects
- Degradation (e.g. cracking)
- Partial shading (e.g. trees, buildings, bird droppings, discolored encapsulant, etc.)
- Higher temperature

Figure 2.12 shows the combined current output of two mismatched parallel connected cells. The combined output is less that the combined output of two identical cells.

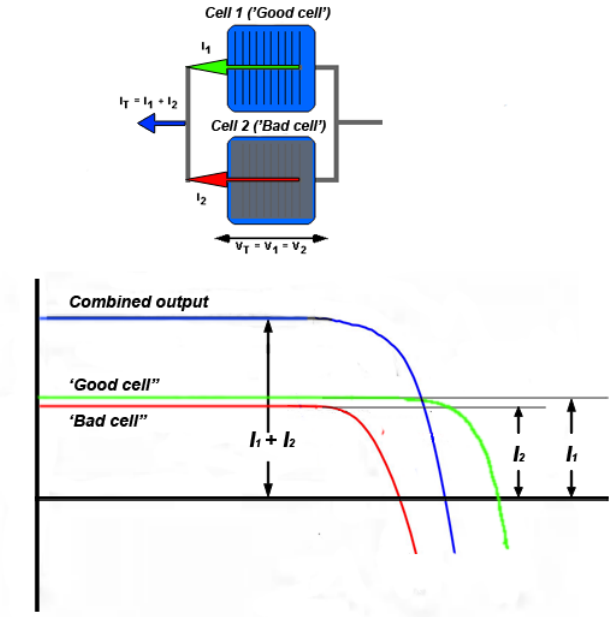

Figure 2.12: Effect of parallel-connected mismatch cells on current output [39]

Figure 2.13 shows combined voltage output of two mismatched series connected cells. The combined output is less than the combined output of two identical cells.

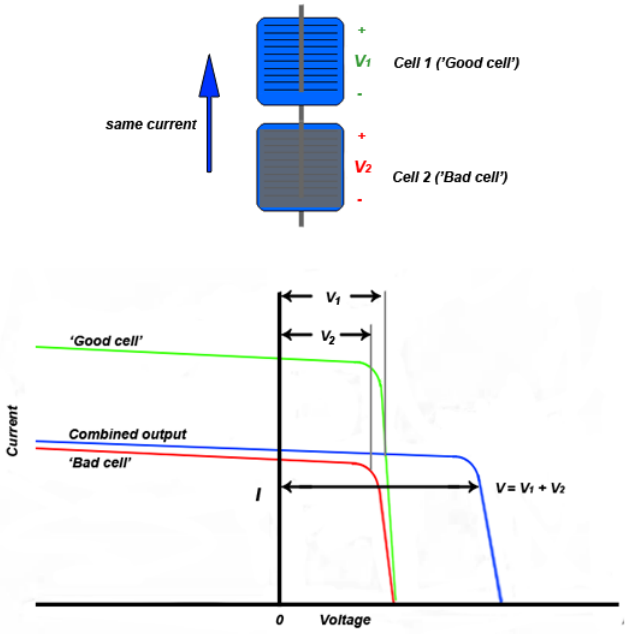

Figure 2.13: Effect of series-connected mismatched cells on voltage output [39]

2.2.4. **Shading Effect on I-V Curve**

Shading affects the performance of PV arrays [39-45]. Partial shading on series connected PV modules is investigated in [39] and the result is shown in Figure 2.14. The result shows that partial shading of PV modules results in reduction of maximum power extracted from the PV system. As more PV modules are shaded, the photo current available from the PV system reduces and this results in downward shift of the I-V characteristic curve. In this study [39], by-pass diodes are suggested to extract maximum power from unshaded PV modules.

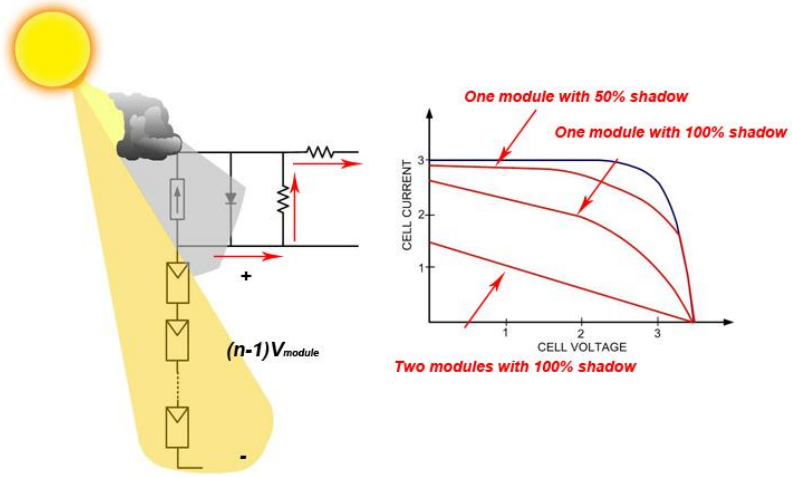

Figure 2.14: Shading effect on PV array I-V characteristic curve [39]

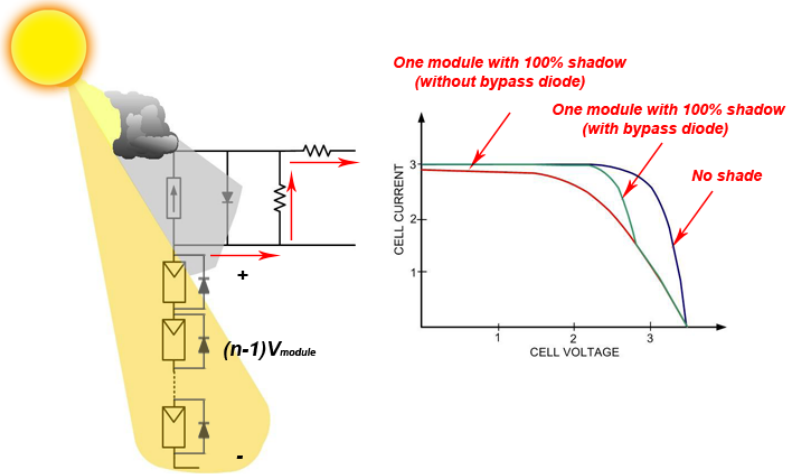

Figure 2.15: Effect of bypass diode on shading [39]

2.3. Grid-Tied PV Inverter Component

The most important component of a grid-tied PV system is its inverter. The main function of a PV inverter is to convert DC power generated by PV arrays into grid-synchronized AC power with high efficiency and low total harmonic distortion (THD). Some of the functions of a grid-tied inverter are:

- Control the DC voltage in order to ensure that the PV system always operates at maximum power point (i.e. maximum power point tracking)
- Power decoupling between the AC and DC side
- Active power curtailment
- Fault ride-through
- Anti-islanding
- Comply with international regulator bodies

Figure 2.16 shows a two-level, three-phase, grid-tied inverter. In the Power Module, six switches and a filter capacitor are located whereas in the Control Module, a controller and a modulation strategy are located. The inverter's output is connected to a filter inductor before it is connected to the grid.

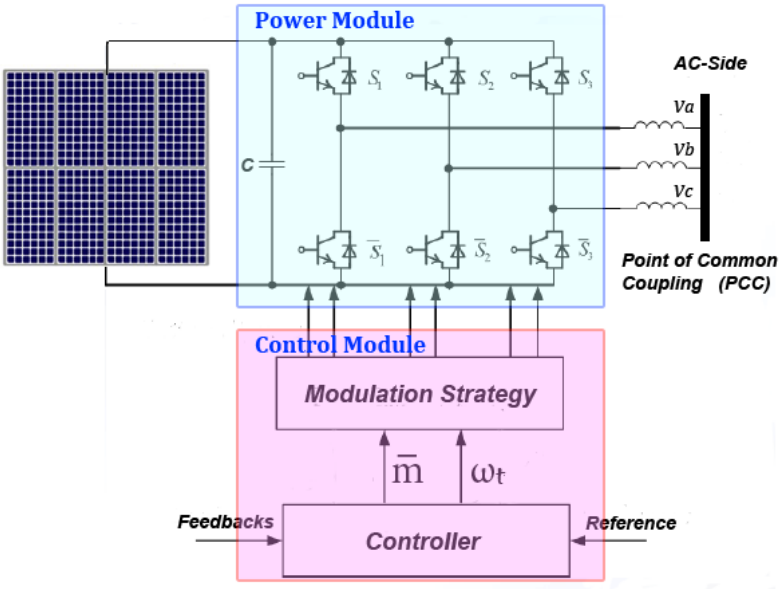

Figure 2.16: Three-phase inverter

The purpose of the capacitor is to filter out and smooth the DC bus voltage. If the PV arrays' output voltage is lower than the DC bus voltage, a DC-DC Boost converter is usually used to connect the PV arrays to the DC bus. The controller accepts grid voltage and current as feedback and using reference values, it computes the modulating signal magnitude. This allows injection or absorption of the required real and reactive power. The Modulation Strategy block accepts a modulation signal magnitude from the controller and converts it to six gating signals to turn ON/OFF each of the six switches in the Power Module. There are different Pulse Width Modulation (PWM) strategies discussed in [46-50]. The most commonly used PWM strategies are the Sine-Triangle Comparison (with third harmonic injection) and the Space Vector Modulation (SVM) techniques. Both methods utilize 115% of the DC bus voltage; as a result the DC bus voltage can be reduced by 15%. The Controller and the Modulation Strategy are discussed in detail in Chapter 6.

2.3.1. **PV System Configurations**

Based on the PV array's configuration, a PV inverter can be categorized as a central inverter, a string inverter, a multi string inverter, and a module integrated inverter as shown in Figure 2.17 [51].

- Central inverter: - in this configuration, multiple PV panels are connected in series and in parallel to get the desired voltage and power levels and are finally connected to a single converter at the end. Since a single inverter is used, this kind of configuration has low total harmonic distortion (THD) and low inverter losses. Hence, it is the first choice for medium to large-scale PV systems. One of its disadvantages is that a variable shading in the PV system can cause the inverter to trip and lose total PV system power generation. In this research, central inverter configuration is implemented in PV systems. This type of configuration is shown in Figure 2.17 (a)

- String inverter: - for applications where different PV panels cannot be operated at the same orientation and experience different shading effects (e.g. PV panels on rooftops or on wings of an aircraft), this type of inverter configuration is the best choice. Figure 2.17 (b) shows that each inverter is responsible for series connected PV panels (strings). String inverter configuration based PV systems are available from 0.4 kW up to 2 kW [51]
- Multi string inverter: - this is another type of string inverter configuration when multiple series connected PV panels are connected to multiple DC-DC converters and finally to a single inverter. One of the advantages of this configuration is that a different number of PV panels can be connected in series (as strings) and because of the DC-DC converters connected to each string, the different strings can be connected in parallel to the same DC bus. This type of configuration is shown in Figure 2.17 (c)
- Module integrated inverter: - in this configuration, different PV inverters are connected in parallel to the grid. One of the advantages of this configuration is that one of the inverters could trip but the others remain connected to the grid. This type of configuration is shown in Figure 2.17 (d)

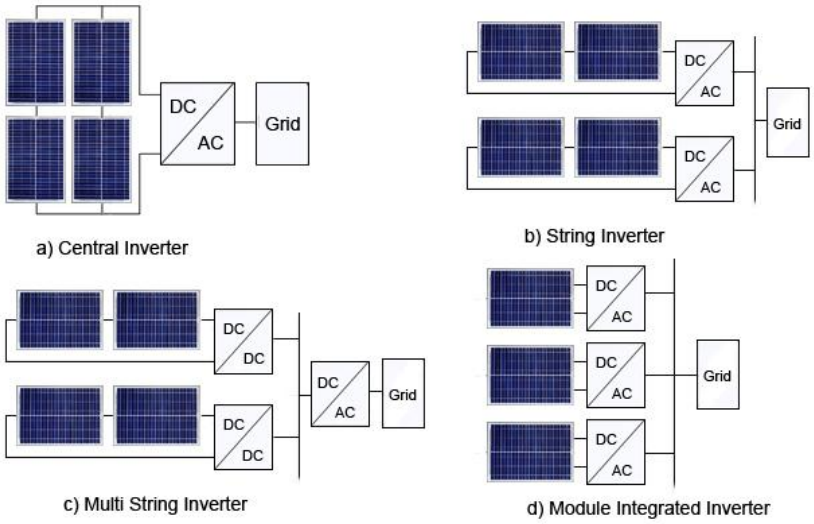

Figure 2.17: Different PV system configurations

2.3.2. **PV Inverter Smart Functionalities**

Most inverters in distribution feeders are made to operate in Unity Power Factor control mode. They do not participate in regulating voltage and they inject only real power when it is available. Slow update and progress in regulatory bodies such as IEEE 1547 (addresses interconnection) and UL 1741 (addresses equipment safety) are some of the reasons for delaying use of advanced inverters [52]. Sections 2.3.2.1 – 2.3.2.5 discuss advanced functions that can be provided by inverters [11].

2.3.2.1. Fixed Power Factor Function

In this mode of control, a fixed power factor is set as leading or lagging. IEEE defines leading power factor as positive (capacitive) and lagging power factor as negative (inductive). Based on the fixed leading/lagging power factor, PV inverters inject active real power and inject/absorb reactive power. This function is useful if the reactive power requirement of the grid or load near the inverter is known. The IEEE PES Smart Inverter Working Group recommends that the California Public Utilities Commission require larger inverters (greater than 15 kW) be allowed to operate within a power factor range of

±0.85, down to 5% of rated power, and ±0.90 power factor for smaller inverters (less than 15 kW), down to 20% of rated power, based on available vars [53].

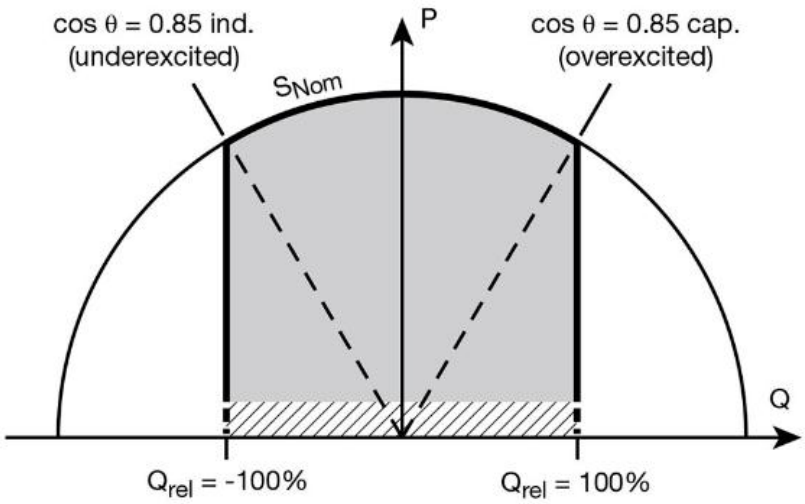

Figure 2.18: Power factor range recommended by SIWG [53]

2.3.2.2. Intelligent Volt-Var Function

In this control mode, inverters either inject or absorb reactive power based on the grid voltages at the points of common coupling. Figure 2.19 shows example settings for the Volt-Var control mode [11].

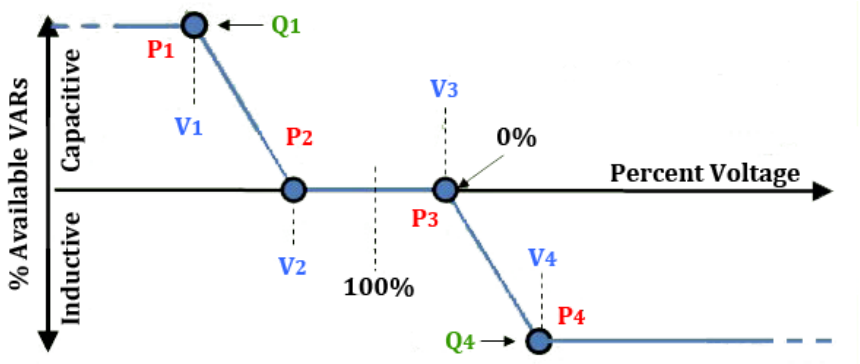

Figure 2.19: Volt-Var settings

Figure 2.19 shows that for a certain voltage range (deadband), inverters do not support reactive power and they operate in Unity Power Factor control mode. As grid

voltage decreases or increases above the deadband, inverters participate in grid voltage control following the curve by injecting or absorbing reactive power.

In the report prepared by EPRI [11], a hysteresis curve is also suggested for dynamic support of reactive power. Figure 2.20 shows two curves for injecting and absorbing reactive power.

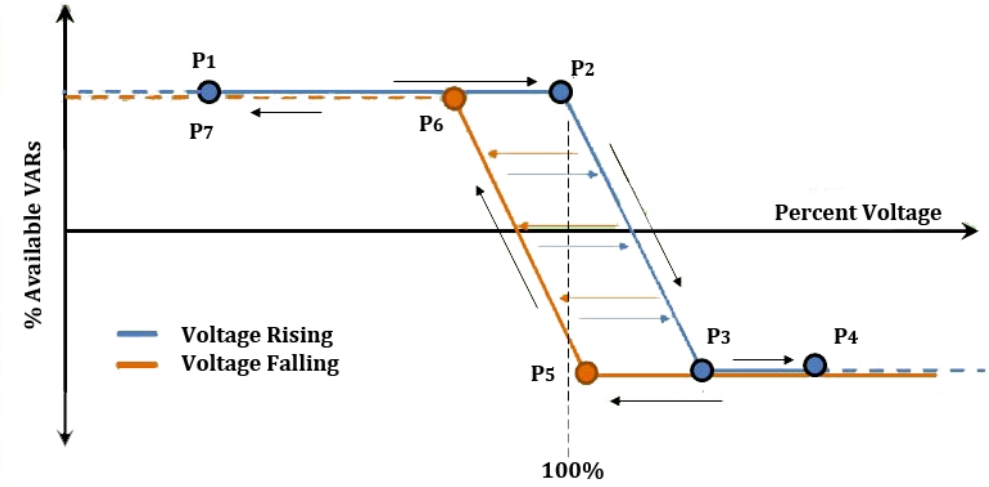

Figure 2.20: Volt-Var control with hysteresis settings

2.3.2.3. Volt-Watt Function

The motivations behind the development of this function are [11]:

- High PV penetration and low load in some distribution feeders resulted in high feeder voltage at certain times. Existing distribution controls are not designed considering high PV penetration and unable to mitigate this occurrence.
- When a large number of customers are served from the same service transformer and when PVs are connected to the transformer, customers have reported high voltages. Because of high voltage and IEEE 1547 interconnection requirements, some PVs are unable to connect to the transformer.

The proposed Volt-Watt function curve is shown in Figure 2.21. When grid voltage increases above maximum voltage setpoint (V_3 in the figure), the inverter ceases to inject power but its controller remains connected to the grid.

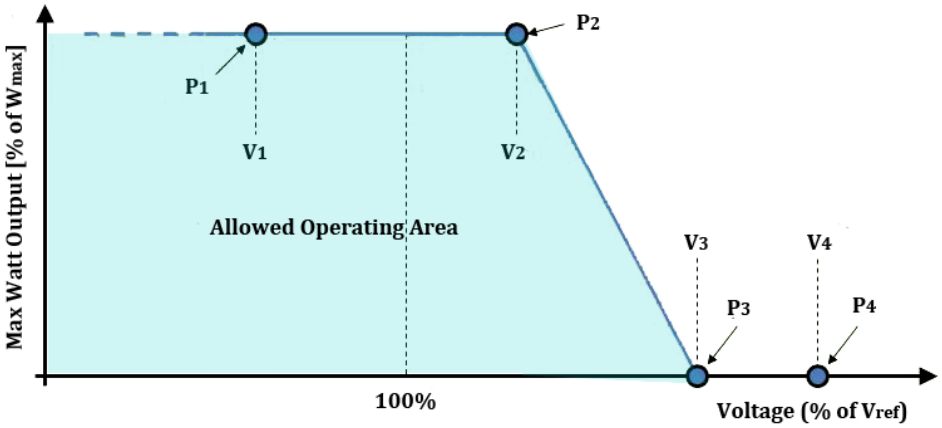

Figure 2.21: Example curve for Volt-Watt function

2.3.2.4. Frequency-Watt Function

The purpose of this function is to enable inverters to participate in stabilizing the grid frequency. When there is a sudden load change or a large conventional generator is suddenly taken offline, the frequency of the system deviates from its nominal operating value. By allowing inverters to curtail their real power output, this function helps to lower and stabilize system frequency. The report by EPRI [11] gives two Frequency-Watt functions (Frequency-Watt Function 1 and Frequency-Watt Function 2). Figure 2.22 and Figure 2.23 show basic settings for Frequency-Watt Function 1 and Frequency-Watt Function 2 respectively.

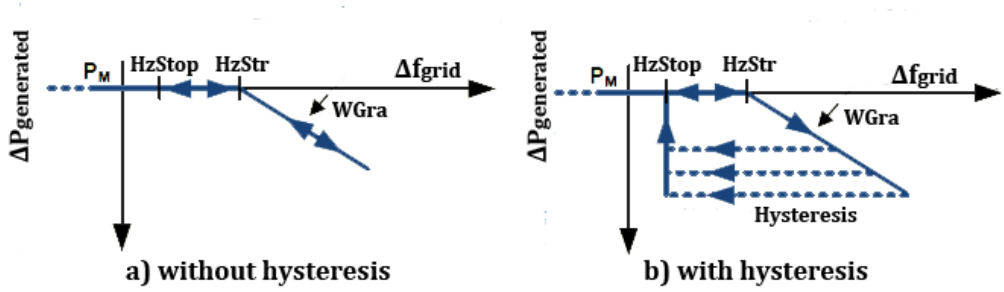

Figure 2.22: Example curve for Frequency-Watt Function 1 [11]

In Figure 2.22,

P_m = Power injected by inverter prior to frequency deviation

$HzStr$ = Frequency deviation at which power curtailment begins

$WGra$ = Power curtailment stop

$HzStop$ = Frequency deviation at which curtailed power may return to Nominal

When frequency deviation is higher than $HzStr$, power curtailment begins at a rate specified by $WGra$ (e.g. 40% P/Hz). Power curtailment continues until power output reaches zero or frequency deviation returns to nominal operating conditions. Once power curtailment begins and if the frequency deviation starts to improve, power output does not start to increase. The inverter waits until frequency deviation returns completely to nominal operating conditions, and then power output level before the beginning of curtailment is delivered.

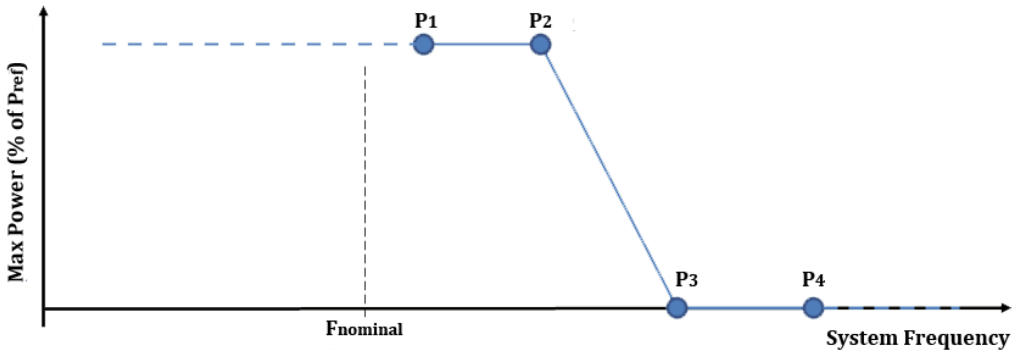

Figure 2.23: Example curve for Frequency-Watt Function 2

Figure 2.23 shows the Frequency-Watt Function 2. Unlike Frequency-Watt Function 1, this function does not wait until frequency deviation returns to nominal operating conditions to increase output level of power. Power output follows frequency deviation level.

2.3.2.5. Watt-Power Factor Function

Using this function, inverters can either inject real power (positive real power) or absorb real power (negative real power) based on the power factor of the system they are connected to. Unlike the Fixed Power Factor Function (section 2.3.2.1), this function uses multiple power factor values to adjust real power output. It is assumed that there is an energy storage system available to store real power absorbed by the inverters. Figure 2.24 shows an example of Watt-Power Factor Function curve. The x-axis is the percentage of real power absorbed or injected by the inverters. The y-axis is the power factor of the system.

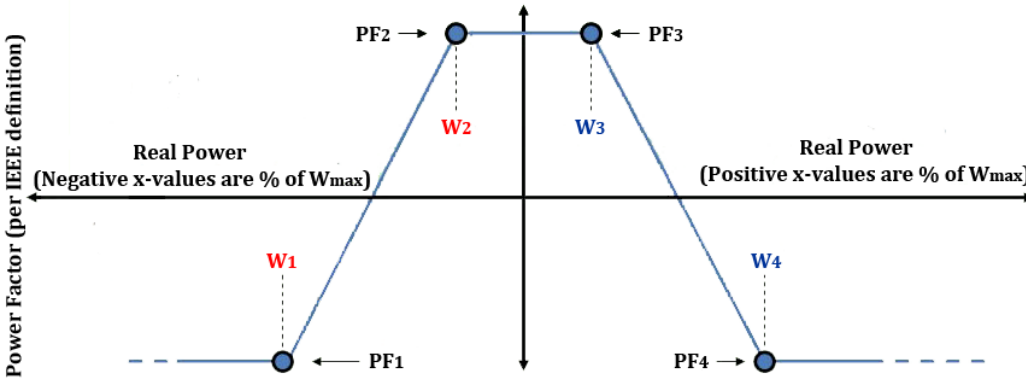

Figure 2.24: Example curve for Watt-Power Factor Function

2.4. Interconnection Requirements of IEEE 1547

Grid-tied PV systems need to comply with standard requirements in order to ensure the safety and the smooth transfer of power to the grid. Institute of Electrical and Electronic Engineers (IEEE) is one of the most relevant international bodies that are developing worldwide standards for the grid. Tables 2.1 to 2.4 summarize some of the most important regulations [54-55].

Table 2.1: Disconnection time for voltage deviations

Voltage range (%)	Disconnection time(s)
V < 45	0.16
0.45 ≤ V < 0.60	1.00
60 ≤ V < 88	2.00
88 ≤ V ≤ 110	Stay connected
110 < V < 120	1.00
V > 120	0.16

* Other static or dynamic voltage and trip times shall be permitted under mutual agreement between DR and EPS (Electric Power System) operators [54]

Table 2.2: Disconnection time for frequency deviations

Frequency range (Hz)	Disconnection time(s)
f < 57	0.16
f < 59.5	2.00
f > 60.5	2.00
f > 62	0.16

* Other modulated power output as a function of frequency shall be permitted under mutual agreement between DR and EPS (Electric Power System) operators [54]

Table 2.3: Conditions for reconnection after trip

IEEE 1547
0.88 < V < 1.10 (pu) AND 59.3 < f < 60.5 (Hz)

Table 2.4: DC current injection

IEEE 1547
$I_{DC} = 0.5$ (%)

* I_{DC} limit is based on % of the rated RMS current

Table 2.5: Maximum current harmonics

IEEE		
Odd harmonic order (%)	$h < 11$	4.0
	$11 \leq h < 17$	2.0
	$17 \leq h < 23$	1.5
	$23 \leq h < 35$	0.6
	$35 \leq h$	0.3
Total harmonic distortion THD (%)	5.0	

* Even harmonics are limited to 25% of above listed odd harmonics

Table 2.6: Anti-islanding requirements

IEEE 1547	
Time a DER should detect unintentional islanding and cease to energize	2s

2.5. PV Intermittency Issues

Power generated by a PV system has an intermittent character due mainly to atmospheric effects such as variable solar insolation resulting from cloud shading. The effects of intermittent PV power generation upon the electric grid are strongly influenced by the type of grid to which a PV system is connected and the type and amount of generation installed.

As the penetration level of PV in a distribution feeder increases, the capacity of a conventional synchronous generator that supplies power to the feeder needs to be reduced relatively. This leads to lower system inertia and higher generator reactance, and hence the power system transient stability would be affected negatively. When a fault occurs in the power system, some PV systems may be disconnected from the grid due to voltage sag. The disconnection causes a further drop in voltage and numerous PV systems may

be disconnected from the grid. In this case, not only would the transient voltage stability be affected, but also the frequency stability would be affected significantly due to the large power imbalance and fewer frequency control generators (conventional generators with inertia) [58-65]. IEEE 1547 and IEC 61727 require distributed generators to stay connected and provide fault-ride through capability as summarized in tables 2.1 and 2.2 (section 2.4).

During normal operational conditions, power from PV systems and conventional generators is balanced and the power system is stable. Power system operators have control over conventional generators but they have less control over the availability and quality of power from PV systems, as weather variations dictate their generation outputs. The following are four normal functions of generator operations that could be affected:

- **Load-frequency control:** Increase or decrease in system frequency is usually an indication of power imbalance in the system. When frequency deviation from the nominal value is detected, power system operators either increase or decrease outputs from conventional generators to match demands from loads. However, intermittent PV systems do not usually participate in frequency regulation and have outputs that are independent of system frequency.
- **Load following:** Due to intermittent PV systems, when solar irradiation increases or decreases and load demand is not increased or decreased at the same time, other power generating systems have to be taken off-line or placed online so that there is power balance in the system and maximum power from PVs can be utilized. This increases duties for conventional generators.
- **Ramp rate:** Conventional generators have inertia and require time (ramp rate) to change their outputs to follow load changes. Because of intermittency issues of PV systems, conventional generators need to

follow not only changes in loads but also output fluctuations from PV systems. This scenario gets worse when loads are suddenly reduced and PV system outputs are increased simultaneously, and vice versa.

- **Energy storage**: Power system operators place energy storage devices, like capacitors and battery banks, in the distribution feeders for emergency power needs. Due to the intermittency issues of PV systems, these storage devices may have to be oversized and become more expensive.

CHAPTER 3: VALIDATION AND VERIFICATION OF NEETRAC MEMBER FEEDERS' MODELING IN OPENDSS AND DIGSILENT

3.1. Introduction

Feeder models and their data obtained from NEETRAC were created by others using OpenDSS software. OpenDSS is a steady state analysis software and it is not suitable for the purpose of this research into transient behavior. DIgSILENT PowerFactory is an alternative power system simulation software, suitable for very large systems and is able to perform a steady state as well as a transient analysis; it is therefore chosen for this research.

However, DIgSILENT PowerFactory does not allow importing OpenDSS models directly. Appendix A discusses the methods and procedures used to import the data of two NEETRAC member feeders from OpenDSS into DIgSILENT PowerFactory software. This chapter discusses the validation and verification of the imported models.

3.2. Validation and Verification of Imported Models from OpenDSS

3.2.1. NEETRAC Member Feeder A

Member Feeder A is located in the Southeast part of the United States. The original feeder is imported from OpenDSS format and into DIgSILENT PowerFactory following the procedures discussed in Appendix A. The single line diagram of the feeder is shown in Figure 3.1 and Table 3.1 summarizes its key characteristics.

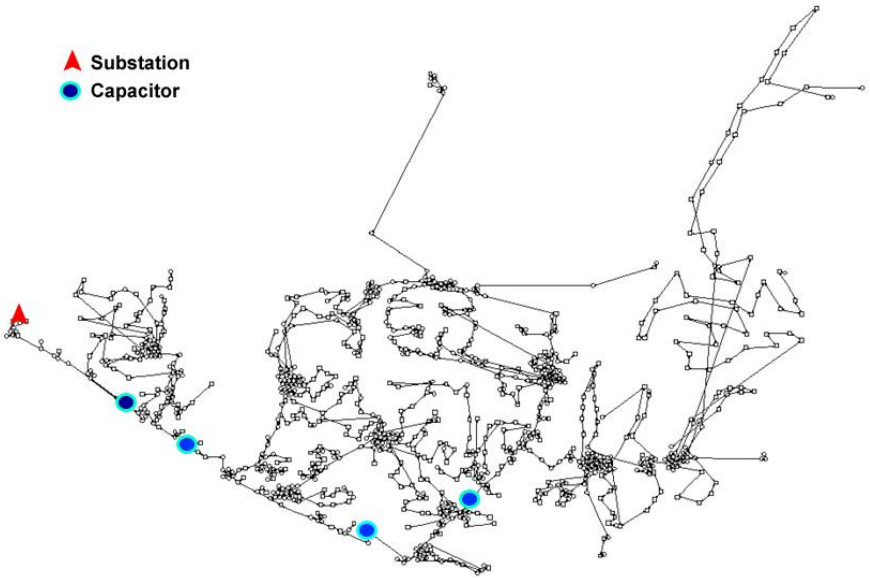

Figure 3.1: Single line diagram of NEETRAC member Feeder A

Table 3.1: Key characteristics of NEETRAC member Feeder A

Feeder Characteristics	Feeder A
Voltage (kV)	115, 34.5, 4.16, 2.4, 0.48, 0.415
Number of Buses	1174 primary and 1526 secondary
Total Active Power (MW)	43.4983
Total Reactive Power (MVAr)	21.939
Total Load	42.259 MW, 16.9993 MVAr
Number of Customers	484
Existing PV (kW)	None
Maximum Primary Three-Phase Short-Circuit Current	66.395 MA

There are four capacitor banks in the feeder. Three of the capacitor banks are rated at 200 kVAr, and have controllers that monitor the flow of reactive power with voltage override settings enabled. One capacitor is rated at 1200 kVAr and is always switched ON (i.e. it does not have a controller).

In the feeder, there are 484 single-phase loads and 484 single-phase transformers. There are also 261 overhead lines and 701 underground cables. The loads are modeled with the following common properties:

- Loads have linear active power and quadratic reactive power demands (Model 4 in OpenDSS).
- Conservative voltage reduction in active power (CVRwatts) and conservative voltage reduction in reactive power (CVRvars) factors of 0.8 and 3 respectively. These values are specific to this feeder.
- Three-phase loads have Wye type connections.
- All loads have a power factor of 0.928.
- Yearly loadshape with constant demand (i.e. load demand does not change throughout the year).

In the feeder, there are 261 overhead lines and 701 underground cables. From the 261 overhead lines, 41 are single-phase lines while the other 220 are three-phase lines. From the 701 underground cables, 583 are single-phase cables while the other 118 are three-phase cables.

OpenDSS and DIgSILENT models of the feeder are run, and their steady state solutions of voltages at all the network nodes are compared in Figure 3.2 to verify that the importation of the feeder models and data into DIgSILENT has been done correctly. The maximum percent difference between OpenDSS and DIgSILENT results is 0.00099 pu or 0.099%. The average percent difference is 0.047%, and the standard deviation is 0.003. The iteration techniques, number of loops, and result rounding used by the two software are different, but their steady state results difference is within acceptable tolerance at 0.099%. Based on the comparison results, it can be concluded that the DIgSILENT model of the feeder is validated at steady state using the OpenDSS model.

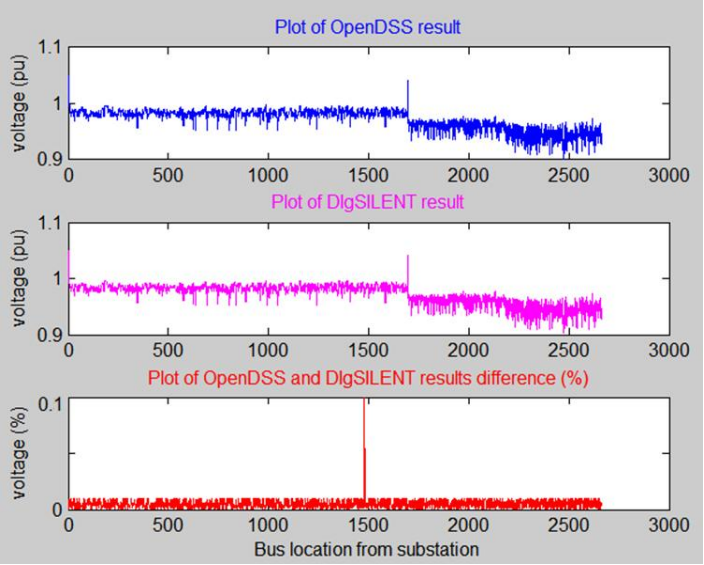

Figure 3.2: Comparison of OpenDSS and DIgSILENT results – NEETRAC member Feeder A

3.2.2. **NEETRAC Member Feeder B**

Member Feeder B is located in the Northeast part of the United States. The single line diagram of the feeder in DIgSILENT PowerFactory is shown in Figure 3.3 while Table 3.2 summarizes some of the key characteristics of the feeder.

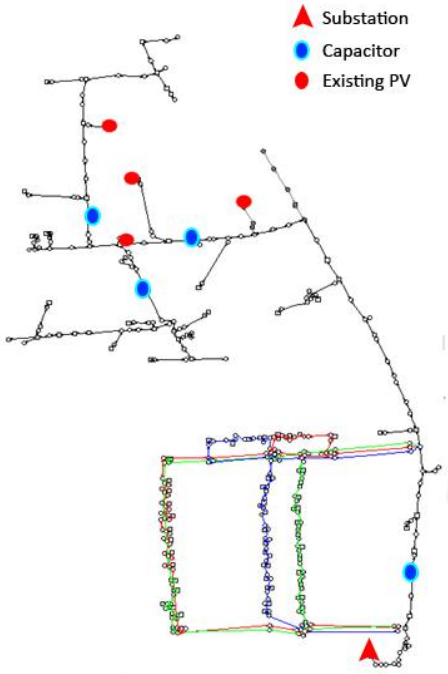

Figure 3.3: Single line diagram of NEETRAC member Feeder B

Table 3.2: Key characteristics of NEETRAC member Feeder B

Feeder Characteristics	Feeder B
Voltage (kV)	34.5, 12.46, 0.415, 0.208
Number of Buses	1434
Peak Load (MW)	4.6027
Minimum Load (MW)	1.35631
Number of Customers	247 Commercial and 851 Residential
Existing PV (kW)	668
Number of Capacitor Banks	4
Substation LTC Setpoint	1.029 pu (123.5 V)
Maximum Primary Three-Phase Short-Circuit Current	9.4148 kA

There are four capacitors banks in the feeder. Three of these capacitor banks are rated at 600 kVAr, while one capacitor is rated at 900 kVAr. One of the 600 kVAr rated capacitors is not switchable and remains ON all the time.

There are 94 distribution transformers in the feeder. From the 94 transformers, 28 are overhead transformers while the remaining 66 of them are underground transformers.

The loads in the feeder are divided into two groups: - residential and commercial loads. There are 851 single-phase residential loads and 247 commercial loads. The commercial loads are split between 78 single-phase loads and 169 three-phase loads.

To simulate the power demand of the feeder for a year, both residential and commercial loads have assigned yearly loadshapes. For one year, per hour load demand is calculated by multiplying base kW by the normalized multiplier (i.e. since there are 8760 hours in a year, there are 8760 multipliers). Figure 3.4 shows the yearly load multipliers of the feeder. The multipliers are higher during summer season resulting in loads reaching peak values

The base kW for both residential and commercial loads is defined as shown in equation 3.1[1].

$$kW = XFKVA * allocationfactor * pf \quad (3.1)$$

Where

- $XFKVA$ is rated kVA of service transformer
- $allocationfactor$ is a multiplier for allocating loads based on connected kVA of transformer
- pf is load power factor

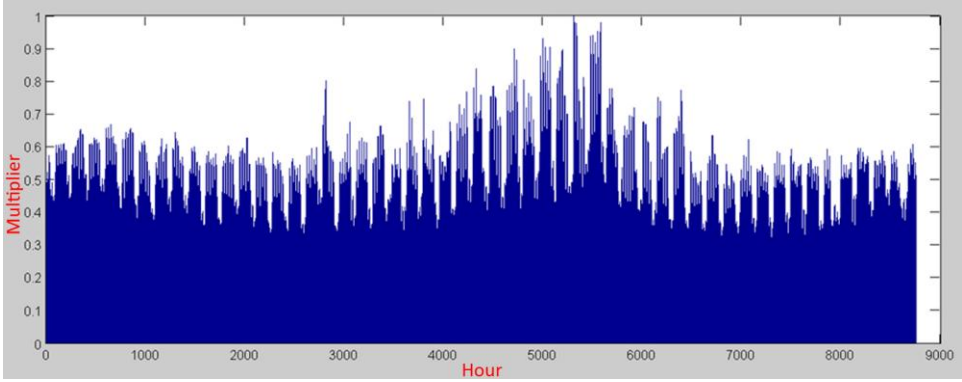

Figure 3.4: Yearly loadshape multipliers for NEETRAC member Feeder B

There are 160 overhead primary lines and 116 underground cables in the feeder. Out of the 160 overhead lines, 114 are three-phase lines while the remaining 46 overhead lines are single-phase lines. All 160 overhead primary lines fall into 14 types based on line geometry and type of wires used to define them in the OpenDSS model. Out of the 116 underground cables, 92 are three-phase cables while the other 24 are single-phase cables. Underground cables fall into seven types based on line codes used to define them in OpenDSS model of the feeder.

Four PV sites exist within this feeder with a combined total capacity of 668 kW, as shown in Table 3.3. All inverters at the four PV sites are controlled in Unity Power Factor mode of operation.

Table 3.3: Existing PV sites in NEETRAC member Feeder B

PV Site	Number of PV Systems	Total PV Capacity	Inverter Mode of Operation
1	5	200 kW	Unity Power Factor
2	8	168 kW	Unity Power Factor
3	9	231 kW	Unity Power Factor
4	2	69 kW	Unity Power Factor

OpenDSS and DIgSILENT models of the feeder are simulated and steady state solutions of voltages at all the network nodes are compared in Figure 3.5. The maximum percent difference between OpenDSS and DIgSILENT results is 0.0009 pu or 0.099%. The average percent difference is 0.0378% while the standard deviation is 0.0246. Based on the comparison results in Figure 3.5, it can be concluded that the DIgSILENT model of the feeder is validated at steady state using the OpenDSS model.

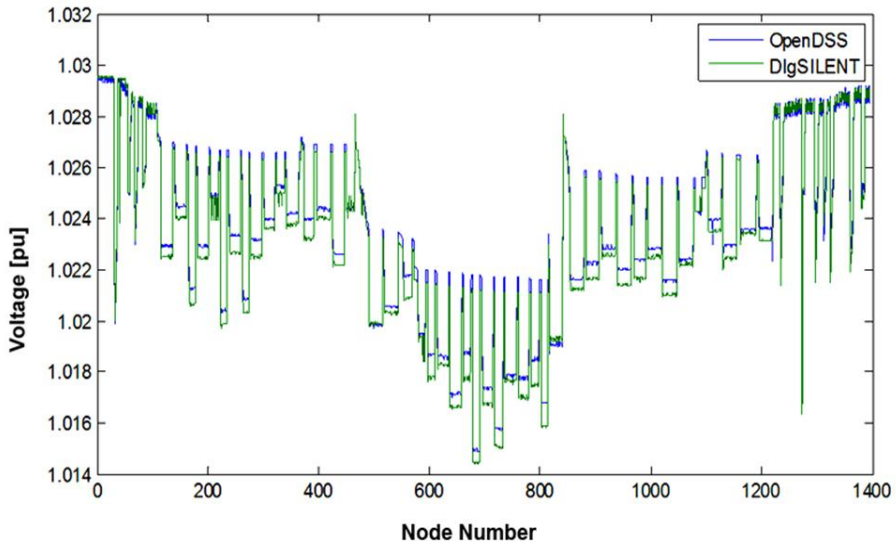

Figure 3.5: Comparison of OpenDSS and DIgSILENT results – NEETRAC member Feeder B

3.3. Summary

Two feeder models received from NEETRAC in OpenDSS file format are imported into DIgSILENT PowerFactory software. Since DIgSILENT PowerFactory

does not allow for the direct import of models created in OpenDSS software, different methods and procedures are followed to convert data in these models into DGS formatted Microsoft Excel files before importing them into DIgSILENT PowerFactory.

The imported models in DIgSILENT PowerFactory have been verified and validated at steady state against OpenDSS models. The maximum difference between the models in the two software at steady state is 0.099% and is well within acceptable tolerance.

Per recommendation from the DIgSILENT PowerFactory helpdesk, the photovoltaic (PV) system that comes as a template with the software is suitable for root mean square (RMS) simulations only and is not valid for electromagnetic transient (EMT) simulations. In chapter 4, DIgSILENT PowerFactory's RMS simulation results are compared and validated against PSCAD's EMT simulations using simple networks with PV, induction motor, and load

.

CHAPTER 4: TRANSIENT PERFORMANCE VALIDATION OF DIGSILENT POWERFACTORY

4.1. Introduction

In order to investigate the impacts of increasing amounts of PV on the transient behaviors of a distribution system, a detailed model of a PV system is needed. DIgSILENT PowerFactory has a "0.5 kVA PV System" template. This PV system model is highly customizable and contains different user interfaces for editing parameters of the PV modules, DC bus, and inverter sections of the system.

According to the DIgSILENT helpdesk [3], the PV system model that comes as a template cannot be used for electromagnetic transient (EMT) simulations, and therefore suitable only for RMS modes of simulation. An RMS simulation uses symmetrical components (i.e. positive-sequence, negative-sequence and zero-sequence) representation of a feeder, and only takes into account the fundamental components of voltages and currents. An EMT simulation uses dynamic equations to represent a feeder, and is ideally suited for small feeders as the simulation takes considerable time. As summarized in Table 3.1 and Table 3.2, NEETRAC member Feeder A has 1174 buses and NEETRAC member Feeder B has 1434 buses. Simulations of these feeders in EMT mode will take considerable time, and the PV system template in DIgSILENT is developed for RMS mode of simulation (i.e. the controller in the PV system uses RMS voltage and power measurements to control the d-axis and q-axis currents to inject to the grid).

To investigate whether valuable information is lost by using the RMS mode, simple networks with a load, PV, and an induction motor are constructed in DIgSILENT and PSCAD software. In PSCAD, simulations are run in EMT, final results are converted to RMS, and comparisons are done against the DIgSILENT RMS simulation results.

4.2. Comparison of DIgSILENT and PSCAD Results Using Simple Network with PV System and Load

A PV system model in PSCAD is constructed in the same fashion as is done in DIgSILENT [66]. PSCAD is well-known power simulation software for analyzing power system transients [67]. If any module of the DIgSILENT PV system model is modified, the PSCAD PV system model can easily be modified by updating the corresponding module. Figure 4.1 and Figure 4.2 show single line diagrams of a simple network with 45 kW PV system and 45 kW load created in DIgSILENT and PSCAD software respectively.

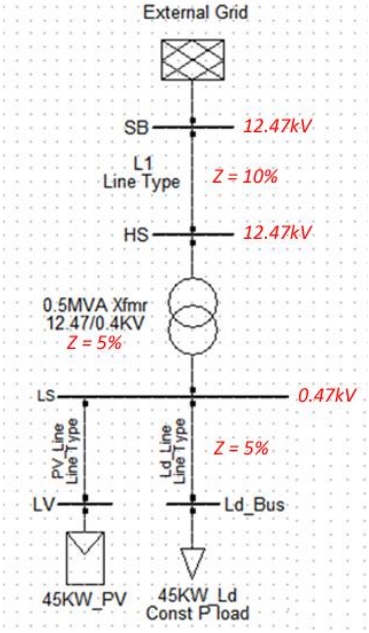

Figure 4.1: Simple network with PV system and load in DIgSILENT

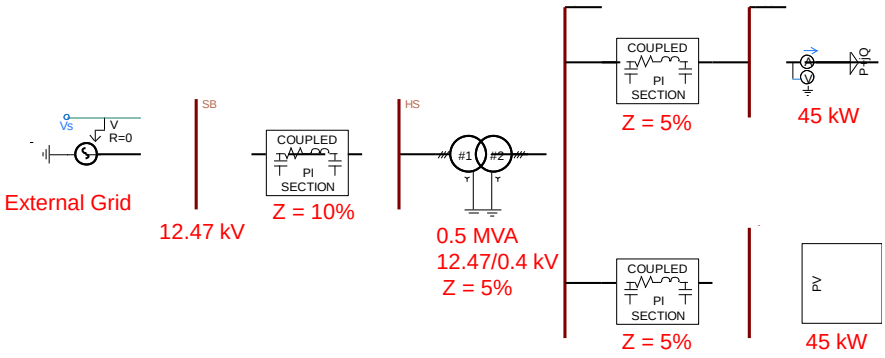

Figure 4.2: Simple network with PV system and load in PSCAD

4.2.1. **Simulation Scenario and Results**

A simple network that consists of the following elements is constructed within both DIgSILENT and PSCAD:

- External grid with 1 pu voltage (12.47 kV) setpoint
- Transmission line with 10% impedance
- Step-down transformer, Y-Y connection, 0.5 MVA,12.47/0.4 kV
- Distribution line with 5% impedance
- 45 kW PV system
- Three-phase, 45 kW load. Constant power model

PSCAD does not pre-initialize a model at the beginning of a simulation (unlike DIgSILENT or Matlab/Simulink). A timed breaker is inserted between the external grid and the simple network and this breaker is closed after 14.25 s to let the initialization process complete before any simulation scenarios are applied to the system

The following simulation scenarios are used:

1. Enable the inverter in the PV systems to operate in a Volt-Var control mode and set the deadband, max reactive power setpoint, and min reactive power setpoint as shown in Figure 4.3.

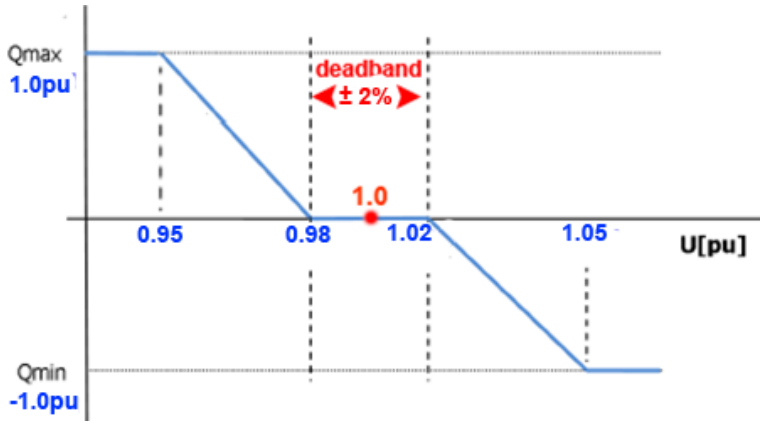

Figure 4.3: PV inverter Volt-Var setpoints

2. Run the simulation for 14.25 s for the initialization process to complete, and then cause a step decrease in the external grid supply voltage from 1 pu to 0.9 pu (i.e. 10 % voltage drop on the external grid).
3. Return the external grid voltage in a step fashion to 1 pu after 150 ms (i.e. at 14.40 s).
4. Measure RMS voltage at the point of common coupling (i.e. voltage at the bus to which the PV system is connected)
5. Measure active and reactive power injected by the PV system

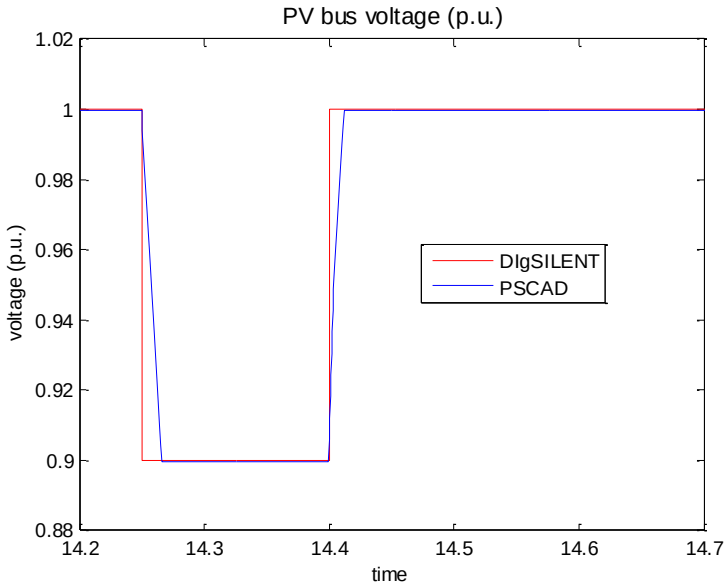

Figure 4.4: Voltage at the PCC – DIgSILENT and PSCAD PV system models

Voltage, active, and reactive powers delivered by the PVs in the two models are shown in Figure 4.4, Figure 4.5, and Figure 4.6 respectively.

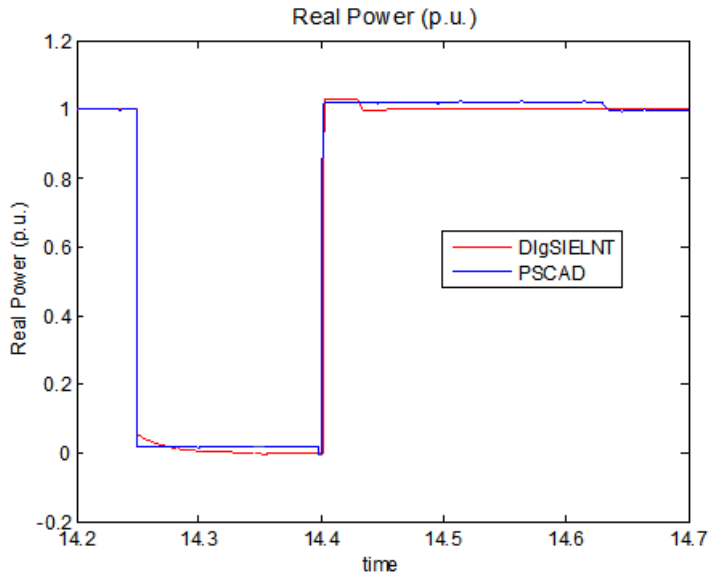

Figure 4.5: PV active power – DIgSILENT and PSCAD PV system models

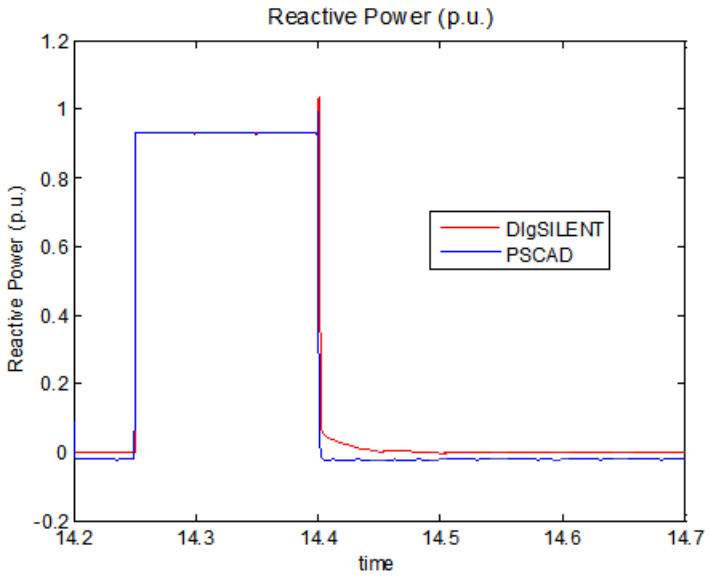

Figure 4.6: PV reactive power – DIgSILENT and PSCAD PV system models

Figure 4.5 and Figure 4.6 show that the results of PSCAD and DIgSILENT PV system models are relatively close. Spikes are present on the PSCAD PV system model since there is no filter circuit connected between the inverter and grid to filter out harmonics and switching transients. In the DIgSILENT PV system model, there is a lack

of detailed information to show what kind of filter circuit is implemented in the "Static Generator" or inverter model of the PV system.

4.3. Comparison of Induction Motor Starting in DIgSILENT and PSCAD

Loads in the distribution feeder models received from NEETRAC members are modeled based on active and reactive power demands. In real world scenarios, there are induction motor loads present in distribution feeders in order to drive fans, air-conditioning units, etc. In order to replace 30% of loads in the NEETRAC distribution feeder models by equivalent induction motors and to investigate the behaviors of these feeders during voltage drop, a simple network with an induction motor is constructed both in DIgSILENT and PSCAD software along with a comparison of the results. Table 4.1 summarizes the parameters used for the induction motor in DIgSILENT and PSCAD software.

Table 4.1: Induction motor parameters used

Power Rating:	100 MW
Voltage	11 kV
Frequency	60 Hz
Number of Poles	6
R_1	0.4 Ω
R_2	0.5 Ω
$X_1 = X_2$	2.08 Ω
X_m	30 Ω
Inertia Constant, H(s)	0.5 s
Load	Fan Type, T = 0.8*ω^2

Figure 4.7 shows the single line diagram of the simple network with induction motor created in DIgSILENT and PSCAD.

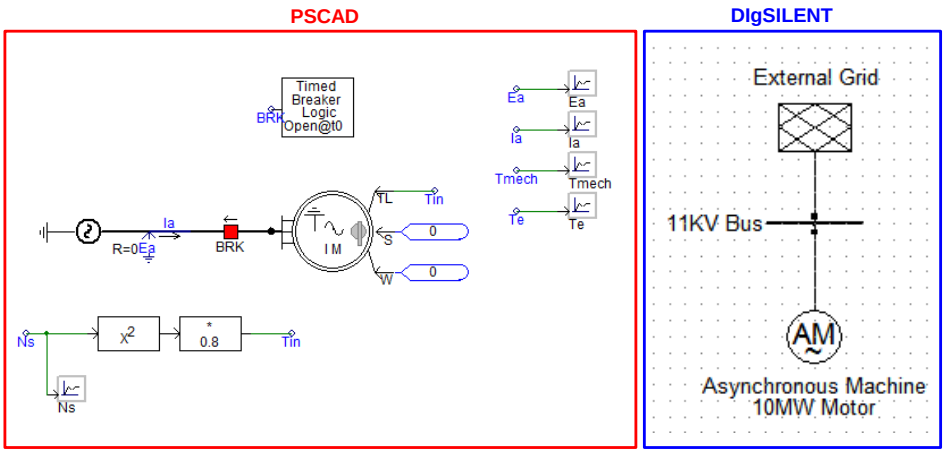

Figure 4.7: Induction motor starting test in DIgSILENT and PSCAD

To simulate motor start up, the PSCAD model is run for 14.25 s and then the breaker is closed. Hence, the motor start up is not affected by PSCAD initialization issues. Figure 4.8 shows a side-by-side comparison of the motor speed and torque curves of PSCAD and DIgSILENT models plotted along the same axis.

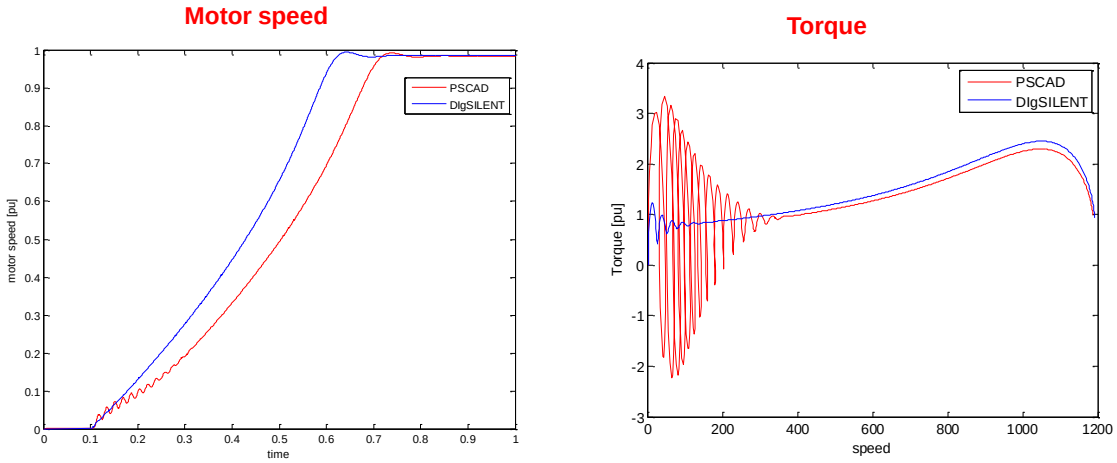

Figure 4.8: DIgSILENT and PSCAD motor speed and torque comparison plots

Figure 4.8 shows that motors in both PSCAD and DIgSILENT reach their rated speed but the motor in the DIgSILENT model reaches its rated speed about 0.1s ahead of the motor in the PSCAD model. The torque-speed curves show motors reach their full-

load torque at rated speed. DIgSILENT uses RMS, and it displays less oscillation at the beginning of the simulation.

To compare current drawn by the two motor models, instantaneous currents from the PSCAD model are converted to RMS positive-sequence current using equations 4.1 and 4.2. The results are compared with RMS current from the DIgSILENT model (i.e. PSCAD uses an EMT simulation mode and positive-sequence equations. Current values from the EMT simulation mode are converted to RMS values in a similar fashion to how DIgSILENT measures current in RMS simulation mode).

$$i = \frac{1}{3}\left(i_a + i_b \cdot e^{j\frac{2}{3}\pi} + i_c \cdot e^{j\frac{4}{3}\pi}\right) = i_r + j \cdot i_i \tag{4.1}$$

$$i_{rms} = \sqrt{{i_r}^2 + {i_i}^2} \tag{4.2}$$

Figure 4.9 shows instantaneous currents in PSCAD and comparisons of PSCAD and DIgSILENT RMS currents.

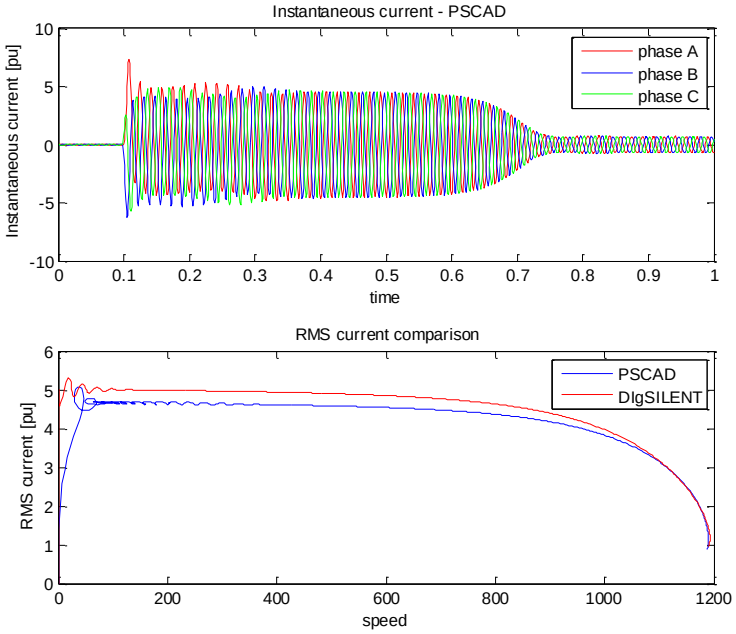

Figure 4.9: DIgSILENT and PSCAD RMS current comparison plots

From Figure 4.9, it can be seen that motors in PSCAD and DIgSILENT draw unbalanced three-phase currents at the beginning of the simulation. This behavior is to be

expected due to the fact that the starting current of a motor (which is typically 5 to 7 times the full-load current) has asymmetrical components. This asymmetrical current is well captured by PSCAD (PSCAD uses differential equations while DIgSILENT uses symmetrical components). Once steady state is reached, current demand by both motors attains rated value. Therefore, it can be concluded that the motors in both softwares behave similarly, thus providing similar results during startup.

4.4. Comparison of DIgSILENT and PSCAD Results Using Simple Network with PV system, Load, and Induction Motor

As part of the validation and verification of the DIgSILENT simulation results, a simple network with 45 kW PV system, 10 MW induction motor, and 45 kW constant load is constructed in both DIgSILENT and PSCAD software. The PV system and induction motor used in the simple network are discussed in sections 4.2 and 4.3 respectively. Figure 4.10 shows the single line diagram of the simple network in both software.

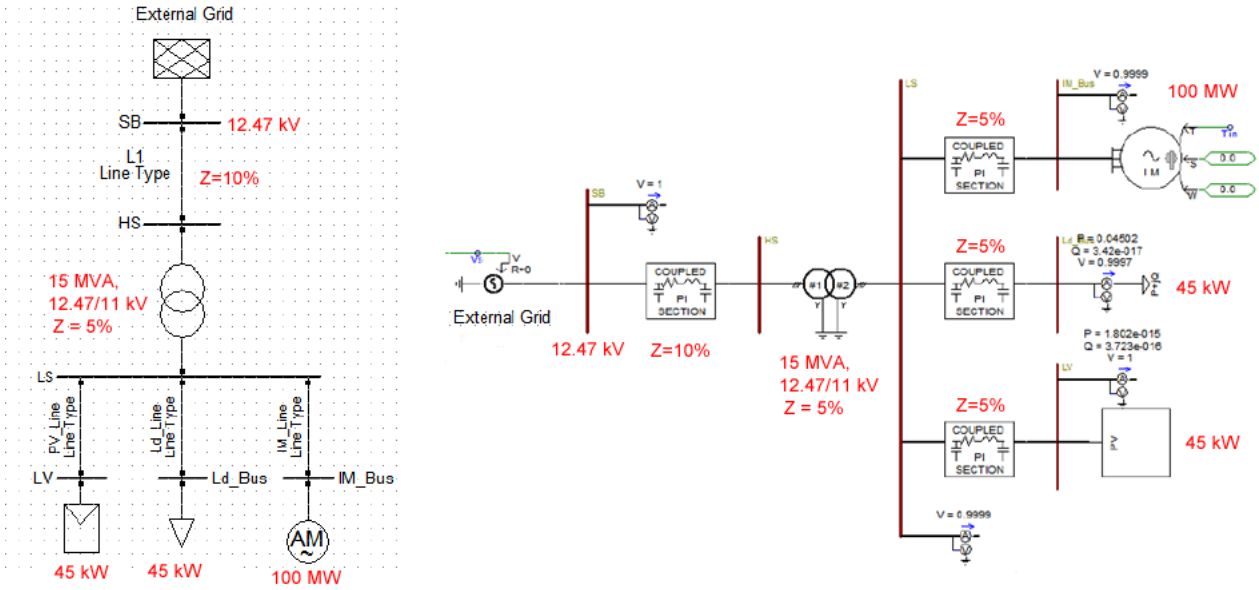

Figure 4.10: Simple test networks with PV system, load, and induction motor (a) DIgSILENT (b) PSCAD

The following simulation scenarios are used:

1. The external grid voltage is reduced from 1.0 pu to 0.9 pu. After 150 ms, it is raised back to its original value of 1.0 pu.
    - In DIgSILENT, a “Parameter Event” is created to lower the external grid voltage to 0.9 pu at 14.25 s. Another “Parameter Event” is created to raise the external grid voltage from 0.9 pu to 1.0 pu at 14.4 s.
    - In PSCAD, a timer is used to lower and then raise the external grid voltage.
    - 14.25 s is chosen in order to avoid the initialization by PSCAD at the beginning of the simulation.
2. Inverters in both models are enabled to operate in Volt-Var mode with settings as shown in Figure 4.3
3. PV bus, load bus and motor bus RMS voltages are measured
4. Active and reactive power delivered by PVs in the two models are measured

PSCAD and DIgSILENT RMS voltage measurements at the low side of transformer bus, PV bus, load bus, and induction motor bus are shown in Figure 4.11. Active and reactive powers delivered by the PVs in the two models are shown in Figure 4.12.

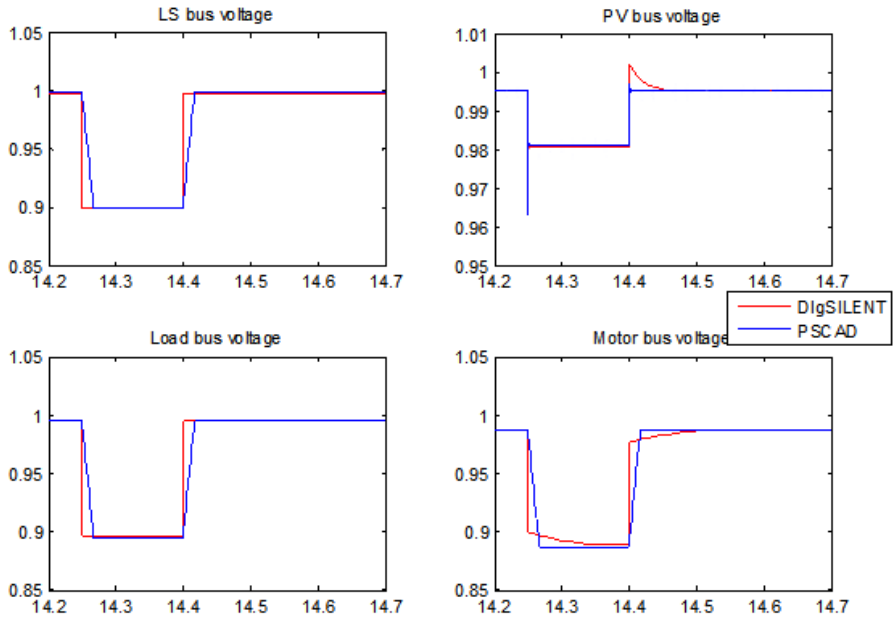

Figure 4.11: Bus voltages – simple test network with PV system, load, and induction motor

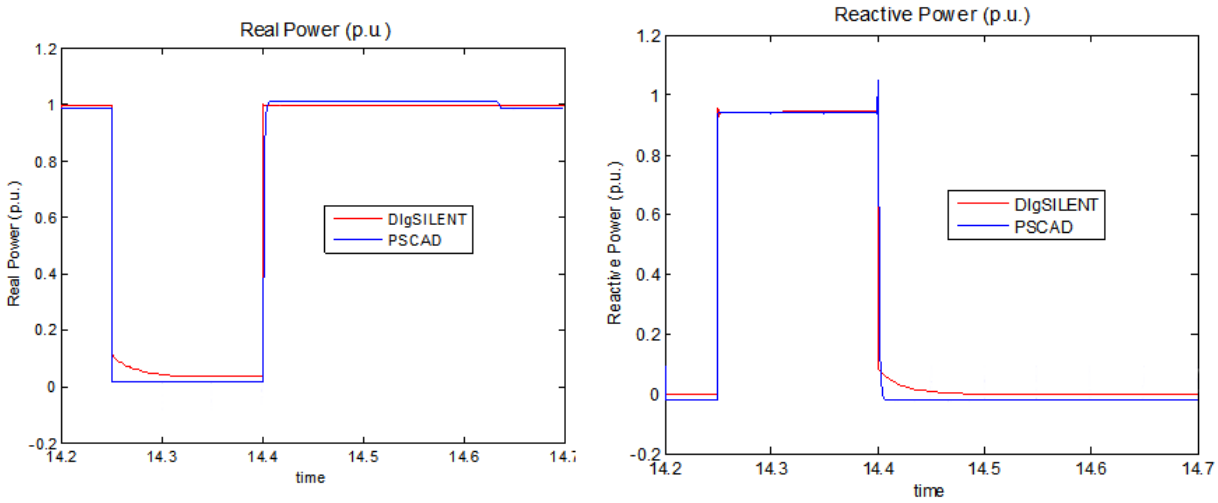

Figure 4.12: PV power - simple test network with PV system, load, and induction motor

PSCAD uses differential equations to represent the network while DIgSILENT uses symmetrical components. This difference is reflected in voltage and power plots of DIgSILENT and PSCAD. PSCAD plots show slow changes at the moment fault is applied and cleared while DIgSILENT plots show sharp changes.

4.5. Summary

According to the DIgSILENT helpdesk, the PV system model in DIgSILENT cannot be used for EMT type simulations and is suitable only for RMS type simulations. To investigate whether valuable information is lost by using RMS instead of EMT to study the transient behaviors of NEETRAC members' feeders, a similar PV system is created in PSCAD. The EMT simulation results of PSCAD are converted to RMS and compared with results of DIgSILENT. As discussed in section 4.2, their results are comparable. RMS converted EMT simulation results of PSCAD show similar behavior to that of DIgSILENTs' RMS simulation results with acceptable tolerance.

Feeder models studied in this research contain buses, lines, PVs, and loads. In NEETRAC member Feeder B, 30% of commercial loads are replaced with equivalent induction motors. Therefore, to investigate if valuable information is lost by using RMS simulation in DIgSILENT, simple networks with load, PV system, and induction motor are constructed in DIgSILENT and PSCAD software. As discussed in section 4.3 and section 4.4, their results are comparable with acceptable tolerance. Based on the simple networks simulation results studied in this section, actual NEETRAC members' feeder models are studied using DIgSILENT PowerFactory

CHAPTER 5: TRANSIENT PERFORMANCE OF NEETRAC MEMBER FEEDER B

5.1. Introduction

Two NEETRAC member feeder models that are originally modeled using OpenDSS software are imported into DIgSILENT PowerFactory. The two DIgSILENT models are validated and verified against their OpenDSS models at steady state (discussed in Chapter 3). NEETRAC member Feeder B is chosen for further transient performance analysis. Unlike Feeder A, this feeder has time varying loads and four pre-existing PV sites. Its single line and feeder characteristics are shown in **Error! Reference ource not found.** and **Error! Reference source not found.** respectively.

The four pre-existing PV sites have a combined total capacity of 668 kW. According to EPRI's report [15], the maximum PV capacity that can be installed in the feeder without violating the ANSI 105% voltage threshold (i.e. 1.05 pu) is 6 MW. In the report, the maximum PV capacity is calculated assuming no pre-existing PVs in the feeder.

In the DIgSILENT model of the feeder, an additional 5th PV site is added at the farthest end of the feeder. The capacity of this PV site is calculated by subtracting the existing four PV sites capacity from 6 MW and assuming a 20% overrated inverter (i.e. 6 MW – 0.668 kW = 5.332 MW PV, total PV system becomes ≈ 6.5 MVA). A 6.5 MVA, 0.48/12.47 kV, Δ-Yg connected step-up transformer is used to connect PV_5 directly to the 12.47 kV bus. Figure 5.1 shows the location of the five PV sites in the feeder.

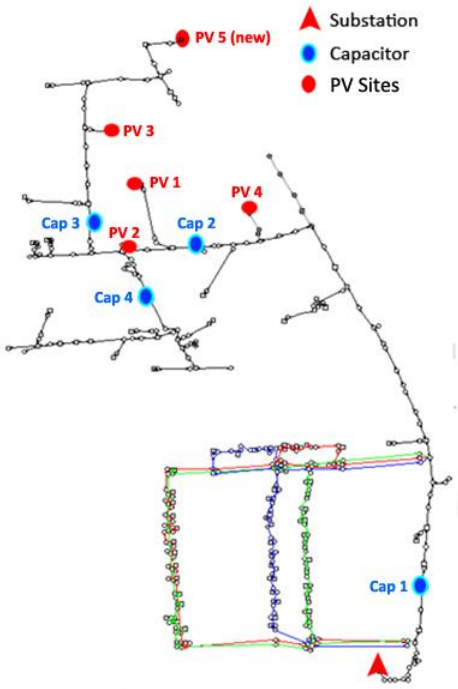

Figure 5.1: Single line diagram of NEETRAC member Feeder B with five PV sites

After PV_5 is added, the feeder model is run at steady state, and voltages at the five PV buses are measured. Table 5.1 shows comparison results of PV bus voltages before and after the addition of PV_5 .

Table 5.1: PV bus voltages before and after the addition of PV_5

PV bus voltages before the addition of PV_5 [pu]						
PV site	Phase A	Phase B	Phase C			
PV_1	1.0149	1.0150	1.0166			
PV_2	1.0271	1.0266	1.0271			
PV_3	1.0272	1.0264	1.0263			
PV_4	1.0131	1.0132	1.0148			
PV_5	1.0231	1.0231	1.0246			
PV bus voltages after the addition of PV_5 [pu]						
PV site	Phase A	Phase B	Phase C	% difference		
				Phase A	Phase B	Phase C
PV_1	1.02557	1.02506	1.02522	1.05	0.99	0.85
PV_2	1.03799	1.03643	1.03570	1.06	0.96	0.84
PV_3	1.03793	1.03511	1.03384	1.04	0.85	0.73
PV_4	1.02074	1.02056	1.02090	0.75	0.73	0.60
PV_5	1.04113	1.03956	1.03915	1.76	1.61	1.42

Table 5.1 shows adding PV_5 with 6.5 MW capacity results in a 1.76% voltage rise at the bus where PV_5 is connected. No threshold violation of 105% is observed on any other bus in the feeder.

After discussions with the representative of the feeder, it is learned that the inverters in the existing four PV sites are enabled to operate only in Unity Power Factor control mode. Furthermore, 30% of the commercial loads in the feeder are industrial type loads. To investigate the inverters interaction with the system, the following modifications are made to the feeder.

- Replace 30% of commercial loads by equivalent induction motors
- Increase impedances of selected lines between PV sites

5.2. Modifications Made to NEETRAC Member Feeder B

5.2.1. Replace 30% of Commercial Loads by Equivalent Induction Motors

Feeder B consists of both, there are residential and commercial loads. After discussions with an advisor from the utility that operates the feeder, it is assumed that 30% of commercial loads in the feeder are induction type loads. Therefore, 30% of commercial loads in the feeder are replaced by equivalent induction motors. Table 5.2 is used as reference to select parameters of an induction motor based on its kW rating [68].

Table 5.2: Typical per unit parameters for induction motors [68]

Rating (kW)	Full load efficiency (%)	Full load power factor (%)	Full load slip (%)	X_m(pu)	X_e(pu)	R_1(pu)	R_2(pu)
Up to 5	75-80	75-85	3.0-5.0	1.6-2.2	0.10-0.14	0.04-0.08	0.04-0.08
5-25	80-88	82-90	2.5-4.0	2.0-2.8	0.12-0.16	0.035-0.05	0.035-0.05
25-200	86-92	84-91	2.0-3.0	2.2-3.2	0.15-0.17	0.03-0.04	0.03-0.04
200-1000	91-93	85-92	1.5-2.5	2.4-3.6	0.15-0.17	0.025-0.03	0.02-0.03
Over 1000	93-94	88-93	1.0	2.6-4.0	0.15-0.17	0.015-0.02	0.015-0.025

Most of the buses have multiple commercial loads connected to them with no impedance between the loads (i.e. multiple commercial loads connected to one node). Therefore, multiple commercial loads on a bus are added together and represented as one large commercial load, while 30% of that load is replaced by an equivalent induction motor. Figure 5.2 shows this process for one of the buses in the feeder. Steady state simulations are run before and after the changes are applied to ensure that any changes made to the feeder are within acceptable tolerance. The maximum voltage difference on a bus before and after replacing 30% of its commercial load by an induction motor is 0.009 pu or 0.9%.

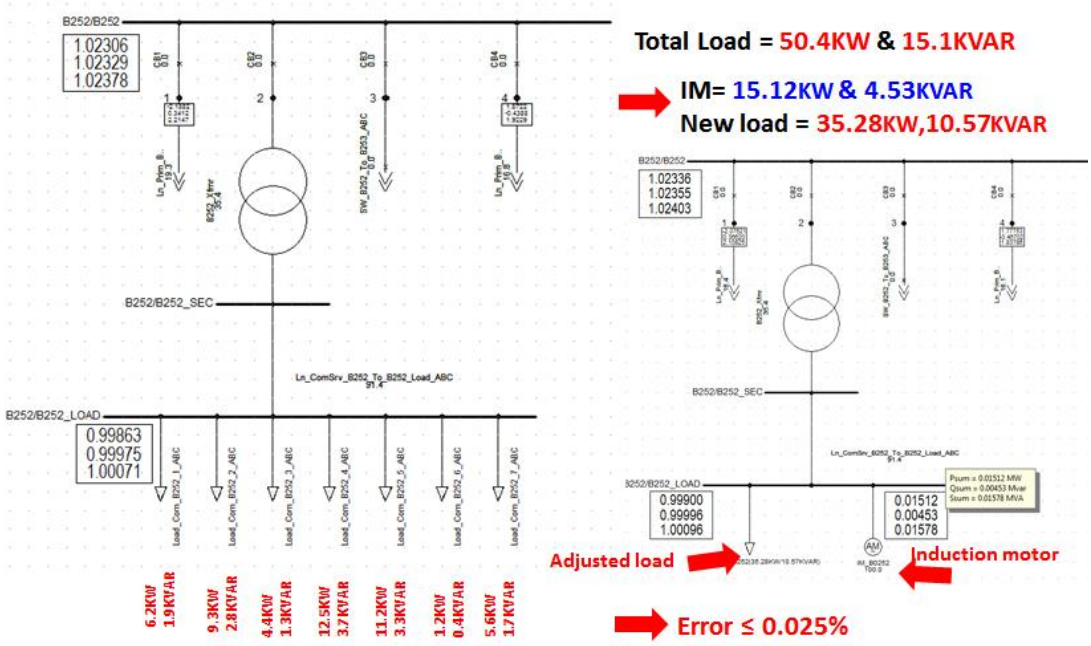

Figure 5.2: Replacing 30% of commercial load by an equivalent induction motor on a bus

Figure 5.2 shows seven loads with different ratings but similar load types (constant P-type) connected to the same bus without any impedance between them. These loads are combined into one load (50.4 kW and 15.1 kVAr), and 30% of that load is replaced by an equivalent induction motor (15.12 kW and 4.53 kVAr). The load is then reduced by 30% to account for the addition of an induction motor. The voltage on the bus before and after the replacement of 30% of the load by an equivalent induction motor has

a percentage difference of 0.025% (i.e. 0.025 pu) which is within acceptable tolerance. Figure 5.3 shows location of induction motors in the modified feeder.

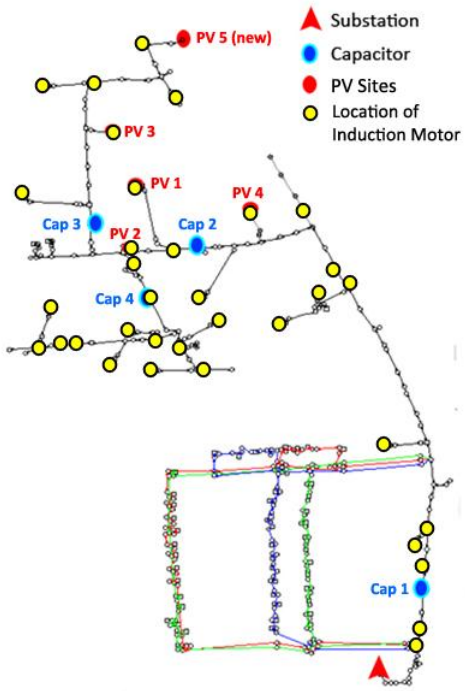

Figure 5.3: Location of induction motors in the modified feeder

5.2.2. **Increase Line Impedance**

The four existing PV sites are located in close proximity. To investigate the effect of inverters operating in Volt-Var control mode, line impedances between the existing PVs and neighbor buses are increased by 20 times. Figure 5.4 shows location of lines with modified impedances in the feeder. After the line impedances are increased, the model is run at steady state.

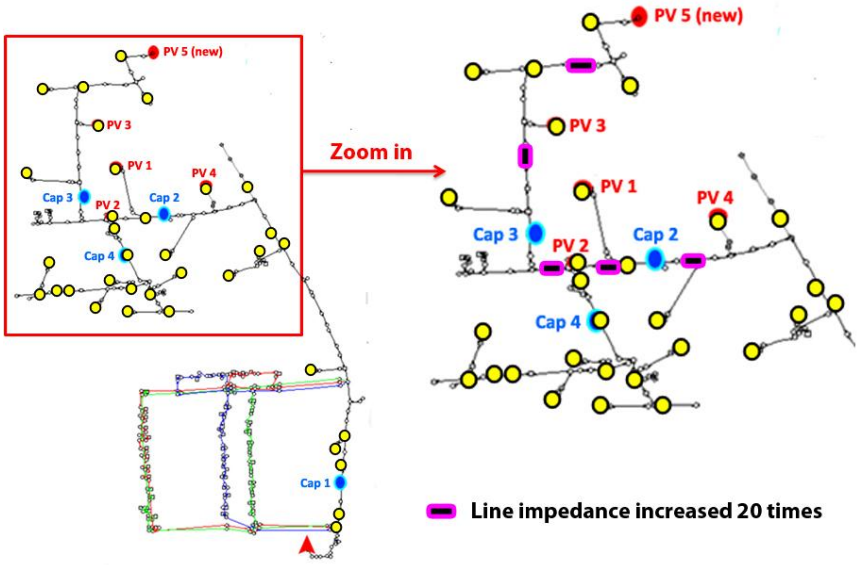

Figure 5.4: Location of lines in the feeder with increased impedance

Figure 5.5 shows voltages measured at PV buses after all modifications are applied to the feeder. Increasing those line impedances results in an ANSI 105% voltage threshold violation only on PV Site 2 (1.061 pu) and PV Site 3 (1.064 pu) buses. Table 5.3 shows data points extracted from Figure 5.5.

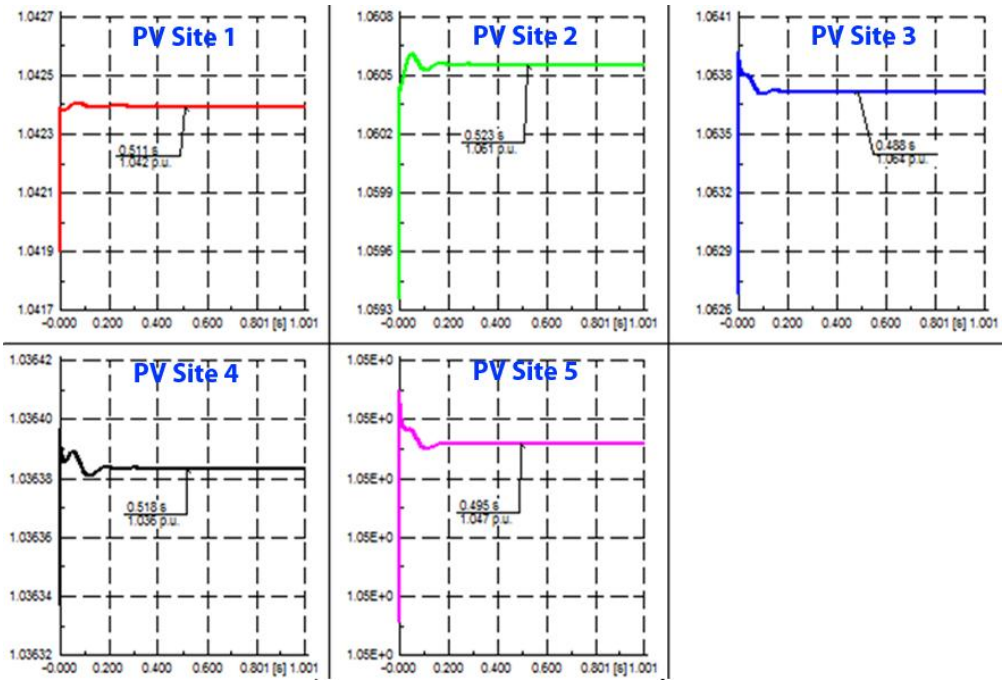

Figure 5.5: Voltages measured at PV buses after all modifications are applied to the feeder

Table 5.3: Data points extracted from Figure 5.5

PV Site	Voltage [pu]
1	1.042
2	1.061
3	1.064
4	1.036
5	1.047

5.3. Different Scenarios Considered for Transient Simulations of NEETRAC Member Feeder B

This section describes the different scenarios constructed for studying the transient behaviors of the feeder.

Scenario 1 – No disturbance in the system: The feeder model is run with no disturbance applied to the system and with the inverters in Unity Power Factor control mode. This scenario serves to simulate steady state conditions where no disturbance occurs in the system. The simulation is repeated with inverters enabled to operate in Volt-Var mode of control.

Scenario 2 – Three-phase fault on the external grid: While inverters operate in Unity Power Factor control mode, the external grid voltage is reduced by 10%. After 150 ms, the external grid voltage is returned to its original value. This scenario serves to simulate a situation where a three-phase fault occurs somewhere in the external grid resulting in a 10% decrease in voltage where the fault is cleared after 150 ms. The simulation is repeated with inverters enabled to operate in Volt-Var control mode.

Scenario 3 – Fluctuating cloud covering PV sites: A 0.5 Hz fluctuating solar irradiation (cloud) is created in DIgSILENT. Fluctuating and out-of-phase cloud cover is allowed to exist within the five PV sites at different rates. This scenario serves to

simulate the effect of a fluctuating cloud covering PVs in the feeder at different rates. Run the simulation for 6 s with inverters enabled to operate in the following control modes:

- Case A – All inverters operate in Unity Power Factor control mode
- Case B – All inverters operate in Volt-Var control mode
- Case C – Inverter at PV Site 5 (large PV site) operates in Unity Power Factor control mode while all the other inverters operate in Volt-Var control mode
- Case D – Inverter at PV Site 5 (large PV site) operates in Volt-Var control mode while all the other inverters operate in Unity Power Factor control mode

Scenario 4 – Effects of losing a large PV site: While running at steady state, suddenly disconnect PV Site 5 from the feeder. This scenario serves to simulate the effects of suddenly losing a large PV site in the feeder. Run the simulation with inverters controlled to operate in Unity Power Factor and Volt-Var control modes.

5.4. Transient Simulation Results

5.4.1. Simulation Scenario 1: No Disturbance Applied to the System

As a base case scenario, the inverters are enabled to operate in Unity Power Factor control mode and no disturbance is applied to the system. The voltage measured at PV buses and power delivered by PVs are shown in Figure 5.6 and Figure 5.7 respectively. Table 5.4 shows data points extracted from Figure 5.6 and Figure 5.7.

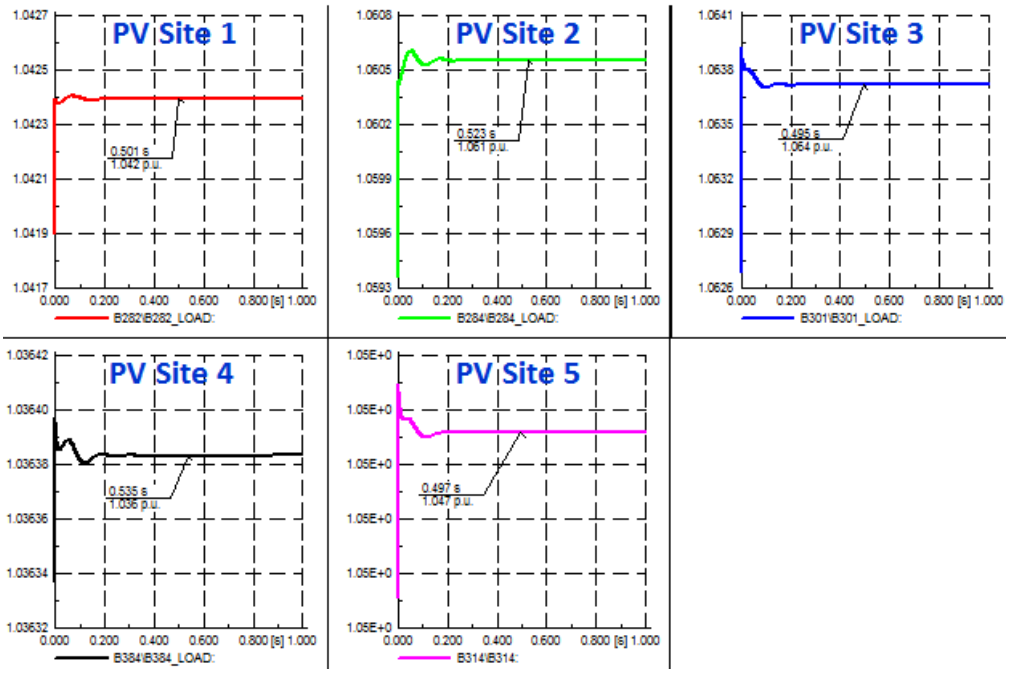

Figure 5.6: Simulation Scenario 1 – Voltages measured at PV buses when inverters operate in Unity Power Factor control mode

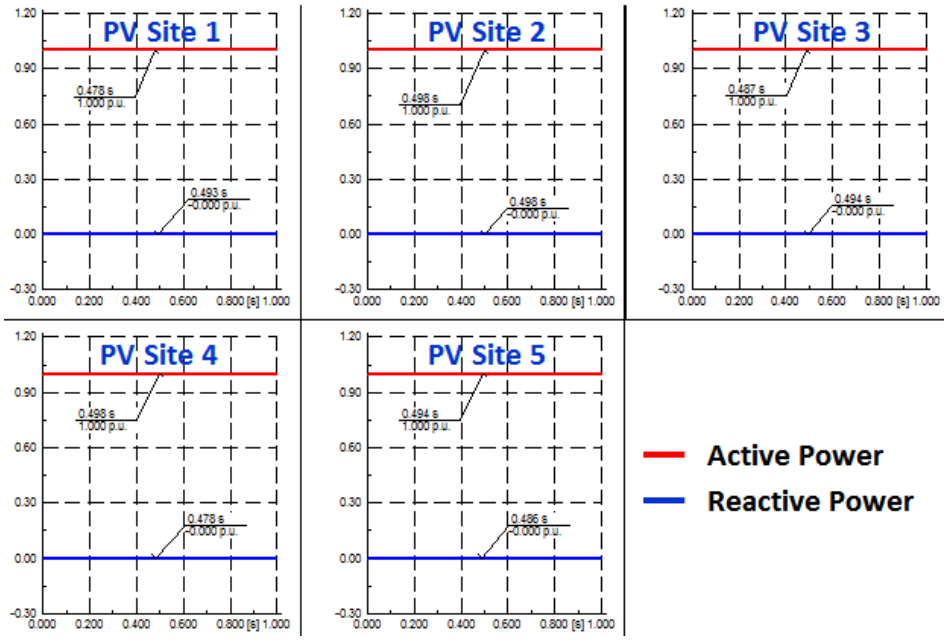

Figure 5.7: Simulation Scenario 1 – Power delivered by PVs when inverters operate in Unity Power Factor control mode

Table 5.4: Data points extracted from Figure 5.6 and Figure 5.7

PV Site	Voltage [pu]	Real Power [pu]	Reactive Power [pu]
1	1.042	1.000	0.000
2	1.061	1.000	0.000
3	1.064	1.000	0.000
4	1.036	1.000	0.000
5	1.047	1.000	0.000

Figure 5.7 shows that the inverters deliver only their rated real power (1 pu), and do not regulate voltage at the PCC. Because of the modifications made to the feeder, there are ANSI 105% voltage threshold violations at PV Site 2 (1.061 pu) and PV Site 3 (1.064 pu) buses.

With no disturbance applied to the system and inverters enabled to operate in Volt-Var control mode, the model is run again for 1.2 s. Figure 5.8 shows inverters' controllers Volt-Var setpoints used. In Volt-Var control mode, reactive power is given priority over real power. Figure 5.9 and Figure 5.10 show voltages measured at PV buses and power delivered by the PVs respectively. Table 5.5 shows data points extracted from Figure 5.9 and Figure 5.10.

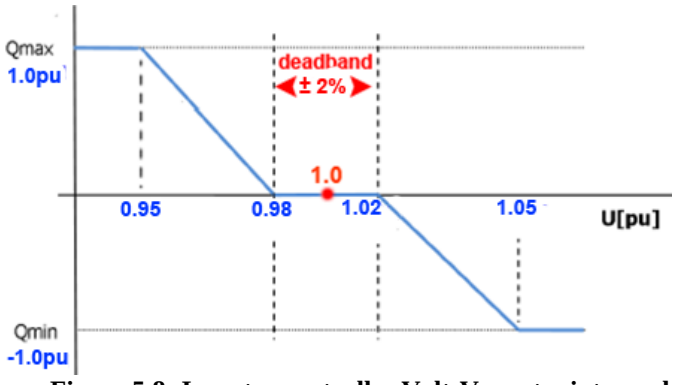

Figure 5.8: Inverter controller Volt-Var setpoints used

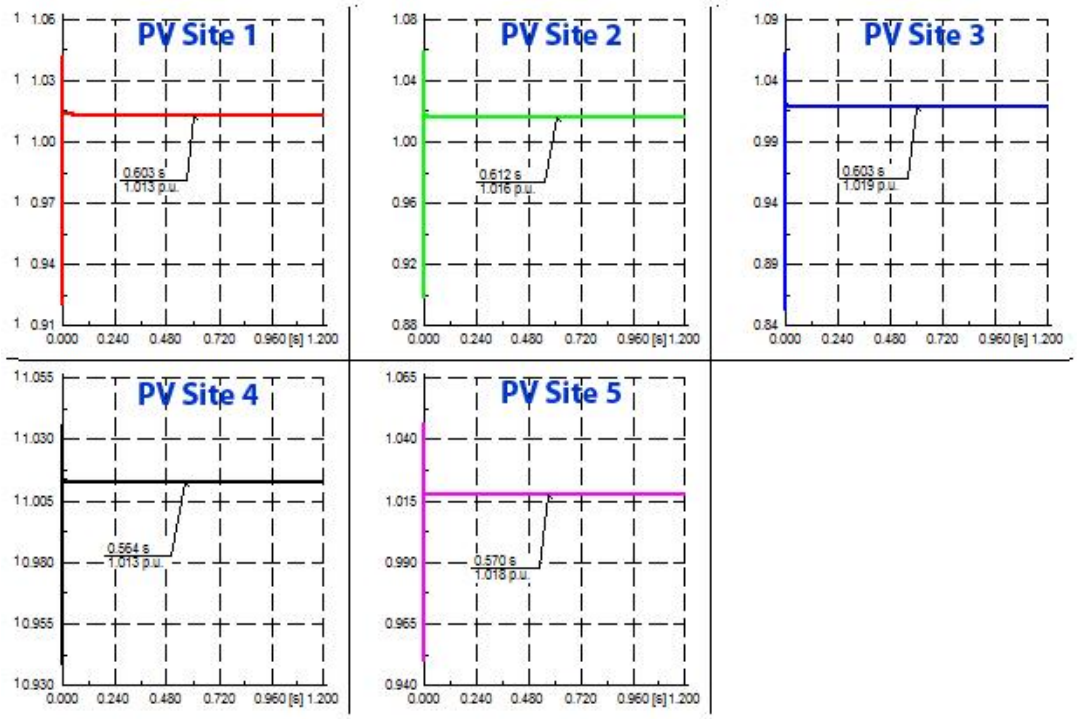

Figure 5.9: Simulation Scenario 1 – Voltages measured at PV buses when inverters operate in Volt-Var control mode

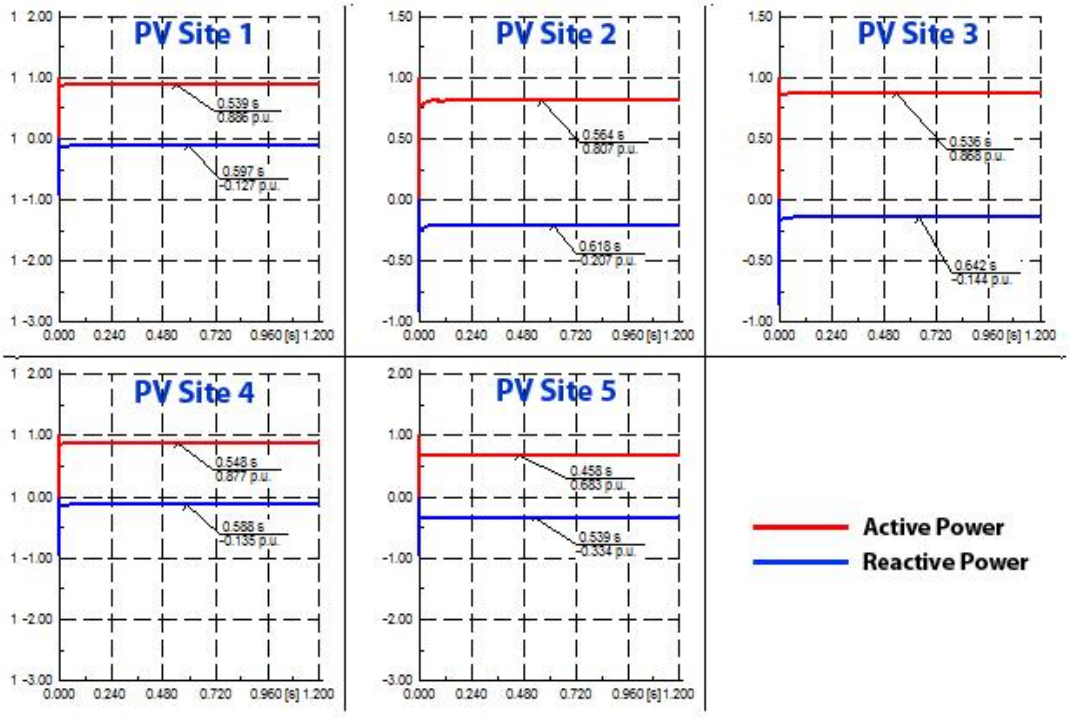

Figure 5.10: Simulation Scenario 1 – Power delivered by PVs when inverters operate in Volt-Var control mode

Table 5.5: Data points extracted from Figure 5.9 and Figure 5.10

PV Site	Voltage [pu]	Real Power [pu]	Reactive Power [pu]
1	1.013	0.886	-0.127
2	1.016	0.807	-0.207
3	1.019	0.868	-0.144
4	1.013	0.877	-0.135
5	1.018	0.683	-0.334

Figure 5.9 shows that voltages measured at PV buses are within the deadband limit (i.e. between 0.98 pu and 1.02 pu). The inverters actively regulate voltages at the PCC by absorbing reactive power (Figure 5.10), and thus keep local voltages at PCC within the deadband limits. In order to compare results of the two simulations, voltage and power measurements are plotted on the same X-Y axis. Figure 5.11 and Figure 5.12 show comparison plots of voltages and power for the two simulations respectively.

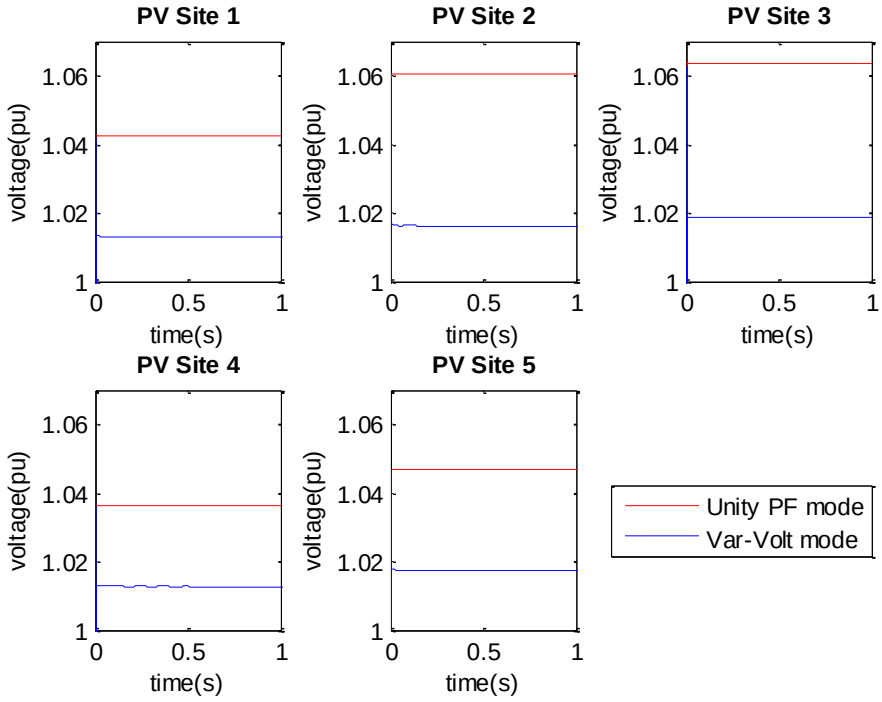

Figure 5.11: Simulation Scenario 1 – Voltage comparison plots when inverters operate in Unity Power Factor and Volt-Var control modes

Figure 5.11 shows when inverters operate in Volt-Var control mode, all bus voltages at the PCC are within the deadband limit. When inverters operate in Unity Power Factor control mode, PV Site 2 and PV Site 3 bus voltages violate the ANSI 105% voltage threshold.

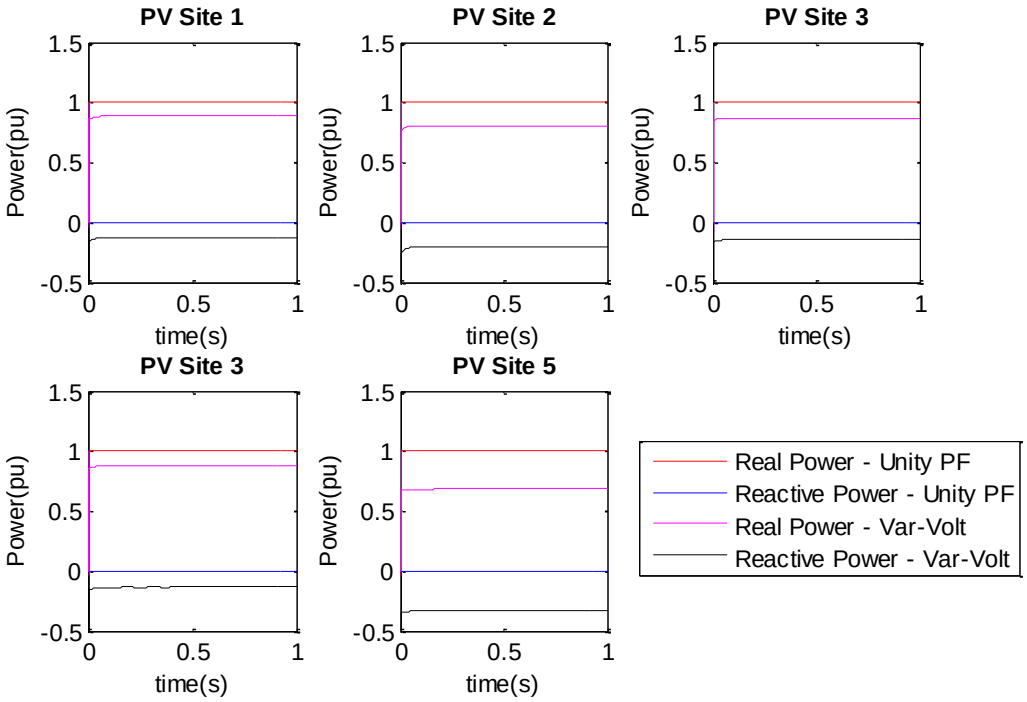

Figure 5.12: Simulation Scenario 1 – Power comparison plots when inverters operate in Unity Power Factor and Volt-Var control modes

Figure 5.12 shows when inverters operate in Unity Power Factor control mode, no reactive power is absorbed from the grid. In Volt-Var control mode, PV inverters absorb reactive power to maintain the bus voltages at the PCC within the deadband limit. From the comparison plots, it can be concluded that when inverters in the feeder are enabled to operate in Volt-Var control mode and there is no disturbance in the system, the inverters help to maintain local bus voltages within their deadband limits.

5.4.2. **Simulation Scenario 2: Fault on the External Grid**

To investigate the interaction of inverters with the system when a sudden fault occurs on the external grid resulting in a 10% voltage drop in the feeder, the model is first run at steady state for 0.5 s, and a sudden three-phase fault is applied on the external grid. The fault is then cleared after 150 ms.

In order to achieve the objective of this simulation scenario, a "Parameter Event" is created in DIgSILENT to lower the external grid voltage from 1 pu to 0.9 pu at 0.5 s. Another "Parameter Event" is created to raise the external grid voltage back to its original value after 150 ms (i.e. at 0.65 s). The simulation is run for 1 s by enabling inverters to operate first in Unity Power Factor control mode and second in Volt-Var control mode with setpoints shown in Figure 5.8. Figure 5.13 and Figure 5.14 show voltages measured at PV buses and power delivered by PVs when inverters are enabled to operate in Unity Power Factor control mode respectively.

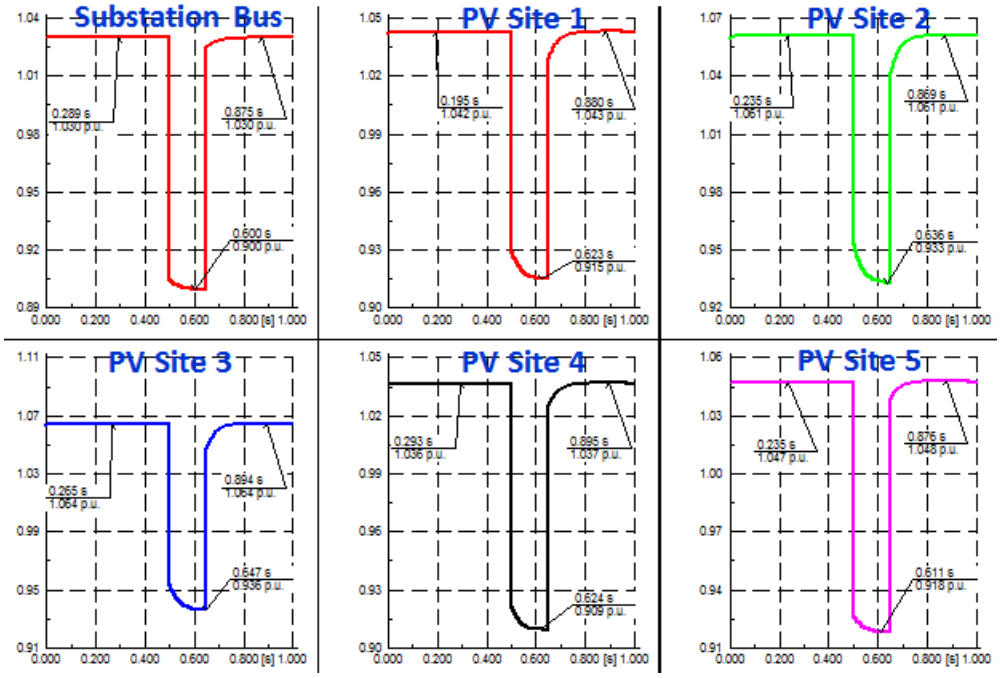

Figure 5.13: Simulation Scenario 2 – Voltages measured at PV buses when inverters operate in Unity Power Factor control mode

Table 5.6: Data points extracted from Figure 5.13

	Peak Voltage Before Fault [pu]	Peak Voltage During Fault [pu]	Peak Voltage After Fault [pu]
Substation Bus	1.030	0.900	1.030
PV Site 1	1.042	0.915	1.043
PV Site 2	1.061	0.933	1.061
PV Site 3	1.064	0.936	1.064
PV Site 4	1.036	0.909	1.037
PV Site 5	1.047	0.918	1.048

As shown in Figure 5.13, when the external grid voltage is suddenly reduced by 10%, the bus voltages at the PCC are reduced by about the same percentage amount. Hence, the active power outputs of the PVs are also reduced by about the same percentage (Figure 5.14). There is no reactive power contribution from the PVs since they are enabled to operate in Unity Power Factor control mode. All buses in the feeder violated the ANSI 95% voltage threshold during the fault period.

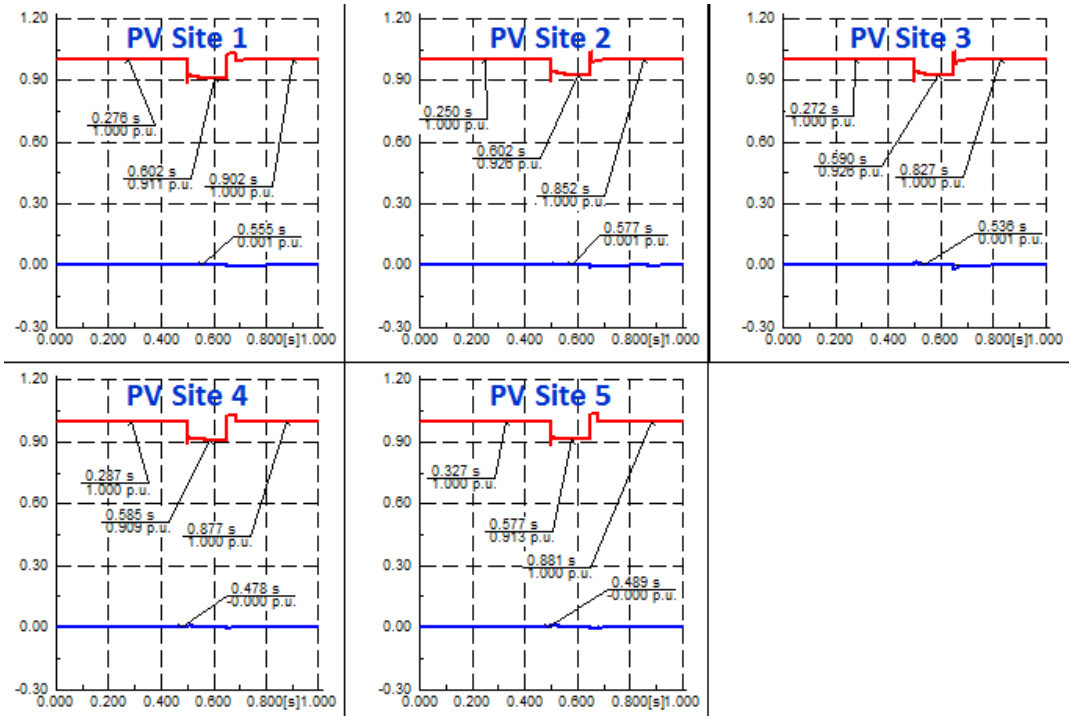

Figure 5.14: Simulation Scenario 2 – Power delivered by PVs when inverters operate in Unity Power Factor control mode

Table 5.7: Data points extracted from Figure 5.14

	Peak Power Before Fault [pu] (Real/Reactive)	Peak Power During Fault [pu] (Real/Reactive)	Peak Power After Fault [pu] (Real/Reactive)
PV Site 1	1.000/0.000	0.911/0.000	1.000/0.000
PV Site 2	1.000/0.000	0.926/0.000	1.000/0.000
PV Site 3	1.000/0.000	0.926/0.000	1.000/0.000
PV Site 4	1.000/0.000	0.909/0.000	1.000/0.000
PV Site 5	1.000/0.000	0.913/0.000	1.000/0.000

Figure 5.15 and Figure 5.16 show voltages measured at PV buses and power delivered by PVs respectively when inverters are enabled to operate in Volt-Var control mode. Figure 5.16 shows that the inverters inject reactive power during the fault period and as a result, voltages at the PCC do not violate the ANSI 95% voltage threshold (Figure 5.15). Data points shown in Figure 5.15 and Figure 5.16 are summarized in Table 5.8 and Table 5.9 respectively.

At the beginning and at end of the fault period, voltage spikes are observed when the inverters operate in Volt-Var control mode. These spikes are the results of voltage measurement delays in the inverters controllers' voltage feedback loops. At the moment the fault occurs, the inverters keep absorbing the same amount of reactive power they were absorbing before the fault. After the voltage measurements time delay, the inverters start to inject reactive power based on the curve shown in Figure 5.8. These time delays before the inverters start to inject reactive power result in voltage spikes on PV buses. Right after the fault is cleared, there are again voltage measurement delays in the controllers of the inverters. The inverters keep injecting the same amount of reactive power they were injecting before the fault is cleared, resulting in voltage spikes.

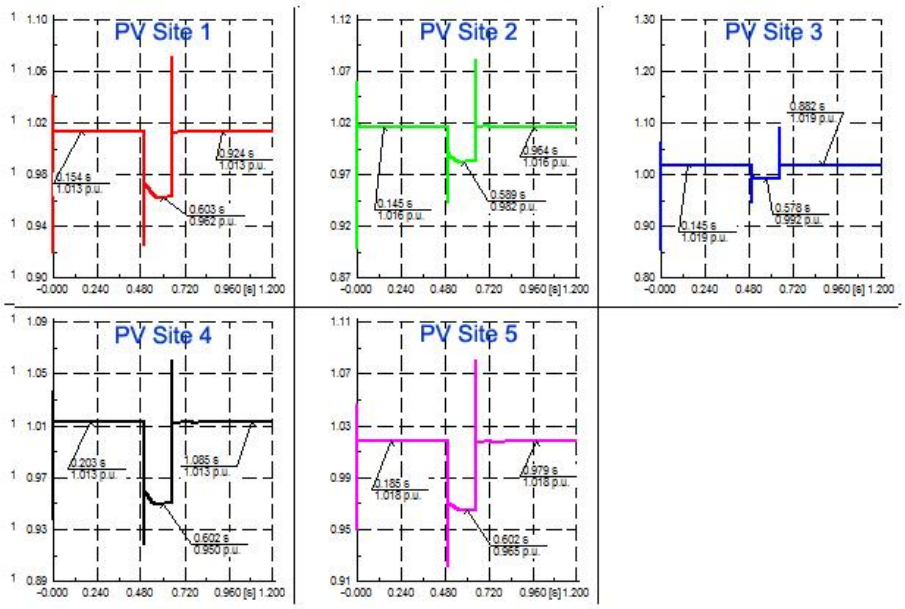

Figure 5.15: Simulation Scenario 2 –Voltages measured at PV buses when inverters operate in Volt-Var control mode

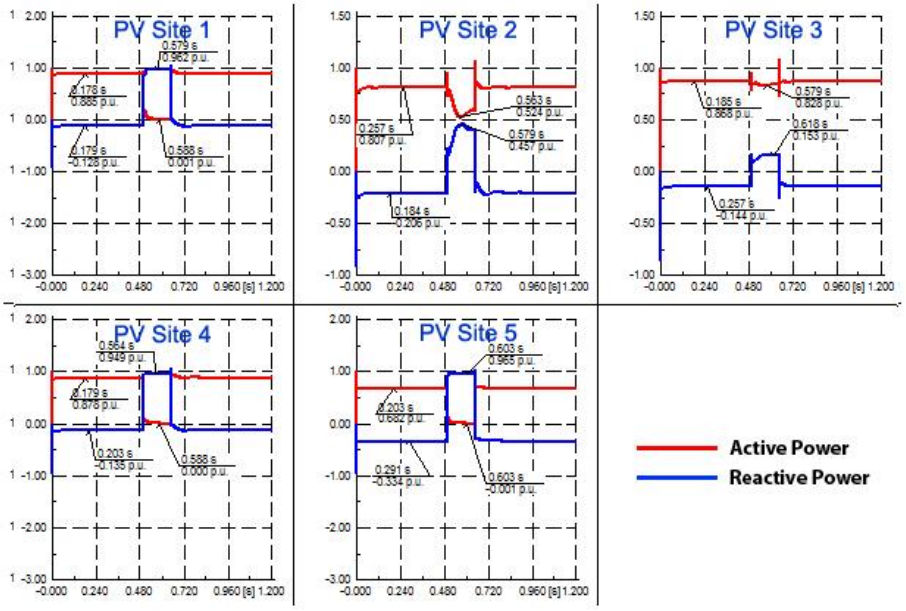

Figure 5.16: Simulation Scenario 2 – Power delivered by PVs when inverters operate in Volt-Var control mode

Table 5.8: Data points extracted from Figure 5.15

	Peak Voltage Before Fault [pu]	Peak Voltage During Fault [pu]	Peak Voltage After Fault [pu]
PV Site 1	1.013	0.962	1.013
PV Site 2	1.016	0.982	1.016
PV Site 3	1.019	0.992	1.019
PV Site 4	1.013	0.962	1.013
PV Site 5	1.018	0.965	1.018

Table 5.9: Data points extracted from Figure 5.16

	Peak Power Before Fault [pu] (Real/Reactive)	Peak Power During Fault [pu] (Real/Reactive)	Peak Power After Fault [pu] (Real/Reactive)
PV Site 1	0.885/-0.128	0.001/0.962	0.885/-0.128
PV Site 2	0.807/-0.206	0.524/0.457	0.807/0.206
PV Site 3	0.868/-0.144	0.828/0.153	0.868/-0.144
PV Site 4	0.878/-0.135	0.000/0.949	0.878/-0.135
PV Site 5	0.682/-0.334	-0.001/0.965	0.682/-0.334

In order to compare results of the two simulations, voltage and power measurements are plotted on the same X-Y axis. Figure 5.17 and Figure 5.18 show voltage and power comparison plots respectively

The comparison plots show that during a temporary fault on the external grid, voltages at PV buses violate the ANSI 95% voltage threshold when operated in Unity Power Factor control mode. When inverters operate in Volt-Var control mode, the PV buses do not violate the 95% threshold since the inverters inject reactive power to the grid (Figure 5.18).

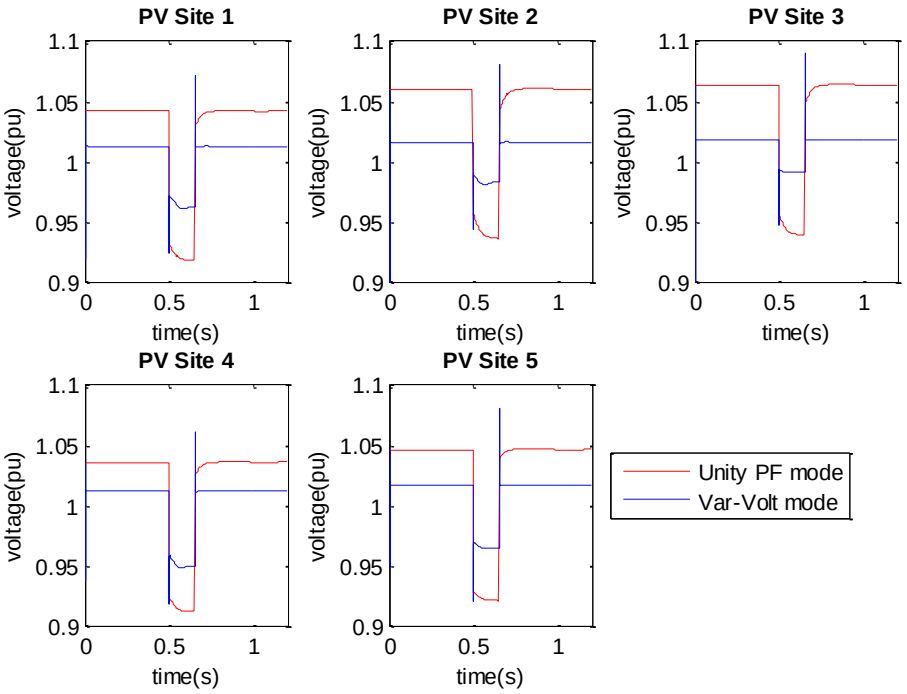

Figure 5.17: Simulation Scenario 2 – Voltage comparison plots when inverters operate in Unity Power Factor and Volt-Var control modes

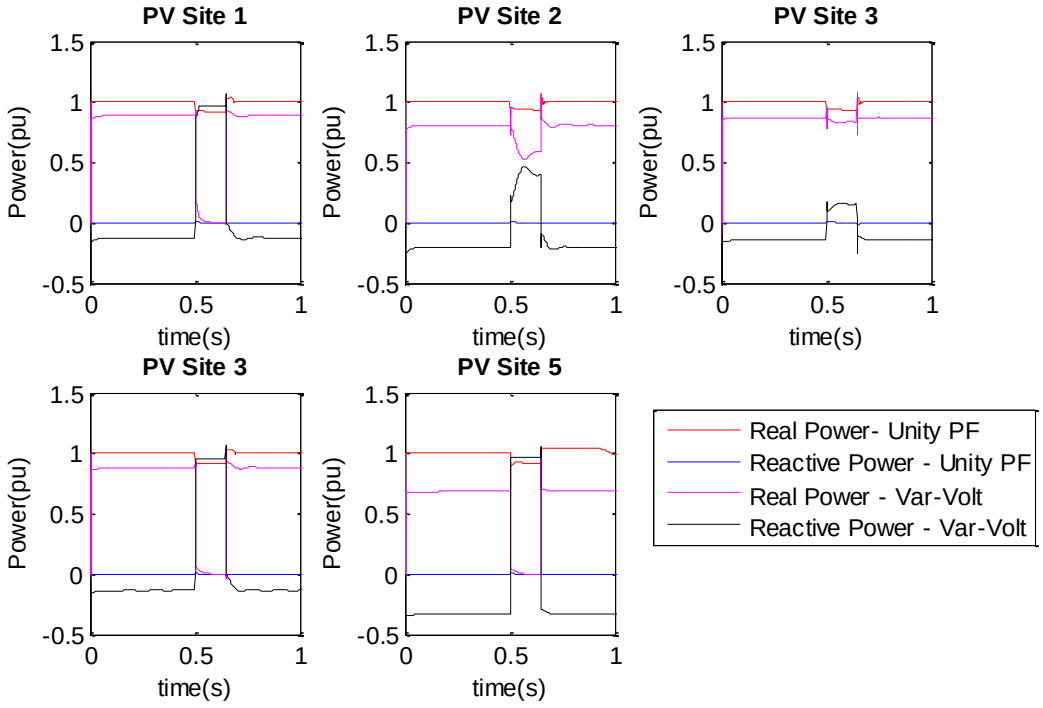

Figure 5.18: Simulation Scenario 2 – Power comparison plots when inverters operate in Unity Power Factor and Volt-Var control modes

From the comparison plots, it can be concluded that when inverters in the feeder operate in Volt-Var control mode, they help in the voltage stability of the feeder when temporary faults occur on the external grid.

5.4.3. **Simulation Scenario 3: Fluctuating Cloud**

In order to study the effect of a fluctuating cloud covering different PV sites at different rates and responses of the inverters in the feeder, a solar irradiation that fluctuates at 0.5 Hz between maximum irradiance of 1000 $\frac{\omega}{m^2}$ and irradiance of 500 $\frac{\omega}{m^2}$ is applied to the PV sites. The fluctuating solar irradiance applied at PV_5 (large PV site) is out of phase with the other sites, and solar irradiations at the other sites are time shifted by 0.2 s from each other. Figure 5.19 shows the solar irradiation applied at the five PV sites.

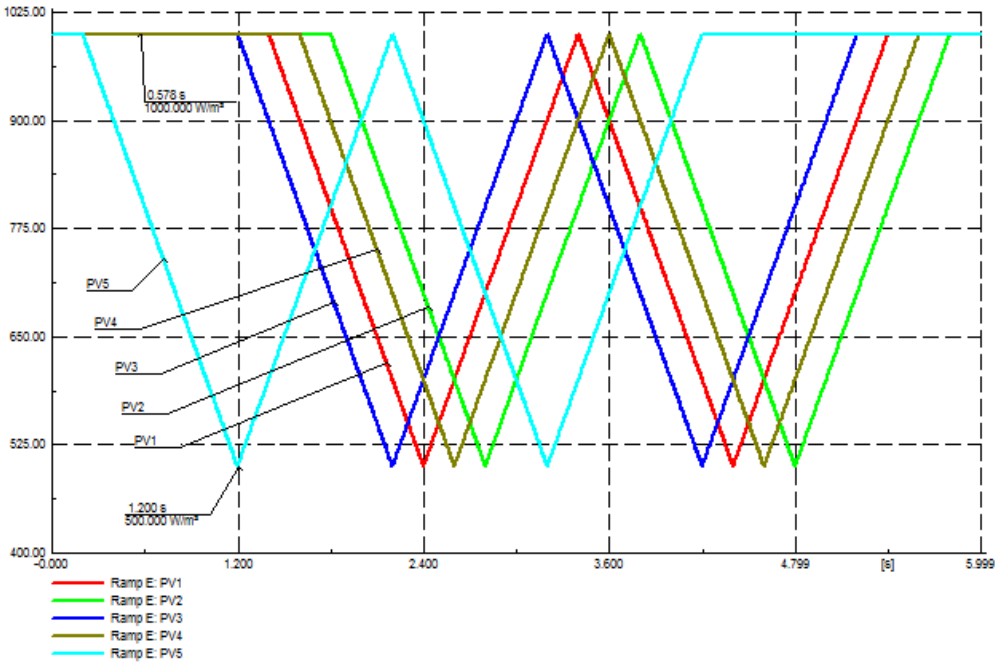

Figure 5.19: Fluctuating solar irradiation applied at the different PV sites

5.4.3.1. Case A – All Inverters in the Feeder Operate in Unity Power Factor Control Mode

The simulation is run for 6 s by enabling the inverters in the feeder to operate in Unity Power Factor control mode. Figure 5.20 and Figure 5.21 show voltages measured at PV buses and power delivered by PVs respectively.

Figure 5.20 shows that PV bus voltages fluctuate with the changing solar irradiation. Solar irradiation at PV_3 is exactly out of phase with that of PV_5 (Figure 5.21), and PV_3 is located in close proximity to PV_5. Hence, the PV bus voltage at PV_3 does not change significantly as compared to the other PV site buses with fluctuating solar irradiation. Data points in Figure 5.20 and Figure 5.21 are summarized in Table 5.10 and Table 5.11 respectively.

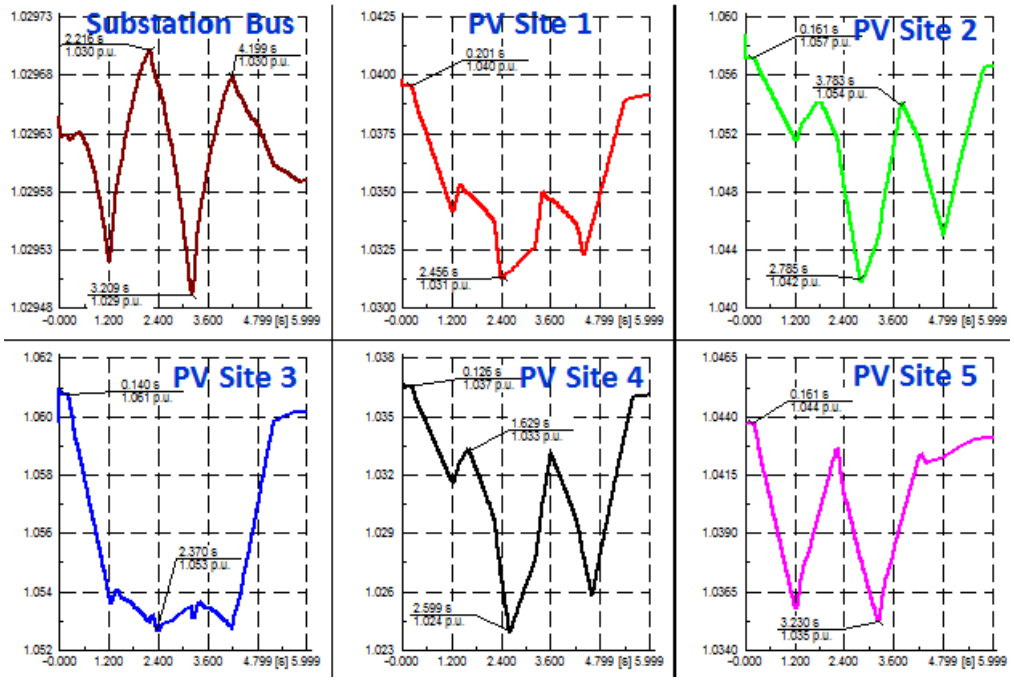

Figure 5.20: Simulation Scenario 3 (Case A) – Voltages measured at PV buses

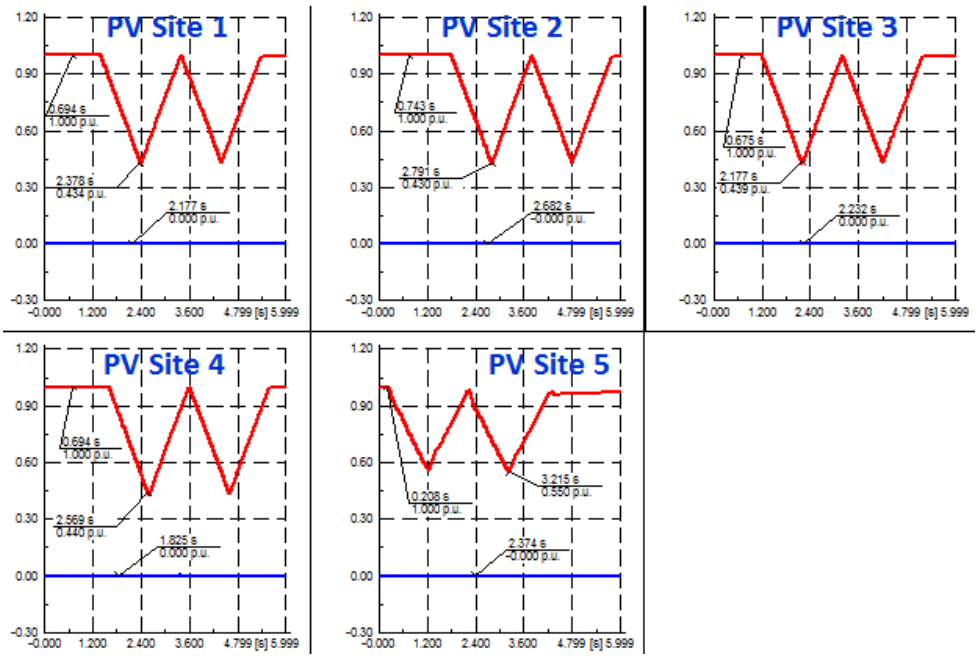

Figure 5.21: Simulation Scenario 3 (Case A) – Power delivered by PVs

Table 5.10: Data points extracted from Figure 5.20

	Peak Voltage [pu]	Lowest Voltage [pu]
Substation Bus	1.030	1.029
PV Site 1	1.040	1.031
PV Site 2	1.057	1.042
PV Site 3	1.061	1.053
PV Site 4	1.037	1.024
PV Site 5	1.044	1.035

Table 5.11: Data points extracted from Figure 5.21

	Peak Power [pu] (Real/Reactive)	Lowest Power [pu] (Real/Reactive)
PV Site 1	1.000/0.000	0.434/0.000
PV Site 2	1.000/0.000	0.430/0.000
PV Site 3	1.000/0.000	0.439/0.000
PV Site 4	1.000/0.000	0.440/0.000
PV Site 5	1.000/0.000	0.550/0.000

5.4.3.2. Case B – All Inverters in the Feeder Operate in Volt-Var Control Mode

While inverters are enabled to operate in Volt-Var control mode with setpoints shown in Figure 5.8, a 0.5 Hz fluctuating and out of phase solar irradiation is applied to the PV sites (Figure 5.19). Figure 5.22 and Figure 5.23 show voltages measured at PV buses and power delivered by the PVs respectively.

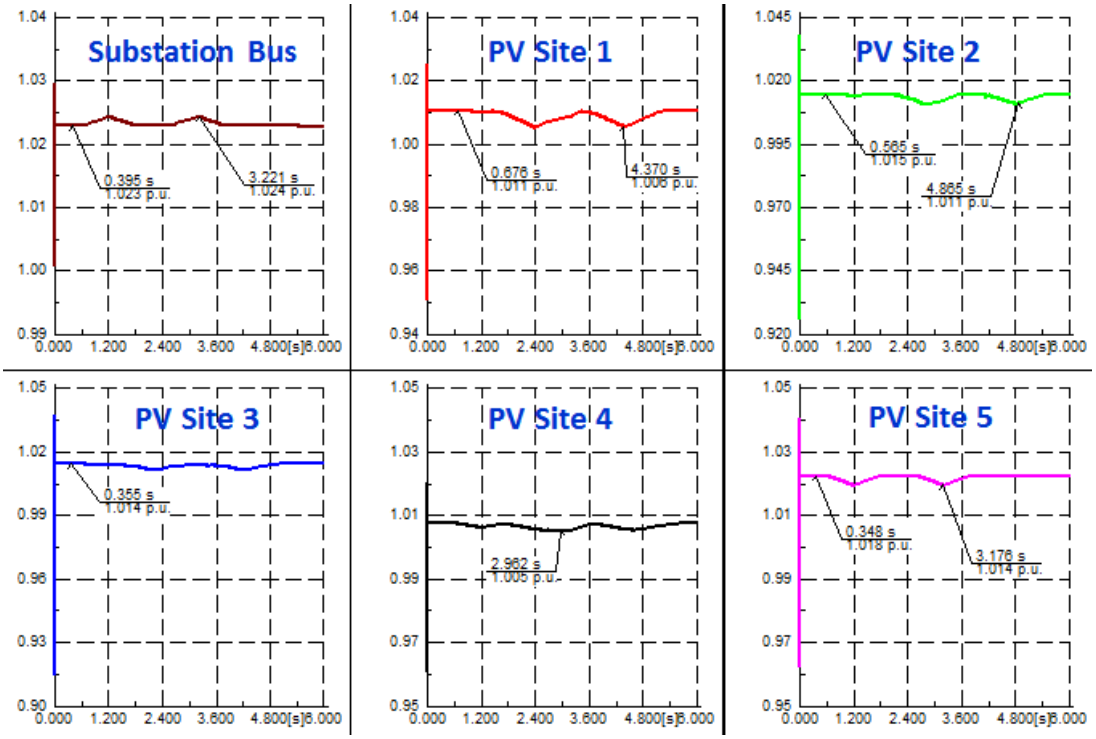

Figure 5.22: Simulation Scenario 3 (Case B) – Voltages measured at PV buses

Figure 5.22 shows that Volt-Var controlled inverters help to mitigate the effects of fluctuating and out-of-phase solar irradiation. They maintain voltages at PV buses within the deadband limit. In order to compare results of the two simulations, voltage and power measurements are plotted on the same X-Y axis. Figure 5.24 shows voltage comparison plots for Cases A and B, while Figure 5.25 shows power comparison plots for Cases A and B.

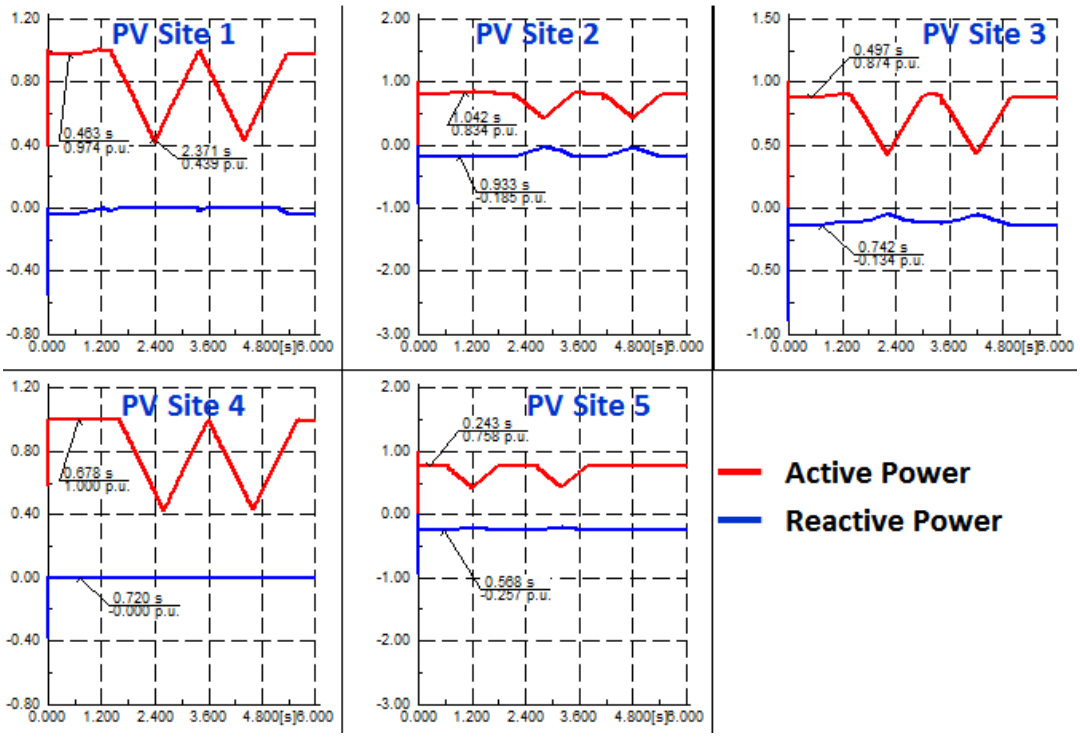

Figure 5.23: Simulation Scenario 3 (Case B) – Power delivered by PVs

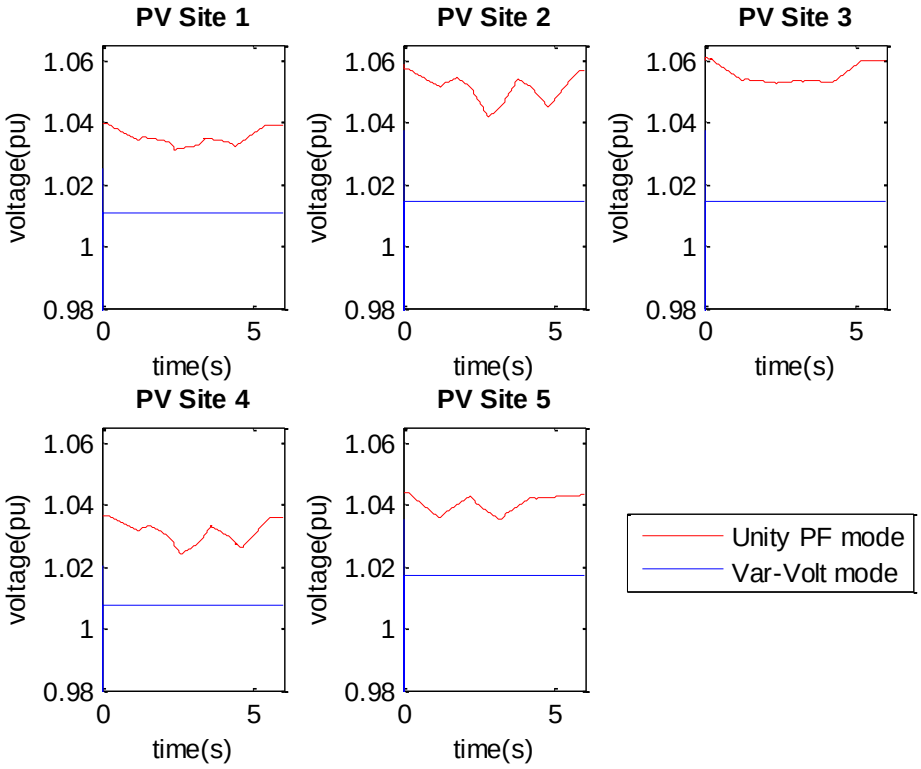

Figure 5.24: Simulation Scenario 3 – Cases A and B voltage comparison plots

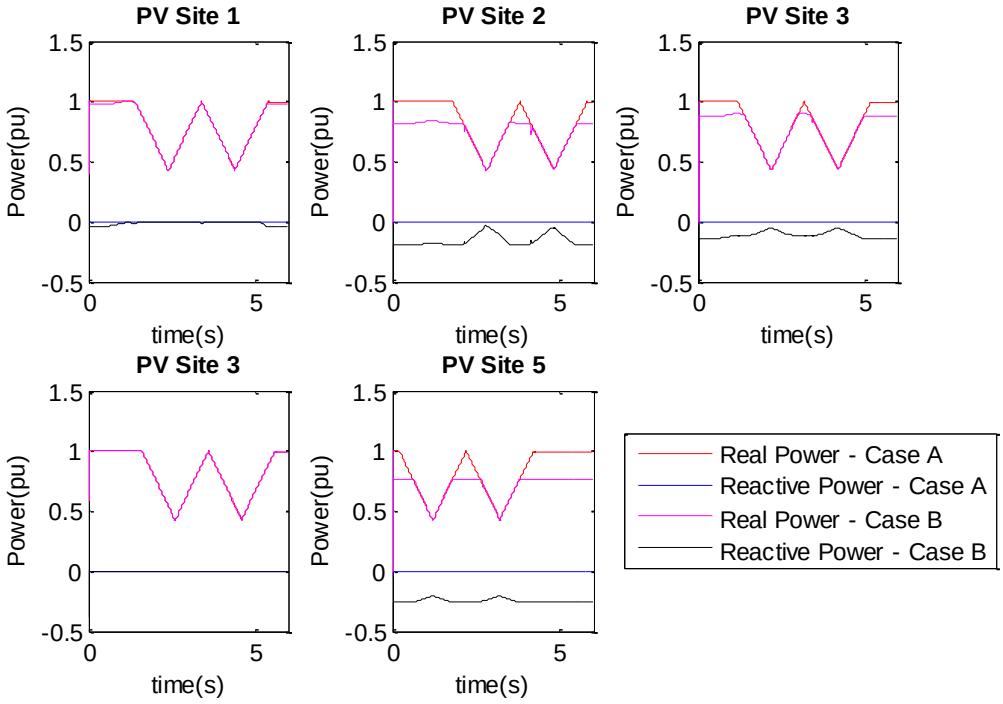

Figure 5.25: Simulation Scenario 3 – Cases A and B power comparison plots

Figure 5.24 and Figure 5.25 show that when inverters in the feeder operate in Volt-Var control mode, they participate in local voltage control, and help to mitigate the effects of fluctuating solar irradiation.

5.4.3.3. Case C – Inverter at PV Site 5 Operate in Unity Power Factor Control Mode and Other Inverters Operate in Volt-Var Control Mode

In this simulation, inverter at PV_5 is enabled to operate in Unity Power Factor control mode while the other PV inverters in the feeder are enabled to operate in Volt-Var control mode with setpoints as shown in Figure 5.8. Solar irradiation similar to simulation scenario 3 is applied at the five PV sites. Figure 5.26 and Figure 5.27 show voltages measured at PV buses and power delivered by the PVs respectively.

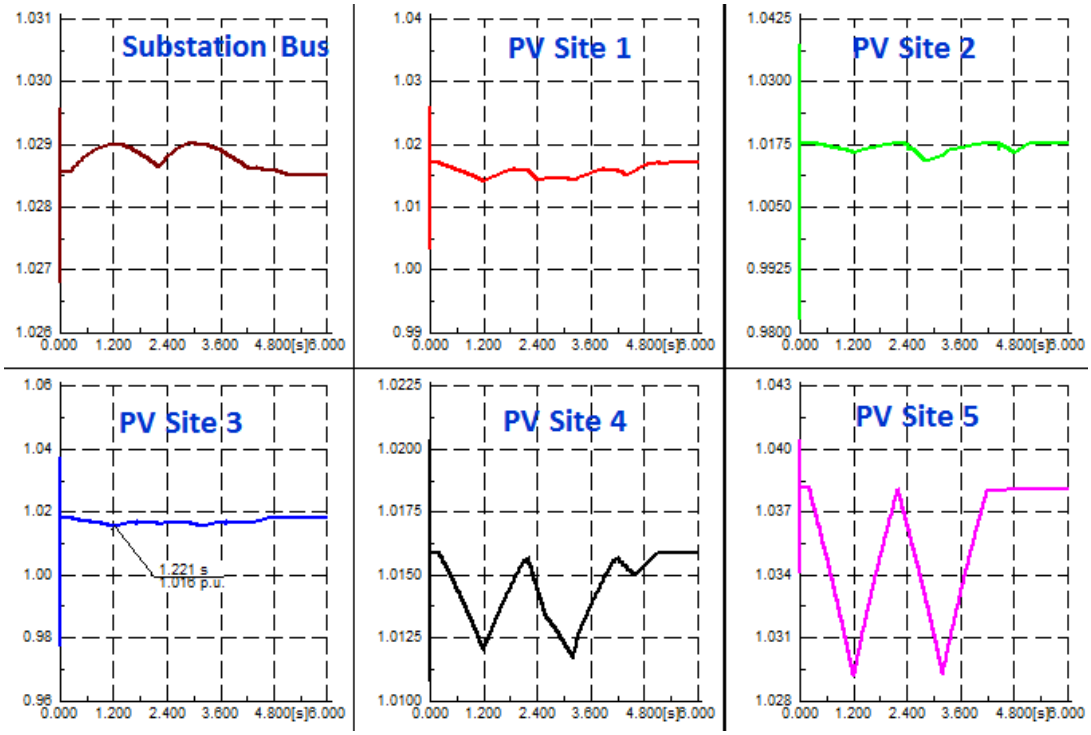

Figure 5.26: Simulation Scenario 3 (Case C) – Voltages measured at PV buses

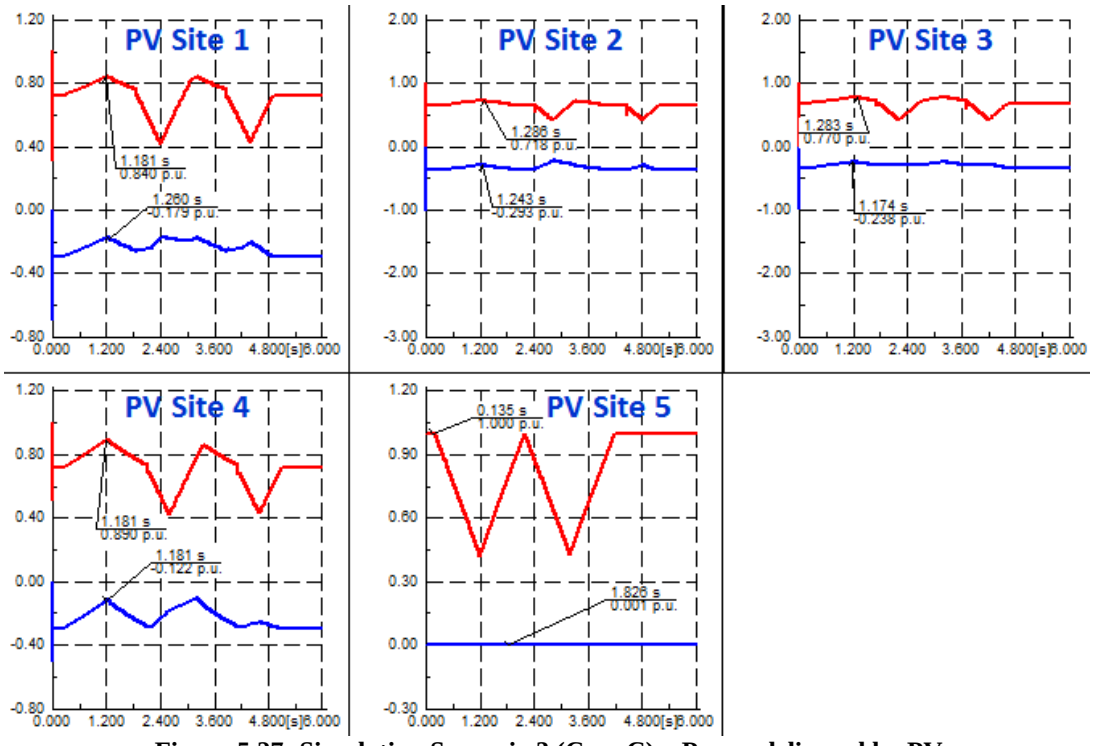

Figure 5.27: Simulation Scenario 3 (Case C) – Power delivered by PVs

Figure 5.26 shows that inverters controlled in Volt-Var mode maintain PV bus voltages within the deadband limit, while bus voltage at PV_5 changes with the fluctuating solar irradiation (PV_5 inverter is controlled in Unity Power Factor mode). Figure 5.27 shows that inverters with Volt-Var control mode inject reactive power when solar irradiation fluctuates, maintaining local bus voltages within the deadband limit. The inverter of PV_5 injects real power in phase with the fluctuating solar irradiation. It does not inject reactive power.

Figure 5.28 and Figure 5.29 show voltage and power comparison plots of Cases A, B, and C simulation scenarios.

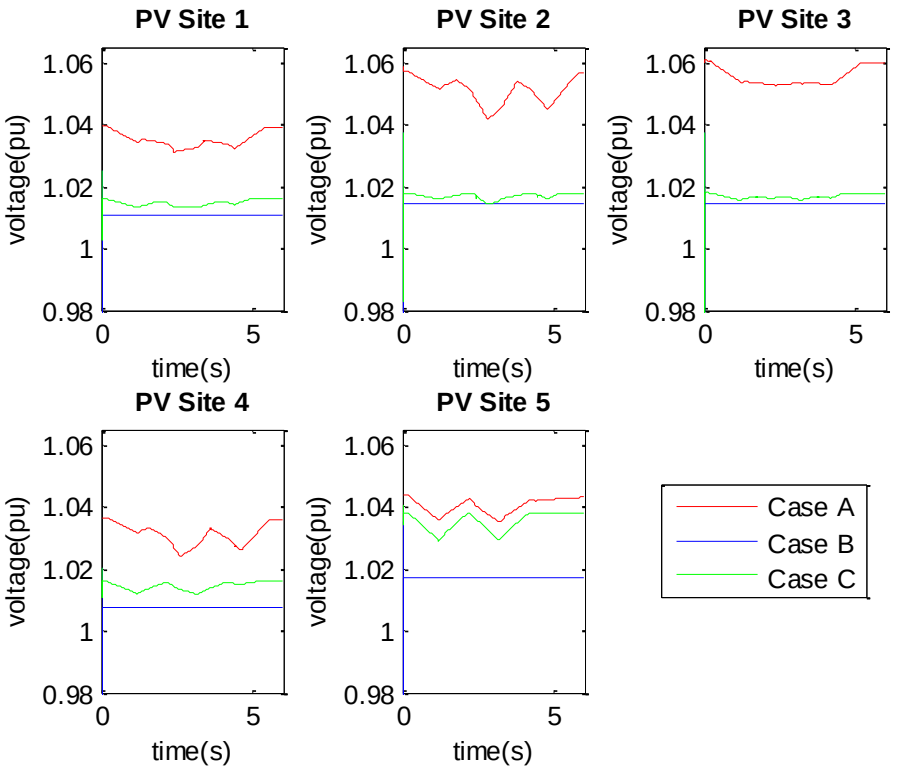

Figure 5.28: Simulation Scenario 3 – Cases A, B, and C voltage comparison plots

From the voltage comparison plots, the best-case scenario is when all inverters operate in Volt-Var control mode (Case B).

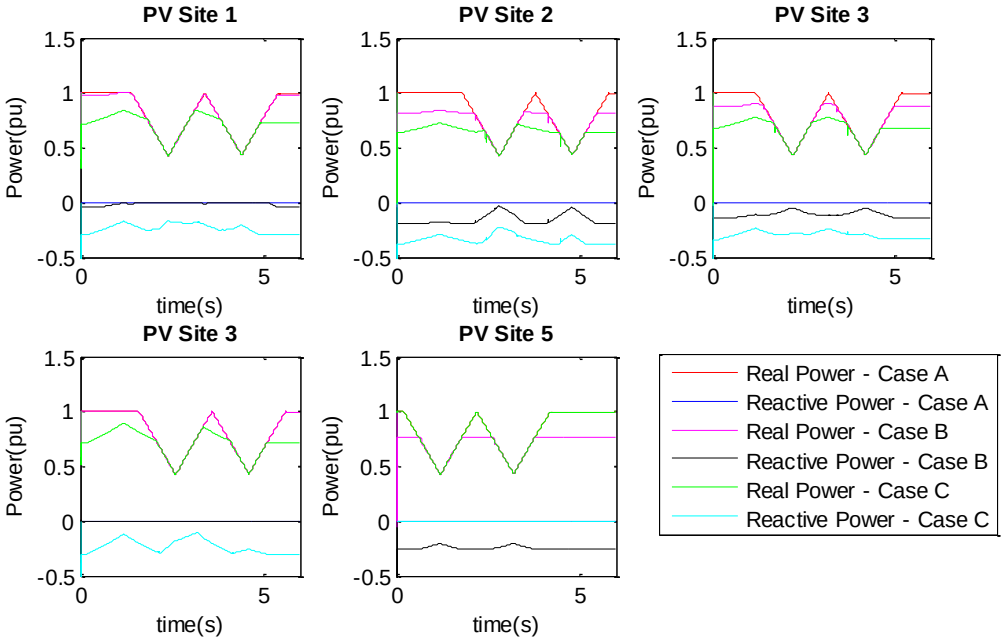

Figure 5.29: Simulation Scenario 3 – Cases A, B, and C power comparison plot

When a fluctuating cloud occurs in the feeder, maximum real power is injected when inverters operate in Unity Power Factor control mode (Case A) and maximum reactive power is injected when inverters operate in Volt-Var control mode (Case B) as shown in Figure 5.29. When an inverter at the larger PV site (PV_5) operates in Unity Power Factor control mode and all other smaller PV inverters in the feeder operate in Volt-Var control mode, PV bus voltages are maintained within the deadband at PV buses with inverters controlled in Volt-Var mode. The smaller inverters reactive power contribution during fluctuating cloud cover is not sufficient to regulate voltage at the larger PV site (Case C).

5.4.3.4. Case D – Inverter at PV Site 5 Operate in Volt-Var Control Mode and Other Inverters Operate in Unity Power Factor Control Mod

In this simulation, the inverter at PV_5 is enabled to operate in Volt-Var control mode with setpoints as shown in Figure 5.8, while the other PV inverters in the feeder are enabled to operate in Unity Power Factor control mode. Solar irradiation similar to what

is shown in Figure 5.19 is applied at the five PV sites. Figure 5.31 and Figure 5.31 show voltages measured at PV buses and power delivered by the PVs respectively.

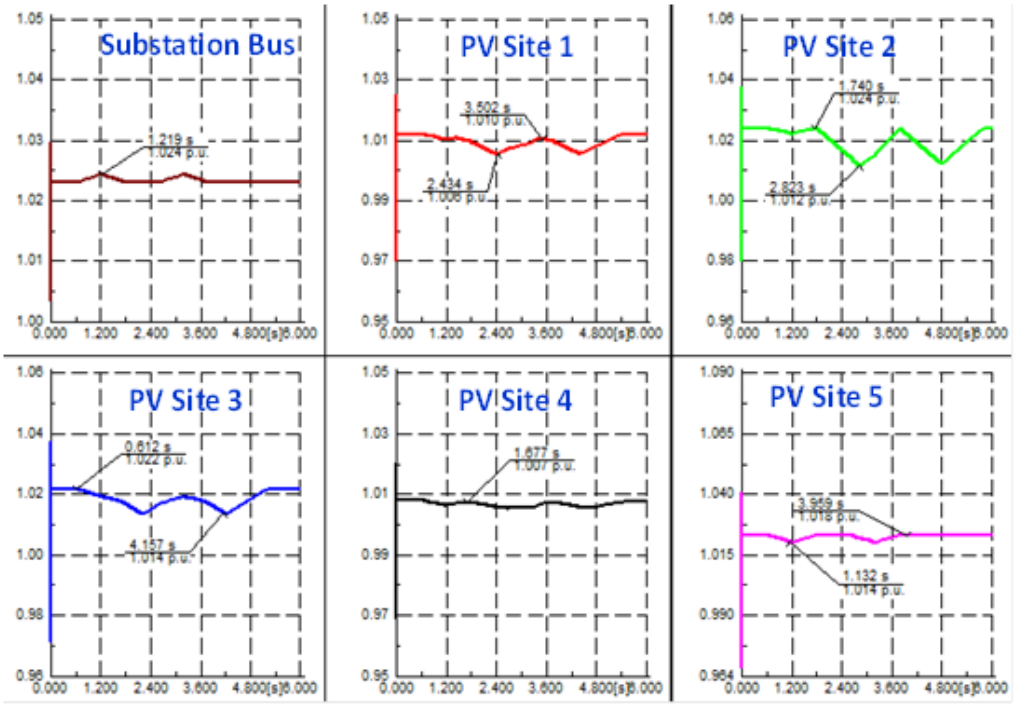

Figure 5.30: Simulation Scenario 3 (Case D) - Voltages measured at PV buses

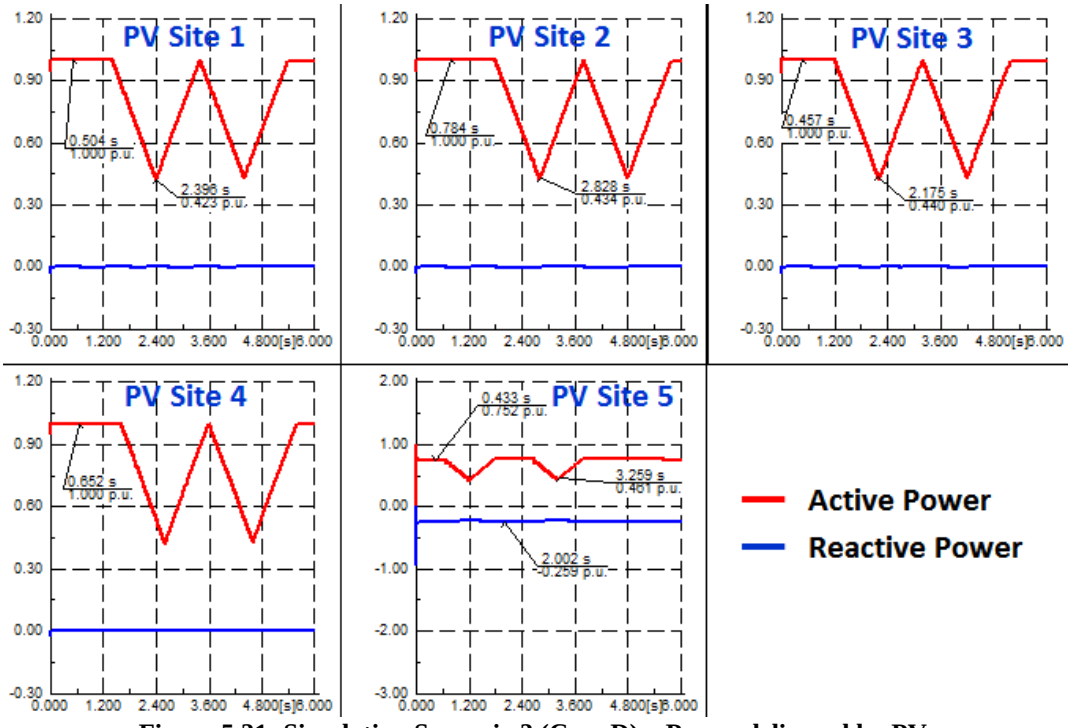

Figure 5.31: Simulation Scenario 3 (Case D) – Power delivered by PVs

Figure 5.31 shows that the bus voltage at PV_5 is within the deadband limit while bus voltages at the other PV sites are above the limit of the deadband (i.e. above 1.02 pu) and changing with the fluctuating solar irradiation. Only the inverter of PV_5 injects reactive power when solar irradiation fluctuates (Figure 5.31).

Figure 5.32 and Figure 5.33 show voltage and power comparison plots of Cases A, B, C, and D simulation scenarios respectively.

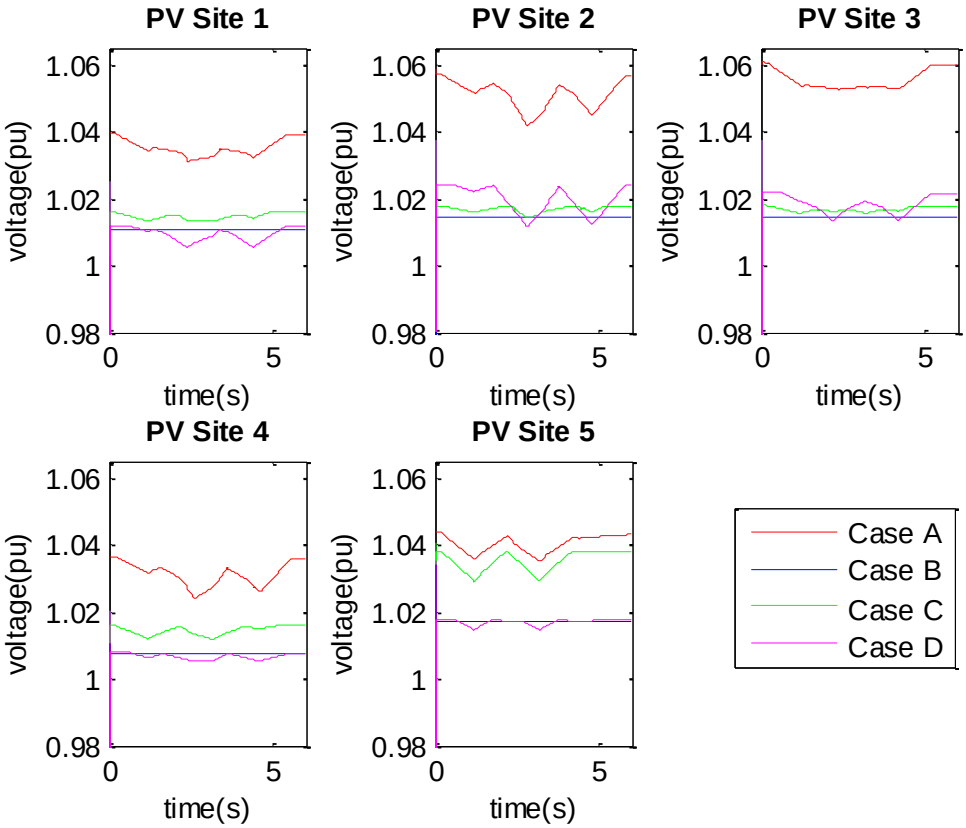

Figure 5.32: Simulation Scenario 3 – Cases A, B, C, and D voltage comparison plots

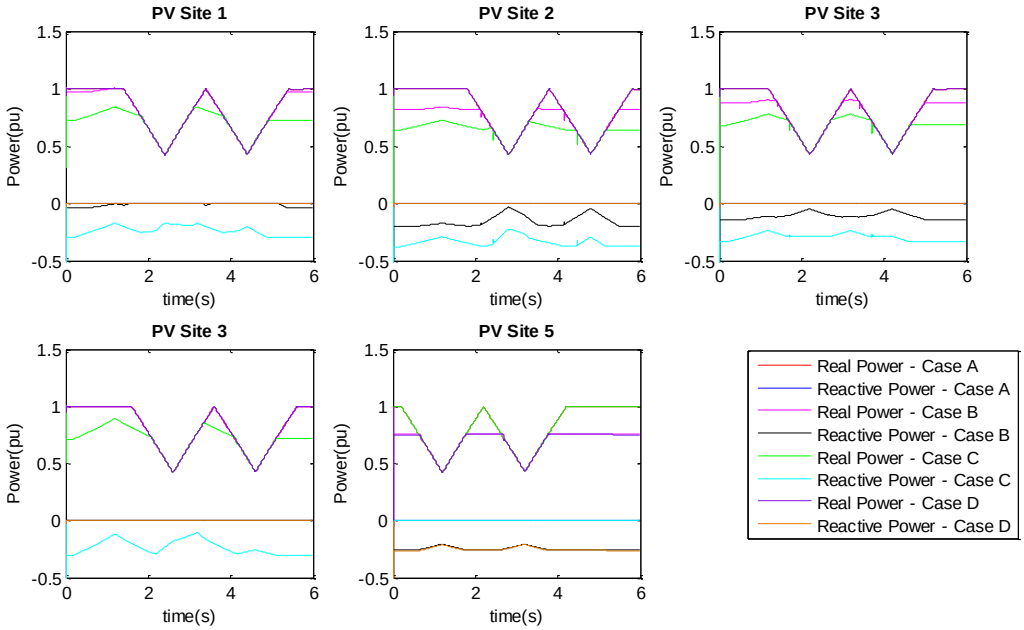

Figure 5.33: Simulation Scenario 3 – Cases A, B, C, and D power comparison plots

From the above comparison figures, it can be seen that the best-case scenario exists when all the inverters in the feeder operate in Volt-Var control mode (i.e. Case B), and the worst-case scenario exists when all inverters operate in Unity Power Factor control mode (i.e. Case A). It is observed from Cases C and D, that the larger PV site (PV_5) does not have a significant impact on bus voltages of the other PV sites. Reactive power injected by PV_5 helps to raise PV bus voltages at other buses when solar irradiation fluctuates, but this reactive power is insufficient to keep the bus voltages in the feeder within the deadband limit. From the comparison plots of Cases A, B, C, and D, it can be concluded that PV inverters operating in Volt-Var mode maintain the voltage on their buses within the deadband irrespective of the mode of operation of PV_5.

5.4.4. **Simulation Scenario 4: Effect of Losing a Large PV Site**

To simulate the transient response of the feeder when a large PV site is suddenly disconnected, a "Switching Event" is created in DIgSILENT to disconnect PV_5 at 0.5 s. The simulation is run for 1s by enabling the inverters in the feeder to first operate in

Unity Power Factor control mode and second in Volt-Var control mode with setpoints shown in Figure 5.8. Figure 5.34 and Figure 5.35 show voltages measured at PV buses and power delivered by the PVs respectively.

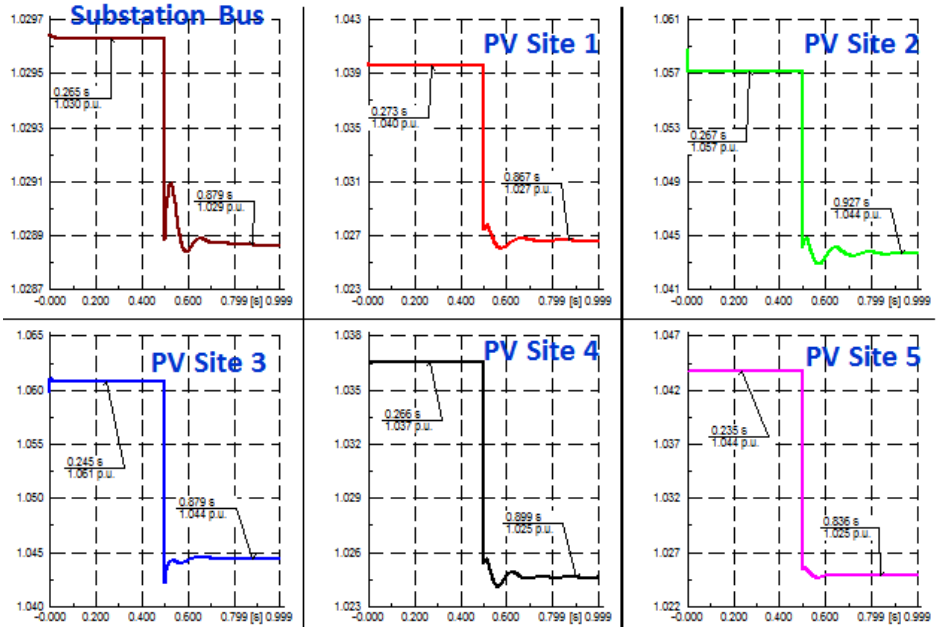

Figure 5.34: Simulation Scenario 4 – Voltages measured at PV buses when inverters operate in Unity Power Factor control mode

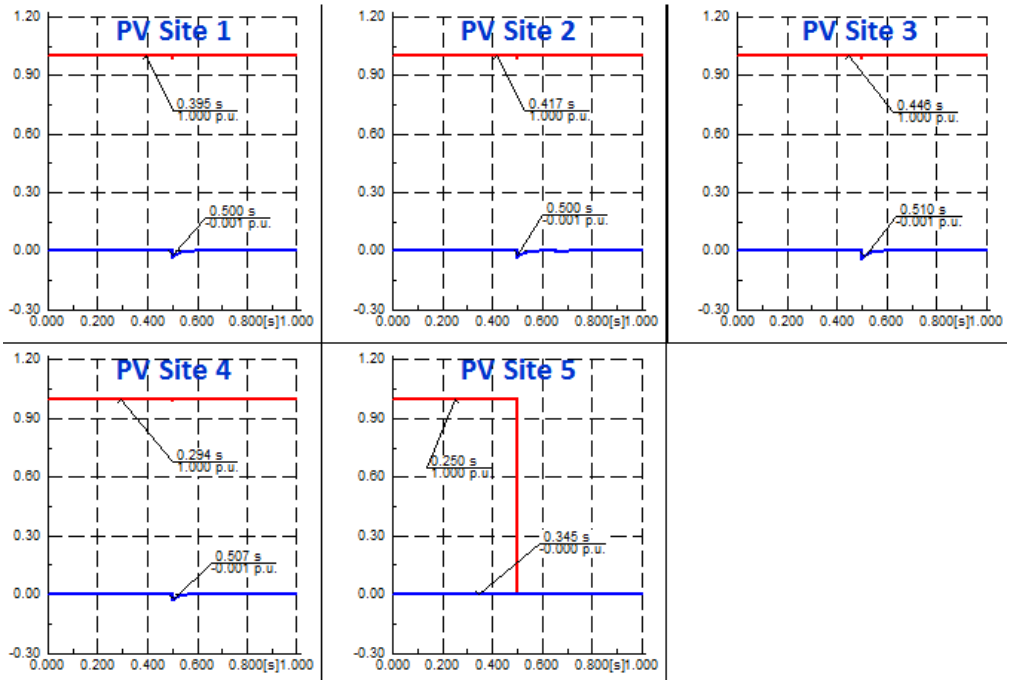

Figure 5.35: Simulation Scenario 4 – Power delivered by PVs when inverters operate in Unity Power Factor control mode

Figure 5.34 shows that losing PV_5 (large PV site) while other inverters in the feeder are enabled to operate in Unity Power Factor control mode, results in a 1.6% average voltage drop. There is no reactive power injected by the PVs (Figure 5.35).

The simulation is repeated by enabling the inverters to operate in Volt-Var mode. Figure 5.36 and Figure 5.37 show voltages measured at PV buses and power delivered by the PVs respectively.

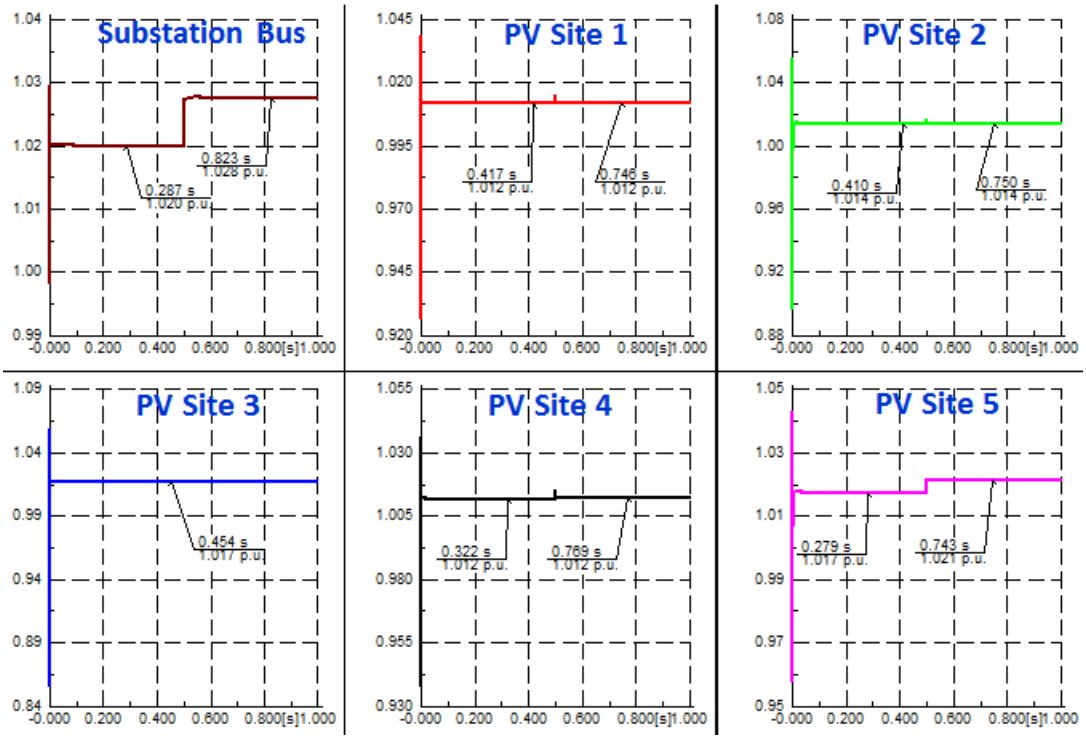

Figure 5.36: Simulation Scenario 4 –Voltages measured at PV buses when inverters operate in Volt-Var control mode

As seen in Figure 5.36, when all inverters operate in Volt-Var control mode and when PV_5 is suddenly disconnected from the feeder, the voltage drop on bus voltages at PCC is negligible. However, it is observed that the substation bus (i.e. the bus on the low side of the substation transformer) has a voltage increase of 0.78%. Figure 5.38 and Figure 5.39 show voltage and power comparison plots respectively

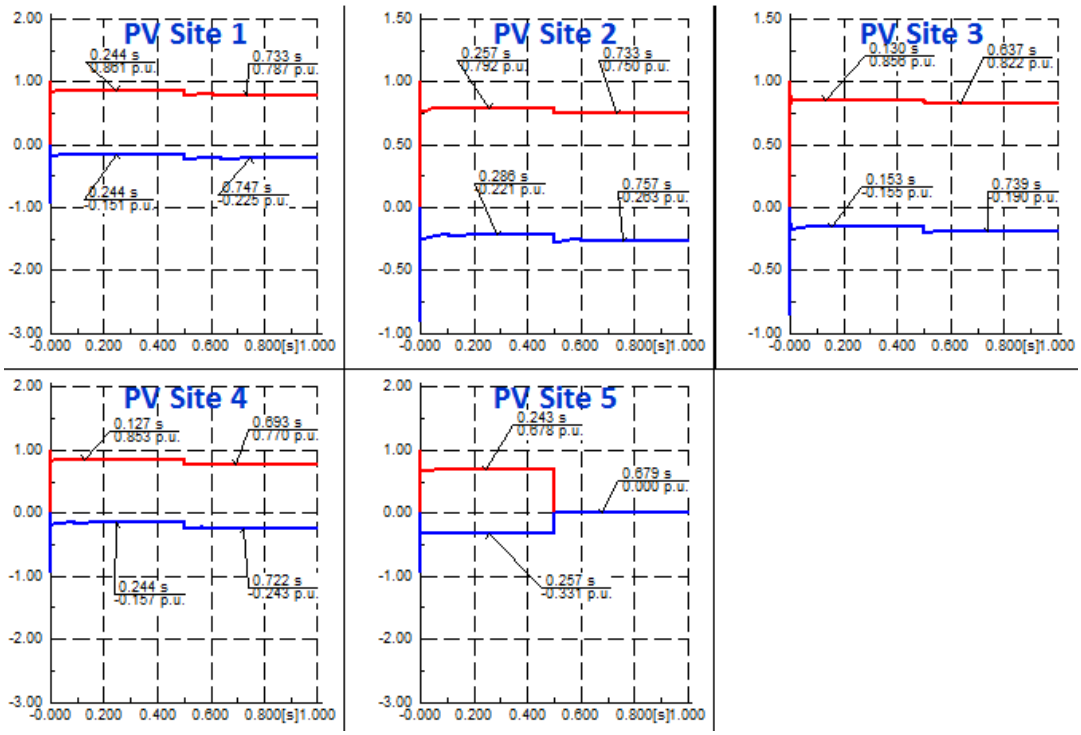

Figure 5.37: Simulation Scenario 4 – Power delivered by PVs when inverters operate in Volt-Var control mode

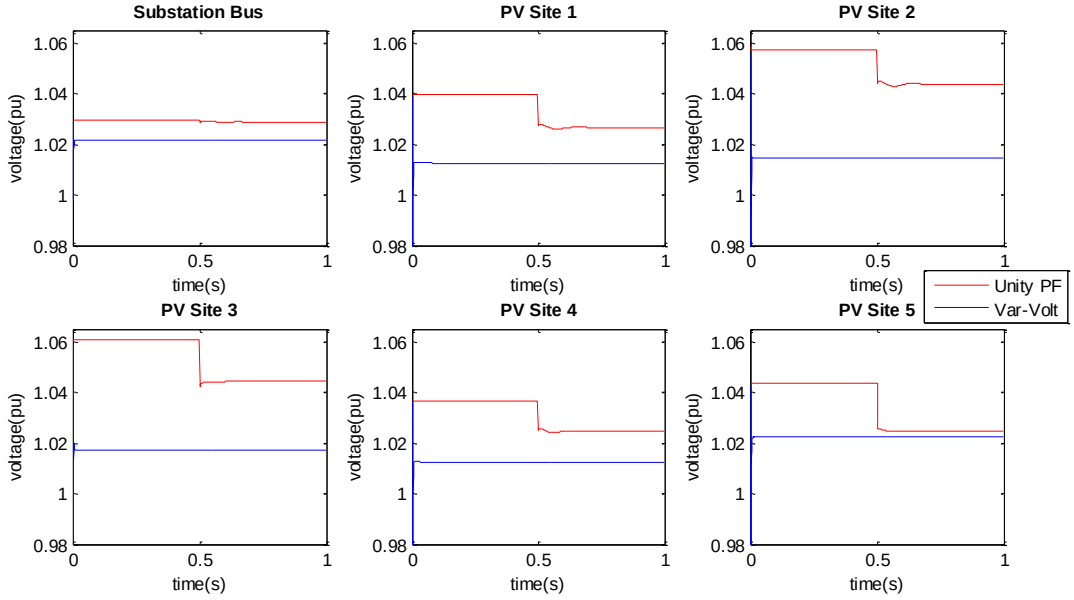

Figure 5.38: Simulation Scenario 4 – Voltage comparison plot

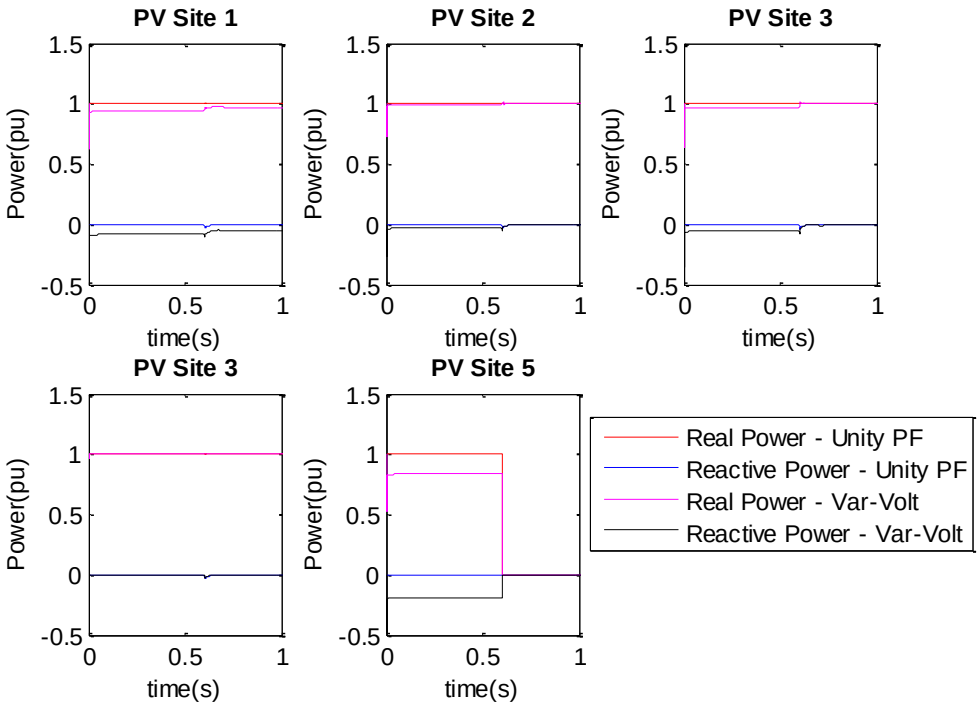

Figure 5.39: Simulation Scenario 4 – Power comparison plot

Figure 5.38 and Figure 5.39 show that losing a large PV site results in negligible voltage drop when the inverters operate in Volt-Var control mode. When the inverters operate in Unity Power Factor control mode, the average voltage drop at PV buses is 1.6%.

5.5. Summary

In this chapter, NEETRAC member Feeder B's transient performance is investigated under different scenarios. To study the inverters interaction with the system, 30% of commercial loads are replaced with equivalent induction motors. At steady state, the maximum voltage difference on a bus before and after replacing 30% commercial load with an induction motor is 0.009 pu or 0.9%. Impedances of selected five lines that are located between the PV sites are increased by 20 times. This resulted in an ANSI 105% threshold voltage violation only on PV Site 2 and PV Site 3 buses when all PVs operate in Unity Power Factor mode.

By applying no disturbance to the system, the steady state behavior of the feeder is studied when the PV inverters operate in Unity Power Factor and Volt-Var control modes. When the inverters operate in Volt-Var control mode with ±2% deadband, bus voltages at the point of common coupling (PCC) are within 0.98 pu to 1.02 pu. There is no threshold voltage violation of 105% observed unlike the case when the inverters operate in Unity Power Factor control mode (Figure 5.11 and Figure 5.12).

By applying a three-phase fault to the external grid that results in a 10% voltage decrease in the feeder, the transient behaviors of the feeder are studied. When the inverters operate in Volt-Var control mode, the bus voltages at the PCC are above 0.95 pu and inject reactive power during the fault period. When the inverters operate in Unity Power Factor control mode, the bus voltages at the PCC are below 0.95 pu and the inverters' real power output decreased by almost 10% (Figure 5.17 and Figure 5.18). When the fault is cleared, under both inverter modes of operation, there are no transient violations that propagate to make the whole system unstable. The system goes back to its previous steady state condition. It is observed that there is no interaction between the inverters when they operate in Volt-Var control mode that adversely affect the stability of the system. This could be due to the capacity and location of PVs in the feeder.

By applying a fluctuating cloud (solar irradiation) at the PV sites, the transient behavior of the feeder is studied. The applied fluctuating cloud has a frequency of 0.5 Hz and reaches the different PV sites at different times (i.e. out-of-phase). It is observed that when all inverters work in Volt-Var control mode, the bus voltages at the PCC remain within 0.98 pu to 1.02 pu. The worst-case scenario is observed when all inverters work in Unity Power Factor control mode (Figure 5.32 and Figure 5.33).

The effect of losing a large PV site on the transient behavior of the feeder is studied by disconnecting PV Site 5. When the inverters work in Unity Power Factor control mode, losing PV Site 5 results in a 1.6% average voltage decrease at the other PV

sites. This is not observed when the inverters operate in Volt-Var mode (Figure 5.38 and Figure 5.39).

CHAPTER 6: MODELING AND SIMULATION OF A SMART INVERTER IN MATLAB/SIMULINK

6.1. Introduction

In the Matlab/Simulink software library, no DC-AC smart inverter model exists to date. In this chapter, a grid-tied smart inverter with smart functions discussed in Chapter 2 is modeled in Matlab/Simulink. The model meets IEEE 1547 interconnection requirements and disconnects from the grid during voltage and frequency deviations from the nominal values after the suggested time delays. One of the main objectives of this inverter is its reusability. A user-interface is provided to change the DC side parameters, the inverter controller, and grid parameters so that multiple copies of the model can be deployed in a feeder. Section 6.2 discusses the dynamic equations of a current-controlled grid-tied inverter. In Section 6.3, a smart inverter is modeled in Matlab/Simulink. Section 6.4 discusses the validation and verification of the inverter. Section 6.5 summarizes the work performed in this chapter.

6.2. Dynamic Equations of a Current-Controlled Grid-Tied Inverter

Figure 6.1 shows a schematic diagram of a current-controlled grid tied inverter system [68]. The system consists of a controlled DC port, a three-phase voltage-source converter, dq0-frame based controller, and a filter circuit. Any DC power source can be connected (e.g. PV plant, battery, etc.) to the controlled DC port. The voltage-source converter studied in this research is a two-level converter. The controller contains compensators that operate in dq0-reference frame. It accepts real and reactive power inputs as references and generates gating signals for switches in the two-level converter. The filter circuit is an L-type circuit with internal resistance. To account for conduction

losses in the inverter, a small resistance (r_{on}) is connected in series with the internal resistance of the filter circuit. Finally, the system is directly connected to the grid.

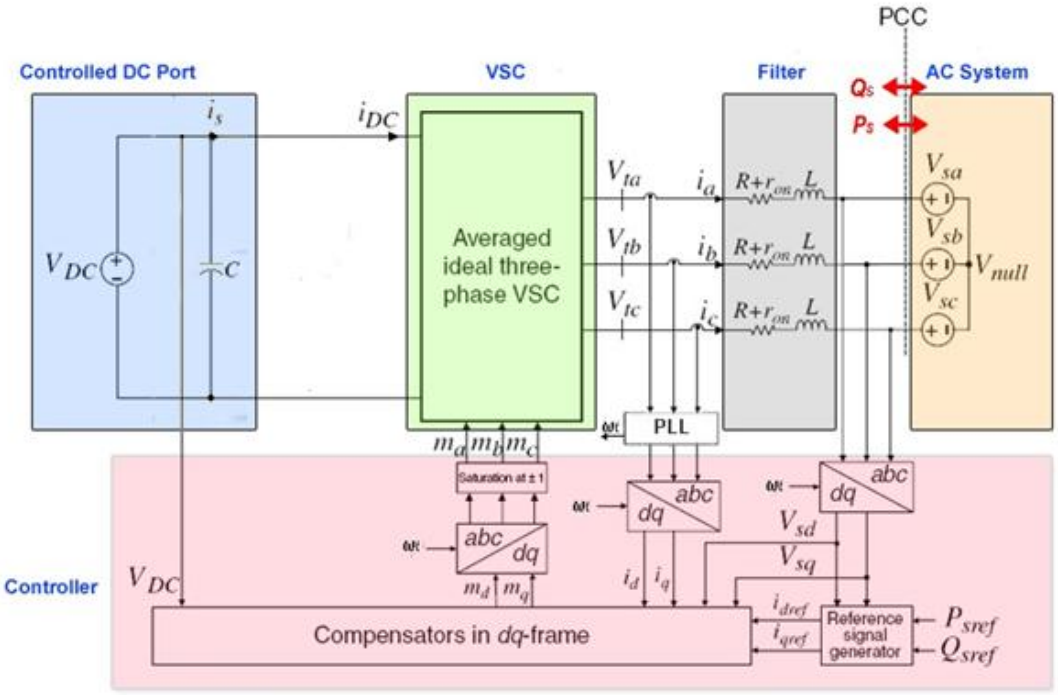

Figure 6.1: Schematic diagram of a current-controlled grid-tied inverter system [68]

Equation (6.1) below describes the relationship between terminal voltage of the inverter, voltage drop at the filter circuit, and grid voltage (AC-side dynamics of the system) [68].

$$L\frac{di_{abc}}{dt} = -(R + r_{on})i_{abc} + V_{t_{abc}} - V_{s_{abc}} \tag{6.1}$$

Where L is filter inductance [H], R is filter inductor internal resistance [Ω], r_{on} is inverter conduction loss [Ω], i_{abc} current supplied to grid ($i_{abc} = [i_a, i_b, i_c]^T$[A]), $V_{t_{abc}}$ is inverter terminal voltage ($V_{t_{abc}} = [V_{ta}, V_{tb}, V_{tc}]^T$[V]), and $V_{s_{abc}}$is grid side voltage ($V_{s_{abc}} = [V_{sa}, V_{sb}, V_{sc}]^T$[V]).

Usually AC-side three-phase quantities are assumed balanced and thus, the zero-sequence components can be ignored. In dq-frame, the equation (6.1) is described by

$$L\frac{di_d}{dt} = L\omega_0 i_q - (R + r_{on})i_d + V_{t_d} - V_{s_d} \tag{6.2}$$

$$L\frac{di_q}{dt} = -L\omega_0 i_d - (R + r_{on})i_q + V_{t_q} - V_{s_q} \tag{6.3}$$

Where ω_0 is grid nominal frequency.

Equations (6.4) and (6.5) describe the relationship between the DC bus and inverter terminal voltages in dq-frame.

$$V_{t_d}(t) = \frac{V_{DC}}{2} m_d(t) \tag{6.4}$$

$$V_{t_q}(t) = \frac{V_{DC}}{2} m_q(t) \tag{6.5}$$

Where V_{DC} is DC bus voltage [V], $m_d \; and \; m_q$ are modulating signal amplitudes in dq-frame, ($0 \leq m_d, m_q \leq 1$).

Because of $L\omega_0$ terms in (6.2) and (6.3), i_d and i_q are coupled. Equations (6.6) and (6.7) determine dq-frame modulating signals by introducing two new control inputs, u_d and u_q[68].

$$m_d = \frac{2}{V_{DC}}\left(u_d - L\omega_0 i_q + V_{s_d}\right) \tag{6.6}$$

$$m_q = \frac{2}{V_{DC}}\left(u_q + L\omega_0 i_d + V_{s_q}\right) \tag{6.7}$$

Substituting $m_d \; and \; m_q$ from (6.6) and (6.7) in V_{t_d} and V_{t_q} equations (6.4 and 6.5), and substituting V_{t_d} and V_{t_q} in equations (6.1) and (6.2), decoupled dynamics of i_d and i_q can be described as shown below by equations (6.8) and (6.9).

$$L\frac{di_d}{dt} = -(R + r_{on})i_d + u_d \tag{6.8}$$

$$L\frac{di_q}{dt} = -(R + r_{on})i_q + u_q \tag{6.9}$$

Equations (6.8) and (6.9) describe two decoupled, first-order, linear systems. i_d and i_q can be controlled by u_d and u_q independently. Figure 6.2 shows control block diagram of a current-controlled voltage-source converter system [68].

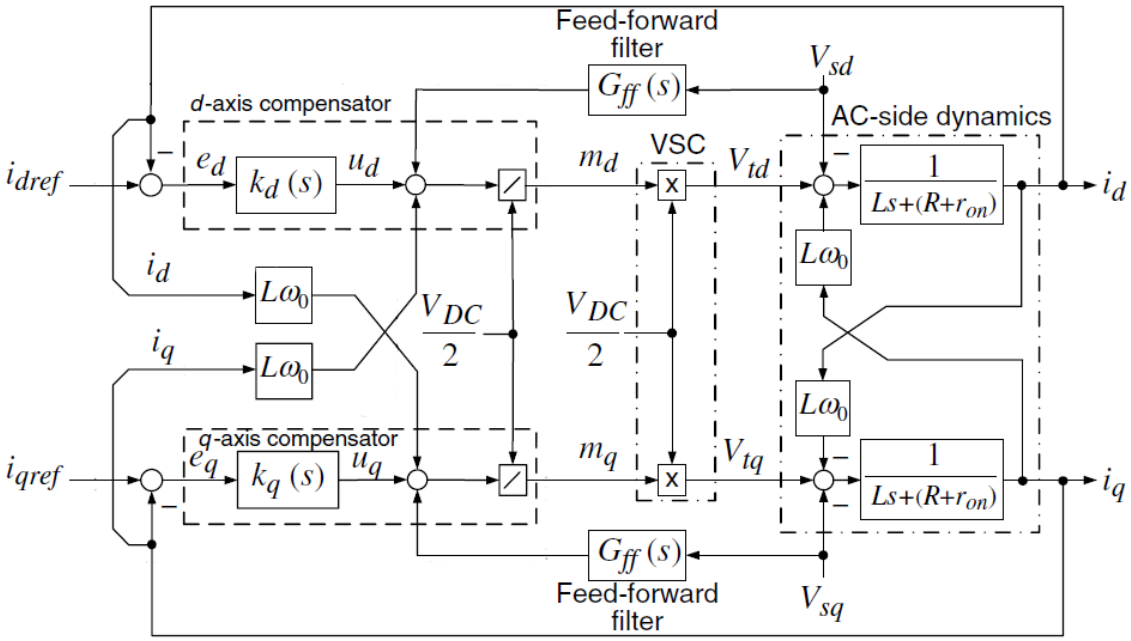

Figure 6.2: Control block diagram of a current-controlled voltage-source converter system [68]

Figure 6.2 shows that u_d and u_q are outputs of d-axis and q-axis compensators respectively. Parameters shown in equation (6.6) and (6.7) are added to the compensators output to obtain dq-frame inverter modulating signals (m_d *and* m_q). The inverter multiplies the modulating signals by $\frac{V_{DC}}{2}$ to generate its output terminal voltages (V_{t_d} and V_{t_q}). V_{t_d} and V_{t_q} in turn control i_d *and* i_q (equations (6.2) and (6.3)). Figure 6.3 shows a simplified and equivalent control block diagram.

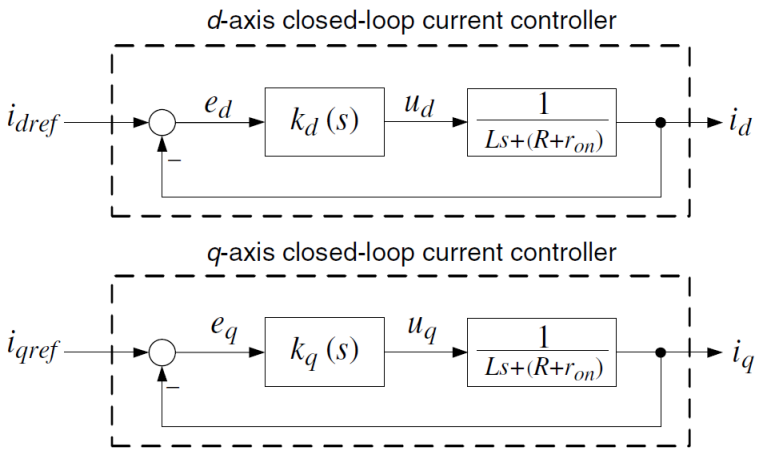

Figure 6.3: Simplified block diagram of a current-controlled voltage-source converter [68]

Figure 6.3 shows that d-axis and q-axis compensators and plants are identical. If a PI compensator is chosen, the proportional and integral gains can be calculated as follows:

$$k_d(S) = k_q(S) = k_p + \frac{k_I}{S} = \frac{k_p S + k_I}{S} \tag{6.10}$$

Where k_p and k_I are proportional and integral gains of the compensator.

The open-loop gain of the system, $l(S)$

$$l(S) = \left(\frac{k_p S + k_I}{S}\right)\left(\frac{1}{LS + (R + r_{on})}\right)$$

$$= \left(\frac{k_p}{LS}\right)\left(\frac{S + \frac{k_I}{k_P}}{S + \frac{(R + r_{on})}{L}}\right) \tag{6.11}$$

The plant pole is canceled by the compensator's zero, $S = -\frac{k_I}{k_P}$, and the loop gain becomes $\frac{k_p}{LS}$. The closed-loop transfer function, $H(S)$ can be described as

$$G_i(S) = \frac{l(S)}{1 + l(S)}$$

$$G_i(S) = \frac{\left(\frac{k_p}{LS}\right)\left(\frac{S + \frac{k_I}{k_P}}{S + \frac{(R + r_{on})}{L}}\right)}{1 + \left(\frac{k_p}{LS}\right)\left(\frac{S + \frac{k_I}{k_P}}{S + \frac{(R + r_{on})}{L}}\right)}$$

$$= \frac{\frac{1}{S}\frac{(Sk_P + k_I)}{\left(SL + (R + r_{on})\right)}}{1 + \frac{1}{S}\frac{(Sk_P + k_I)}{\left(SL + (R + r_{on})\right)}}$$

$$= \frac{Sk_P + k_I}{S\left(SL + (R + r_{on})\right) + Sk_P + k_I}$$

$$= \frac{1}{\frac{S(SL + (R + r_{on}))}{Sk_P + k_I} + 1}$$

Let $k_p = \frac{L}{\tau_i}$ and $k_I = \frac{(R+r_{on})}{\tau_i}$, then

$$G_i(S) = \frac{I_d}{I_{d_{ref}}} = \frac{1}{\tau_i S + 1} \tag{6.12}$$

Where τ_i is the time constant of the resultant closed-loop system. It is usually selected between 0.5-5 ms [68].

Instantaneous power in abc-frame must match instantaneous power in dq-frame. Assuming a balanced three-phase system, real and reactive powers are described by equations (6.13) and (6.14).

$$P_s(t) = \frac{3}{2}\left[V_{sd}(t)i_d(t) + V_{sq}(t)i_q(t)\right] \tag{6.13}$$

$$Q_s(t) = \frac{3}{2}\left[-V_{sd}(t)i_q(t) + V_{sq}(t)i_d(t)\right] \tag{6.14}$$

Where P_s and Q_s are real and reactive powers in dq-frame respectively

When the PLL is at steady state (Figure 6.1), $V_{sq} = 0$. Thus equation (6.13) and (6.14) can be described as shown below.

$$P_s(t) = \frac{3}{2}[V_{sd}(t)i_d(t)] \tag{6.15}$$

$$Q_s(t) = \frac{3}{2}[-V_{sd}(t)i_q(t)] \tag{6.16}$$

Figure 6.2 shows $I_{dref}\ and\ I_{qref}$ are inputs to the current compensators. Using equations (6.15) and (6.16), $I_{dref}\ and\ I_{qref}$ can be computed as shown below.

$$I_{dref}(t) = \frac{2}{3V_{sd}} P_{sref}(t) \tag{6.17}$$

$$I_{qref}(t) = -\frac{2}{3V_{sd}} Q_{sref}(t)] \tag{6.18}$$

6.2.1. **DC Bus Voltage Level Selection**

Based on the PWM technique used to gate the inverters' switches, the DC bus voltage must satisfy the expressions in equations (6.4) and (6.5). Equation (6.19) describes the DC bus voltage if sine-triangle comparison PWM technique is used. Equation (6.20) describes DC bus voltage if Space Vector Modulation (SVM) or sine-triangle with 3rd harmonic injection techniques are used.

$$V_{DC} \geq 2\hat{V}_t \tag{6.19}$$

$$V_{DC} \geq 1.74\hat{V}_t \tag{6.20}$$

$$\hat{V}_t = \sqrt{{V_{td}}^2 + {V_{tq}}^2} \tag{6.21}$$

As shown in equations (6.19) and (6.20), V_{DC} level depends on inverter terminal voltage ($\hat{V}_t$). Therefore, it must satisfy the worst-case inverter operating condition. Ignoring filter inductor internal resistance and inverter conduction losses, equations (6.2) and (6.3) become

$$V_{td} = L\frac{di_d}{dt} - L\omega_0 i_d + V_{s_d} \tag{6.22}$$

$$V_{tq} = L\frac{di_q}{dt} + L\omega_0 i_d \tag{6.23}$$

Substituting for $i_d \; and \; i_q$ from (6.15) and (6.16) in (6.22) and (6.23),

$$V_{td} = \left(\frac{2L}{3V_{sd}}\right)\frac{dP_s}{dt} + \left(\frac{2L\omega_0}{3V_{sd}}\right)Q_s + V_{sd} \tag{6.24}$$

$$V_{tq} = -\left(\frac{2L}{3V_{sd}}\right)\frac{dQ_s}{dt} + \left(\frac{2L\omega_0}{3V_{sd}}\right)P_s \tag{6.25}$$

To calculate the maximum value for $\hat{V}_t$, the following worst-case scenario is considered:

- Initially, the system is at steady state (i.e. $P_s = P_{ref} \; and \; Q_s = Q_{ref}$)
- At $t = t_0$, $P_{ref} and \; Q_{ref}$ are subjected to step changes (i.e. $P_s = P_{ref} + \Delta P_s \; and \; Q_s = Q_{ref} + \Delta Q_s$)
- $P_s \; and \; Q_s$ respond to step change command as described below

$$V_{td} = \left(\frac{2L\omega_0}{3V_{sd}}\right)\left(\frac{\Delta P_s}{\omega_0\tau_i} - \Delta Q_s\right)e^{\frac{-(t-t_0)}{\tau_i}} + \left(\frac{2L\omega_0}{3V_{sd}}\right)(Q_{ref} + \Delta Q_s) + V_{sd} \tag{6.26}$$

$$V_{tq} = -\left(\frac{2L\omega_0}{3V_{sd}}\right)\left(\frac{\Delta Q_s}{\omega_0\tau_i} + \Delta P_s\right)e^{\frac{-(t-t_0)}{\tau_i}} + \left(\frac{2L\omega_0}{3V_{sd}}\right)\left(P_{ref} + \Delta P_s\right) \tag{6.27}$$

The worst-case scenario is immediately after $t = t_0$ (i.e. $t = t_o{}^+$)

$$V_{td}(t_o{}^+) = \left(\frac{2L}{3\tau_i V_{sd}}\right)\Delta P_s + \left(\frac{2L\omega_0}{3V_{sd}}\right)Q_{ref} + V_{sd} \tag{6.28}$$

$$V_{tq}(t_o{}^+) = \left(\frac{2L\omega_0}{3V_{sd}}\right)P_{ref} - \left(\frac{2L}{3\tau_i V_{sd}}\right)\Delta Q_s \tag{6.29}$$

Depending on steady state operating conditions of P_{ref} *and* Q_{ref}, $\hat{V}_t(t_o{}^+)$ can be computed using equation (6.21).

6.2.2. **DC Bus Voltage Control**

The DC port of the inverter is usually connected to a variable DC source (e.g. PV, battery packs, etc.), and thus control of the DC port is necessary. The DC bus voltage control method discussed in [68] is adopted in this work. Figure 6.4 shows the overall control schematic diagram of the inverter system. The outer DC bus control loop is added to the inner current control loop.

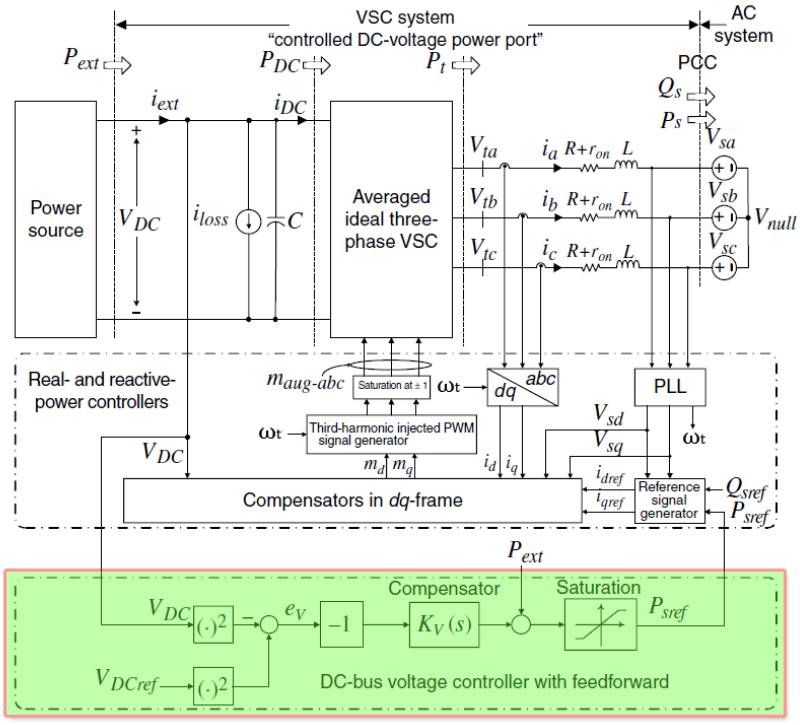

Figure 6.4: Schematic diagram of controlled DC-port [68]

Figure 6.4 shows ${V_{DC}}^2$ is compared with ${V_{DCref}}^2$ and the difference is passed to a compensator. To rapidly reflect changes in the output power of the inverter, a feedforward signal, P_{ext0}, is added to the output of the compensator. A saturation block is used to limit overcurrent and protect the inverter. Equation (6.30) describes the dynamics of ${V_{DC}}^2$ based on the power balance of the inverter system [68].

$$\frac{d\left({V_{DC}}^2\right)}{dt} = \frac{2}{C}P_{ext} - \frac{2}{C}P_{loss} - \frac{2}{C}\left[P_s + \left(\frac{2LP_s}{3{\hat{V}_S}^2}\right)\frac{dP_s}{dt}\right] + \frac{2}{C}\left[\left(\frac{2LQ_s}{3{\hat{V}_S}^2}\right)\frac{dQ_s}{dt}\right] \quad (6.30)$$

P_{ext} represents power supplied by the external DC source, while P_{loss} is power loss at the DC port, and $P_s \; and \; Q_s$ are real and reactive power supplied by the inverter to the grid respectively.

Linearizing equation (6.30) about steady state operating points and computing $\tilde{P}_S$ to ${\tilde{V}_{DC}}^2$ transfer function in Laplace domain results in expression described by equation (6.31).

$$G_V(S) = \frac{{\tilde{V}_{DC}}^2}{\tilde{P}_S} = -\left(\frac{2}{C}\right)\frac{\tau S + 1}{S} \quad (6.31)$$

where

$$\tau = \frac{2LP_{ext0}}{3{\hat{V}_S}^2} \quad (6.32)$$

In equation (6.31), "~" denotes small perturbation around the steady state operating point. Equation (6.32) indicates that τ is proportional to the steady state real power flow, P_{ext0}. For smaller P_{ext0}, τ is insignificant and the plant is predominantly an integrator. However, for larger P_{ext0}, phase of $G_V(S)$ gets shifted as τ becomes larger. For a DC-AC inverting mode of operation, the P_{ext0} is positive. Hence, τ is also positive and adds to the phase of $G_V(S)$. For an AC-DC rectification mode of operation, both the $P_{ext0} and \; \tau$ are negative, and phase of $G_V(S)$ gets reduced. The plant, $G_V(S)$, has a zero

at $S = \frac{-1}{\tau}$. In a rectification mode of operation, negative τ represents a nonminimum-phase system in the controlled DC bus port.

Figure 6.5 shows the control block diagram of the DC bus voltage control based on equation (6.30).

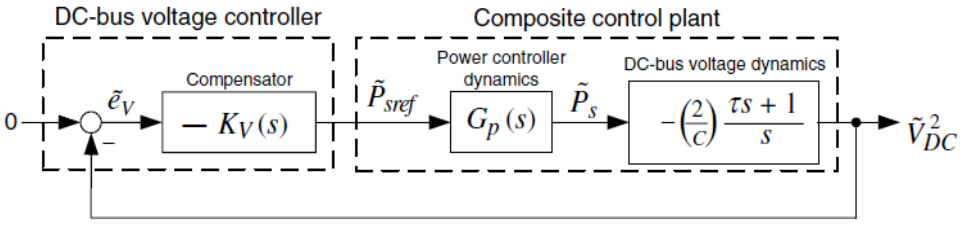

Figure 6.5: Control block diagram of DC bus voltage [68]

In Figure 6.5, $K_V(S)$ is the compensator of the DC bus voltage controller, $G_p(S)$ is the compensator of the current controller (discussed in section 6.2), and $G_V(S)$ is the dynamics of the DC bus voltage or the plant (described by equation (6.31). The open-loop gain of the system is shown below.

$$l(S) = -K_V(S)G_p(S)G_V(S) \tag{6.33}$$

As expressed in equation (6.33), $K_V(S)$ is multiplied by -1 to compensate for the negative sign of $G_V(S)$. In designing $K_V(S)$, the objective is to select parameters of $K_V(S)$ such that magnitude of $l(j\omega)$ crosses the 0dB point in the bode plot of the transfer function with a slope of $\frac{-20dB}{dec}$ at $\omega = \omega_c$ while the phase of $l(j\omega)$is larger than -180° by a reasonable margin. The cut-off frequency, ω_c, should be chosen sufficiently lower than the bandwidth of the current controller ($G_p(j\omega)$) such that $G_p(j\omega_c) \approx$ 1+j0. ω_c is usually selected to be about 0.1-0.5 times the bandwidth of $G_p(j\omega)$ [68].

6.2.3. **DC Bus Capacitor Sizing**

The sizing of DC bus capacitor should allow for storing the maximum instantaneous power for each switching cycle. Its size determines the voltage ripple on the DC bus and limits fluctuations in the input DC power drawn by the inverter. Figure 6.6 shows the DC and AC power ports of the inverter while **Error! Reference source not found.** shows voltage, current, and power waveforms for one cycle of grid frequency.

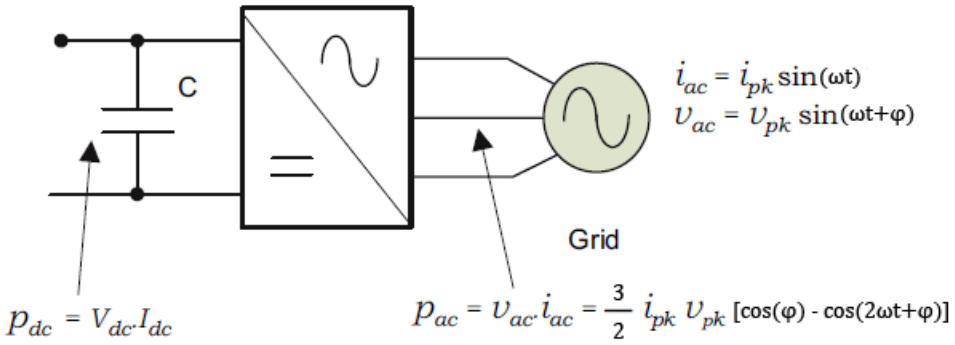

Figure 6.6: DC and AC power ports of an inverter [69]

Let the AC current and voltage supplied to the grid per phase be:

- $i_a(\omega t) = I_{pk} \sin(\omega t + \varphi)$
- $v_a(\omega t) = V_{pk} \sin(\omega t)$

Then, three-phase power supplied by the inverter is:

$$P_a(\omega t) = v_a(\omega t) i_a(\omega t)$$

$$P_a(\omega t) = \frac{V_{pk} I_{pk}}{2} [\cos(\varphi) - \cos(2\omega t + \varphi)] \quad (6.34)$$

$$P_a(\omega t) = P_b\left(\omega t - \frac{2\pi}{3}\right) = P_c\left(\omega t + \frac{2\pi}{3}\right)$$

Error! Reference source not found. shows that the capacitor needs to store nergy for $\frac{1}{8}^{th}$ period of the grid frequency. Equation (6.35) describes energy balance on the DC bus capacitor for $\frac{1}{8}^{th}$ period of grid frequency [69].

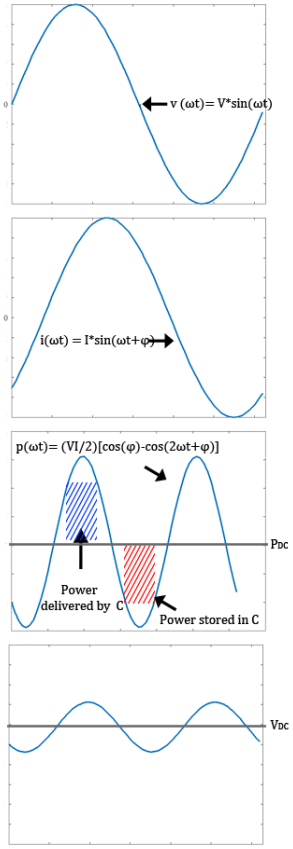

Figure 6.7: Power balance and ripple on DC bus capacitor

$$P_{ac} = \frac{\Delta E}{\frac{T}{8}} = \frac{\frac{1}{2}C{V_{DC}}^2 - \frac{1}{2}C(V_{DC} - \Delta V_{DC})^2}{\frac{1}{(8 * f_{AC})}} \tag{6.35}$$

$$P_{ac} = 4 * f_{AC} * C * \left[{V_{DC}}^2 - (V_{DC} - \Delta V_{DC})^2\right]$$

$$C = \frac{P_{ac}}{4 * f_{AC} * \left[{V_{DC}}^2 - (V_{DC} - \Delta V_{DC})^2\right]} \tag{6.36}$$

6.2.4. **Filter Inductance Sizing**

The L-type filter circuit is used to filter out lower order harmonics created by high frequency switching of inverter's switches. Care must be given in sizing the inductor since it is undesirable for the inductor to participate in power flow of the inverter. Figure 6.8 shows per phase inductor current and voltage for one switching cycle [70].

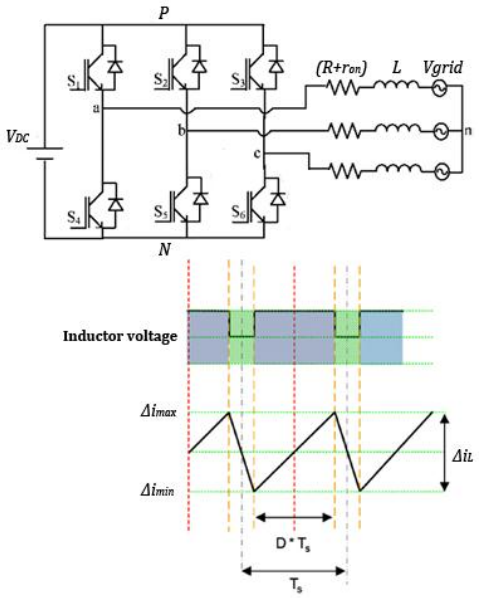

Figure 6.8: Inductor voltage and current waveforms for one switching cycle

Voltage across the inductor is given by:

$$V_L = L\frac{di_L}{dt} \tag{6.37}$$

For one switching cycle,

$$(V_{DC} - V_{Grid}) = L\frac{\Delta i_L}{DT_S} \tag{6.38}$$

Where T_S is the switching period ($T_S = \frac{1}{F_{SW}}$) and D is the duty cycle. Rearranging (6.38),

$$\Delta i_L = \frac{D * T_S * (V_{DC} - V_{Grid})}{L} \tag{6.39}$$

The duty cycle, D, can be expressed in terms of modulating index, m_a, as shown below.

$$D(\omega t) = m_a * \sin(\omega t) \tag{6.40}$$

Inverter terminal voltage must match grid side voltage. Equation (6.41) describes the relationship between duty cycle, DC voltage, and grid voltage.

$$V_{Grid} = D * V_{DC} \tag{6.41}$$

Substituting D from (6.40) in (6.41) and substituting V_{Grid} in (6.39),

$$\Delta i_L = \frac{V_{DC} * T_S * m_a * \sin(\omega t) * (1 - m_a * \sin(\omega t))}{L} \tag{6.42}$$

Equation (6.42) shows inductor current ripple, Δi_L, as a function of a sinusoidal waveform. To find the maximum ripple, Δi_L is differentiated with respect to time and equated to 0 as shown below.

$$\frac{d\Delta i_L}{dt} = \frac{V_{DC} * T_S * m_a * \omega * [\cos(\omega t)(1 - 2 * m_a * sin(\omega t)]}{L} = 0 \tag{6.43}$$

$$sin(\omega t) = \frac{1}{2m_a} \tag{6.44}$$

Equation (6.44) gives the modulating index for which ripple is maximum. Substituting (6.44) in (6.42),

$$\Delta i_{L_{max}} = \frac{V_{DC} * T_S}{4L} \tag{6.45}$$

$$\text{L} = \frac{V_{DC}}{4 * F_{S*} \Delta i_{L_{max}}} \tag{6.46}$$

Equation (6.46) describes the inductor size based on allowed maximum inductor current ripple.

6.3. Developing a Smart Inverter Model in Matlab/Simulink

The dynamic equations of a current-controlled, two-level, three-phase inverter system is discussed in section 6.2. In this section, a smart inverter is developed in Matlab/Simulink software. One of the objectives of the model is reusability. A user is able to customize the DC bus, the inverter, and the filter circuit parameters using a user-interface (mask) created on top of different building blocks. Customized inverters with different parameters can be deployed at different nodes of a feeder, and both steady state and transient simulations can be performed. Figure 6.9 shows the user-interface mask created.

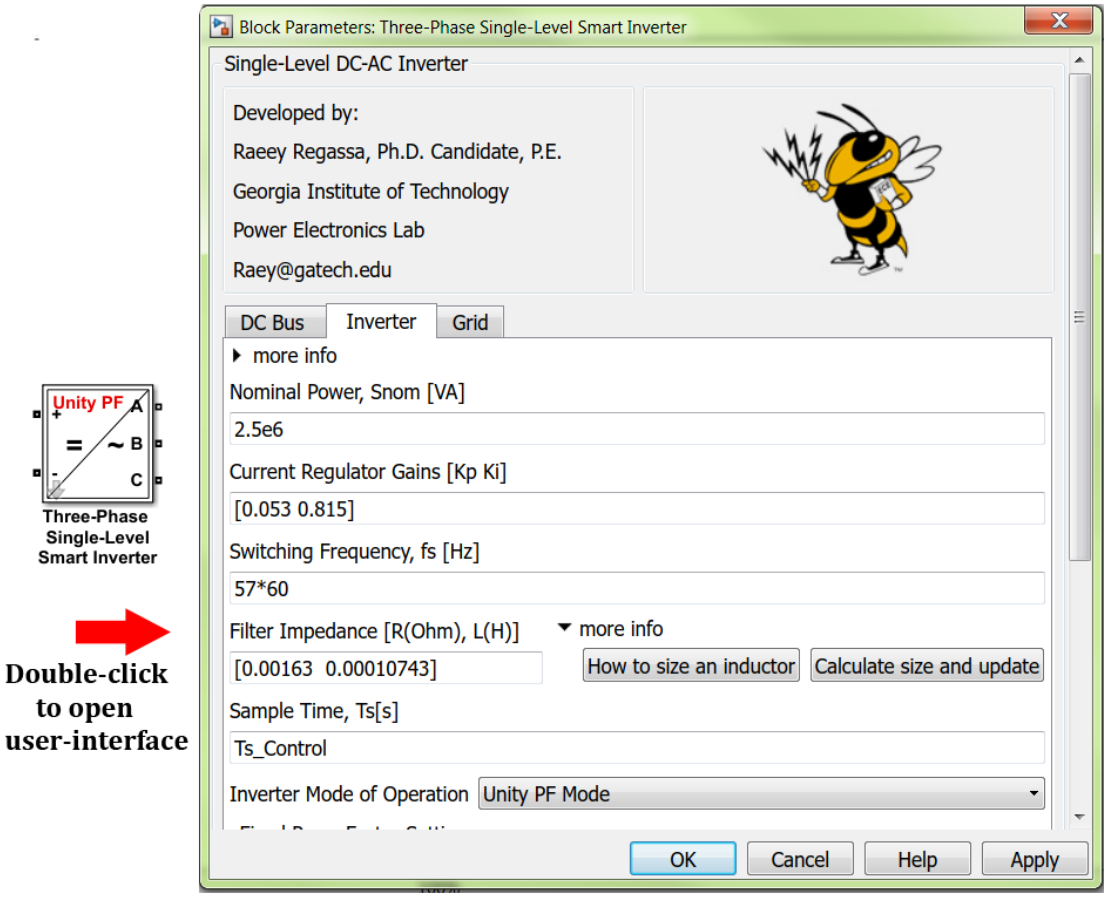

Figure 6.9: User-interface of the smart inverter model in Simulink

Figure 6.9 shows the “DC bus”, “Inverter”, and “Grid” taps created for entering parameters by a user. The “DC bus” tap contains fields for the entering information about the DC bus voltage level, DC bus capacitor, and DC bus controller. The DC bus voltage level should be calculated as discussed in equations (6.28) and (6.29). The “Inverter” tap contains the following fields:

- Nominal power of the inverter [VA]
- Gains for the proportional and integral components of the current compensator
- Switching frequency of the inverter switches
- Filter circuit impedance (i.e. values for filter inductance and internal resistance of the filter inductor)
- Sample time of the controller
- Inverter mode of operation. A user can choose one of the following control modes for the inverter and enter setpoints:
    - Unity Power Factor
    - Fixed Power Factor
    - Volt-Var
    - Volt-Watt
    - Frequency-Watt

An option is provided for a user to automatically calculate and update the filter inductance value based on the inverter’s switching frequency, DC bus voltage, and rated power (“Calculate size and update” button shown in Figure 6.9). When this option is selected, a callback function written inside the user-interface is executed. This callback function calculates the size of the inductor needed as described by equation (6.46). Another button, “How to size an inductor”, is provided as additional information. Clicking this button opens up a pdf file that contains equations discussed in section 6.2.2.

Finally, a user enters the grid side voltage ($V_{L-L,rms}$) and frequency in the "Grid" tap. After a user enters all the necessary parameters to customize the inverter and clicks the "ok" button, the user-interface mask initializes the underlying building blocks of the inverter model by passing the inputs as parameters. It also displays the selected inverter control mode. As an example, the inverter model shown in Figure 6.9 displays "Unity PF" message since Unity Power Factor control mode is selected in the "Inverter" tap. Figure 6.10 shows the initialization codes written in the user-interface mask.

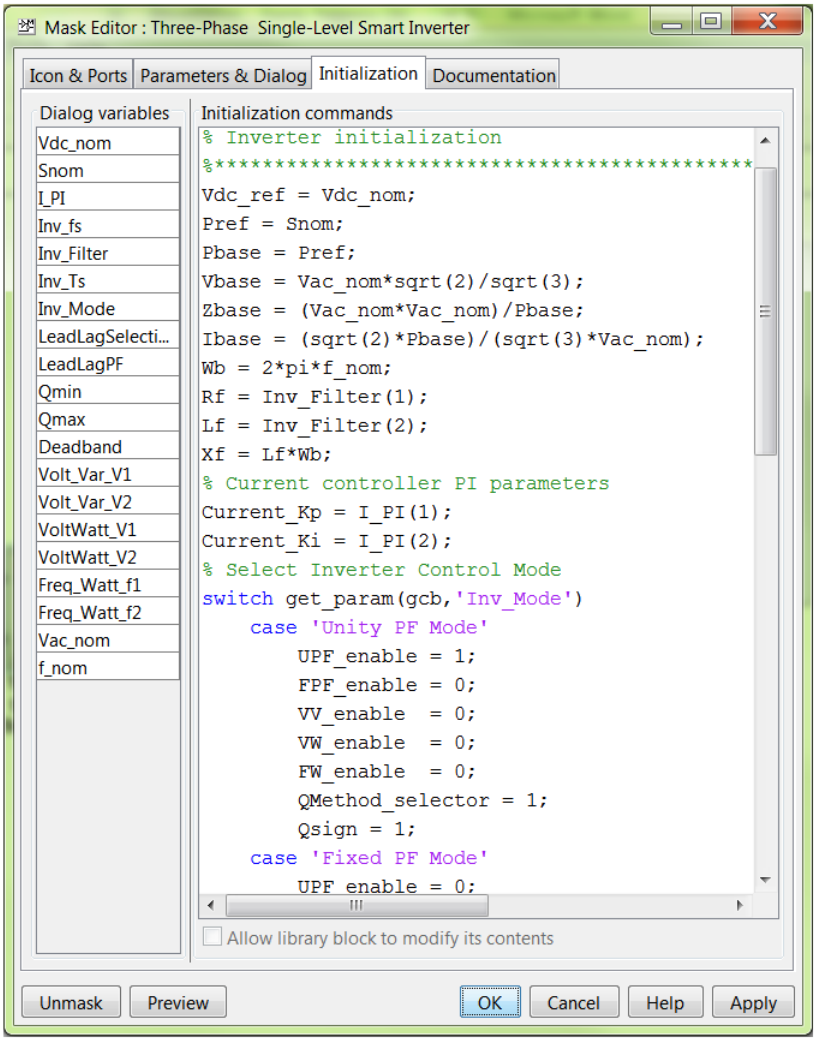

Figure 6.10: Model initialization by user-interface mask

Figure 6.10 shows the codes written in the initialization of the user-interface mask. Base values are calculated for power, voltage, current and impedance. Based on

the user selected inverter mode of operation, a flag is enabled to run the model in the selected control mode.

The second layer of the model is shown in Figure 6.11. In this layer, six-IGBTs (semiconductor switches), a controller subsystem, a measurement subsystem, a filter circuit, and a three-phase breaker exist. The switches are gated by output signals of the controller block. The three-phase breaker is also controlled by a signal from the controller block. The controller trips the breaker in the case of voltage and/or frequency deviations as per IEEE 1547 interconnection rules. Inductance and resistance parameters of the filter circuit and parameters of the controller are passed from the user-interface during initialization of the user-interface mask (Figure 6.10).

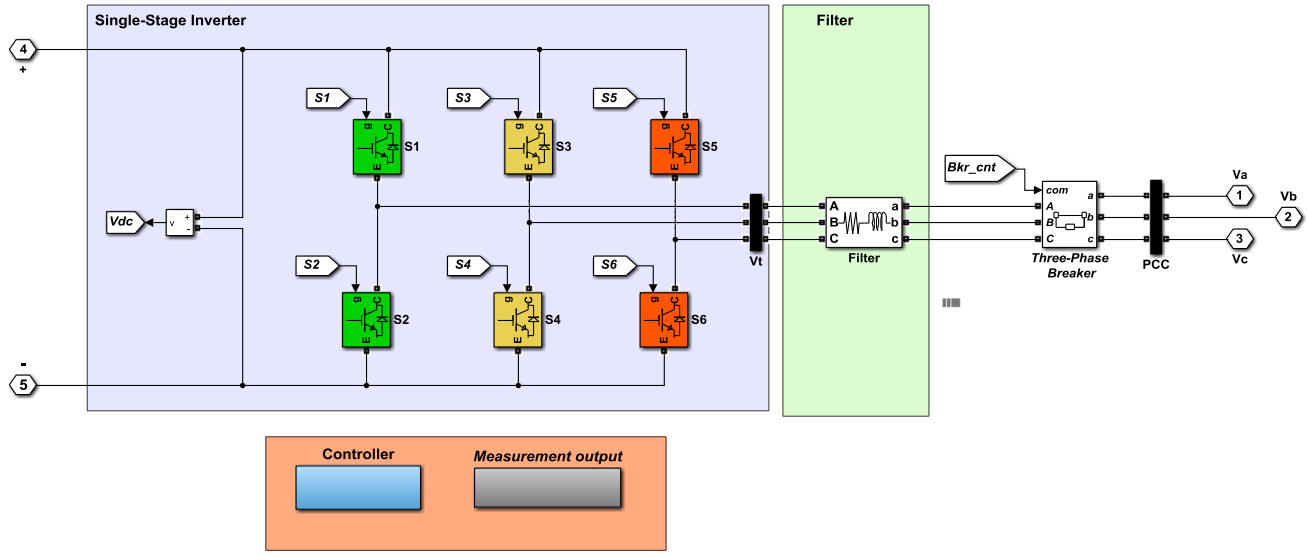

Figure 6.11: Second layer of the smart inverter model in Simulink

In the "Controller" subsystem, six subsystems are created to control the DC bus voltage and power output of the inverter as discussed in section 6.2. Figure 6.12 shows these six subsystems.

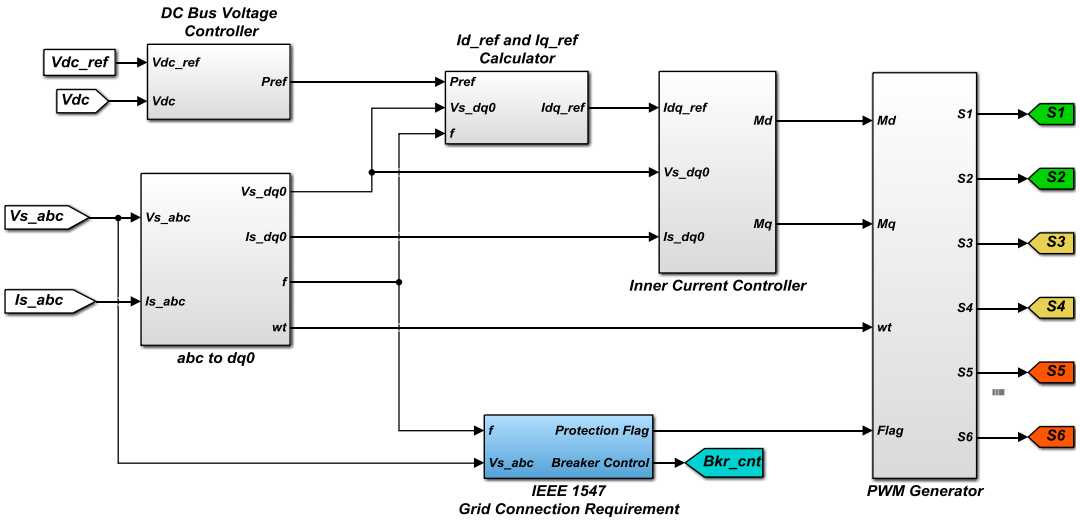

Figure 6.12: Third layer of the model - Inside the Controller block

Inside the Controller subsystem, the following six subsystems exist:

1. **<u>abc to dq0</u>**:- this subsystem transforms voltage and current measurements at a point of common coupling into dq0 reference frame (i.e. transform $v_{s_{abc}}$ and $i_{s_{abc}}$ at PCC into $v_{s_{dq0}}$ and $i_{s_{dq0}}$) using a phase-locked loop (PLL) block and abc to dq0 transformation blocks. Figure 6.13 shows this subsystem.

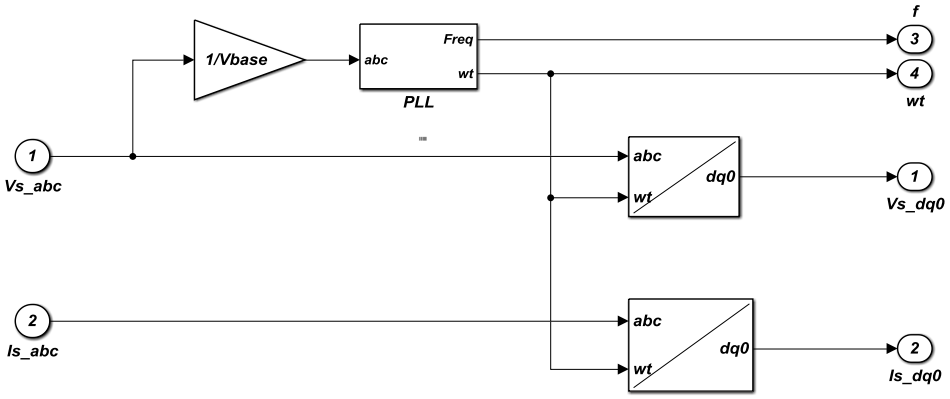

Figure 6.13: Inside the Controller subsystem - abc to dq0 subsystem

2. **<u>DC Bus Voltage Controller</u>**:- This subsystem generates P_{ref} based on DC bus voltage and DC bus controller parameters set by the user. It

implements the DC bus control method discussed in section 6.2.2. Figure 6.14 shows blocks used inside this subsystem.

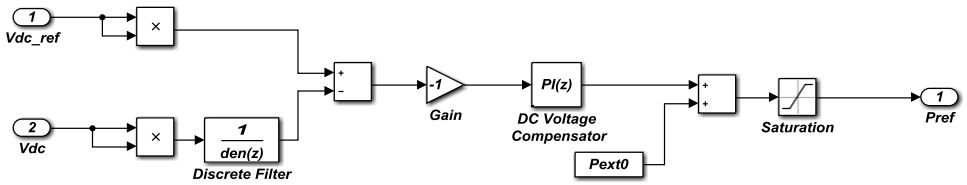

Figure 6.14: Inside DC Bus Voltage Controller subsystem

3. **I_{dref} and I_{qref} Calculator**:- Based on the inverter control mode selected by a user (i.e. Unity Power Factor, Volt-Var, etc.), this subsystem generates $I_{d_{ref}}$ and $I_{q_{ref}}$ using equations (6.17) and (6.18) respectively. Figure 6.15 shows five subsystems created to compute $I_{d_{ref}}$ and $I_{q_{ref}}$. During simulation, only one of the five subsystems is enabled based on the user selected inverter control mode.

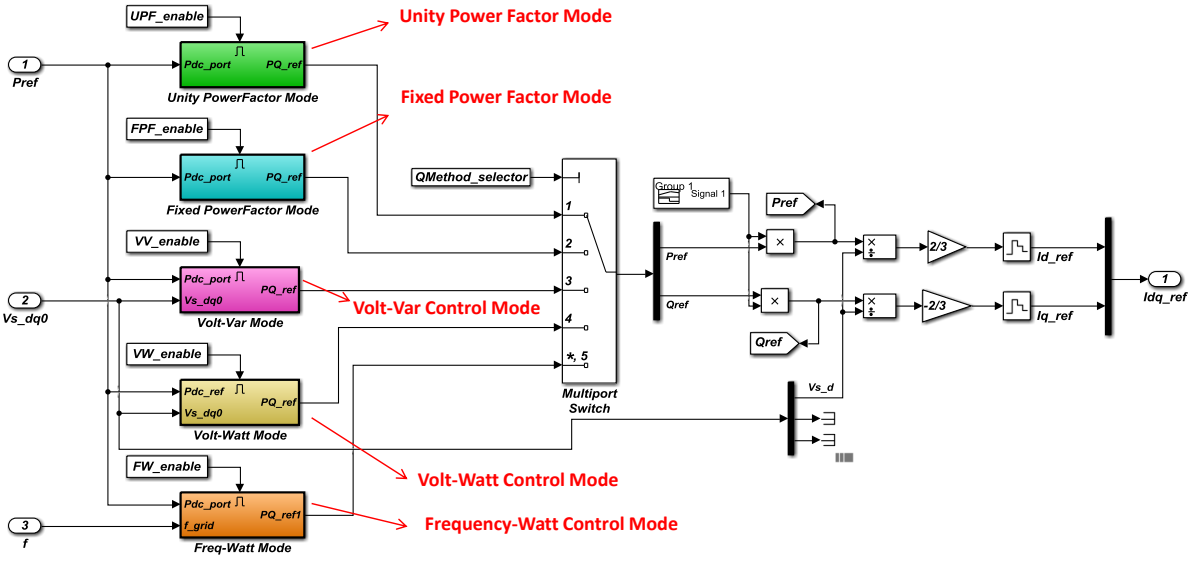

Figure 6.15: Idref and Iqref Calculator subsystem

4. **Current Controller**: - This subsystem implements equations (6.6) and (6.7) to compute dq-frame modulating signals (m_d *and* m_q). It contains PI compensators and feedforward dq-axis grid voltages. The saturation block

(limiter) maintains the modulation signals within ±1. Figure 6.16 shows building blocks used inside this subsystem.

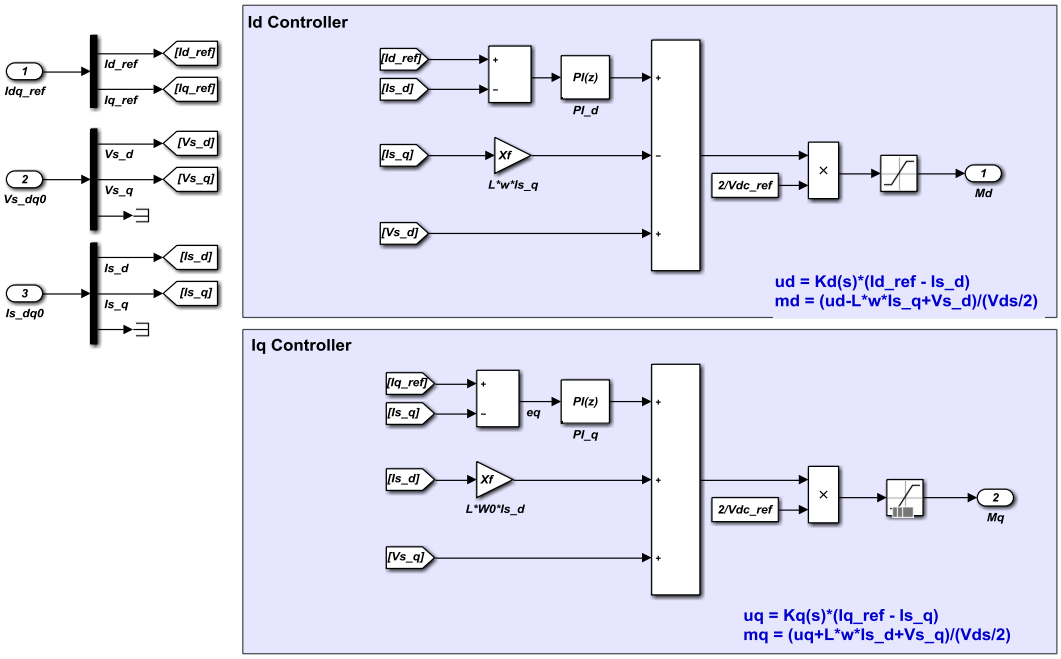

Figure 6.16: Current controller subsystem

5. **<u>IEEE 1547 Grid Connection Requirement</u>**:- Grid interconnection requirements of IEEE 1547 are implemented in this subsystem. As discussed in chapter 2 and summarized in tables 2.1-2.2, the inverter remains connected to the grid for different time durations depending on levels of voltage and frequency deviations from nominal operating points. This is done to give inverters fault ride-through capabilities during faults in the system. Figure 6.17 shows building blocks used inside this subsystem.

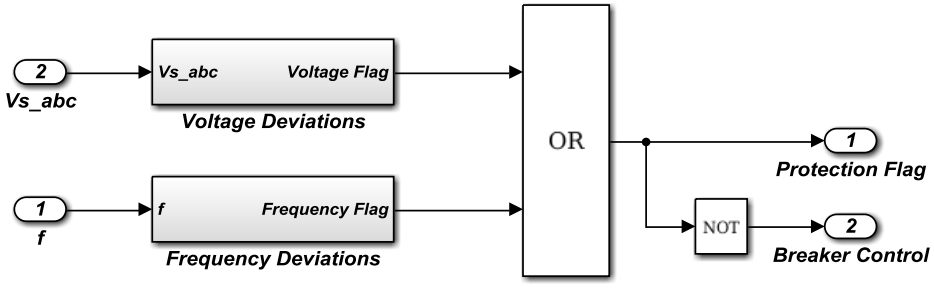

Figure 6.17: IEEE Grid Interconnection Requirement Subsystem

Grid voltage and frequency are measured at PCC and passed to the "Voltage Deviation" and "Frequency Deviations" subsystems respectively. These subsystems compare the measured values against IEEE 1547 standards. If deviations are detected, they block the inverters' IGBTs (switches) and trip the breaker that connects the inverter to the grid. Figure 6.18 and Figure 6.19 show building blocks used in "Voltage Deviations" and in "Frequency Deviations" subsystems respectively.

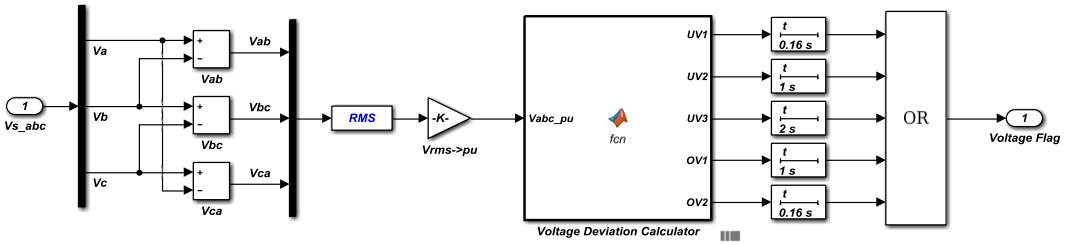

Figure 6.18: Building blocks in the Voltage Deviation subsystem

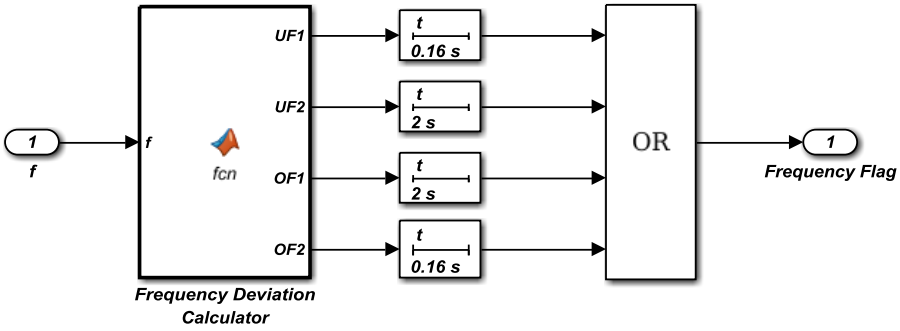

Figure 6.19: Building blocks in the Frequency Deviation subsystem

Figure 6.18 shows that grid voltages are converted from physical units to per unit system and passed to the "Voltage Deviations Calculator" Matlab function. This function compares measured voltages against voltage deviation values summarized in Table 2.1. This function also sets one of its four output flags to "ON" if a deviation is detected. Different "ON time delay" blocks are connected to the Matlab functions' output ports. The "ON time delay" blocks delay tripping of the inverter for time durations specified in IEEE 1547 requirements. If the measured voltage

value returns to its nominal value before the time delay expires, the inverter is not tripped. The code used in the "Voltage Deviations Calculator" Matlab function is shown in Appendix B.

Figure 6.19 shows building blocks used in the "Frequency Deviations" subsystem. Similar to the "Voltage Deviations" subsystem, it compares measured grid frequency values against deviations summarized in Table 2.2 and sets one of its two output flags to "ON" if a deviation is detected. Two "ON time delay" blocks are connected to the "Frequency Deviations Calculator" function to delay tripping of the inverter for time durations per IEEE 1547 grid interconnection requirements. This Matlab function is shown in Appendix C.

6. **PWM Generator**:- This subsystem generates gating signals for the IGBTs of the inverter. It converts dq-frame modulating signals (m_d and m_q) generated by the "Current Controller" subsystem into abc-frame (m_{abc}), injects 3rd harmonics to maximize the use of the DC bus voltage by 15%, and compares the augmented abc-frame gating signals against a triangular waveform to generate final gating signals. The frequency of the triangular waveform is specified by the user at the top-layer (user-interface). Figure 6.20 shows the building blocks used inside this subsystem.

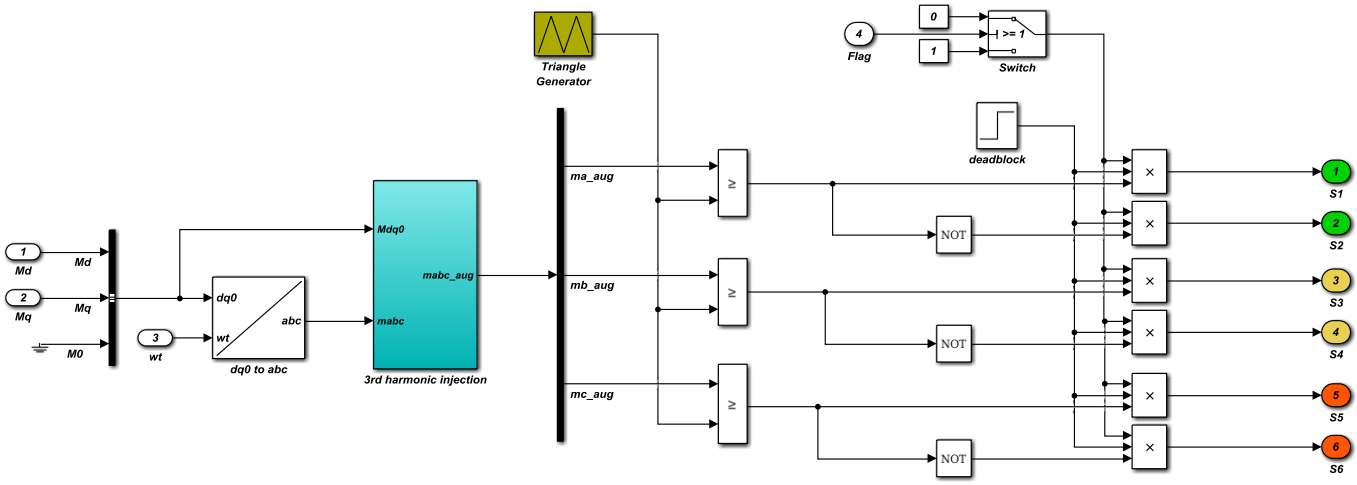

Figure 6.20: PWM Generation subsystem

In the PWM Generation subsystem, $m_d \; and \; m_q$ signals are converted into m_{abc} signals using an inverse Park transformation block. After 3rd harmonics are added to m_{abc} signals, they are compared with a high frequency triangular waveform. The frequency of the triangular waveform is set by the user. A deadblock is used to delay gating of inverters' IGBTs at the beginning of the simulation to let the DC bus capacitor charge. This time delay is set by the user via the user-interface. A switch is used to trip the breaker that connects the inverter to the grid and block IGBTs of the inverter during voltage and frequency violations (i.e. switch is enabled when "IEEE 1547 Grid Requirements" subsystem sends out a flag to trip the breaker).

Equations (6.47) – (6.49) describe 3rd harmonic injection to m_{abc} signals. Figure 6.21 shows implementation of 3rd harmonic injection in "3rd harmonic injection" subsystem (Figure 6.20).

$$m_{a_{aug}} = \hat{m}\sin(\omega t) + \frac{1}{6}\hat{m}\sin(\omega t) \tag{6.47}$$

$$m_{b_{aug}} = \hat{m}\sin\left(\omega t - \frac{2\pi}{3}\right) + \frac{1}{6}\hat{m}\,3\sin\left(\omega t - \frac{2\pi}{3}\right) \tag{6.48}$$

$$m_{c_{aug}} = \hat{m}\sin\left(\omega t - \frac{4\pi}{3}\right) + \frac{1}{6}\hat{m}\,3\sin\left(\omega t - \frac{4\pi}{3}\right) \tag{6.49}$$

Where $\hat{m}$ is the magnitude of the m_{abc} signal and $\hat{m}^2 = {m_d}^2 + {m_q}^2$.

Using the identity, $\sin(3\omega t) = -4sin^3(\omega t) + 3\sin(\omega t)$, equation (6.47)-(6.49) are rewritten as:

$$m_{a_{aug}} = \hat{m}\left[\frac{3}{2}sin(\omega t) - \frac{2}{3}sin^3(\omega t)\right] \tag{6.50}$$

$$m_{b_{aug}} = \hat{m}\left[\frac{3}{2}sin\left(\omega t - \frac{2\pi}{3}\right) - \frac{2}{3}sin^3\left(\omega t - \frac{2\pi}{3}\right)\right] \quad (6.51)$$

$$m_{c_{aug}} = \hat{m}\left[\frac{3}{2}sin\left(\omega t - \frac{4\pi}{3}\right) - \frac{2}{3}sin^3\left(\omega t - \frac{4\pi}{3}\right)\right] \quad (6.52)$$

Multiplying the right side terms of equations (6.50)-(6.52) by $\frac{\hat{m}^2}{\hat{m}^2}$,

$$m_{a_{aug}} = \hat{m}\frac{3}{2}sin(\omega t) - \frac{2}{3}\frac{[\hat{m}\,sin(\omega t)]^3}{\hat{m}^2} \quad (6.53)$$

$$m_{b_{aug}} = \hat{m}\frac{3}{2}sin\left(\omega t - \frac{2\pi}{3}\right) - \frac{2}{3}\frac{[\hat{m}\,sin\left(\omega t - \frac{2\pi}{3}\right)]^3}{\hat{m}^2} \quad (6.54)$$

$$m_{c_{aug}} = \hat{m}\frac{3}{2}sin\left(\omega t - \frac{4\pi}{3}\right) - \frac{2}{3}\frac{[\hat{m}\,sin\left(\omega t - \frac{4\pi}{3}\right)]^3}{\hat{m}^2} \quad (6.55)$$

Substituting $\hat{m}^2$ by ${m_d}^2 + {m_q}^2$, equations (6.53)-(6.55) are rewritten as:

$$m_{a_{aug}} = \frac{3}{2}m_a(t) - \frac{2}{3}\left(\frac{m_a(t)^3}{{m_d}^2 + {m_q}^2}\right) \quad (6.56)$$

$$m_{b_{aug}} = \frac{3}{2}m_b(t) - \frac{2}{3}\left(\frac{m_b(t)^3}{{m_d}^2 + {m_q}^2}\right) \quad (6.57)$$

$$m_{c_{aug}} = \frac{3}{2}m_c(t) - \frac{2}{3}\left(\frac{m_c(t)^3}{{m_d}^2 + {m_q}^2}\right) \quad (6.58)$$

Figure 6.21 shows implementation of equations (6.56)-(6.58) in "3rd harmonic injection" subsystem.

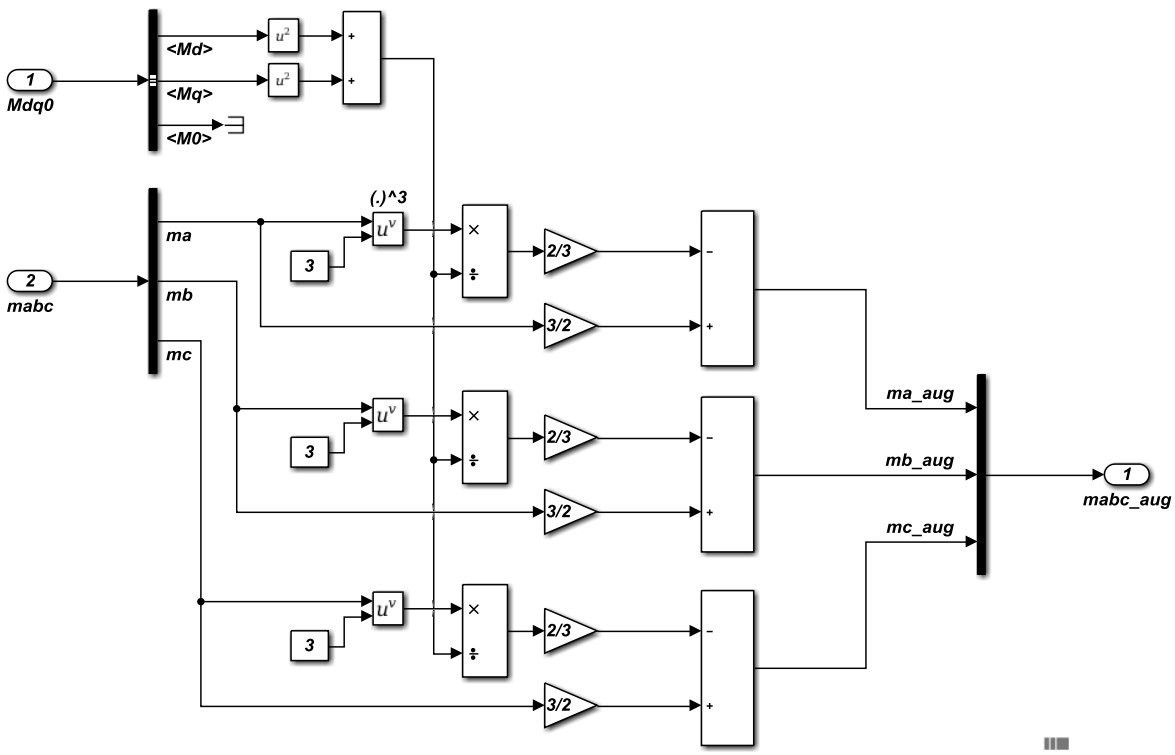

Figure 6.21: 3rd Harmonic Injection subsystem

6.4. Validation and Verification of the Smart Inverter Model in Matlab/Simulink

In order to validate and verify the smart inverter model, a 600 kVA inverter system is designed and connected to a 4.16 kV grid. The following parameters are used:

- Grid side voltage, $v_{grid} = 4.16$ kV (L-L, rms)
- Current supplied to the grid, $i_{grid} = \frac{600\ kVA}{\sqrt{3} * v_{grid}} = 83.27 A_{rms}$
- Select 3420 Hz (i.e. 57*60 Hz) as inverter switching frequency
- Allow 20% ripple on filter inductor current (i.e. $\Delta i_{L_{max}} = 23.55\ A_{peak}$). Assume DC bus voltage is twice the grid side voltage (i.e. $V_{DC} = 2\left(\sqrt{\frac{2}{3}} v_{grid}\right) \approx 6800\ V$). Inductor size is calculated using equation (6.46)

$$L = \frac{V_{DC}}{4 * F_{S*} \Delta i_{L_{max}}} \approx 30\ m\text{H}$$

- Inductor internal resistance and conduction losses in the inverter are approximated as 0.75 mΩ and 0.88 mΩ respectively.
- Time constant (τ_i) for inner current control loop is selected to be 2 ms. K_P and $K_I$values of the current compensator are calculated ($k_p = \frac{L}{\tau_i} = 15$ and $k_I = \frac{(R+r_{on})}{\tau_i} = 0.815$)
- Using equations (6.28), (6.29) and (6.21), DC bus voltage level is calculated for the following worst-case operating scenario:
    - Inverter is initially not injecting real or reactive power. It suddenly starts to inject its rated real power (600 kW).

      $V_{td}(t_o{}^+) = \left(\frac{2L}{3\tau_i V_{sd}}\right)\Delta P_s + V_{sd} = 5163.01$ V

      $V_{tq}(t_o{}^+) = 0$

      $\hat{V}_t = \sqrt{{V_{td}}^2 + {V_{tq}}^2} = 5163.01$ V

      $V_{DC} = 1.74\hat{V}_t = 8900$ V
- DC bus capacitance is calculated using equation (6.36). Allowing 20% voltage ripple on the DC bus voltage,

$$C = \frac{P_{ac}}{4 * f_{AC} * \left[{V_{DC}}^2 - (V_{DC} - \Delta V_{DC})^2\right]} = 150\ \mu\text{F}$$

Parameters calculated above are entered into the smart inverter model using the user-interface. A constant 8900 DC source is connected to the inverter's DC port. The AC port of the inverter is connected to a 4.16 kV grid (swing source). Figure 6.22 shows the single line diagram of the test system.

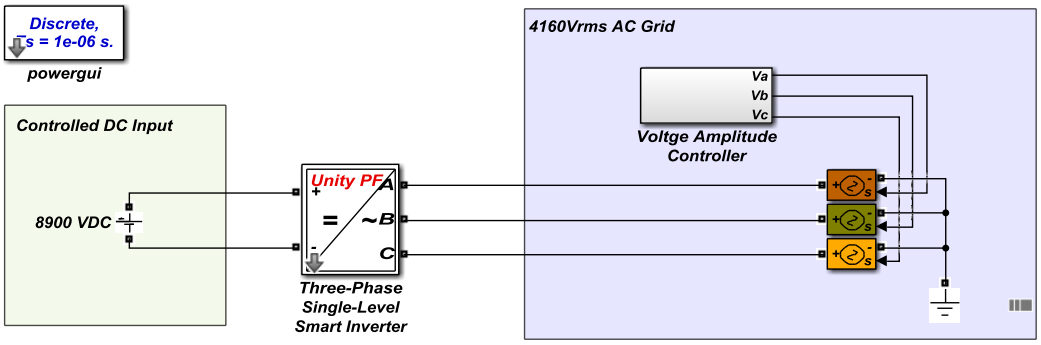

Figure 6.22: Single line diagram of smart inverter test circuit

The AC port of the inverter is connected to a "4160 Vrms AC Grid" subsystem. This subsystem simulates different grid voltages and frequencies in order to validate and verify the performance of the inverter under different grid conditions. Figure 6.23 shows the building blocks used in this subsystem.

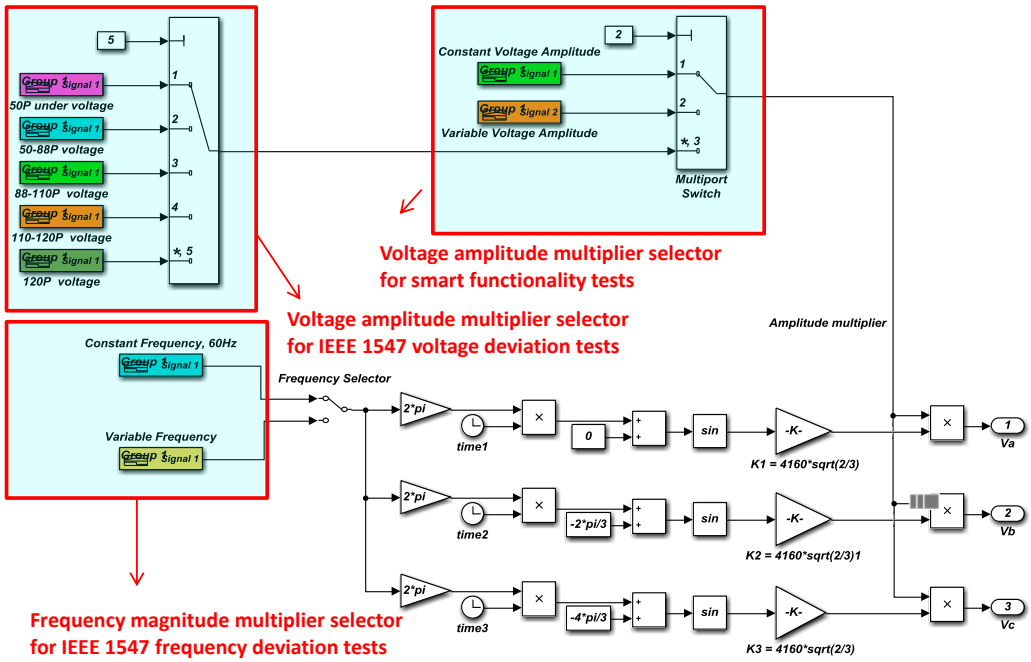

Figure 6.23: 4160 Vrms AC Grid subsystem

<u>Scenario 1 – No disturbance in the AC system:</u> The model is run with no disturbance applied to the system and with the smart inverter in Unity Power Factor control mode. Initially, inverter switches are blocked for 0.2 s. Figure 6.24 shows scope

captures of voltage, current, and power measurements at the point of common coupling of the inverter to the grid.

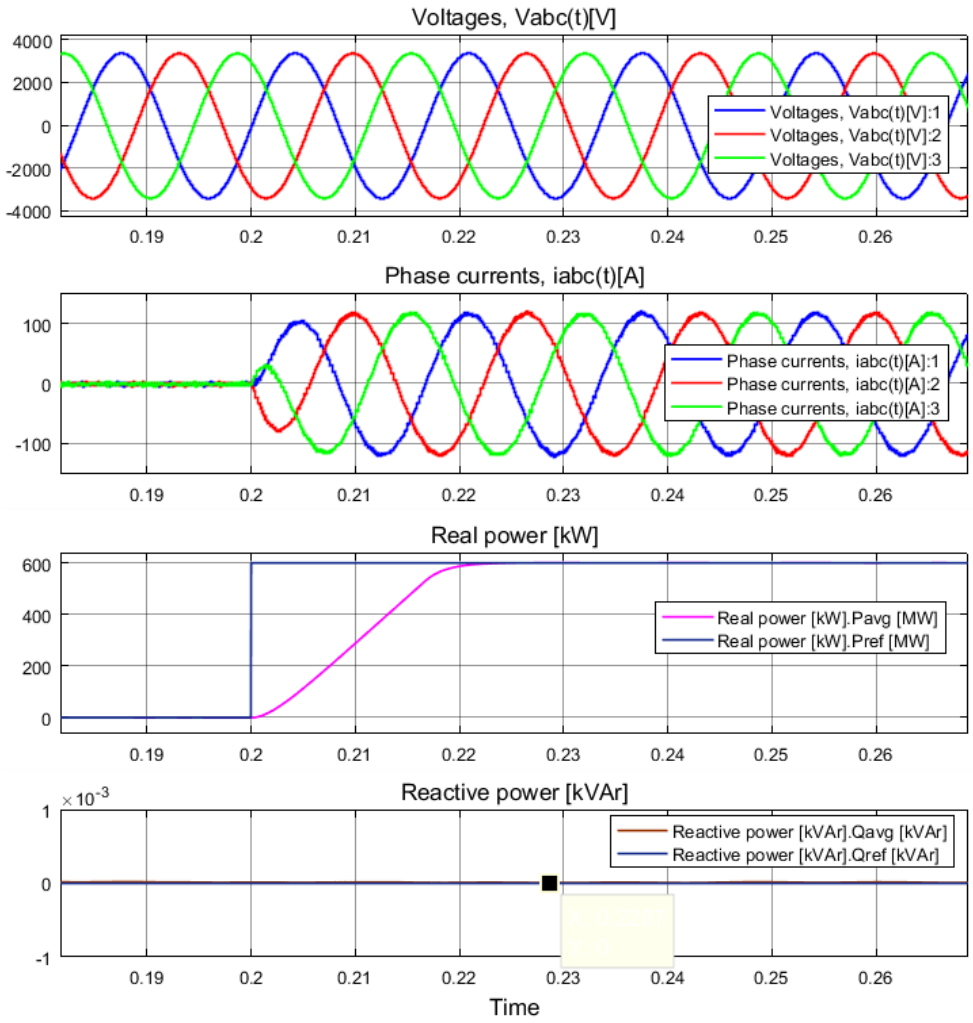

Figure 6.24: Smart inverter test - No disturbance applied to the system and inverter in Unity Power Factor control mode

Figure 6.24 shows that the inverter injects 600 kW real power after 0.225 s. Since it is controlled in Unity Power Factor control mode, the reactive power injected is very small (i.e. an average of 15 Var) as compared to 600 kW. The inverter current compensator tracked the step change in power very well with no overshoot and 25 ms settling time. Figure 6.25 shows the harmonic analysis of current supplied by the inverter.

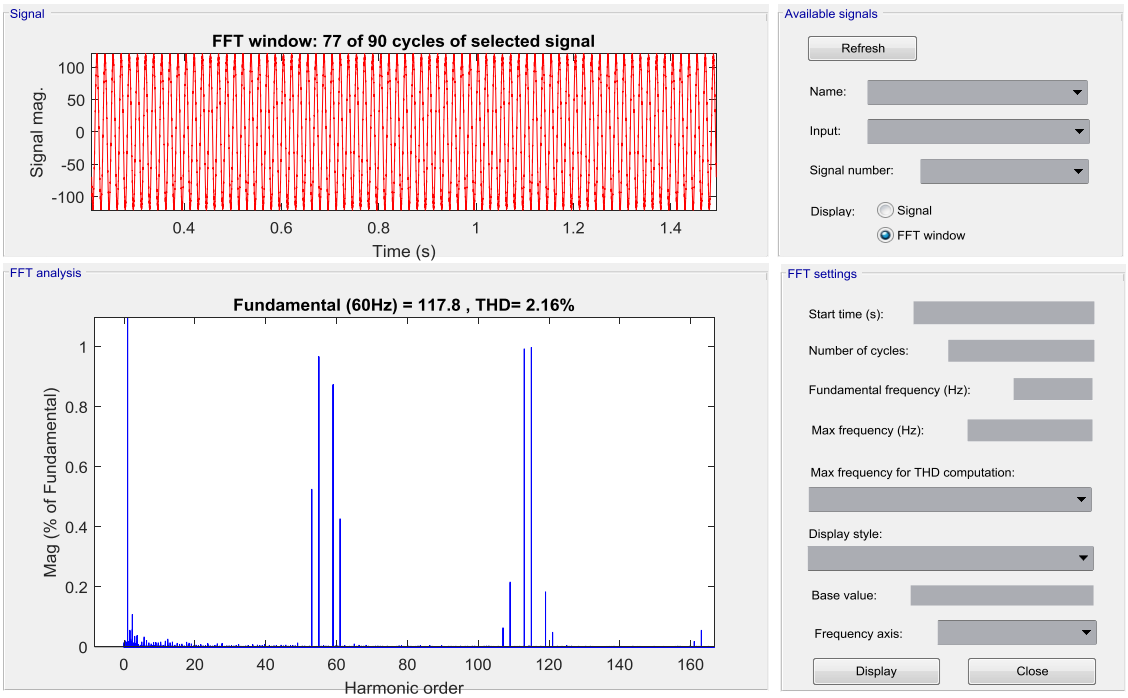

Figure 6.25: Smart inverter test - Current harmonics analysis

The total harmonic distortion (THD) of current supplied to the grid is 2.16%, which is well below the IEEE 1547 requirement of 5%. As expected with a switching modulating frequency of 57, the odd harmonics present in the current are (57±2), (2*57±1), (3*57±2), etc.

<u>Scenario 2 – Variable voltage in the AC system:</u> The grid voltage is varied as shown in Figure 6.26. The simulation is run first with inverter in Unity Power Factor, second in 0.85 lagging Fixed Power Factor, and third in Volt-Var control modes with settings shown in Figure 5.8. Figure 6.27, Figure 6.28, and Figure 6.29 show scope captures of power measurements at point of common coupling of the inverter to the grid.

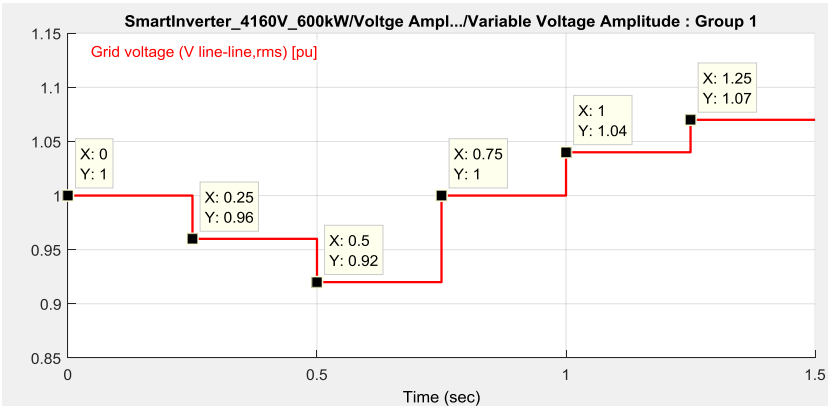

Figure 6.26: Variable Grid voltage

The grid voltage is 1 pu for the first 0.25 s and is changed to 0.96 pu for the next 0.25 s. It is further reduced to 0.92 pu from 0.5 s-0.75 s. The grid voltage is raised to 1 pu from 0.75 s to 1s. It is raised again to 1.04 pu from 1s-1.25 s. Finally, it is raised to 1.5 s from 1.25 s-1.5 s. This is done to make the grid voltage fall into the five regions shown in the Volt-Var curve (Figure 5.8).

Time intervals for the voltage deviations are selected considering the IEEE 1547 interconnection requirements. In this simulation scenario, the objective is for the inverter to stay connected to the grid. If longer time intervals are selected, the inverter disconnects from the grid as discussed in section 6.3 and shown in Figure 6.18

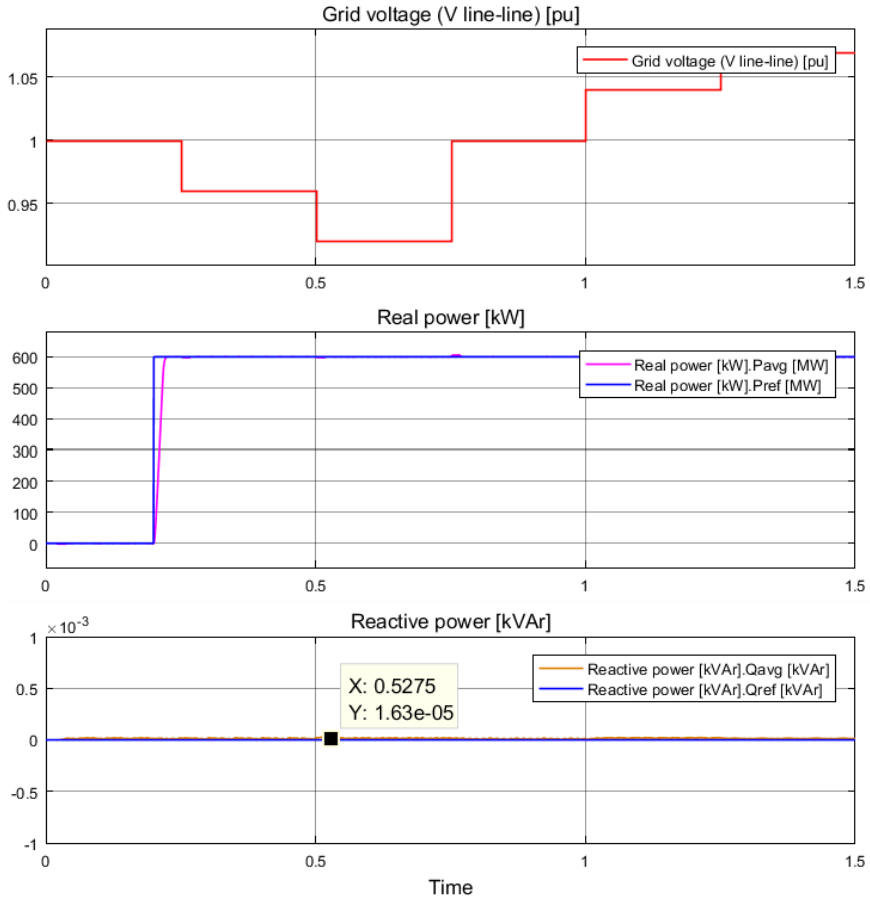

Figure 6.27: Smart inverter test – Variable grid voltage applied to the system and inverter in Unity Power Factor control mode

Figure 6.27 shows the inverter supplies 600 kW real power when the grid voltage varies. Its current output varies with varying grid voltage but its real power output is kept constant. No reactive power is delivered or absorbed from the grid.

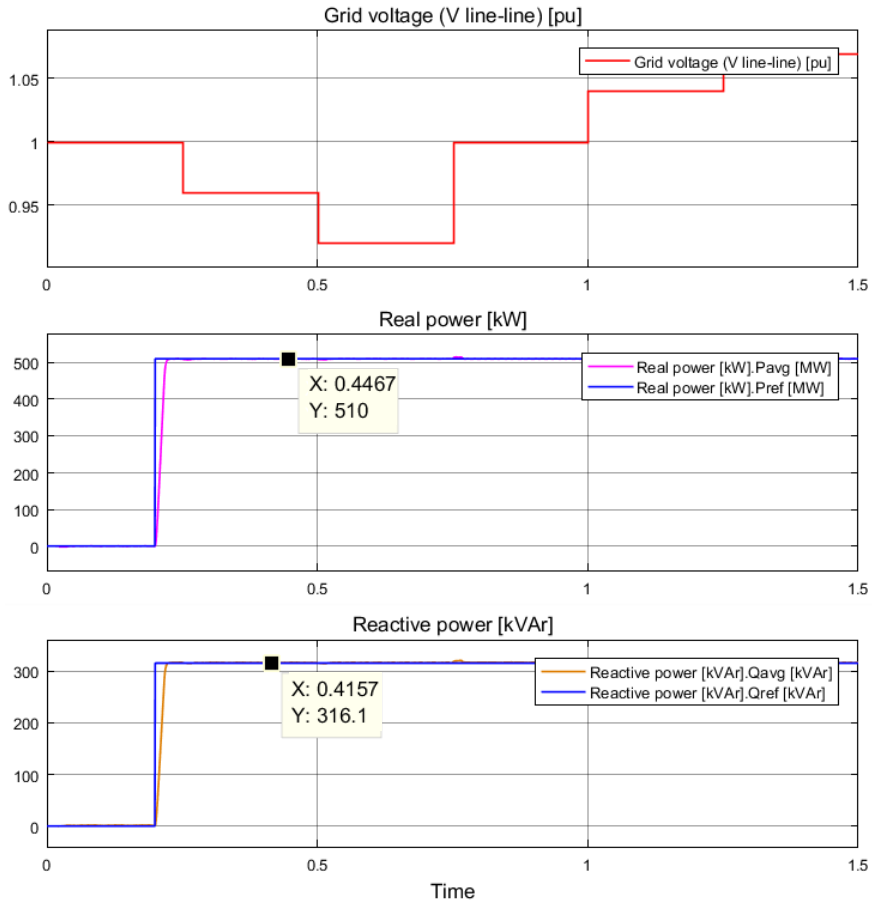

Figure 6.28: Smart inverter test – Variable grid voltage applied to the system and inverter in 0.85 lagging Fixed Power Factor control mode

Figure 6.28 shows the inverter supplies fixed real power (510 kW) and fixed reactive power (316.1 kVAr) when the grid voltage varies. The reactive power output remains constant as the grid voltage varies.

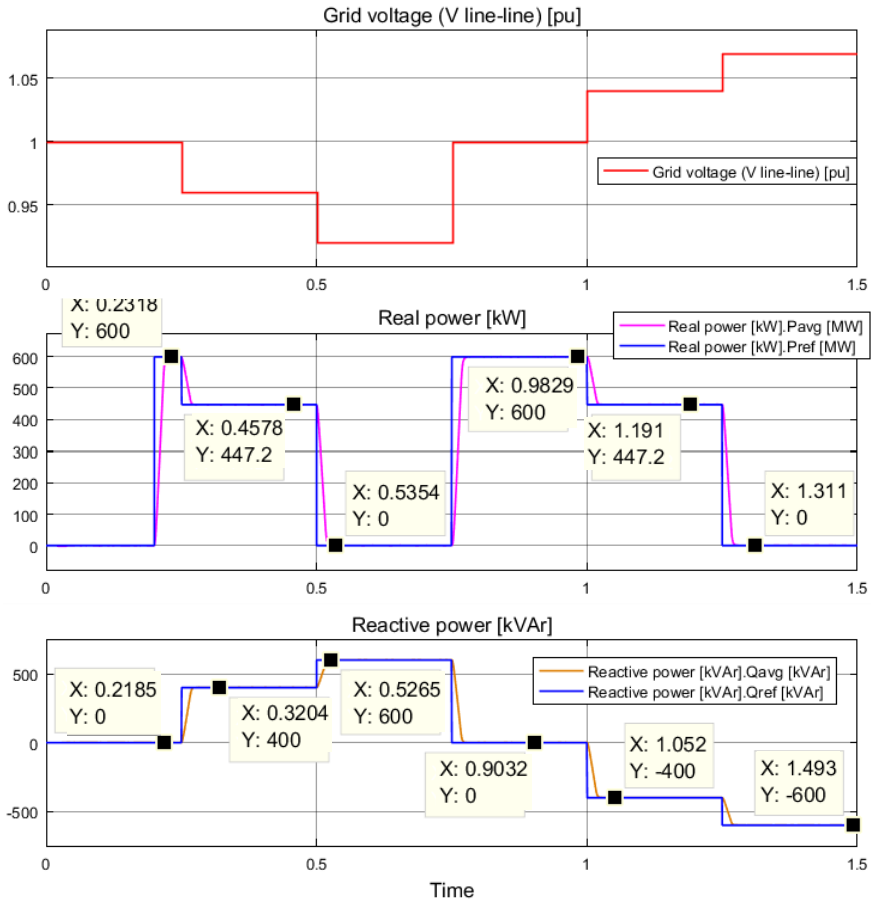

Figure 6.29: Smart inverter test – Variable grid voltage applied to the system and inverter in Volt-Var control mode

Figure 6.29 shows that the inverter absorbs and injects different amounts of reactive power as the grid voltage varies. In the Volt-Var control mode, reactive power is given priority over real power. Hence, the inverter's real power output depends on the amount of reactive power injected or absorbed by the inverter.

Scenario 3 – IEEE 1547 requirements – voltage deviation: The objective of this simulation is to test whether the inverter remains connected to the grid or disconnects when a voltage violation is detected for a duration of time specified by IEEE 1547 grid interconnection requirements. The inverter is controlled in Unity Power Factor mode and the grid voltage is reduced as shown in Figure 6.30. IEEE 1547 requires inverters to remain connected for 0.16 s when voltage deviations are less than 0.45 pu (Table 2.1).

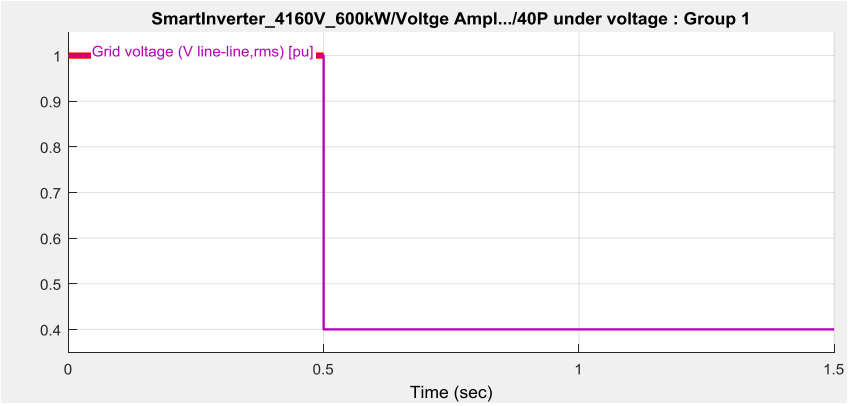

Figure 6.30: Grid voltage for simulation scenario 3

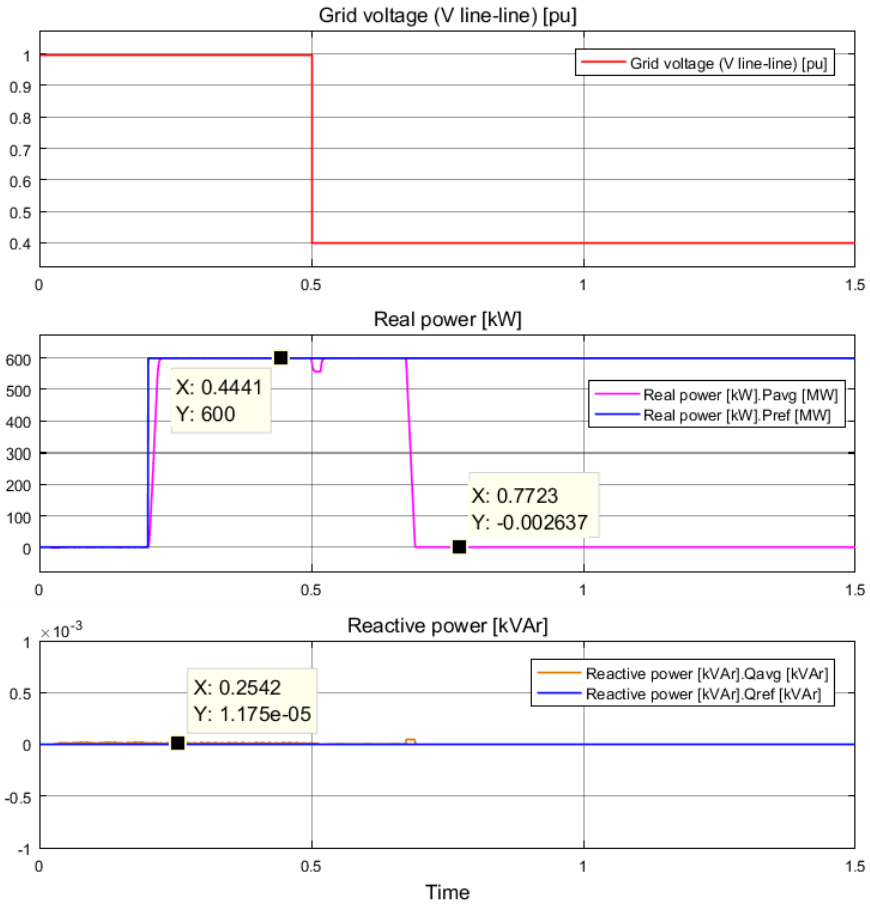

Figure 6.31: IEEE 1547 test – 0.4 pu grid voltage deviation and inverter in Unity Power Factor control mode

Figure 6.31 shows that the inverter remains connected for 0.16 s when the grid voltage is reduced to 0.5 pu. When the grid voltage is reduced to 0.5 pu at 0.5 s, the current output of the inverter increases to keep its power output at 600 kW. After 0.16 s

time duration (i.e. at 0.66 s), the inverter disconnects from the grid and current injection stops. The inverter's controller remains connected to the grid, as required by IEEE 1547, so that the inverter connects to the grid when grid voltage returns to its nominal value.

The simulation is repeated with grid voltage deviation shown in Figure 6.32. For voltage deviation of 0.5 pu $\leq v_{grid} <$ 0.88 pu, IEEE 1547 requires the inverter to stay connected for 2 s.

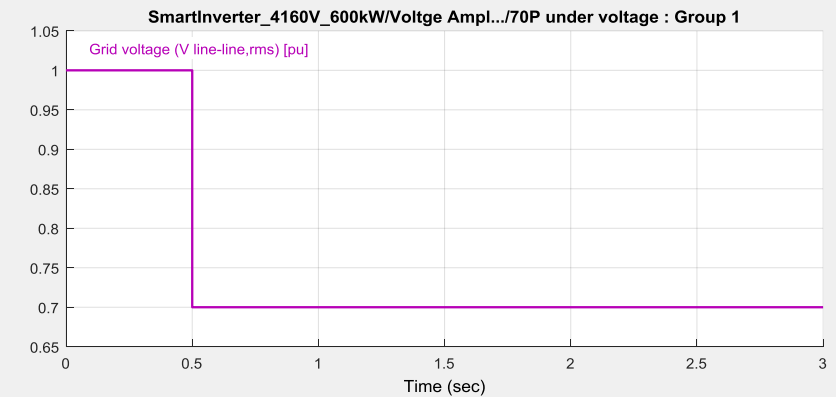

Figure 6.32: Grid voltage for simulation scenario 3

Figure 6.33 shows that the inverter remains connected for 2 s when the grid voltage is reduced to 0.7 pu. When the grid voltage is reduced to 0.7 pu at 0.5 s, the current output of the inverter increases to keep its power output at 600 kW. After 2 s time duration (i.e. at 2.5 s), the inverter disconnects from the grid and current injection stops. The inverter's controller remains connected to the grid, as required by IEEE 1547, thus the inverter connects to the grid when grid voltage returns to its nominal value.

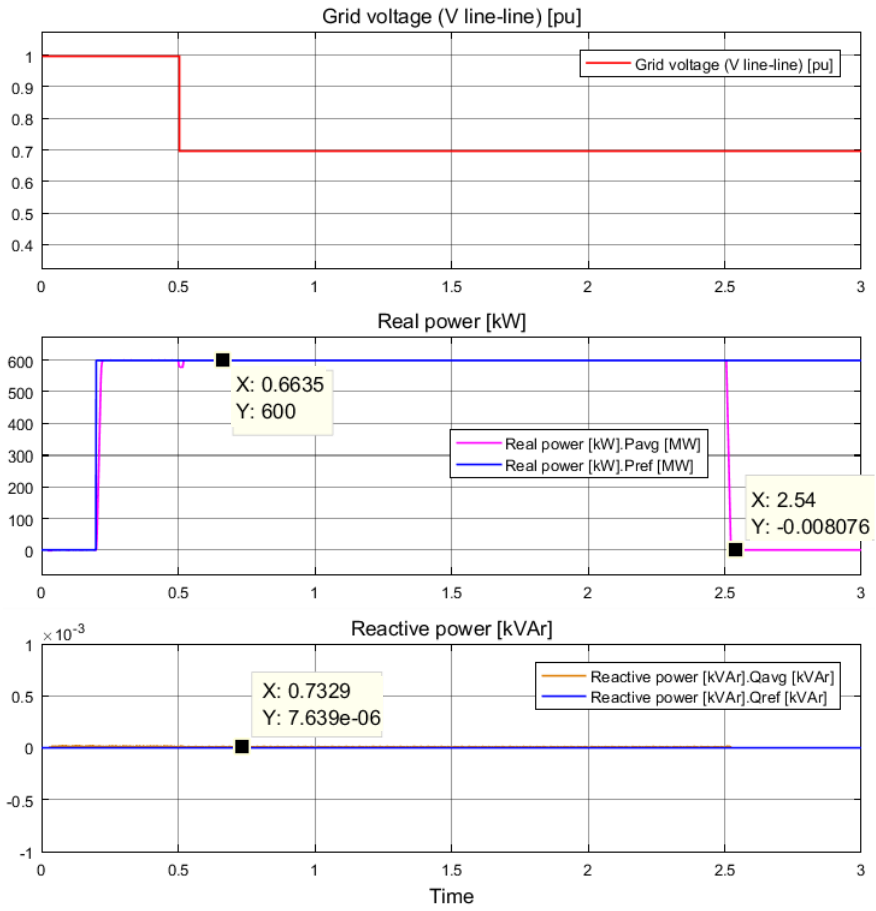

Figure 6.33: IEEE 1547 test – 0.5 pu ≤ v_{grid} < 0.88 pu deviation and inverter in Unity Power Factor control mode

<u>Scenario 4 – IEEE 1547 requirements – frequency deviation:</u> The objective of this simulation is to test whether the inverter remains connected to the grid or disconnects when a frequency violation is detected for duration of time specified by IEEE 1547 grid interconnection requirements. The inverter is controlled in Unity Power Factor mode and the grid frequency is increased as shown in Figure 6.34. IEEE 1547 requires inverters to remain connected for 2 s when frequency deviation is 60.5 < f < 62 (Table 2.2).

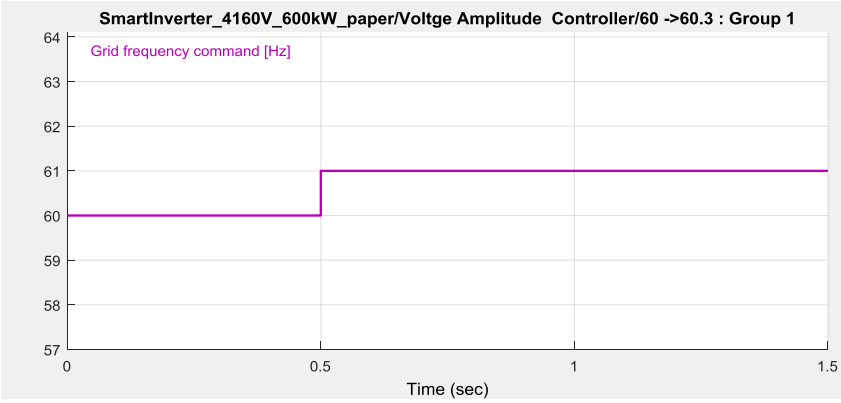

Figure 6.34: Grid frequency for simulation scenario 4

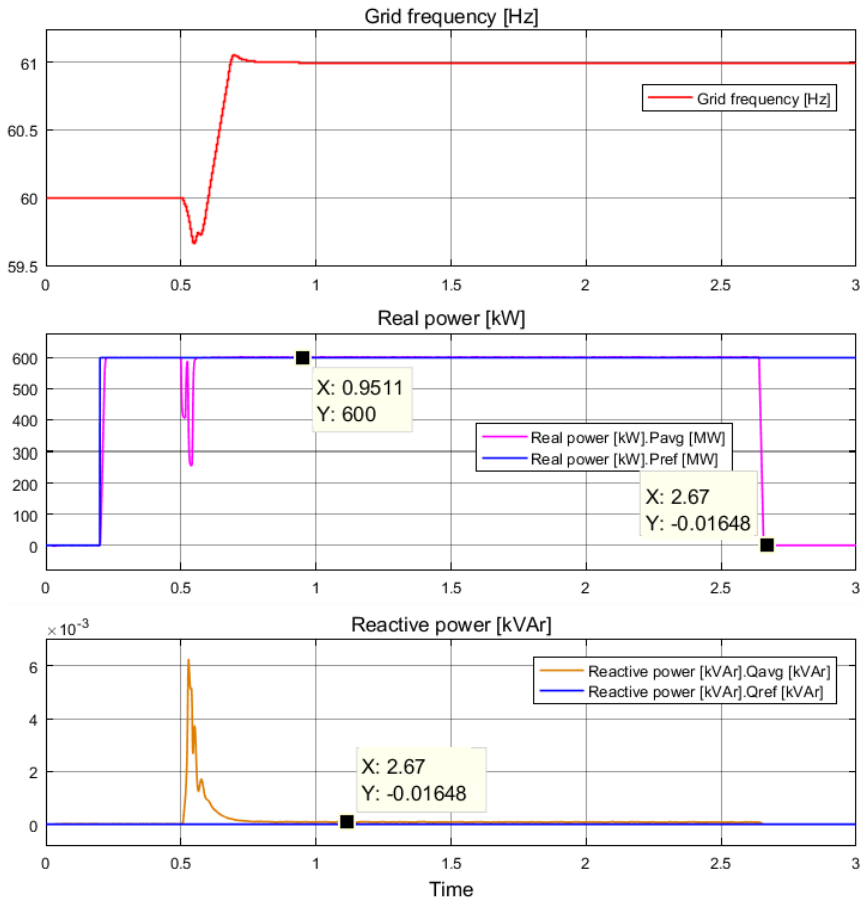

Figure 6.35: IEEE 1547 test – 60.5< f < 62 deviation and inverter in Unity Power Factor control mode

Figure 6.35 shows that the inverter remains connected for 2 s when the grid frequency is increased from 60 Hz to 61 Hz.

6.5. Chapter Summary

In this chapter, dynamic equations of a current-controlled, two-level, three-phase inverter are investigated. Based on the dynamic equations, open-loop and close-loop gains of the inverter system are formulated. A compensator for real and reactive power control is designed based on circuit time constant (t) and inductance of the filter circuit. Waveforms of filter inductor current and DC bus capacitor are analyzed to determine required inductor and capacitor sizes. DC port control method is investigated in case of a variable DC source being connected to the inverter.

A smart inverter model is developed in Matlab/Simulink software. One of the objectives of this model is reusability. Therefore, user-interface is provided to customize the DC bus, inverter, and AC side parameters of the inverter system. Grid interconnection requirements of IEEE 1547 are implemented in the inverter model. The inverter stays connected for set durations of time, as required by IEEE 1547, in the case of grid voltage and frequency deviations from their nominal values.

In order to verify and validate the smart inverter, a 600 kVA test system is created. DC bus voltage level, filter inductor size, DC bus capacitor size, and real and reactive power compensator values are calculated. The smart inverter model parameters are updated via the user-interface to reflect the calculated values. Grid voltage and frequency values are varied to different levels, and the inverters' performance under these variable grid conditions is investigated. The inverter tracks step change with no overshoot and 20 ms settling time. The Total Harmonic Distortion (THD) of current supplied by the inverter is 2.16%, which is well below the 5% requirement of IEEE 1547. The inverter injects no reactive power when it is controlled in Unity Power Factor mode. It injects fixed real and reactive power when it is controlled in Fixed Power Factor mode. The inverter injects variable real and reactive power when controlled in Volt-Var control

mode. Finally, the inverter remains connected to the grid for variable time durations during various voltage and frequency deviations as required by IEEE 1547.

CHAPTER 7: TRANSIENT PERFORMANCE OF IEEE 13 NODE TEST FEEDER

7.1. Introduction

As the penetration level of PV in a distribution feeder increases, the capacity of a conventional synchronous generator that supplies power to a feeder needs to be reduced relatively. During normal operational conditions, power from a PV system and conventional generators is balanced and the power system remains stable. An increase or decrease in system frequency is usually an indication of power imbalance in the system. When a frequency imbalance occurs in a system, conventional generators try to adjust their power outputs. However, adjustments in power outputs take time due to inertia. PV systems do not have a rotating mass. They have no inertia and do not participate in frequency regulation. Their power output goes from 100% to 0% in just few milliseconds.

When a large synchronous generator is tripped or a large load is suddenly connected to the system, the frequency of the system reduces. Utility operators have load-shedding schemes and disconnect loads from feeders when frequencies vary from the nominal value. This load-shedding effect is significant when PV penetration in the system is higher. Since the PV system is also tripped due to low frequency, further load-shedding is needed in order to keep the system frequency at its nominal value. In order to mitigate the effects of frequency deviation, incorporation of virtual inertia (artificial inertia) in a feeder with higher PV penetration level, lower number of conventional generators, and fast but inertia-less PV systems is needed.

In order to investigate the transient behavior of a feeder with higher PV penetration than power demand by its loads, the IEEE 13 Node Test Feeder is modeled in Matlab/Simulink software. PVs are connected at different nodes of the feeder with a total

penetration level of 120%. An Energy storage system is connected to the feeder to provide virtual inertia during frequency deviations. Section 7.2 describes the modeling, validation, and verification of the IEEE 13 Node Test Feeder in Matlab/Simulink. Section 7.3 describes the modeling of PV system using the Smart Inverter model discussed in chapter 6. Section 7.4 describes the modeling of a battery management system while section 7.5 describes the transient simulation of the IEEE 13 Node Test Feeder with 120% a PV penetration and a battery management system. Section 7.6 summarizes the work performed in this chapter.

7.2. IEEE 13 Node Test Feeder Model in Matlab/Simulink

This feeder is small and relatively short in length (8200 ft) compared to other IEEE test feeders. Larger feeders, as experienced from NEETRAC member feeders, take considerable simulation time. The purpose of this simulation is to investigate and mitigate the transient effect of system frequency deviations for short duration of time, hence, this feeder is selected. Some of key characteristics of this feeder are [71]:

- It has 13 nodes (buses) and a total length of 8200 ft. The longest line in the feeder is 2000 ft long.
- There exists one substation voltage regulator consisting of three single-phase transformers connected in wye (star) configuration. Each phase of the voltage regulator is controlled independently.
- There are single-phase, two-phase, and three-phase overhead and underground lines in the feeder.
- The feeder has two capacitor banks located at nodes 611 and 675. The capacitor bank at node 611 is a single-phase bank with a capacity of 100 kVAr while the capacitor bank at node 675 is a three-phase bank with 200 kVAr capacity on each phase.

- There exists one 500 kVA, 4.16/0.48 kV in-line transformer connected between nodes 633 and 634.
- There are balanced and unbalanced spot and distributed loads with Constant PQ, I, and Z-type connected in delta or wye configurations.

Figure 7.1 shows the single line diagram of the feeder [71].

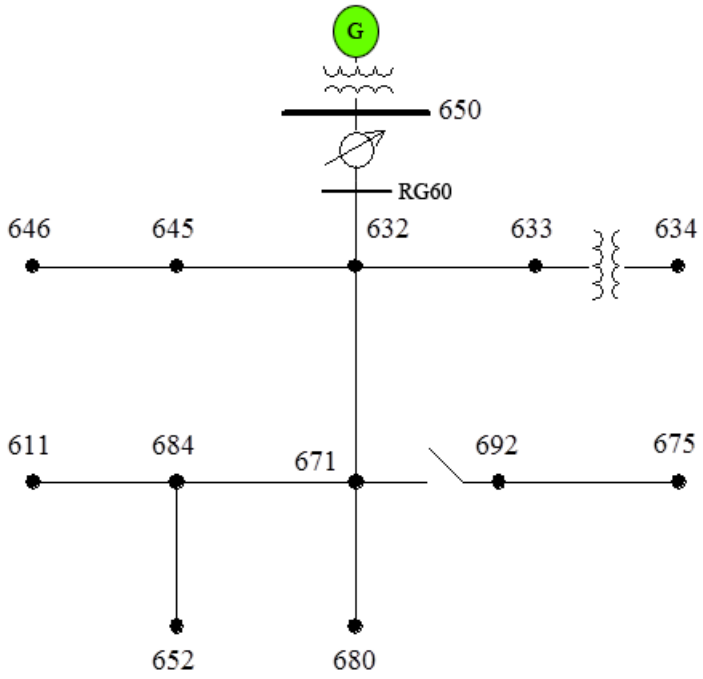

Figure 7.1: Single line diagram of IEEE 13 Node Test Feeder [71]

Figure 7.1 shows the location of the 13 nodes in the feeder. The secondary side of the substation transformer is connected to node 650 and node 650 in turn is connected to the voltage regulator. Circuit parameters of the feeder can be downloaded from the IEEE website [71].

In the Simulink library, there is a model of an IEEE 13 Node Test Feeder but this particular model uses phasor simulation type to solve power flow in the feeder [72]. The model does not include a substation transformer or a voltage regulator. A constant voltage source (i.e. external grid) with adjusted voltage outputs that match the published voltages of node 632 is directly connected to node 632, bypassing the substation

transformer and the voltage regulator. Another reason for not using this model is its use of a constant voltage source as external grid. In order to investigate the effect of system frequency deviation, a detailed model of a synchronous generator with inertia is needed.

7.2.1. **Modeling Voltage Regulator in Matlab/Simulink**

The Simulink library does not have an On Load Tap Changer transformer (OLTC transformer) model that uses continuous or discrete simulation type. The model that exists in the library uses phasor simulation type and is not suitable for the purpose of this research. A Type-B voltage regulator is one of the most common types used by utilities [73]. Figure 7.2 shows the control circuit of a typical voltage regulator.

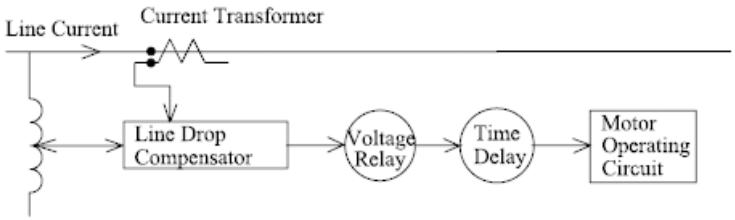

Figure 7.2: Voltage regulator control circuit [73]

Figure 7.2 shows that the control circuit of a typical voltage regulator consists of a Line Drop Compensator, a Voltage Relay, and a Time Delay block. The Line Drop Compensator block receives voltage and current measurements from the terminals of the transformer. Since voltage is not usually regulated at the terminals of the transformer but rather at a bus located at a distance from the regulator, this block calculates the voltage drop in the line connecting the transformer to the controlled bus. Impedance of the line connecting the transformer to the controlled bus is used to compute voltage drop in the line. This impedance is usually provided in units of volt [V]. The Voltage Relay block computes the necessary tap position of the voltage regulator. This is based on the voltage drop computed by the Line Drop Compensator block and the desired voltage level at the controlled bus. The Time Delay block accounts for time delay in the switching

mechanisms of the voltage regulator and provides ride-through capability during the transient period of a load change. Figure 7.3 shows Type-B voltage regulator windings.

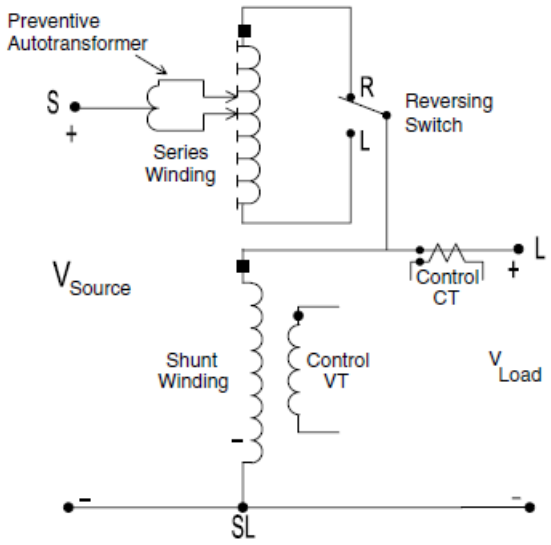

Figure 7.3: Type-B voltage regulator [73]

Figure 7.3 shows that the autotransformer uses a Reversing Switch to raise or lower the output voltage. It typically consists of 16 taps plus a neutral tap in the raise and lower positions. Each tap gives 0.0625 pu voltage increase or decrease (i.e. 16 taps give a total of ±10% voltage difference) on the output voltage of the transformer depending on the position of the Reversing Switch.

Figure 7.4 shows the User-Interface (mask) of the voltage regulator model developed in Simulink. It has two taps: Parameters and Control Settings. In the Parameters tap, the user enters parameters of the autotransformer (i.e. impedance, number of taps, and primary and secondary side voltage levels). In the Control Settings tap, a user enters settings of the controller (i.e. bandwidth, PT and CT ratios, load compensator settings, and desired voltage level at the controlled bus). Each phase of the voltage regulator is controlled individually. The model allows three modes of control: Manual, Automatic, and No Control. In Manual control mode, a user manually enters the tap settings and the voltage regulator maintains that tap position throughout the simulation.

In Automatic Control, the voltage regulator changes the tap position depending on voltage on the controlled bus. In No Control mode, the voltage regulator is disabled and the substation transformer is connected directly to the controlled bus (i.e. controlled bus voltage is not regulated).

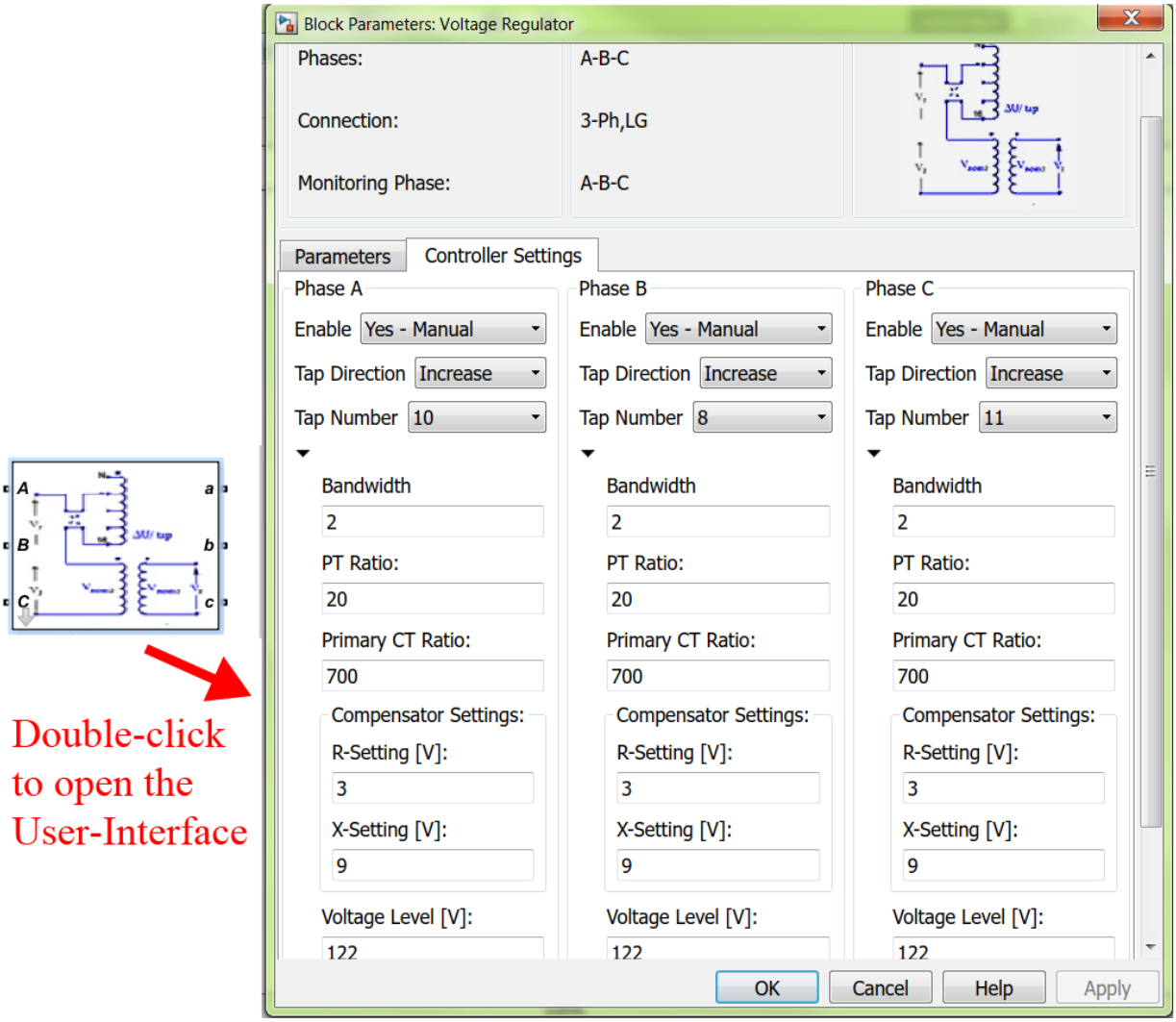

Figure 7.4: User-Interface of the voltage regulator model in Simulink

Figure 7.5 shows the second-layer of the voltage regulator model. There are three single-phase autotransformers connected in Wye (star) configuration. Each phase of the voltage regulator is controlled by its own controller. Parameters of the transformer and

the controller settings are passed from the User-Interface (mask) to the internal building blocks during model initialization by Simulink.

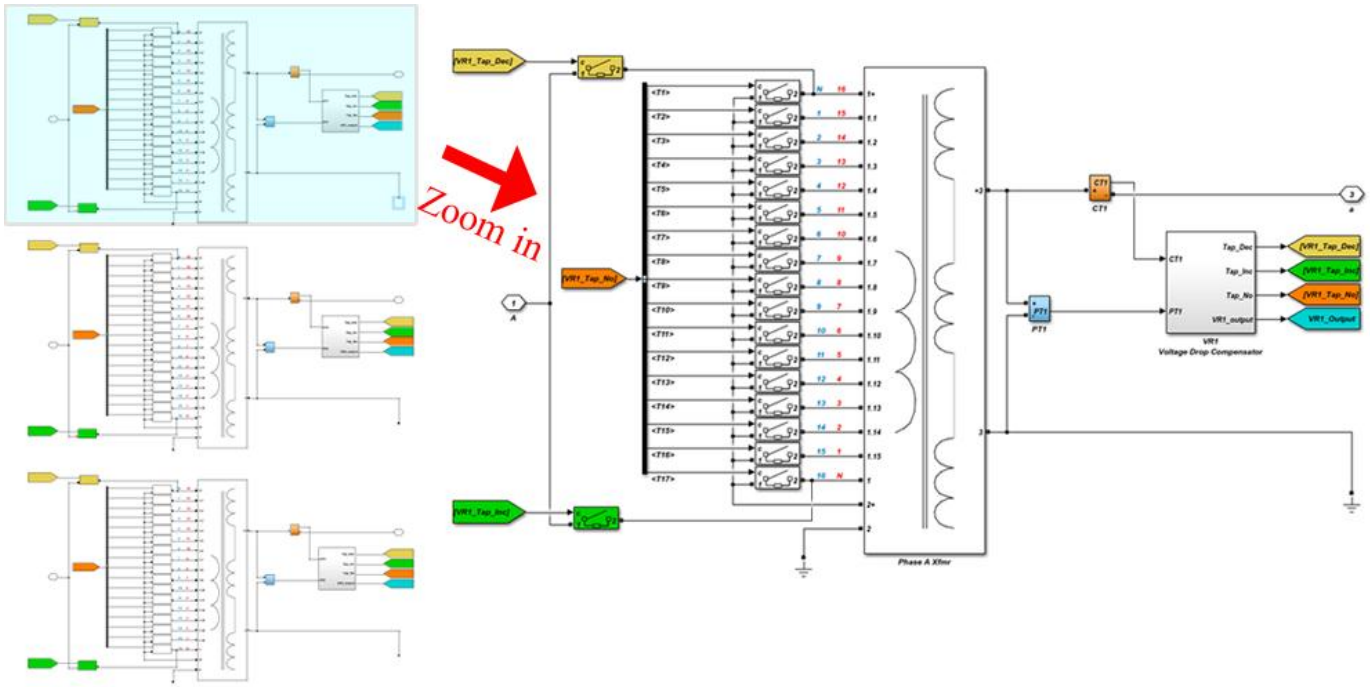

Figure 7.5: Second-layer of the voltage regulator model in Simulink

Figure 7.5 shows three single-phase autotransformers connected in Wye configuration. Each transformer is connected to a current transformer (CT) and a voltage transformer (PT). Individual controllers receive measured voltage and current at the terminals of a transformer. Based on user specified voltage level of the controlled bus, tap positions are adjusted. The primary side of each transformer is connected to 17 switches (including the neutral position switch) to select the required tap number. Two switches are used as Reversing Switch to change the polarity of the 16 tapped windings (upper windings of the primary side of the transformer). By changing the polarity of the 16 tapped windings, the output voltage of the transformer (i.e. the secondary side) is adjusted ±10% of the primary side voltage. The tap position and direction of the Reversing Switch are computed by the controller. Figure 7.6 shows the building blocks used inside a controller subsystem (third-layer of the model).

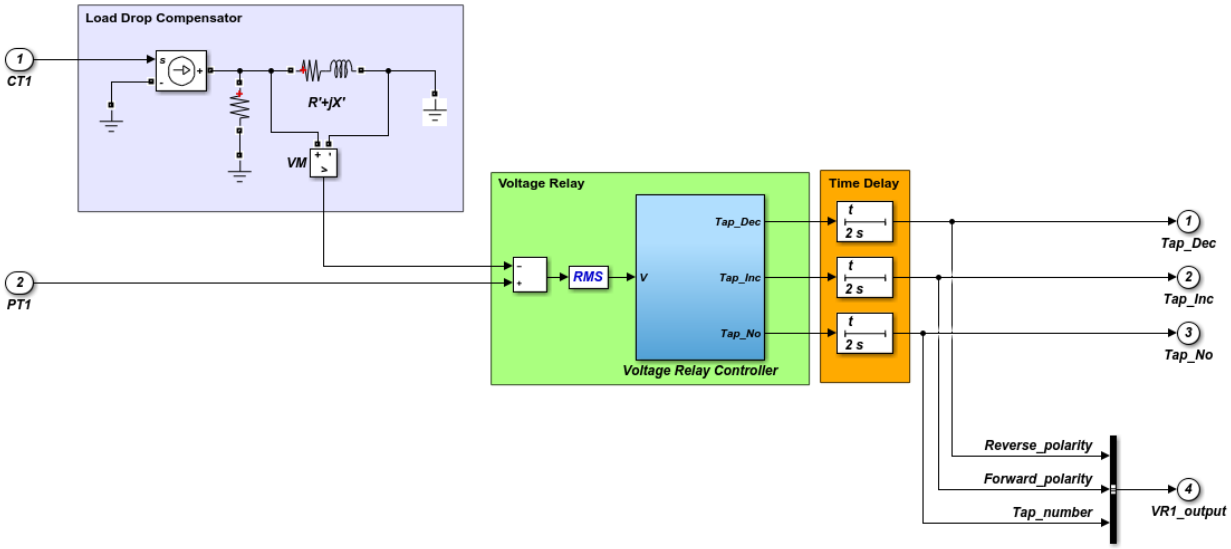

Figure 7.6: Building blocks used inside the Controller subsystem

Figure 7.6 shows the Load Drop Compensator, Voltage Relay, and Time Delay blocks created inside the Controller subsystem. The Load Compensator computes voltage drop on the line connecting the voltage regulator to the controlled bus. The Voltage Relay computes the required tap position of the voltage regulator based on voltage drop on the line and desired voltage level set by a user. The Time Delay block holds the outputs of the voltage regulator for a specified time duration to account for time delay in switching mechanism of the voltage regulator. This Time Delay block is also set to account for ride-through capability during a transient periods of sudden load change.

Figure 7.7 shows the building blocks used inside the Voltage Relay Controller subsystem. Voltage by PTs and Load Drop Compensator output voltage is measured, and the difference is input to the subsystem. A Matlab script is created to compute the necessary tap number and the Reversing Switch position (i.e. it is shown for phase A. Phases B and C scripts are similar to that of phase A).

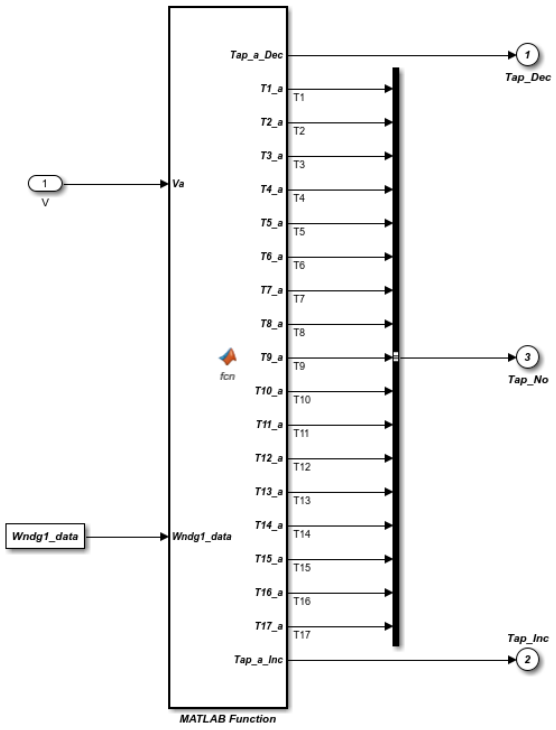

Figure 7.7: Building blocks used inside the Voltage Relay Controller subsystem

To validate and verify the model, published results of the IEEE 13 Node Test Feeder voltage controller settings are used. Table 7.1 summarizes published voltage regulator settings, while Table 7.2 summarizes published voltage profiles of nodes RG60 and 632.

Table 7.1: Voltage regulator settings used in the published results of IEEE 13 Node Test Feeder

Phases A, B, and C, Wye configuration. Bandwidth = 2.00						
Phase	Volt Hold	R [V]	X [V]	PT Ratio	CT Ratio	Tap
1	122	3.00	9.00	20.00	700.00	10
2	122	3.00	9.00	20.00	700.00	8
3	122	3.00	9.00	20.00	700.00	11

Table 7.2: Published voltage profiles of Nodes RG60 and 632

Node	A-N [pu]	B-N [pu]	C-N [pu]
RG60	1.0625	1.0500	1.0687
632	1.0210	1.0420	1.0174

The voltage regulator output is connected to node RG60, but it controls voltage on node 632 that is connected to node RG60 using a 2000 ft overhead line. Figure 7.8 shows the test circuit constructed that is similar to the IEEE 13 Node Test Feeder.

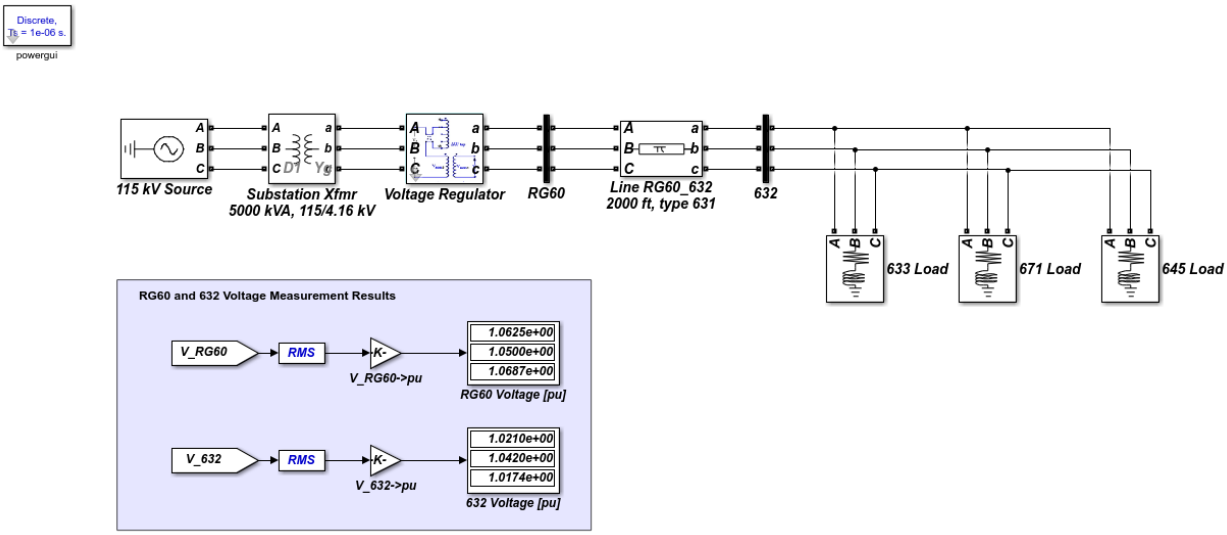

Figure 7.8: Test circuit used to validate the voltage regulator model

Node 632 supplies power to nodes 633, 671, and 645. From the published results of the IEEE 13 Node Test Feeder, the power delivered to these nodes are modeled as loads and connected to node 632 as shown in Figure 7.8. The high side of the substation transformer is connected to a 115 kV voltage source and the low side of the transformer is connected to the voltage regulator. The voltage regulator is configured using the settings in the published result (Table 7.1). A 2000 ft line is connected between nodes RG60 and 632. Impedance of this line is taken from the published data of the line. Measured voltages at nodes RG60 and 632 are similar to the published voltage profiles of the nodes (Figure 7.8 and Table 7.2).

The voltage regulator along with seven PV systems and a battery management system are used in the IEEE 13 Node Test Feeder to investigate the transient performance of the feeder when PV penetration is 120%.

7.2.2. **Steady State Simulation Results**

Figure 7.9 shows the single line diagram of the feeder in Simulink. In the substation subsystem, a 115 kV source, a 5000 kVA step-down transformer, a voltage regulator, and a line connecting the voltage regulator to node 632 exist.

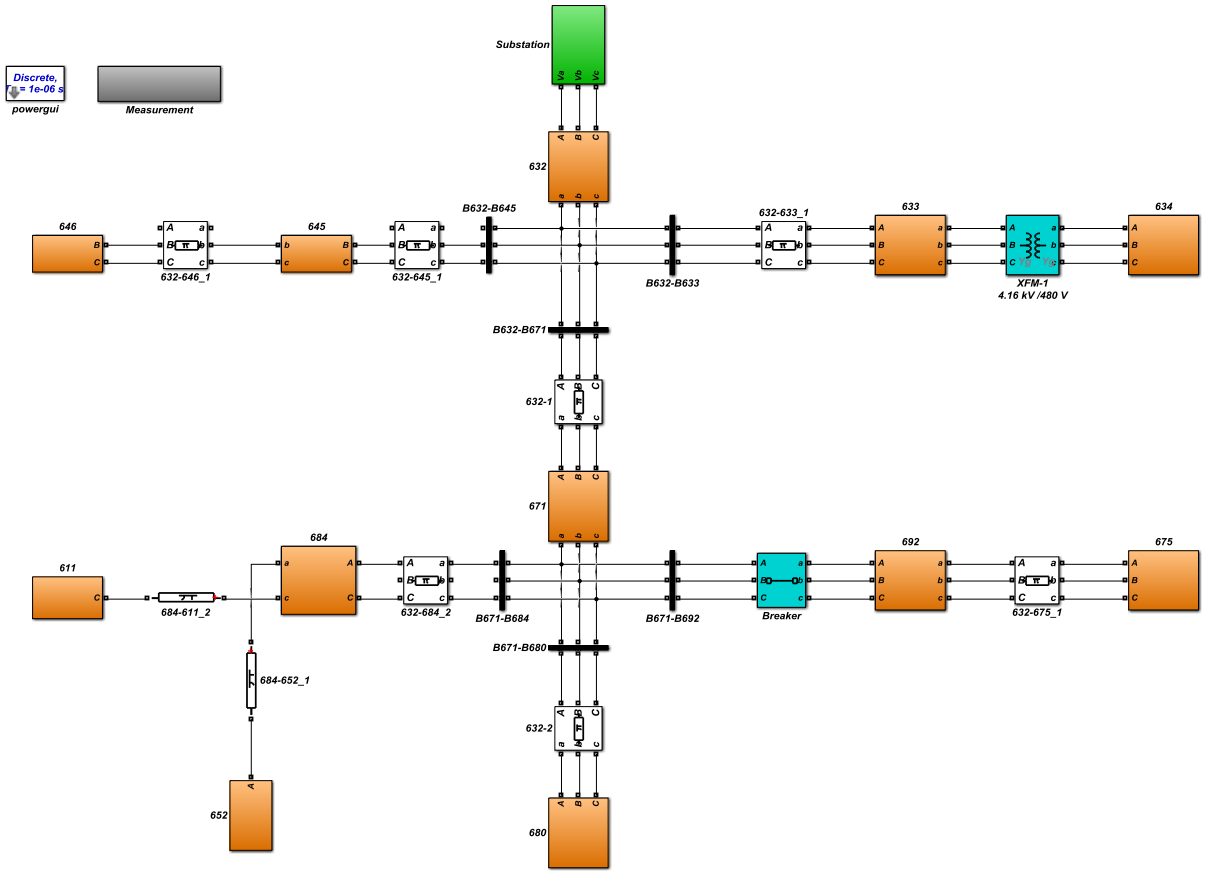

Figure 7.9: Single line diagram of IEEE 13 Node Test Feeder in Simulink

The results of the model are compared against the published results of the feeder, and the maximum percent difference in voltage magnitude and angle are 0.3036% and 4.3421% respectively (node 684, phase A). Table 7.3 summarizes the comparison result.

Table 7.3: Power flow results comparison between Simulink and the published model

	Phase A		Phase B		Phase C	
Node	Magnitude [%]	Angle [%]	Magnitude [%]	Angle [%]	Magnitude [%]	Angle [%]
650	0.0000	0.0000	0.0000	0.0000	0.0000	0.0000
RG60	0.0000	0.0000	0.0000	0.0000	0.0000	0.0000
632	0.0000	0.0000	0.0000	0.0164	0.0393	0.0255
633	0.0000	0.0391	0.0096	-0.0246	-0.0197	0.0170
634	0.0201	-0.1858	-0.0196	0.0164	0.0100	-0.0511
645	-	-	-0.0097	0.0000	0.0492	-0.0339
646	-	-	0.0097	-0.0164	0.0395	0.0000
671	0.2929	-4.3208	0.0855	-0.0490	-0.0205	0.0172
680	0.2929	-4.3208	0.0855	-0.0490	-0.0205	0.0172
684	0.3036	-4.3421	-	-	-0.2362	0.0173
611	-	-	-	-	0.0308	-0.0173
652	0.2952	-4.3238	-	-	-	-
692	0.2929	-4.1055	0.0855	-0.0490	-0.0307	0.0172
675	0.2949	-3.8489	0.1232	-0.0653	-0.0205	0.0259

7.3. PV Power Generation Model in Simulink

The purpose of this model is to connect it to a grid-tied inverter (discussed and modeled in Chapter 6) and create a PV system. The PV system is used in the IEEE 13 Node Test Feeder model.

The PV power generation plant consists of PV arrays connected in series and parallel to a DC-DC boost converter. A maximum power point tracking algorithm (MPPT) tracks the maximum power output of the PV power plant under different solar irradiation and cell temperature conditions. The electrical model of a PV power plant and the maximum power point tracking algorithms are discussed in section 2.2. Simulink provides this PV power plant model in its library. The model is highly customizable and users have the ability to input their own manufacturer data.

The PV array output voltage is usually lower than the DC bus voltage. Hence a DC-DC boost converter is used. As discussed in section 6.2.1 and expressed in equations (6.28) and (6.29), the DC bus voltage level is selected considering the worst-case operational scenario. Figure 7.10 shows a PV power plant connected to a DC-DC boost converter. The controller adjusts the duty cycle of the converter based on PV voltage and MPPT.

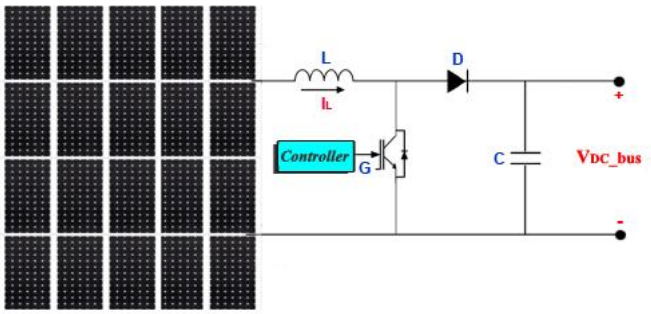

Figure 7.10: PV power plant connected to a DC-DC boost converter

The DC-DC converter consists of a filter inductor, a switch, a diode, and a filter capacitor as shown in Figure 7.10. The MPPT tracks the maximum power point of the PV arrays and the controller provides the duty cycle (D) for the DC-DC boost converter. Equation 7.1 describes the relationship between PV voltage and DC bus voltage (i.e. duty cycle, D). Equation 7.2 describes the inductor size required for continuous current mode of operation (CCM) in the inductor based on allowed ripple current (Δi_L), switching frequency (f), and duty cycle (D) [74].

$$D = 1 - \frac{V_{PV}}{V_{DC}} \tag{7.1}$$

$$L = \frac{V_{PV} D}{\Delta i_L f} \tag{7.2}$$

The size of a filter capacitor that allows for a maximum ripple voltage (ΔV_{DC}) on the DC bus is described by equation (7.3) [74]. Since the PV power plant and the DC-DC

converter are finally connected to a grid-tied inverter, the size of the filter capacitor is calculated for the worst-case scenario DC bus voltage level as described by equation (6.36).

$$C = \frac{D}{R\left(\frac{\Delta V_{DC}}{V_{DC}}\right) f} \tag{7.3}$$

$$R = \frac{{V_{DC}}^2}{P_{PV}} \tag{7.4}$$

Where R is the Thevenin equivalent impedance of the system connected to the DC bus.

A PV power plant with DC-DC boost converter is modeled in Simulink. Figure 7.11 shows the User-Interface of the model. The User-Interface provides two taps: PV Array and DC-DC Boost Converter. In the PV Array tap, a user enters parameters of the PV array (i.e. number of PV modules connected in series and parallel). The model uses SunPower SPR-290-WHT-U PV module manufacturer data provided by the Simulink PV model. Power outputs of the PV array are configured by adjusting the number of PV modules connected in series and parallel. The DC-DC Boost Converter tap allows users to configure sizes of the filter inductor and capacitor and select the switching frequency of the converter. It also provides a user the option of choosing between Perturb and Observe or Incremental Conductance maximum power point tracking algorithms. Figure 7.12 shows the building blocks used under the User-Interface.

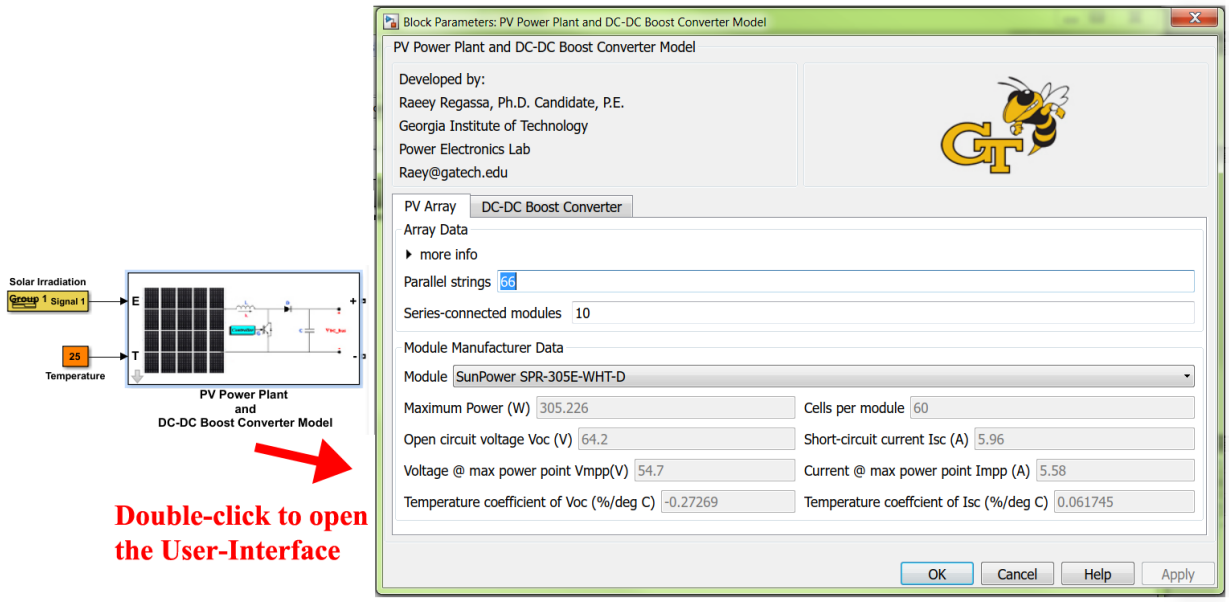

Figure 7.11: User-Interface of the PV Power Plant and DC-DC Boost Converter model in Simulink

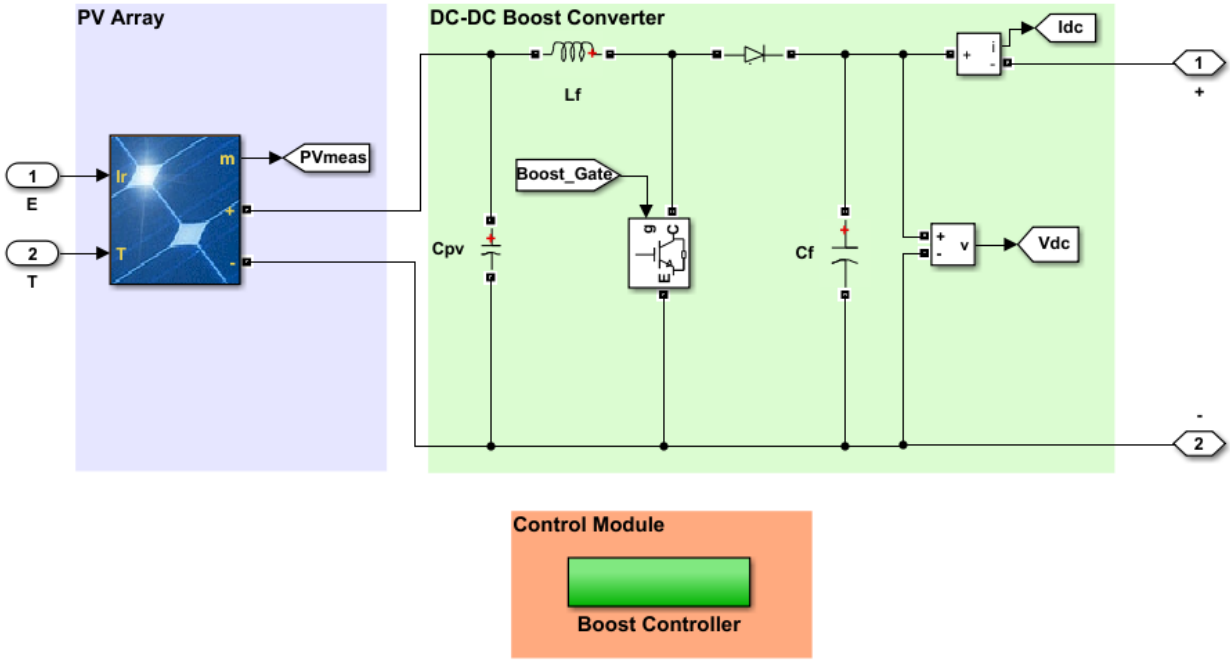

Figure 7.12: Building blocks used under the User-Interface

The number of series and parallel connected PV module parameters are passed from the User-Interface to the PV Array model. This model is provided by the Simulink library. The output terminals of the PV Array model are connected to the DC-DC Boost

Converter. The Boost Controller subsystem implements the MPPT algorithm selected by a user (at the User-Interface) and controls the IGBT switch. Figure 7.13 shows the building blocks used under the Boost Controller subsystem.

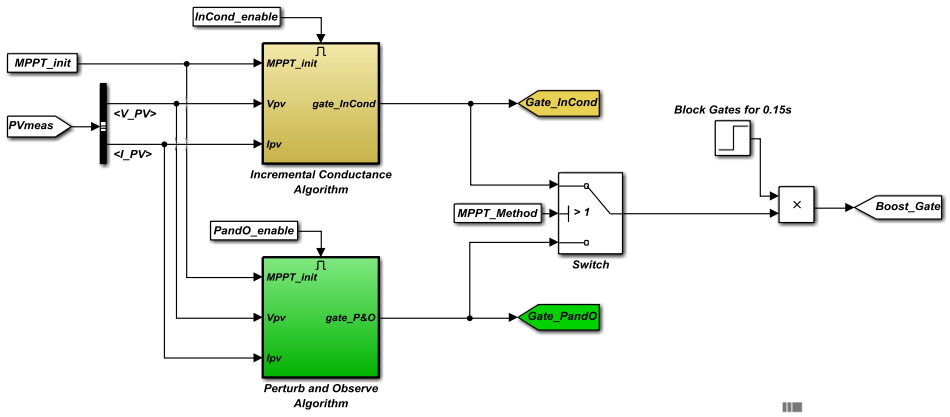

Figure 7.13: Building blocks used inside the Boost Controller subsystem

In the Boost Controller subsystem, an MPPT algorithm is implemented to generate a gating signal. During the simulation, only one of the two MPPT algorithm subsystems shown in Figure 7.13 is enabled based on the user's selected method. Figure 7.14 shows the building blocks used inside the Incremental Conductance Algorithm and Perturb and Observe Algorithm subsystems. Matlab scripts used in the subsystems are shown in Appendix D.

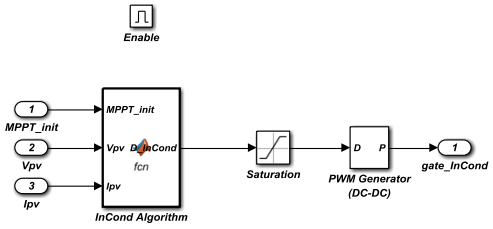

a) Incremental Conductance Subsystem

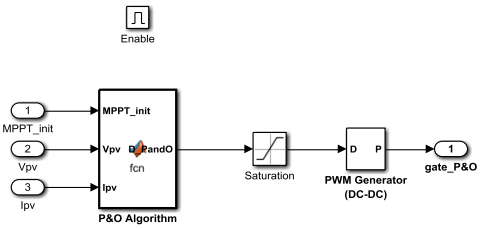

b) Perturb and Observe Subsystem

Figure 7.14: Building blocks used inside the Incremental Conductance and the Perturb and Observe subsystems

In order to validate and verify the model, a 600 kW PV power plant is designed. The PV power plant is connected to a DC-DC boost converter, and the converter is connected to a constant impedance load. The following parameters are used:

- 22 modules are connected in parallel (i.e. $I_{PV} = 119.9$ A)
- 94 modules are connected in series (i.e. $V_{PV} = 5010.2$ V)
- PV array output power at maximum power point, $P_{PV} = 600.7$ kW
- DC bus voltage level is 8900 V
- Using equation (7.1), calculated duty cycle is 0.437056
- 5 kHz is selected for switching the DC-DC converter
- Using equation (7.2) and allowing 10% ripple on filter inductor current, calculated inductor size is 36.5 mH
- Using equations (7.3), (7.4) and allowing 1% ripple on filter capacitor voltage, calculated capacitor size is 66.5 μF
- Using equation (7.4), load connected to output terminals of the DC-DC converter is 131.858 Ω
- Variable solar irradiation as shown in Figure 7.15 and a constant temperature of 25°C is applied to the model
- Perturb and Observe MPPT algorithm is selected
- Block the DC-DC boost converter for 0.01 s at the beginning of the simulation

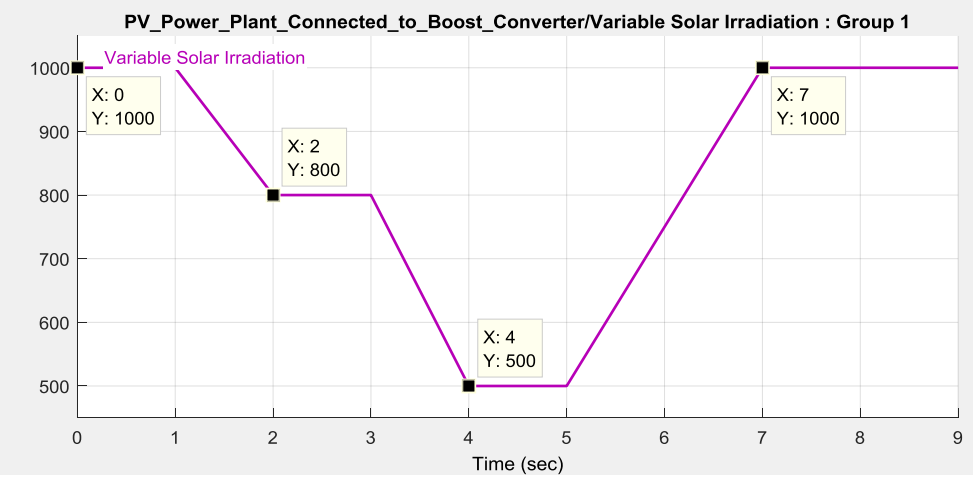

Figure 7.15: Variable solar irradiation applied to the 600 kW PV Power Plant with DC-DC Boost Converter

The simulation begins with 1000 $\frac{w}{m^2}$ solar irradiation. At t=1 s, solar irradiation begins to decrease and reaches 800 $\frac{w}{m^2}$ at t=2 s. It remains constant for the next 1 s and begins to decrease at t=3 s. At t=4 s, it reaches 500 $\frac{w}{m^2}$ and remains constant for the next 1 s. At t=5 s, it begins to increase and reaches 1000 $\frac{w}{m^2}$ at t=7 s. It remains constant for the next 2 s. Figure 7.16 shows the single line diagram of the test circuit, while Figure 7.17 shows scope capture of the PV plant power output and power delivered to the load.

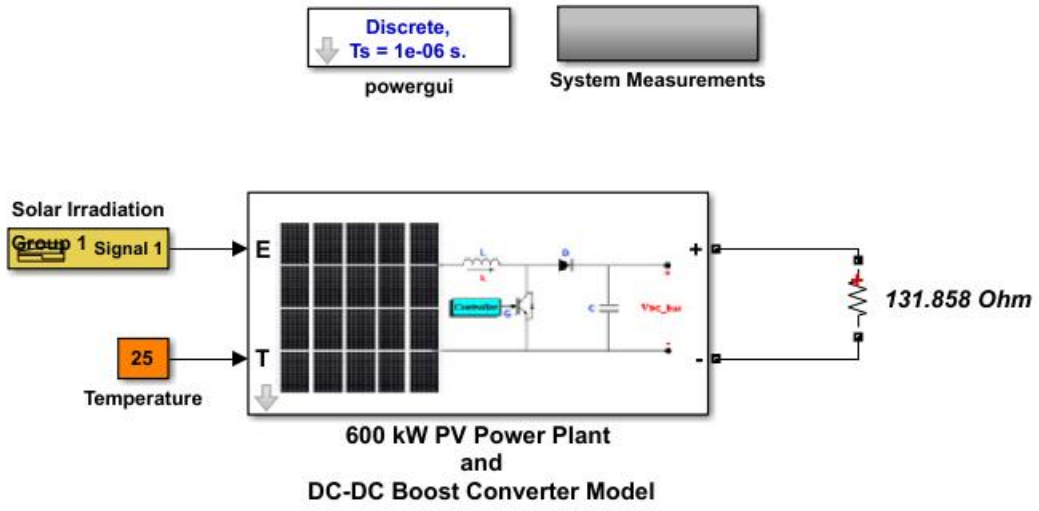

Figure 7.16: Single line diagram of PV power plant with DC-DC boost converter test circuit

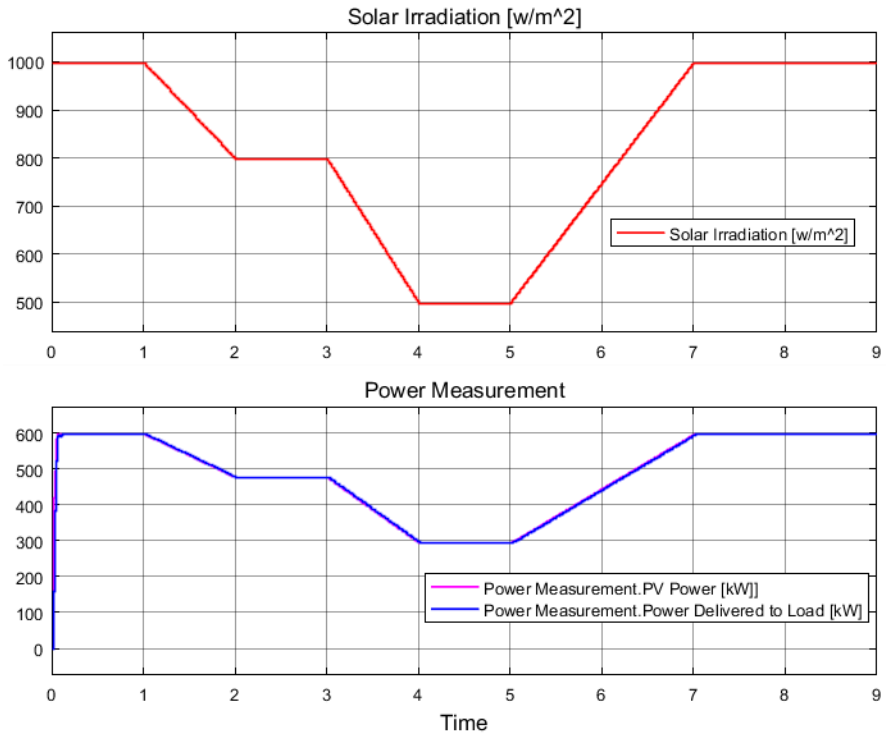

Figure 7.17: PV Array output power and power delivered to the load [kW]

Figure 7.17 illustrates that the MPPT algorithm tracks the maximum power point of the PV array when solar irradiation varies and the DC-DC converter delivers the maximum available power. The output power of the PV array and power delivered to the load vary by the same percentage as the varying solar irradiation.

Next, the model is connected to a smart grid-tied inverter (modeled in Chapter 6) to create a 600 kW PV system. The purpose of this PV system is to deploy it at seven different nodes of the IEEE 13 Node Test Feeder. The seven PV systems give 120% PV penetration level in the feeder.

In Section 6.4 of Chapter 6, a 600 kW smart inverter is designed. Its current controller is tuned by selecting a time constant of 2 ms. In order to tune the DC bus controller, Simulink's PID Tuner App is used. The open-loop transfer function of the inverter, as expressed by equation (6.33) and shown in Figure 6.5, is created in the PID Tuner App. Figure 7.18 and Figure 7.19 show a step response and bode plots of the open-loop gain respectively.

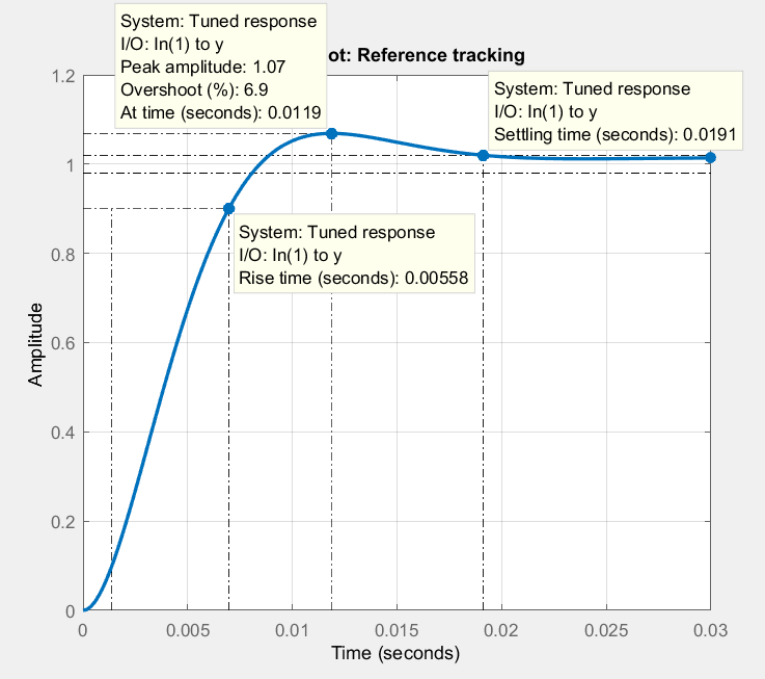

Figure 7.18: Step response of DC bus voltage controller

Figure 7.18 shows that the DC bus voltage controller has an overshoot of 6.9%, a rise time of 5.58 ms, and a settling time of 19.1 ms. The design requirements are for the controller to have less than 10% overshoot, a settling time of less than 10 ms, and a zero steady state error. The tuned controller response satisfies the design requirements.

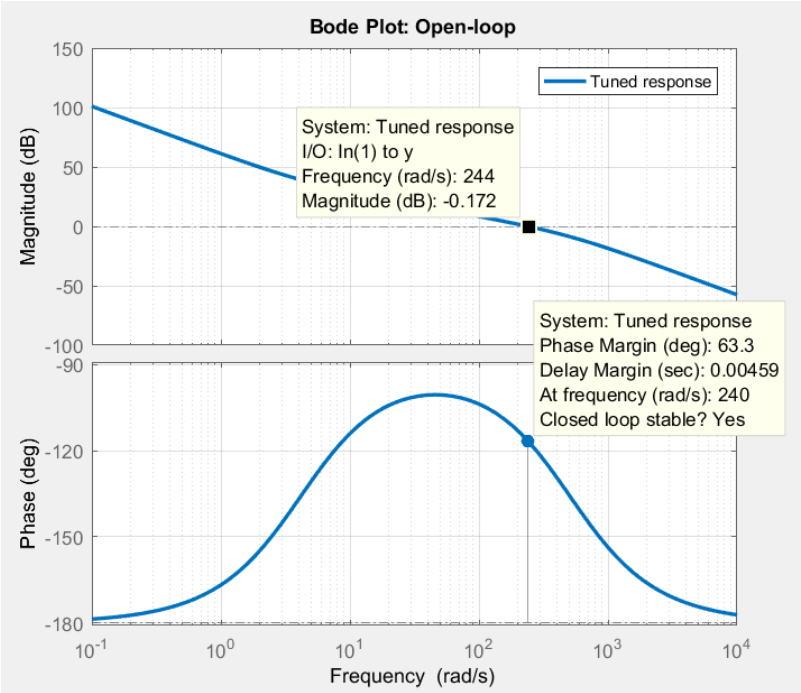

Figure 7.19: Bode plot of the open-loop response

Figure 7.19 shows that the controller has a cut-off frequency of 240 rad/s, which is half the bandwidth of the current controller bandwidth (i.e. for τ_i = 2 ms, the current controller has a bandwidth of 500 rad/s). The magnitude curve crosses the 0dB axis with -20dB/dec slope. The phase margin is 63.3° at the cut-off frequency. The controller is stable in both steady state and transient operations.

To validate and verify the PV system, it is connected to a 4.16 kV grid as shown in Figure 7.20. The smart inverter is controlled in Unity Power Factor mode. Initially the PV system is blocked for 0.02 s, and then allowed to inject real power at a rate of 7500 kW/s (i.e. its rated power of 600 kW at 0.1 s). Scope capture of power measurements at PCC are shown in Figure 7.21.

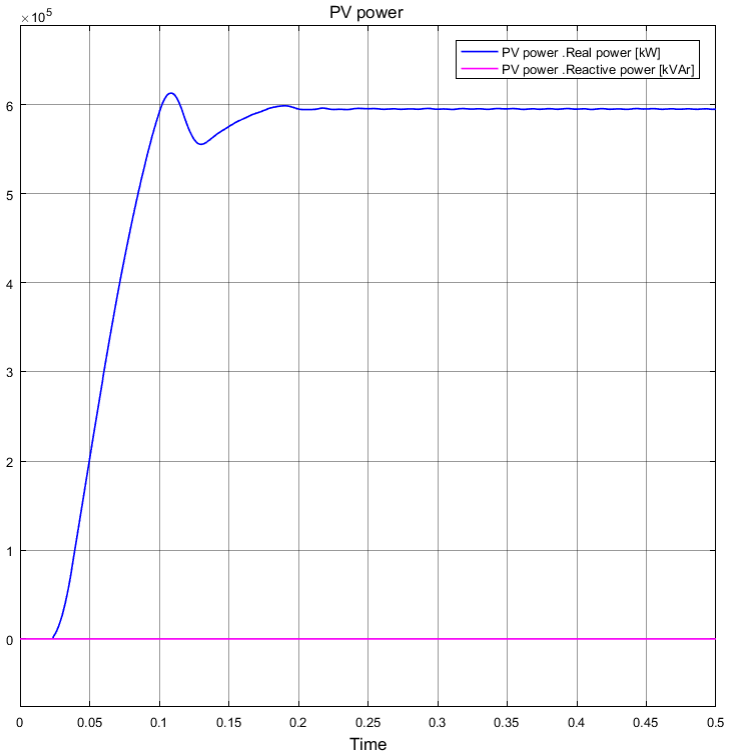

Figure 7.20: Scope capture of PV System's voltage, current, and power measurements at PCC

The DC bus voltage controller tracks step change with 6.9% overshoot, a settling time of 19.1 ms, and provides a reference power signal to the current controller. The PV system supplies its rated power of 600 kW at steady state. Figure 7.21 shows that the total

harmonic distortion on current supplied to the grid is 2.17% at steady state which is lower than the 5% requirement of IEEE 1547.

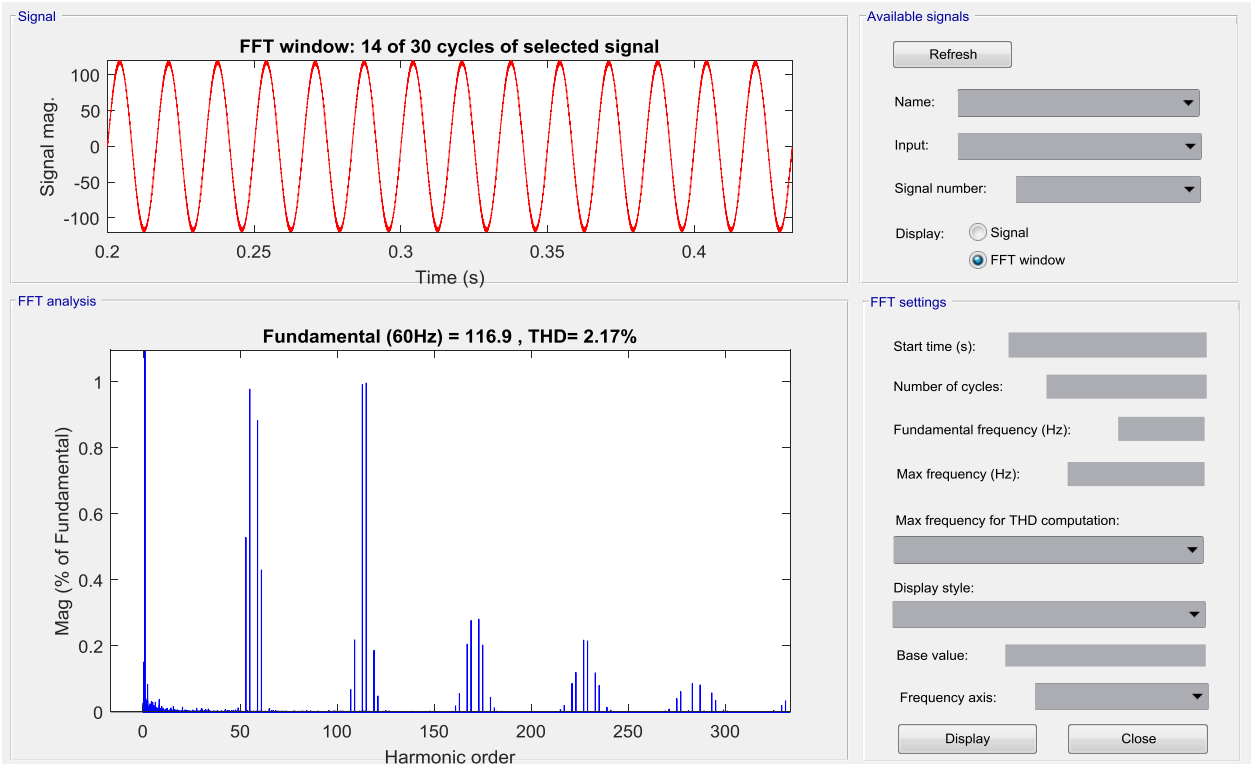

Figure 7.21: FFT analysis of current supplied by the PV system

7.4. Battery Management System Model in Simulink

Frequency deviation from the nominal operating point is often a sign of power imbalance in the system. When there is more power demand than supplied, frequency of the system lowers until the conventional generators adjust their speed and increase their power outputs. Because of their inertia (rotating mass), conventional generators cannot adjust their speed immediately after a sudden change in load demand. Under frequency condition is also observed when a conventional generator is suddenly taken offline. Utilities often engage in load-shedding (disconnecting load from the system) when under frequency conditions are detected in their feeders. Under frequency conditions trip PV inverters as well (per IEEE 1547 rules). With higher PV penetration level in a feeder, further power imbalance occurs and more load-shedding is required to return the system

frequency to its nominal operating point. When there is a sudden decrease in load demand, conventional generators again cannot adjust their speed and lower their power outputs immediately. Hence system frequency increases and PV inverters are tripped (per IEEE over frequency rules).

In order to prevent over/under frequency conditions from tripping PV inverters and thus creating more frequency imbalance in the system, an energy management system is investigated in this research. A lead-acid battery pack is chosen as an energy storage device and connected to the Smart Inverter model discussed in Chapter 6. The smart inverter's Frequency-Watt function is modified as shown in Figure 7.22.

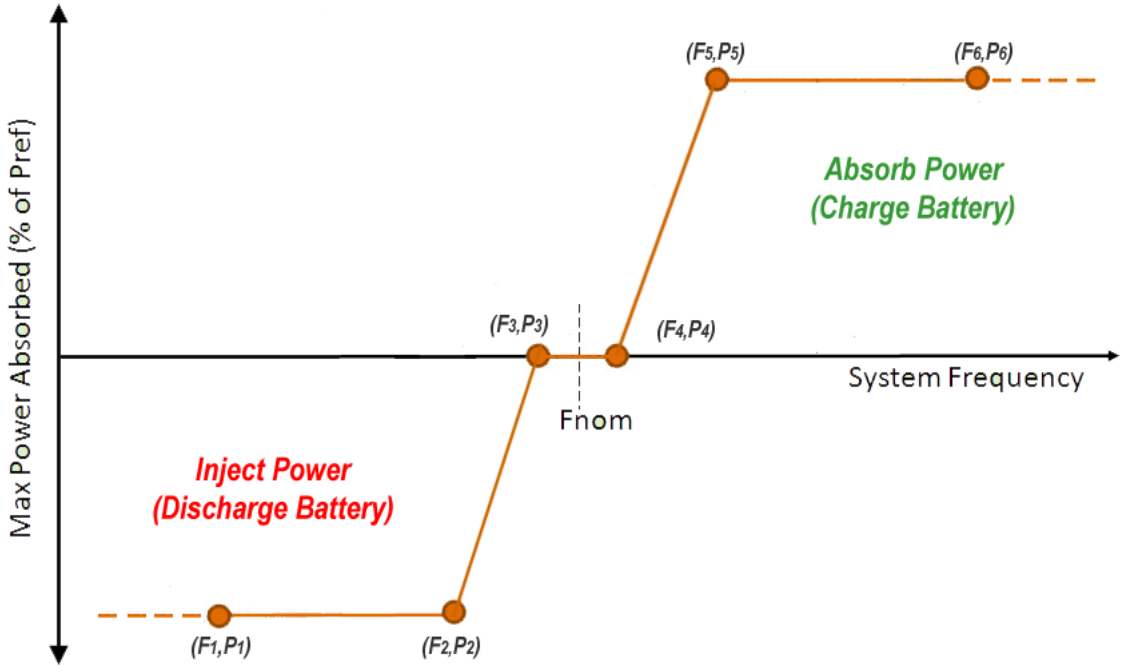

Figure 7.22: Frequency-Watt function used for battery management system

Based on deviation levels of system frequency from its nominal operating point, the battery is allowed to either absorb (i.e. charge) or inject (i.e. discharge) different amounts of real power. When frequency is between certain values (e.g. 59.05 Hz and 60.05 Hz), the battery is allowed to disconnect from the grid. If the State of Charge (SOC) is lower than 60%, the battery is allowed to charge during this time interval

instead of being disconnected. From the User-Interface of the Smart Inverter model, setpoints for frequency and power are entered into the model. Figure 7.23 shows the User-Interface of the Smart Inverter modified to manage battery packs.

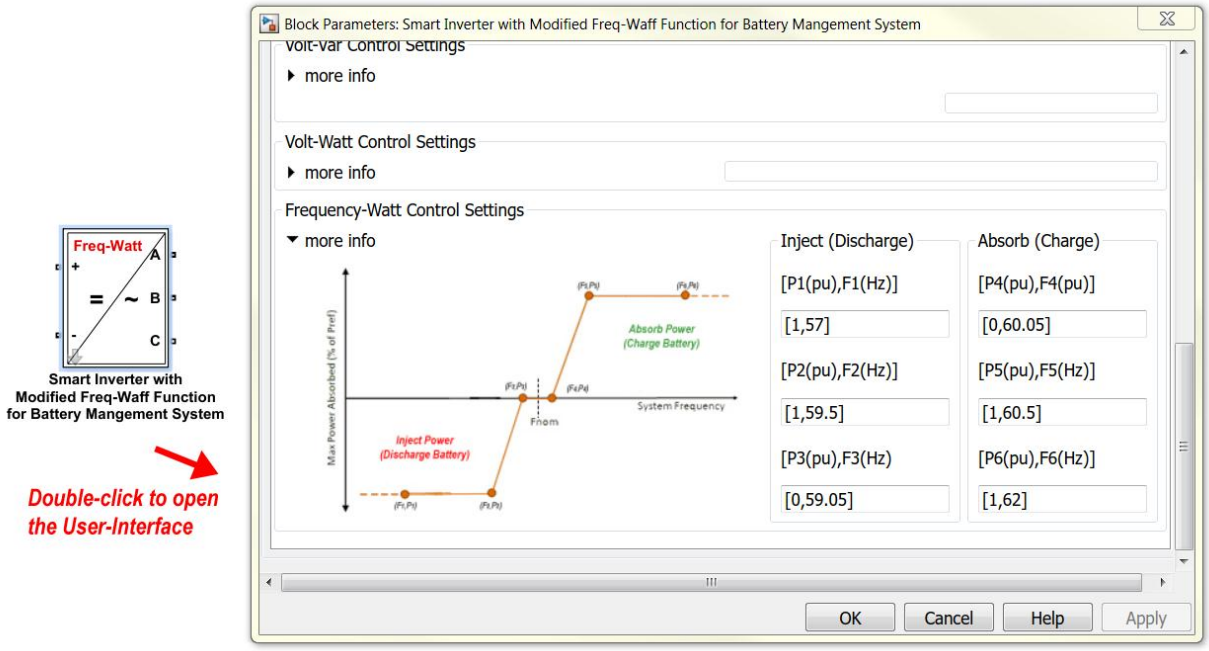

Figure 7.23: Modified Smart Inverter User-Interface for battery management system

A battery model that is part of the Simulink library is connected directly to the Smart Inverter. By changing the direction of current (i.e. changing the direction of real power flow based on the curve shown in Figure 7.22), the Smart Inverter controls the amount of power absorbed or discharged by the battery. To validate and verify the battery management system, a 600 kWh battery system is constructed in Simulink. The nominal voltage of the battery pack is selected to be 8900 V to match the DC-port voltage level of the Smart Inverter modeled in Chapter 6. The Smart Inverter is controlled in Frequency-Watt mode with setpoints as shown in Figure 7.23. The grid side of the Smart Inverter is connected to a 4.16 kV Voltage Source. At the beginning of the simulation, frequency of the Voltage Source is 56 Hz. After 1 s, its frequency slowly begins to increases and reaches 64 Hz at t = 4 s. Figure 7.24 shows the single line diagram of the test circuit,

while Figure 7.25 shows the frequency setpoints of the Voltage Source during the simulation.

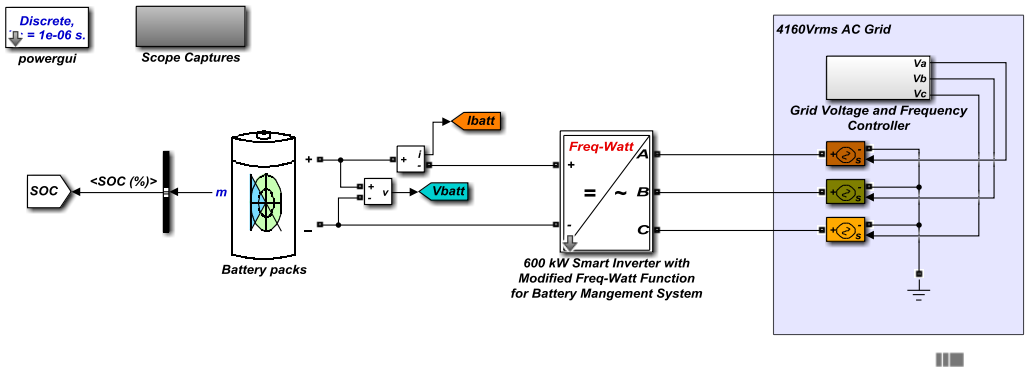

Figure 7.24: Test circuit for validation and verification of battery management system

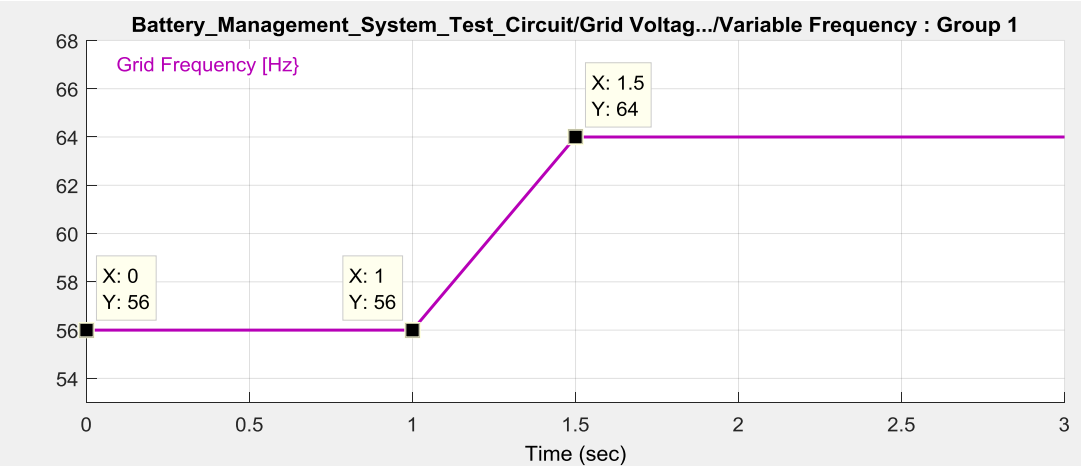

Figure 7.25: Voltage Source frequency setpoints

The simulation is run for 3.5 s and the power delivered/absorbed by the battery packs is measured. At the beginning of the simulation, the State-of-Charge (SOC) of the battery packs is 60 % and the battery management system is set to control the SOC within 30 % and 90 %. Figure 7.26 (a) shows the measured system frequency. Figure 7.26 (b) shows power delivered and absorbed by the battery management system. Figure 7.26 (c) shows the SOC (available current) of the battery packs during the simulation.

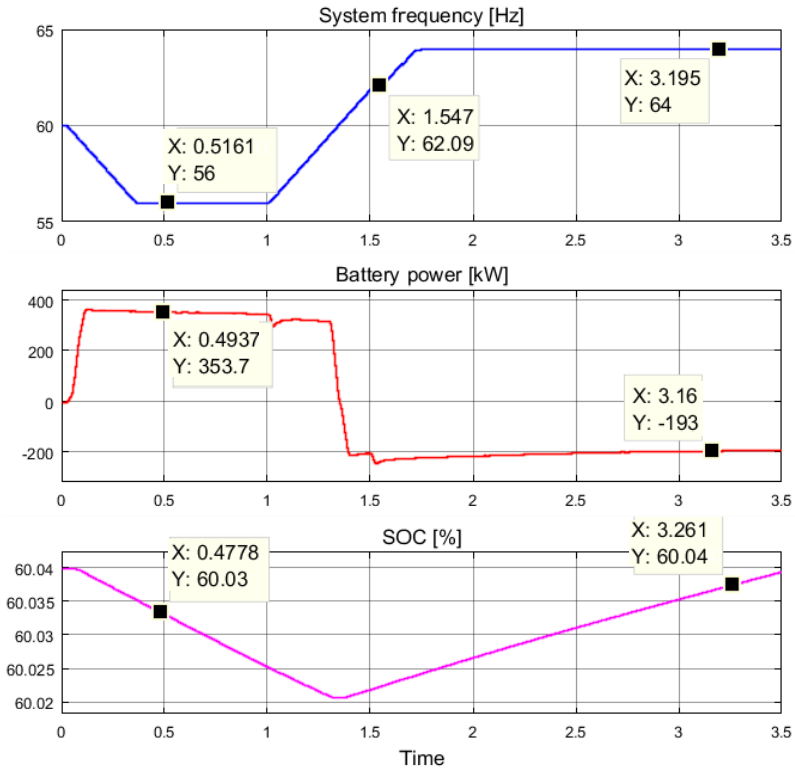

Figure 7.26: Battery power and power reference signal generated by the Smart Inverter

The battery management system charges and discharges the battery packs depending on measured grid frequency. When frequency of the system reaches 56 Hz and the SOC of the battery packs is 60.03%, 353.7 kW power is delivered to the grid (i.e. ≈60% of the available power). When frequency is between 59.95 Hz and 60.05 Hz, the management system charges the battery packs. When frequency increases to 64 Hz, the battery management system further charges the battery packs, and the SOC of the battery packs starts to increase. At the end of the simulation, the SOC of the battery packs reach 60.04%, and 193 kW power is absorbed from the gird (i.e. ≈32.2% of power capacity). The management system keeps the SOC of the battery packs between 30 % and 90 %.

7.5. Transient Simulation of an IEEE 13 Node Test Feeder with a 120% PV Penetration Level

In section 7.2 of Chapter 7, an IEEE 13 Node Test Feeder is modeled, validated and verified in Simulink. In sections 7.3 and 7.4, a PV system and a battery management system are modeled. In this section, seven 600 kW PV systems (with a total penetration level of ≈120%) are connected to seven nodes of the IEEE 13 Node Test Feeder model. Solar irradiation of 1000 $\frac{W}{m^2}$ and 25°C temperature values are supplied to the PV arrays (i.e. the PV arrays operate at STC condition and supply their rated power). A 600 kW battery with its management system is connected to the secondary-side of the substation transformer. Figure 7.27 shows the locations of PV and battery systems, while Figure 7.28 shows PV system connected at node 632. Similar to the PV system connected at Node 632, PV systems are connected to the other six nodes shown in Figure 7.27

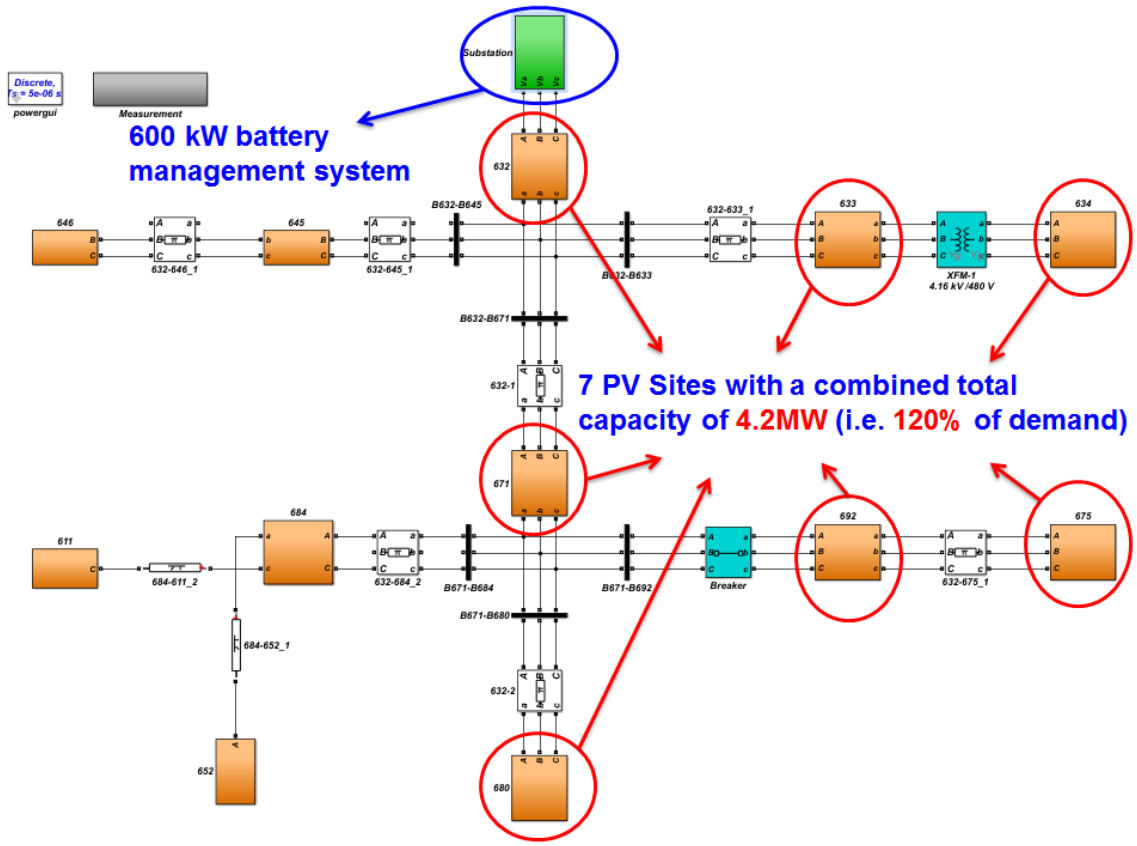

Figure 7.27: PV and Battery Management systems location in the IEEE 13 Node Test Feeder

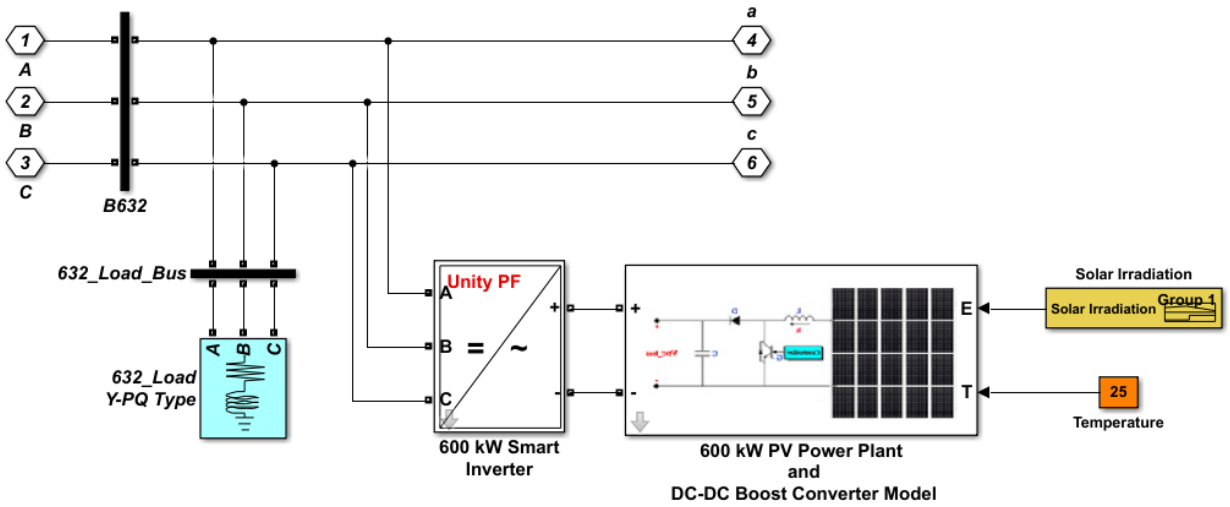

Figure 7.28: PV System connected at Node 632

The high side of the IEEE 13 Node Test Feeder is connected to an external grid. This external grid is modeled as an infinite bus in the published data of the feeder [71]. In real world, synchronous generators located at power plants supply power to feeders in the network. Therefore, the infinite bus is replaced with a detailed model of a 20 MVA synchronous generator with an excitation system and governor (speed) controllers. Parameters used in the synchronous generator, excitation system, and governor are shown in Appendix E.

Two loads, 4.95 MW and 0.25 MW, are connected to the high side of the substation transformer. These loads represent loads that are supplied by the generator in addition to the IEEE 13 Node Test Feeder. The 0.25 MW load is connected to a circuit breaker and is switched ON and OFF during different simulation scenarios investigated in this research. Figure 7.29 shows the modified substation subsystem of the IEEE 13 Node Test Feeder.

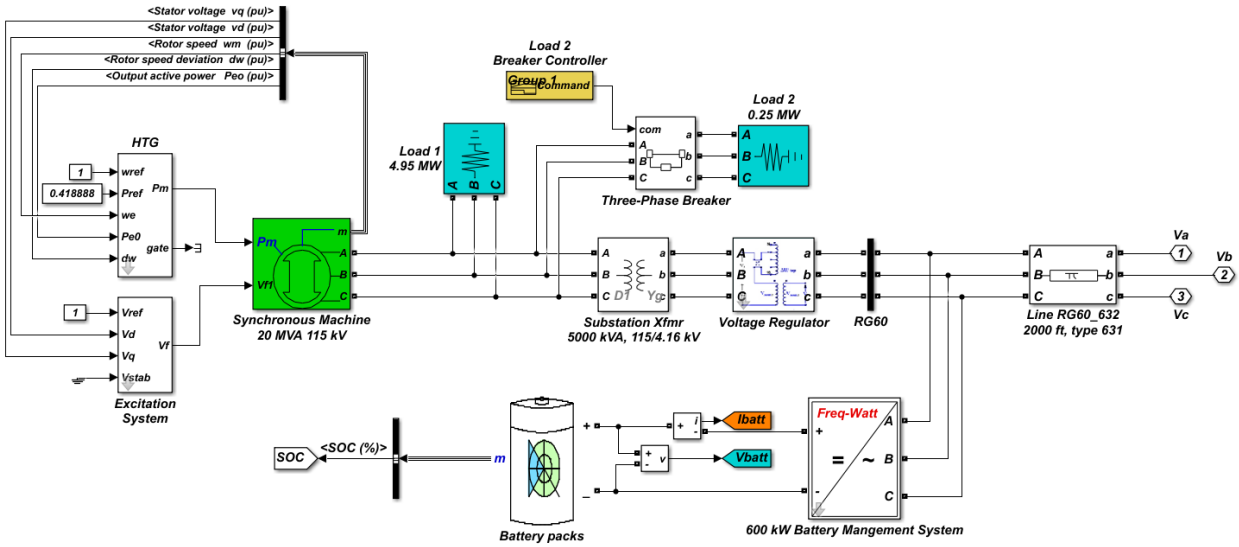

Figure 7.29: Modified substation subsystem of the IEEE 13 Node Test Feeder

Figure 7.29 shows that a 20 MVA, 115 kV hydro-turbine driven, synchronous generator is connected to the high side of the substation transformer. The generator's terminal voltages are controlled by the Excitation System block, and its mechanical speed is controlled by HTG (Hydro-Turbine Governor) block. Load 1 and Load 2, with 4.95 MW and 0.25 MW power demand respectively, are connected to the high side of the transformer. The low side of the transformer is connected to a voltage regulator. A 600 kW battery management system and a 2000 ft line are connected to bus RG60.

Simulink provides an interface, "powergui", to initialize the synchronous generator to steady state. Thus, the synchronous generator delivers its steady state output at the beginning of the simulation. Figure 7.30 shows the initialized parameters of the generator.

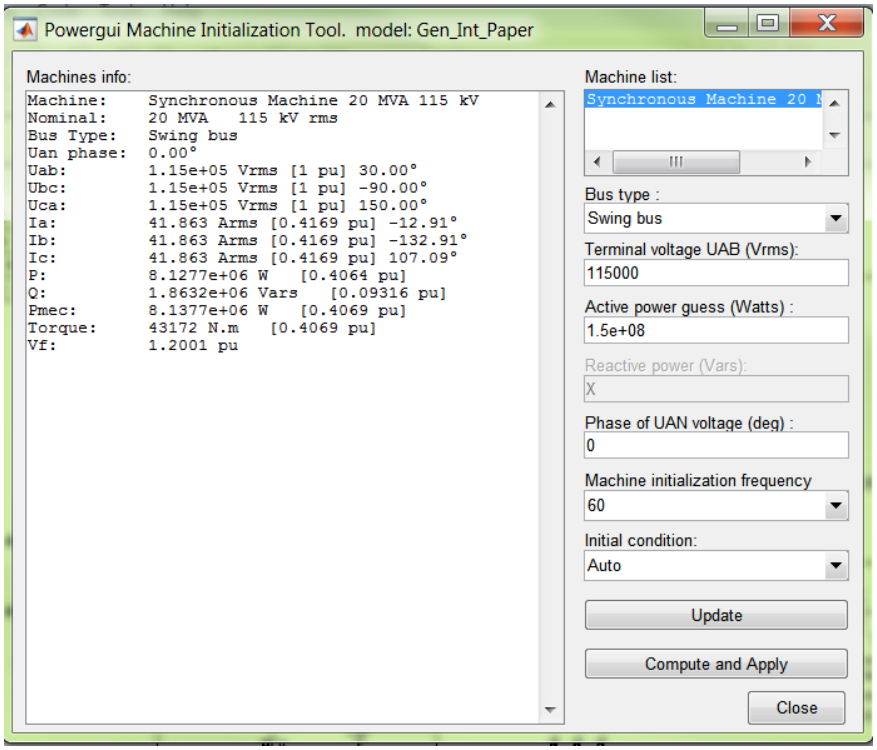

Figure 7.30: Synchronous machine initialization using Simulink's "powergui"

To investigate the feeder when frequency deviates from the nominal value of 60 Hz, the following scenarios are considered:

Scenario 1: All PV systems and the battery management system are disconnected. The simulation is run for 1 s, and suddenly Load 2 (i.e. 0.25 MW) is disconnected from the system. Frequency of the system during the transient period is measured. This scenario serves as a base case scenario when there are no PVs and energy storage systems in the feeder.

Scenario 2: PVs with a total penetration level of 120% are connected to the grid. The battery management system is disconnected from the system. The simulation is run for 1 s, and suddenly Load 2 (0.25 MW) is disconnected from the grid. Frequency of the system and power delivered by PVs are measured. This scenario serves to investigate the transient behaviors of the grid with a 120% PV penetration and without an energy storage system.

Scenario 3: For this scenario, the grid interconnection requirements of IEEE 1547 that is implemented in the PV inverters is disabled. Similar to scenario 2, PVs with a total penetration level of 120% are connected to the grid and the battery management system is disconnected from the system. The simulation is run for 1 s, and suddenly Load 2 (0.25 MW) is disconnected from the grid. Frequency of the system and power delivered by PVs are measured. This scenario serves to investigate the transient behaviors of the grid with a 120% PV penetration, without an energy storage system, and when inverters are allowed to stay connected to the grid during frequency deviations.

Scenario 4: PVs with a 120% penetration level and a 600 kW battery management system are connected to the grid. Load 2 (0.25 MW) is suddenly disconnected from the system. Frequency of the system and power delivered by PVs along with the battery management systems are measured.

To investigate the transient behavior of the feeder with 120% PV penetration level and during under frequency conditions, Load 2 (0.25 MW) is first disconnected. Then, the synchronous generator is initialized using the "powergui" to supply power to the system at steady state (i.e. the output of the generator is configured to supply power only to the IEEE 13 Node Test Feeder and the 4.95 MW load initially). The following simulations scenarios are investigated:

Scenario 5: All PV systems and the battery management system are disconnected. The simulation is run for 1 s, and suddenly Load 2 (i.e. 0.25 MW) is connected to the system. Frequency of the system during the transient period is measured. This scenario serves as a base case scenario when there are no PV and energy storage systems in the feeder with load suddenly connected to the system.

Scenario 5: PVs with a total penetration level of 120% are connected to the grid. The battery management system is disconnected from the system. The simulation is run for 1 s, and suddenly Load 2 (0.25 MW) is connected to the grid. Frequency of the system and power delivered by PVs is measured.

Scenario 6: Similar to Scenario 3, the grid interconnection requirements of IEEE 1547 that is implemented in the PV inverters is disabled and simulation Scenario 5 is repeated. This scenario serves to investigate the transient behaviors of the grid with a 120% PV penetration, without an energy storage system, and when inverters are allowed to stay connected to the grid during frequency deviations.

Scenario 7: PVs with 120% penetration level and a 600 kW battery management system are connected to the grid. Load 2 (0.25 MW) is suddenly connected to the system. Frequency of the system and power delivered by PVs and the battery management systems are measured.

7.5.1. Simulation Scenario 1 – Over Frequency Response of the Feeder without PV and without Battery Management Systems

With no PV and no battery management systems in the feeder, the simulation is run at steady state for 1 s. Load 2 is suddenly disconnected from the grid, and frequency of the system during the transient period is measured. Figure 7.31 shows frequency of the system during the transient period.

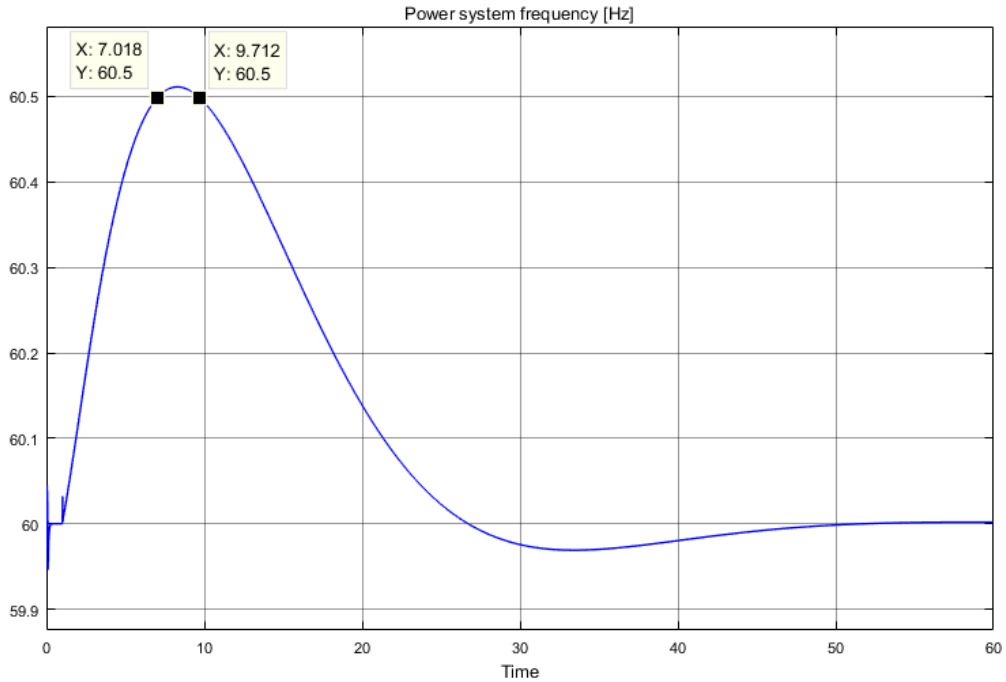

Figure 7.31: Simulation Scenario 1 - Frequency of the system during the transient period

When Load 2 is disconnected at t=1 s, the frequency of the system starts to increase. It passes the 60.5 Hz over frequency threshold from t=7.108 s to t=9.712 s. IEEE 1547 recommends configuring inverters to trip after 2 s time delay when over frequency of 60.5 Hz is measured (Table 2.1). In this simulation scenario, there are no PV and energy management systems installed in the IEEE 13 Node Test Feeder.

7.5.2. Simulation Scenario 2 – Over Frequency Response of the Feeder with 120% PV Penetration Level and without a Battery Management System

With a PV penetration level of 120 % and without a battery management system in the feeder, the simulation is run at steady state for 1 s. Load 2 is suddenly disconnected from the grid. Frequency of the system and power delivered by PVs during the transient period are measured. Figure 7.32 shows frequency of the system and power delivered by a PV system installed at node 632. The other six PVs installed on other nodes in the feeder deliver similar power as shown in Figure 7.32.

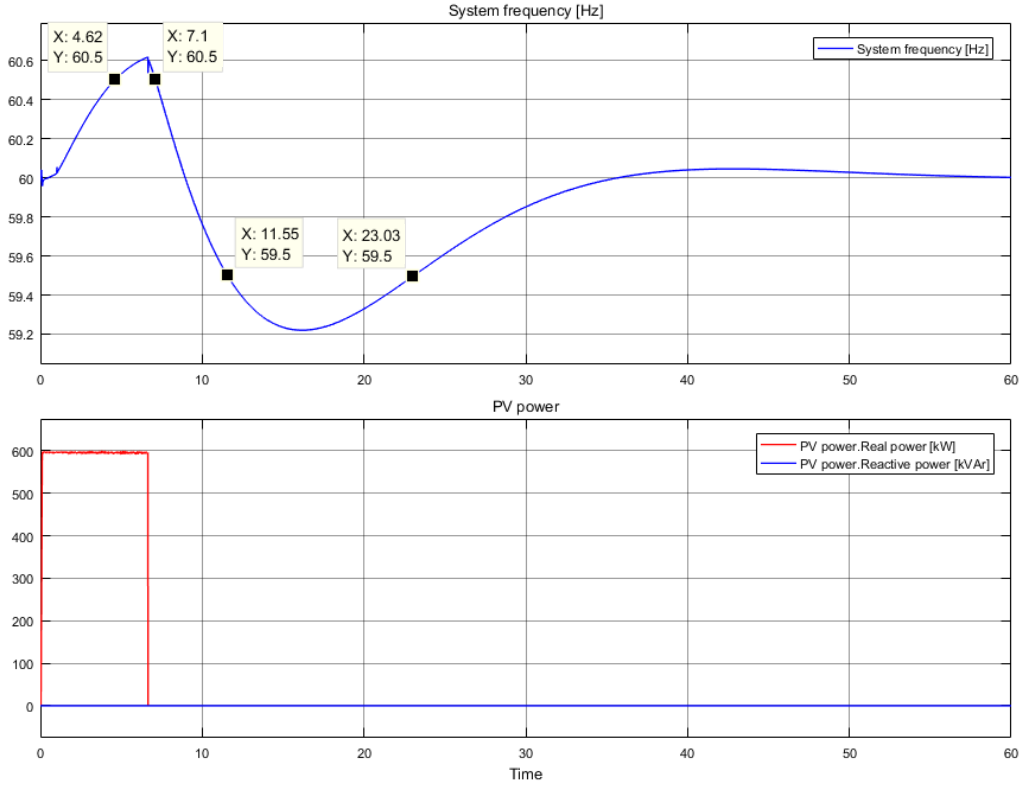

Figure 7.32: Simulation Scenario 2 - Frequency of the system and power delivered by PV during the transient period

With a 120% PV system installed in the feeder, the frequency of the system violates the 60.5 Hz over frequency threshold at t = 4.62 s. Because the frequency of the system remains above 60.5 Hz for a duration of more than 2 s, PV systems are disconnected. When PV systems disconnect, the system frequency experiences more instability, and the 59.5 Hz under frequency threshold is violated from t = 11.55 s to 23.03 s. As it can be from Figure 7.31 and Figure 7.32, a 120% PV penetration level enhances the frequency instability of the system when a sudden load change occurs on the external grid.

7.5.3. Simulation Scenario 3 – Over Frequency Response of the Feeder with 120% PV Penetration Level and without IEEE 1547 Requirements

The IEEE 1547 grid interconnection requirement block is disabled in the inverters' controllers. With a PV penetration level of 120 % and without a battery management system in the feeder, the simulation is run at steady state for 1 s. Load 2 is suddenly disconnected from the grid. Frequency of the system and power delivered by PVs during the transient period are measured. Figure 7.33 shows frequency of the system and power delivered by a PV system installed at node 632.

With no IEEE 1547 interconnection requirements implemented in the inverters and with a 120% PV system installed in the feeder, the frequency of the system violates the 60.5 Hz over frequency threshold at t = 4.62 s. Because the PV systems remain connected to the grid, the system frequency stays above 60.5 Hz from t = 4.62 s to t = 13.54 s (i.e. 6.44 s higher than simulation scenario 3). The inverters remain connected to the grid and supply power during the transient period, unlike simulation scenario 3, and under frequency violation is not observed.

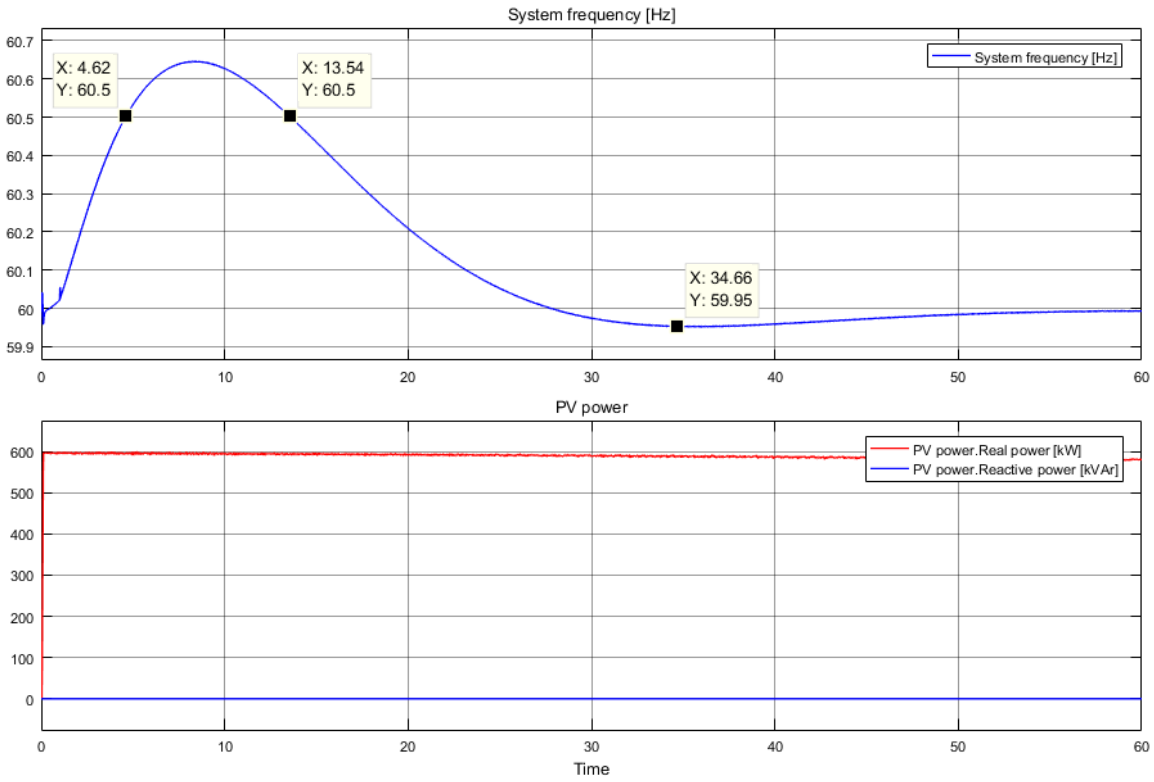

Figure 7.33: Simulation Scenario 3- Frequency of the system and power delivered by PV during the transient period

7.5.4. Simulation Scenario 4 – Over Frequency Response of the Feeder with 120% PV Penetration Level and a 600 kW Battery Management System

With a 120 % PV penetration level and a 600 kW battery management system in the feeder, the simulation is run at steady state for 1 s. Load 2 is suddenly disconnected from the grid. Frequency of the system, power delivered by PVs (Node 632), and power absorbed by the battery management system during the transient period are measured and shown in Figure 7.34.

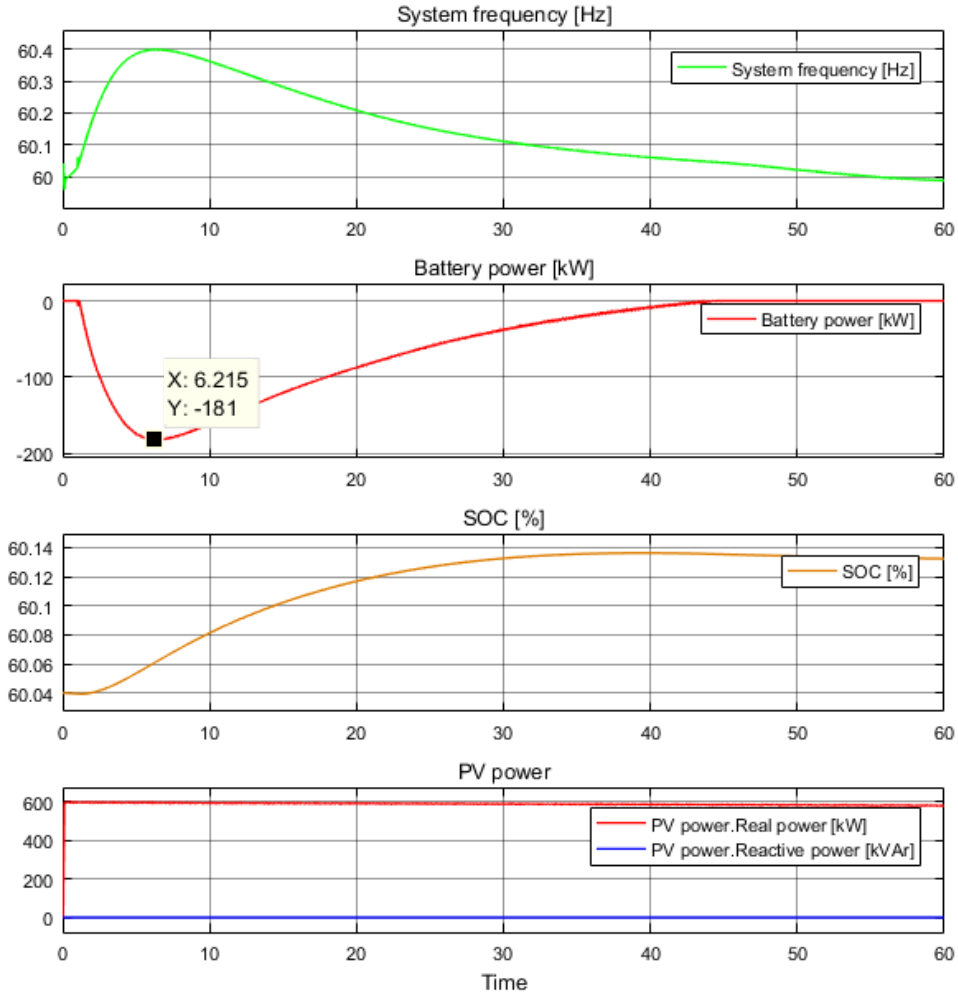

Figure 7.34: Simulation Scenario 4 - Frequency of the system during the transient period

Figure 7.34 shows that the frequency of the system does not violate the 60.5 Hz threshold during the transient period. Both under frequency and over frequency thresholds are not violated. The battery management system absorbed 181 kW power to maintain the frequency of the system below the 60.5 Hz threshold requirement. Figure 7.35 shows a comparison plot of the above four simulation scenarios.

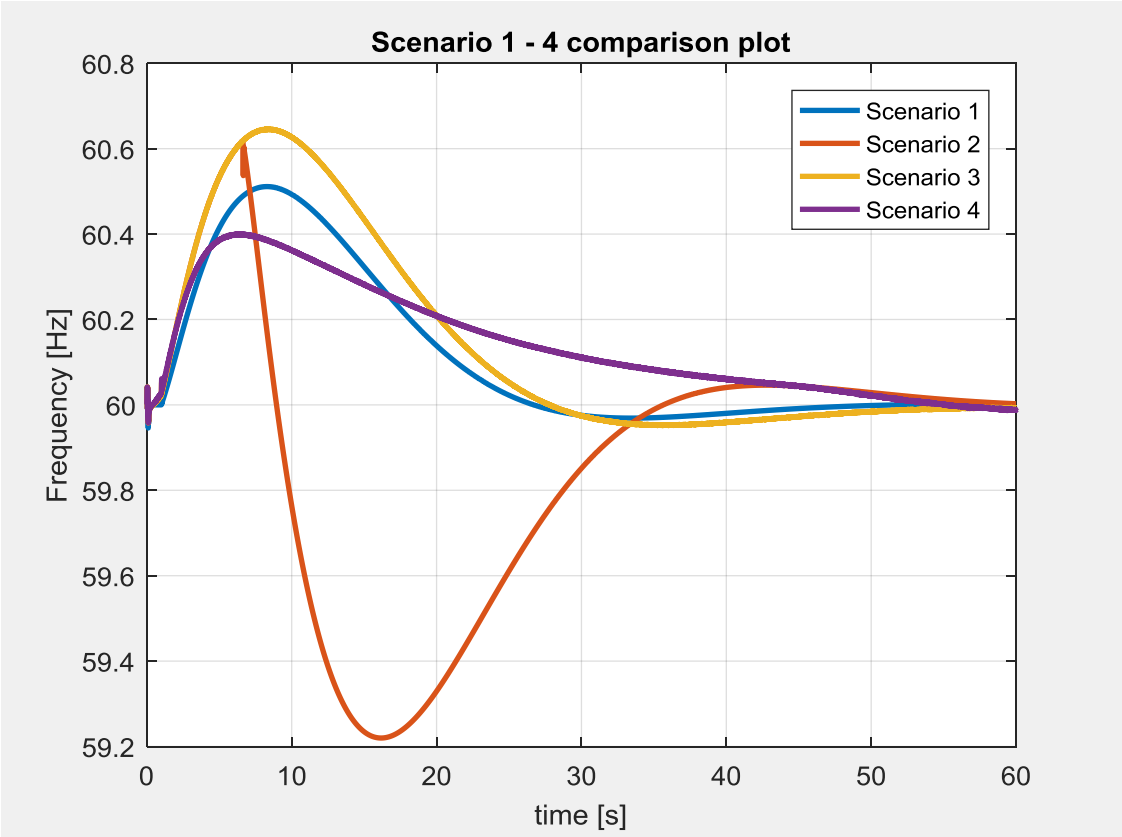

Figure 7.35: Simulation scenarios 1 to 4 comparison plot

7.5.5. Simulation Scenario 5 – Under Frequency Response of the Feeder without PV and without Battery Management Systems

With no PV and no battery management systems in the feeder, the simulation is run at steady state for 1 s. Load 2 is suddenly connected to the grid and frequency of the system during the transient period is measured. Figure 7.39 shows frequency of the system during the transient period

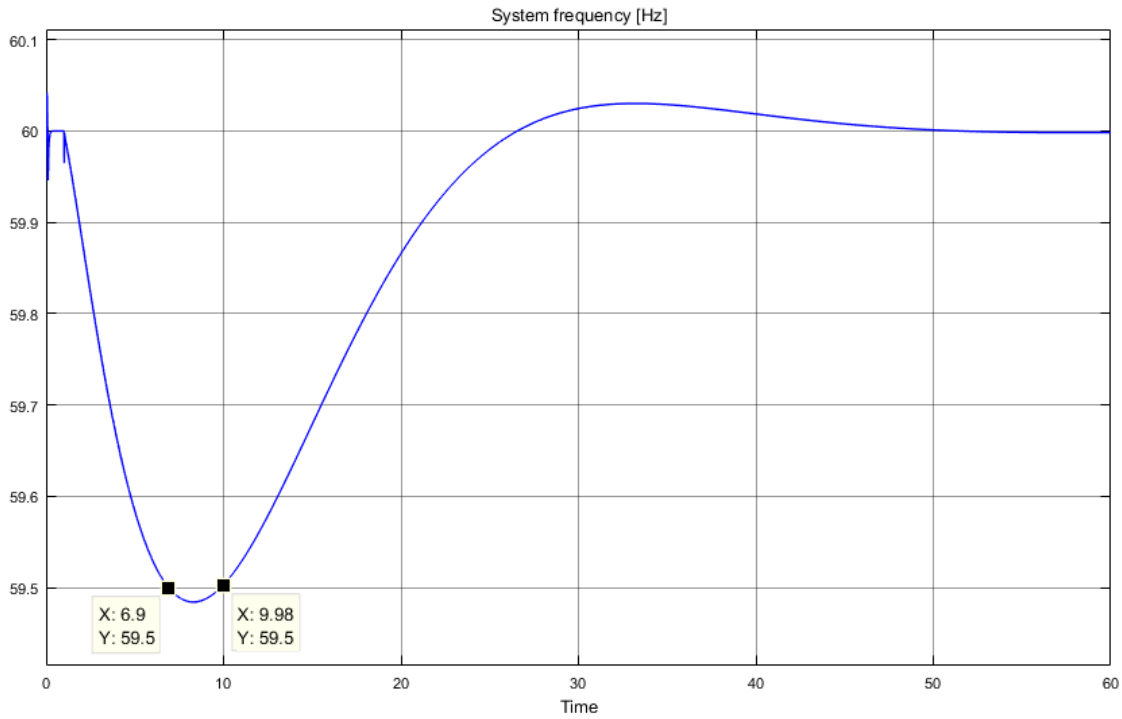

Figure 7.36: Simulation Scenario 5 - Frequency of the system during the transient period

Figure 7.36 shows that when PV and battery management systems are not installed in the feeder, the system frequency violates the 59.5 Hz threshold from t = 6.9 s to 9.98 s. The system frequency does not violate the 60.5 Hz over frequency threshold during the transient period.

7.5.6. Simulation Scenario 6 – Under Frequency Response of the Feeder with a 120% PV Penetration Level and without a Battery Management System

With a 120 % PV penetration level and without a battery management system in the feeder, the simulation is run at steady state for 1 s. Load 2 is suddenly connected to the grid. Frequency of the system and power delivered by PVs during the transient period are measured. Figure 7.37 shows frequency of the system and power delivered by a PV system installed at node 632. The other six PVs installed on other nodes in the feeder deliver similar power as shown in Figure 7.37.

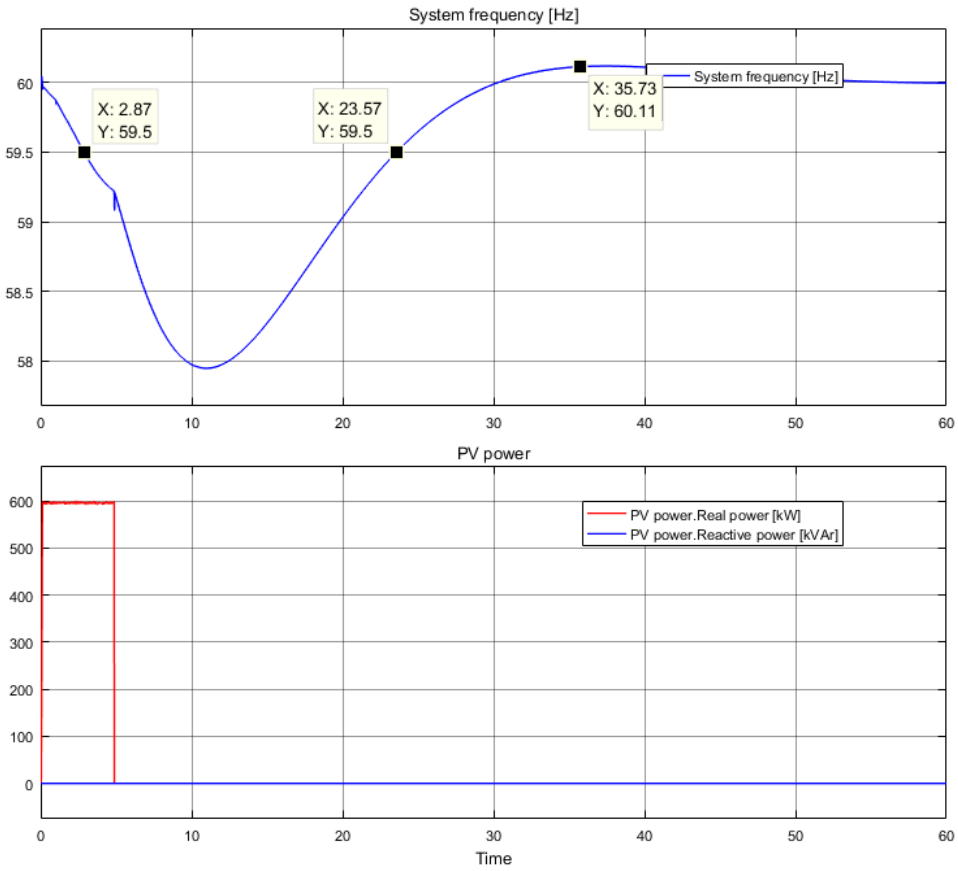

Figure 7.37: Simulation Scenario 6 - Frequency of the system during the transient period

With a 120 % PV system installed in the feeder, the frequency of the system violates the 59.5 Hz under frequency threshold at t = 2.87 s. Because the frequency of the system remains below 59.5 Hz for a duration of more than 2 s, PV systems are disconnected (i.e. after 2 s of passing the 59.5 Hz threshold per IEEE 1547 rules). When PV systems disconnect, the system frequency experiences more instability As it can be seen from Figure 7.36 and Figure 7.37, a 120 % PV penetration level enhances the frequency instability of the system when a sudden load change occurs on the external grid.

7.5.7. Simulation Scenario 7 – Under Frequency Response of the Feeder with 120% PV Penetration Level and without IEEE 1547 Requirements

The IEEE 1547 grid interconnection requirement block is disabled in the inverters' controllers. With a PV penetration level of 120 % and without a battery management system in the feeder, the simulation is run at steady state for 1 s. Load 2 is suddenly connected to the grid. Frequency of the system and power delivered by PVs during the transient period are measured. Figure 7.38 shows frequency of the system and power delivered by a PV system installed at node 632.

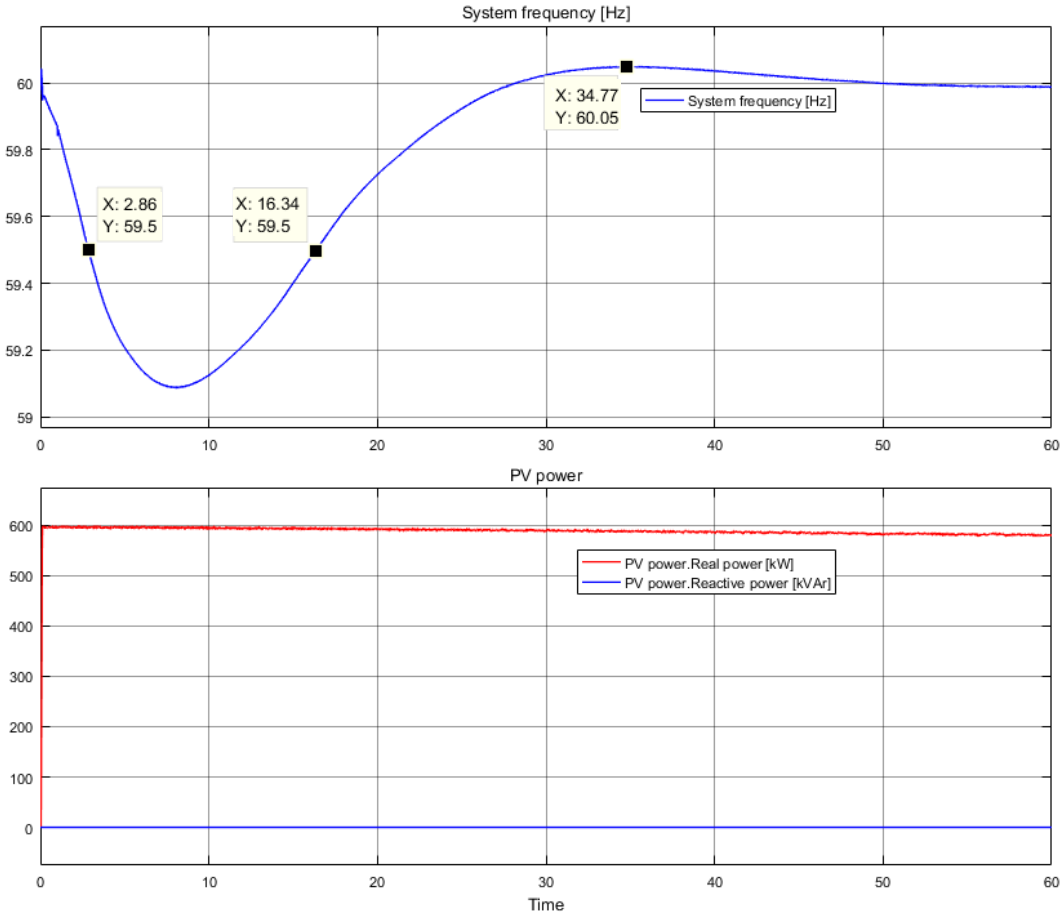

Figure 7.38: Simulation Scenario 7- Frequency of the system and power delivered by PV during the transient period

With no IEEE 1547 interconnection requirements implemented in the inverters and with a 120% PV system installed in the feeder, the frequency of the system violates the 59.5 Hz under frequency threshold at t = 2.86 s. Because the PV systems remain connected to the grid, the system frequency stays below 59.5 Hz from t = 2.86 s to t = 16.34 s (i.e. 7.23 s lower than simulation scenario 3). The inverters remain connected to the grid and supply power during the transient period, unlike simulation scenario 6, and over frequency violation is not observed

7.5.8. Simulation Scenario 8 – Under Frequency Response of the Feeder with a 120% PV Penetration Level and a 600 kW Battery Management System

With a 120 % PV penetration level and a 600 kW battery management system in the feeder, the simulation is run at steady state for 1 s. Load 2 is suddenly connected to the grid. Frequency of the system, power delivered by PVs, and power absorbed by the battery management system during the transient period are measured. Figure 7.39 shows frequency of the system, power absorbed by the battery management system, and power delivered by a PV system installed at node 632.

Figure 7.39 shows that the frequency of the system does not violate the 59.5 Hz threshold during the transient period. Both under frequency and over frequency thresholds are not violated. The battery management system delivers 290.7 kW peak power to maintain the frequency of the system above the 59.5 Hz threshold requirement. Figure 7.40 shows a comparison plot of simulation scenarios 5 to 8.

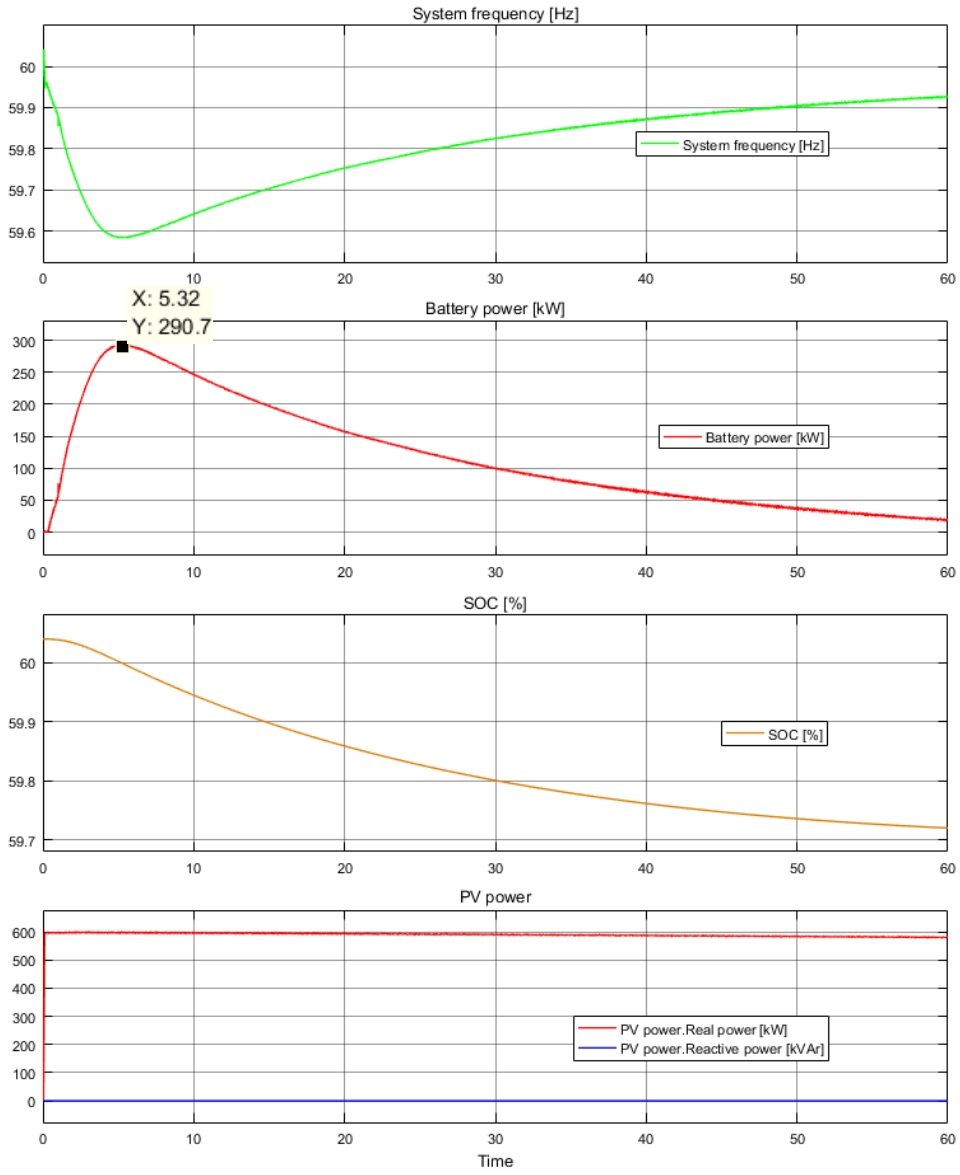

Figure 7.39: Simulation Scenario 6 - Frequency of the system during the transient period

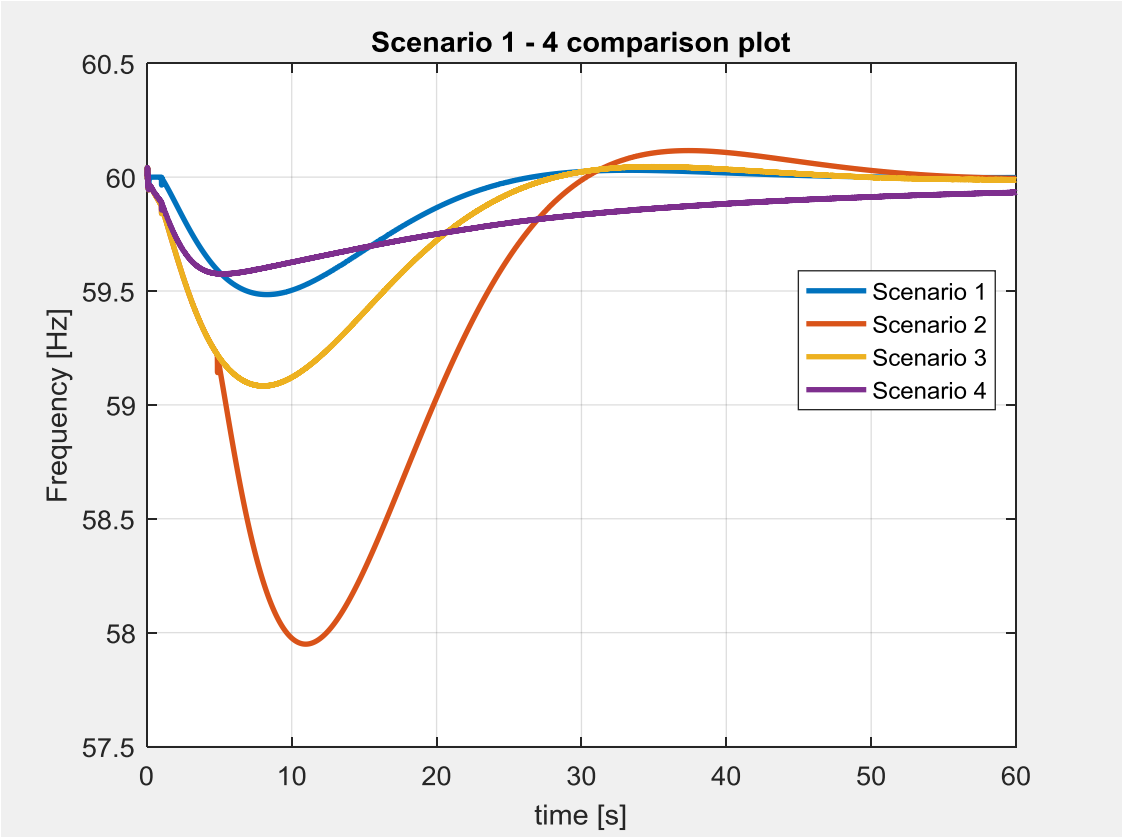

Figure 7.40: Simulation scenarios 5 to 8 comparison plot

7.6. Summary

In this chapter, an IEEE 13 Node Test Feeder is modeled, validated and verified in Matlab/Simulink software. Since the Simulink library does not contain a voltage regulator model that uses either continuous or discrete simulation types, a Type-B Voltage Regulator is modeled. This model provides a user-interface to change parameters of the model. Therefore, it is customizable and can be used in any feeder that has a voltage regulator connected to the substation transformer. In most cases, the voltage control is desired at a bus, which is at a distance from the voltage regulator. The Voltage Regulator compensates for voltage drop in the line connecting it to the controlled bus. The Voltage Regulator model provides three modes of control: Automatic, Manual, and No Control. In Automatic mode of control, the Voltage Regulator dynamically controls

voltage on a controlled bus. In Manual mode, the Voltage Regulator model does not change its transformers' taps to control the voltage on the controlled bus. Instead, it keeps the tap numbers set by the user via the user-interface. In No Control mode, the Voltage Regulator is disabled and the substation transformer is connected directly to the controlled bus.

A PV Power Plant with a user-interface is modeled, validated, and verified under different solar irradiation conditions. The model consists of PV arrays connected in series and parallel and a DC-DC boost converter with MPPT algorithms. The model internally computes the required filter inductor and capacitor sizes based on user allowed percent ripple on current and voltage via the user-interface. The PV arrays along with the DC-DC boost converter are finally connected to the Smart Inverter model discussed in Chapter 6 to create a grid-tied PV system. The DC-bus voltage controller of the Smart Inverter is designed to have its gain cross the 0dB axis at -20dB/dec slope. It has a phase margin of 63.3°, which is well above the -180° needed to have stability during transient periods.

A Battery Management System is modeled with a modified Frequency-Watt function. The setpoints of the Frequency-Watt function are customized via the user-interface of the modified Smart Inverter. The model is validated and verified to absorb and deliver real power depending of the frequency of the system.

Finally, the IEEE 13 Node Test Feeder's infinite bus is replaced with a detailed model of a 20 MVA synchronous generator with Excitation and Governor Systems. Two additional loads, 4.95 MW and 0.25 MW, are connected to the high-side of the substation transformer, and the low-side of the transformer is connected to the IEEE 13 Node Test Feeder. PV systems with a total penetration level of 120 % are installed in the feeder along with a 600 kW Battery Management System. Six simulations are carried out to investigate the behavior of the feeder in under and over frequency conditions. The worst-case scenario observed is when a 120 % PV penetration exists in the feeder and there is no battery management system. The high penetration of PVs enhances the frequency

instability of the system during sudden load changes. It is observed that the battery management system absorbs and delivers real power to mitigate frequency deviations during sudden load change.

.

CHAPTER 8: CONCLUSIONS AND FUTURE WORK

8.1. Conclusions

Power generated by a PV system has an intermittent character due mainly to atmospheric effects such as variable solar insolation resulting from cloud shading. The effects of intermittent PV power generation upon the electric grid are strongly influenced by the type of grid to which a PV system is connected and the type and amount of generation installed.

As the penetration level of PV in a distribution feeder increases, the capacity of a conventional synchronous generator that supplies power to the feeder needs to be reduced relatively. This leads to lower system inertia, and hence the power system transient stability would be affected negatively. When a fault occurs in the power system, some PV systems may be disconnected from the grid due to voltage sag. The disconnection causes a further drop in voltage and numerous PV systems may be disconnected from the grid. In this case, not only will the transient voltage stability be affected, the frequency stability will also be affected significantly due to the large power imbalance and fewer frequency control generators (conventional generators with inertia)

In this research, a NEETRAC member Feeder B is imported into The DIgSILENT PowerFactory software, and its voltage transient stability is investigated under different environmental conditions. ANSI 105% voltage threshold violations are observed in the feeder when all PV inverters are controlled in Unity Power Factor mode. To mitigate this violation, a Volt-Var control mode with ± 2 % deadband, 0.95 pu lower limit, and 1.05 pu upper limit is used. This control scheme mitigates the ANSI 105% voltage violations on NEETRAC member Feeder B during different environmental conditions.

The IEEE 13 Node Test Feeder is modeled in Matlab/Simulink software. PV systems with a total penetration level of 120 % are installed at different nodes of the

feeder, and frequency transient stability of the system is investigated. It is observed that higher penetration of PVs in the feeder adversely affect the frequency stability of the system during sudden load changes. To mitigate this frequency instability, a battery management system with modified Frequency-Watt function is developed and installed at the substation of the feeder. This battery management system emulates inertia and provides the necessary real power to stabilize the frequency of the system

8.2. Summary of Contributions

The first part of this thesis develops a method to import models originally created in OpenDSS software into DIgSILENT PowerFactory. Different methods and procedures are used to prepare and convert OpenDSS formatted files into DIgSILENT compatible DGS files. Matlab scripts are created to automate the preparation and conversion of OpenDSS files into the DGS format, which in turn cuts down on human efforts and error. These scripts can be used as plugins for both OpenDSS and DIgSILENT software.

Four PV inverters that exist in the NEETRAC member Feeder B are currently controlled in Unity Power Factor mode of operation. With the addition of a larger PV site, Site 5, ANSI 105% voltage threshold violations are observed during different environmental conditions. Based on the results of this research, representatives of the utility that operate the feeder are informed and advised about the Volt-Var control mode ability to mitigate the voltage violations.

The second part of this thesis develops a model for a Type-B voltage regulator that is most often used by utilities. The model has three control modes: Automatic, Manual, and No Control. A user-interface is provided to change the parameters of the transformers and the controller settings. Thus, the model is highly customizable and can be used in any feeder that contains a voltage regulator in the substation.

A PV Power Plant is modeled in Simulink that consists of series and parallel connected PV arrays, a DC-DC boost converter, and two MPPT algorithms (Perturb and

Observe and Incremental Conductance). A user is able to configure the power output of the plant by changing the number of series and parallel connected PV modules via the user-interface provided. The model internally calculates the required sizes of the filter inductor and capacitor based on user chosen percent ripple on current and voltage respectively.

A smart inverter that meets grid interconnection requirements of IEEE 1547 is modeled in Simulink. It provides Unity Power Factor, Volt-Var, Volt-Watt, and Frequency-Watt control functions. A user-interface is provided to change parameters of the DC bus, the inverter controller, and the AC side of the inverter. This inverter is reusable and can be installed at any node in a feeder.

A PV system model is created by connecting the PV Power Plant model to the Smart Inverter model. The DC bus voltage controller of the inverter is designed to be stable during transient operations by providing enough gain and phase margins at cut-off frequency.

A battery management system is modeled in Simulink that provides inertia in cases of higher PV penetration in a feeder. The battery management system absorbs and delivers real power depending on the frequency of the system.

Portions of the research in this dissertation have been included in IEEE conference panel presentations, journal papers, and NEETRAC Board Member meetings. A list of the published papers and presentations contributed as part of this research is given below.

Conference Presentations

I. Kim, R. Regassa, and R. G. Harley "The Modeling of Distribution Feeders Enhanced by Distributed Generation in DIgSILENT," in *2015 IEEE 42nd Photovoltaic Specialist Conference (PVSC).*, New Orleans., LA, 2015, 1-5.

I. Kim, R. G. Harley, and R. Regassa "The Investigation of the Maximum Effect of the Volt/Var Control of Distributed Generation on Voltage Regulation," in *2015 IEEE 42nd Photovoltaic Specialis Conference (PVSC).*, New Orleans., LA, 2015, 1-6.

I. Kim, R. G. Harley, R. Regassa, and Y. D. Valle "The Effect of Volt/Var Control of Photovoltaic Systems on the Time-Series Steady-State Analysis of a Distribution Network," in *2015 Clemson University Power Systems Conference (PSC).*, Clemson., SC, 2015, 1-6.

I. Kim, R. G. Harley, R. Regassa, and Y. D. Valle "The Analysis of Voltage Increase Phenomena in a Distribution Network with High Penetration of Distributed Generation," in *2015 Clemson University Power Systems Conference (PSC).*, Clemson., SC, 2015, 1-6.

I. Kim, R. G. Harley, and R. Regassa "Optimal Distributed Generation Allocation on Distributed Networks at Peak Load and theAnalysis of the Impact of Volt/Var Control on the Improvement of the Voltage Profile," in *2014 North America Power Symposium (NAPS).*, Pullman., WA, 2014, 1-5.

Journal Publications (Submitted)

R. Regassa, and R. G. Harley, "Modeling and Simulation of a Smart Inverter in Matlab/Simulink for Transient Analysis," *IEEE Transactions on Power Electronics*, 2017.

R. Regassa, and R. G. Harley, "Modeling and Simulation of a Type-B Substation Voltage Regulator in Matlab/Simulink," *IEEE Transactions on Power Electronics*, 2017.

R. Regassa, and R. G. Harley, "Transient Analysis of IEEE 13 Node Test Feeder with 120 % PV Penetration Level and A Battery Mangement System," *IEEE Transactions on Power Systems*, 2017.

8.3. Recommended Future Work

8.3.1. Faults on Distributed Generation

This research focused on the intermittent nature of PV on the distribution feeder. Smart inverter's Volt-Var function helps to mitigate the ANSI 105% voltage threshold violations in NEETRAC member Feeder B. Research must be carried out to investigate

the effects of faults on a PV system. How will fault in a PV system affect the rest of the system? The following are some of the key questions that need to be addressed:

- Existing system protection scheme during faults on the PV system
- Fault current contribution of PV systems
- Forward/reverse power flow during faults
- Sympathetic breaker tripping due to higher PV penetration
- Reduction of breaker's reach

8.3.2. **Partial Shading within a PV Power Plant**

In this research, the effects of fluctuating and out-of-phase cloud covering five PV sites in NEETRAC member Feeder B is investigated. However, partial shading of a PV power plant is not investigated. If some PV modules in a PV array are partially shaded or not performing as well as the rest of PV modules in the array, the inverter output is affected. Research should investigate the effect of partial shading within an array and the performance of the inverter.

8.3.3. **Non-Ideal Smart Inverter**

A smart inverter with smart functions is modeled in Matlab/Simulink. In the model, ideal IGBT (semiconductor) switches are used. In practice, these semiconductor switches do not turn ON/OFF when gated. To account for time delay in these devices, deadband is used between ON and OFF gating signals. The Smart Inverter model should be revised to include deadbands.

In high power transmission, losses in PV inverters should be minimized. The Smart Inverter model developed in this research is an ideal inverter and it should be revised to include switching losses. The model should also include switching losses

minimization techniques such as Zero Voltage Switching (ZVS) and Zero Current Switching (ZCS).

APPENDIX A: IMPORTING FEEDER MODELS FROM OPENDSS INTO DIGSILENT POWERFACTORY SOFTWARE

A.1. Introduction

Feeder models obtained from NEETRAC were created by others using OpenDSS software. OpenDSS is a steady-state analysis software and it is not suitable for the purpose of transient analysis in this research. DIgSILENT PowerFactory is an alternative power system simulation software that is capable of performing transient analysis and is therefore chosen for this research.

However, DIgSILENT PowerFactory does not allow importing OpenDSS models directly. Section A.2 discusses the methods and procedures used to import two NEETRAC member feeders that are created in OpenDSS into DIgSILENT PowerFactory while section A.3 discusses their validation and verification.

Importing OpenDSS models into DIgSILENT PowerFactory is difficult, labor intensive and time consuming. Some of the difficulties are due to:

- Lack of tutorials available in DIgSILENT PowerFactory explaining how to import models created using other power simulation software.
- The DIgSILENT PowerFactory helpdesk is slow to respond to questions submitted online and often not helpful when engaged in troubleshooting issues.

A.2. Methods and Procedures Used to Import OpenDSS Models into DIgSILENT PowerFactory

A.2.1. Convert File Format and Import into Microsoft Excel

The first step taken to import OpenDSS models into DIgSILENT PowerFactory is to convert the OpenDSS files with file extension ".dss" to files with ".txt" extension using Notepad. Then, Microsoft Excel is used to open the ".txt" files with delimiters and to save them on separate Excel sheets. Figure A.1 shows the flow chart used to convert OpenDSS files into separate Excel sheets.

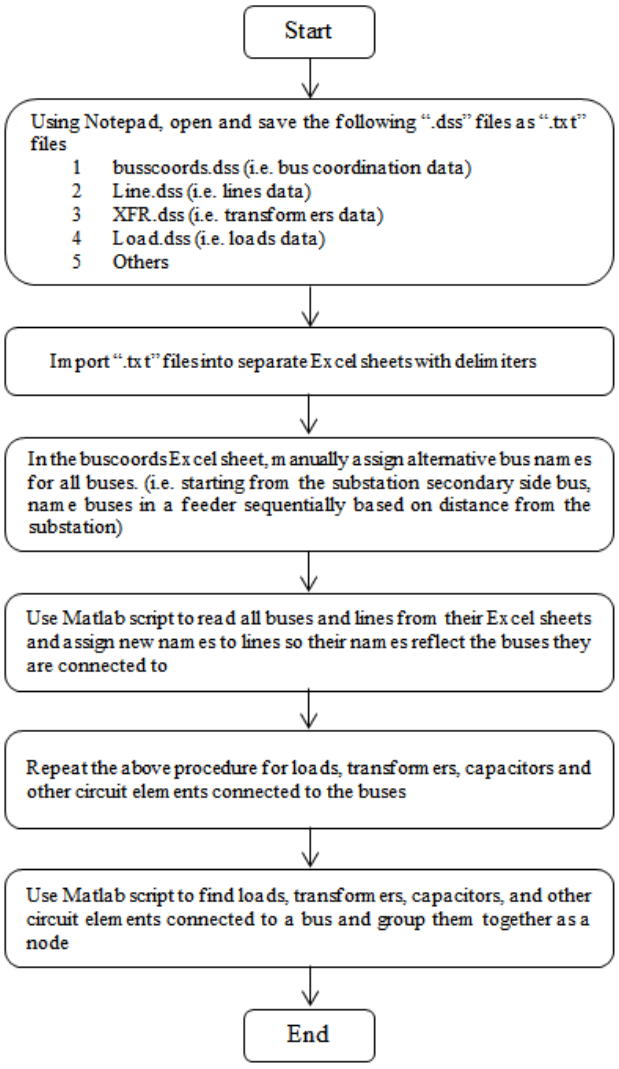

Figure A.1: Flow chart used to extract data from OpenDSS models

Figure A.1 shows that OpenDSS files with ".dss" file extension are opened using Notepad and re-saved with ".txt" file extension. Microsoft Excel is used to open the ".txt" files with delimiters and save them as separate sheets on an Excel file.

Buses and other circuit elements in the OpenDSS models are given longer names, some of them being non-sequential. To give these circuit elements shorter and sequential names, an Excel sheet that contains bus coordinates is used, and bus names are assigned manually starting from the substation bus. The low side of the substation transformer bus is named as "B001" bus and the rest of the buses in a feeder are given sequential names based on their distances from the substation.

Once the buses in the feeders are renamed, circuit elements that are connected to these buses are renamed following the bus name they are connected to. For example, if a transformer is connected to bus "B150" on the high side and to another bus on the low side, the transformer is renamed as "B150_Xfmr", while the low side bus is renamed as "B150_Sec". The same can be said of a line connecting buses "B150" and "B151". This line is renamed as "Ln_B150_To_B151". To make this renaming process automatic, a Matlab script is created to read busses and other circuit elements from different sheets of an Excel file, and then assign new names to the circuit elements based on bus names they are connected to. This Matlab script is shown in Appendix A.

A.2.2. Prepare DGS Formatted Excel File and Import into DIgSILENT

DIgSILENT PowerFactory allows importing data from power simulation software as illustrates in Figure A.2. DGS is an abbreviation for "**D**IgSILENT Interface for **G**eographical Information **S**ystems" and is the method used to import NEETRAC member models into DIgSILENT.

Importing models in DGS format requires all data to be organized into tables. Each table must have a unique name consisting of one or more table columns. There are two types of tables [2]:

1. The General table
2. The Object table

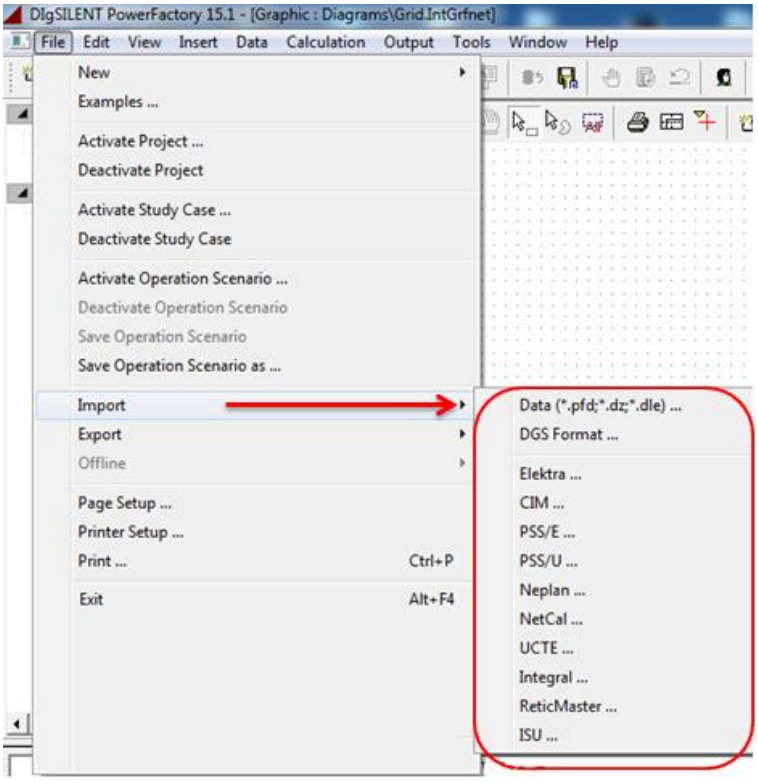

Figure A.2: File formats allowed by DIgSILENT for importing models

The General table is a special table that provides meta information about the DGS file. It consists of "ID", "Descr" and "Val" columns. Values for the "ID" column can be freely chosen but must be unique. In the "Descr" column, at least one entry must contain information about the version of DGS used. The current DGS format version is 5.0 and this value is entered in the "Val" column [2]. Figure 3.3 shows the General table created for NEETRAC member Feeder A.

	A	B	C	D
1	ID(a:40)	Descr(a:40	Val(a:40)	
2	1	Version	5.0	
3				
4				

Figure A.3: General table created for NEETRAC member Feeder A

The Object (data) tables store the actual data of the DIgSILENT PowerFactory objects. For each class of PowerFactory object used, exactly one Object table with its corresponding class name is needed (e.g. “ElmTerm” table for buses, “ElemTr2” table for two-winding transformers, etc.). In addition, the Object tables must be saved on separate sheets within the same Excel file. There is a requirement that the first columns of these tables must contain the “ID”, while the remaining columns could be certain attributes of the class. Actual data values of a particular class are saved in the rows of that Object table. For example, if there are 2000 buses in a feeder, each bus is saved in “ElmTerm” sheet beginning from row 2 to row 2001. Figure 3.4 shows some of the Excel sheets created that contain Object tables for NEETRAC member Feeder A.

Figure A.4: Object tables created for NEETRAC member Feeder A

The following summarizes Excel sheets created for the purpose of importing OpenDSS model into DIgSILENT PowerFactory in DGS format:

- All buses and nodes are saved in sheet “ElmTerm” with unique row IDs.
- All lines are saved in sheet “ElmLne” with unique row IDs.
- All line types (impedance matrices) are saved in sheet “TypLne” with unique row IDs.
- All two-winding transformers are saved in sheet “ElemTr2” with unique row IDs.
- All two-winding transformer parameters (ratings, impedances,…) are saved in sheet “TypTr2” with unique row IDs.
- All loads are saved in sheet “ElmLod” with unique row IDs.
- All switches are saved in sheet “StaCoup” with unique row IDs.

- For graphical display of single line diagram, connections to each element are specified in sheet “StaCubic” (e.g. for connecting bus “B150” to bus “B151” using line “Ln_B150_To_B151”, both bus “B150” and bus “B151” must refer to the unique ID of the line “Ln_B150_To_B151” in “StaCubic” sheet or they will not be connected.
- A Matlab script is created to search for unique IDs of each connected element and reference it in “StaCubic” sheet. This script is shown in Appendix B. Figure 3.5 shows the flow chart used to import models into DIgSILENT using DGS format.

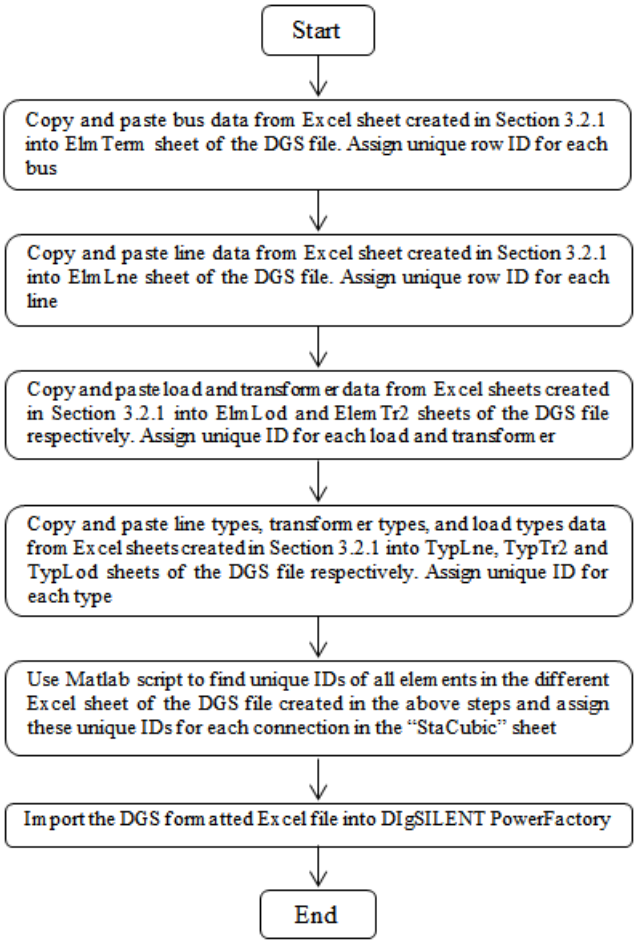

Figure A.5: Flow chart used to import DGS formatted file into DIgSILENT

DIgSILENT PowerFactory will display error messages if the DGS formatted Excel file is not properly imported. However, error messages will not be displayed if unknown settings are found in the Excel file (i.e. no warnings are displayed). As a result, debugging and fixing errors increases in difficulty.

When DIgSILENT PowerFactory imports DGS formatted Excel files, all of the circuit elements and connections are saved in the Data Manager. Upon first glance, the single line circuit elements appear to not be connected to each other. However, when the circuit element is clicked on the single line (e.g. a bus), DIgSILENT PowerFactory opens a window to display what elements are connected to it. Therefore, it requires manual work to reconnect circuit elements on the single line even though they are already connected in the Data Manager. Figure 3.6 shows a single line diagram of NEETRAC member Feeder A immediately after it is imported into DIgSILENT PowerFactory and Figure 3.7 shows the single line diagram of the feeder after the connections have been adjusted manually. Figure 3.8 shows the single line diagram of the feeder in OpenDSS (as received).

Figure A.6: Single line diagram of NEETRAC member Feeder A – right after importation using DGS formatted file

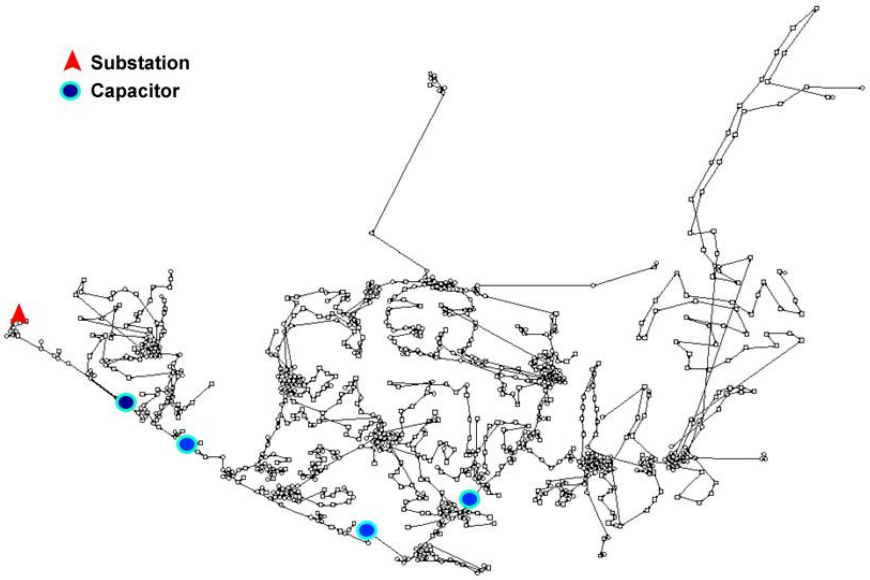

Figure A.7: Single line diagram of NEETRAC member Feeder A – after manually adjusting connections

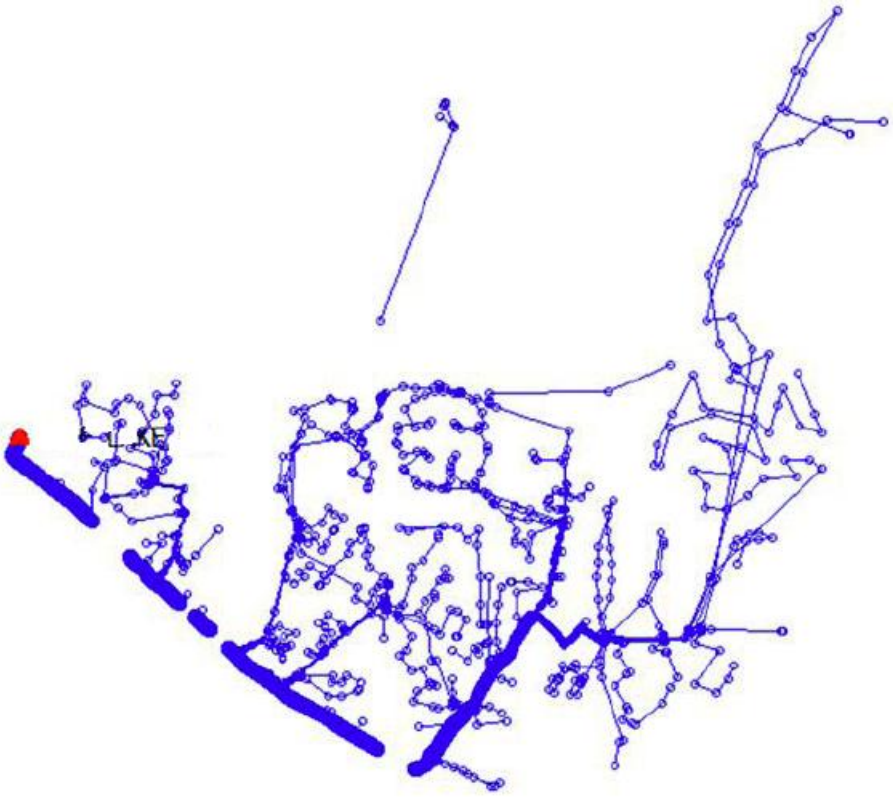

Figure A.8: Single line diagram of NEETRAC member Feeder A – in OpenDSS

A.3. Matlab Script Created to Rename Circuit Elements

```
%#####################################################################
%     This script imports Excel file (Elements.xlsx) and extracts bus names
%     and assigns new names to lines, transformers, loads, and switches based
%     on buses they are connected to
%#####################################################################
[NUM,TXT,RAW]=xlsread('Elements.xlsx','Lines');
[NUM2,TXT2,RAW2]=xlsread('Elements.xlsx','Buses');
[NUM3,TXT3,RAW3]=xlsread('Elements.xlsx','LineProperty');
[NUM4,TXT4,RAW4]=xlsread('Elements.xlsx','Switches');
Line_And_Bus = TXT(1:988,1:3);
Line_short_name = TXT(1:988,4:6);
Bus = TXT(4:984,7:8);
a = size(Line_And_Bus);
b = size(Line_short_name);
c = size(Bus);

 for i=4:988
       d = Line_And_Bus(i,2);
       e = Line_And_Bus(i,3);
       f = Bus(:,1);
       r1 = strmatch(d,f); %
       r2 = strmatch(e,f);

      if(isempty(r1)==1)
         r1 = 1;
      end
      if(isempty(r2)==1)
         r2 = 1;
      end

        Line_short_name(i,2)=cellstr(Bus(r1(1),2));
        Line_short_name(i,3)=cellstr(Bus(r2(1),2));
 end
%*******************************************************
%*******************************************************
Transformer = TXT(996:1479,1:3);
Tr = TXT(996:1479,4:6);
Bus1 = TXT2(3:985,1:2);
Bus2 = TXT2(987:1368,1:2);

for i=1:484
   xfmr1 = Transformer(i,2);
   xfmr2 = Transformer(i,3);
   B1 = Bus1(:,1);
   B2 = upper(Bus2(:,1));

   r1 = strmatch(xfmr1,B1);
   r2 = strmatch(xfmr2,B2);
```

```
    Tr(i,2) = cellstr(Bus1(r1,2));
    Tr(i,3) = cellstr(Bus2(r2,2));
end
%*********************************************************
%*********************************************************
Sec_line = TXT(1482:1974,1:3);
SecLn = TXT(1482:1974,4:6);
Bus1 = TXT2(987:1368,1:2);
Bus2 = TXT2(1370:1750,1:2);

for i=1:493
    SLn1 = Sec_line(i,2);
    SLn2 = Sec_line(i,3);
    B1 = upper(Bus1(:,1));
    B2 = upper(Bus2(:,1));

    r1 = strmatch(SLn1,B1);
    r2 = strmatch(SLn2,B2);

    SecLn(i,2) = cellstr(Bus1(r1,2));
    SecLn(i,3) = cellstr(Bus2(r2,2));
end
%*********************************************************
%*********************************************************
Load = TXT(1988:2471,1:2);
Ld_txt = TXT(1988:2471,4:6);
Bus = TXT2(1370:1750,1:2);
for i=1:484
    Ld1 = Load(i,2);
    B1 = upper(Bus(:,1));

    r1 = strmatch(Ld1,B1);

    Ld_txt(i,2) = cellstr(Bus(r1,2));

end
%*********************************************************
%*********************************************************
Line = TXT(4:988,1:9);
Line_Prop = TXT3(3:1021,1:9);
for i=1:985

    Ln = upper(Line(i,1));
    Ln_prop = upper(Line_Prop(:,1));
    r1 = strmatch(Ln,Ln_prop);
    Line(i,7)=cellstr(num2str(NUM3(r1,2)));
    Line(i,8)=cellstr(Line_Prop(r1,7));
    Line(i,9)=cellstr(num2str(NUM3(r1,5)));
end
%*********************************************************
```

```
%*******************************************************
Bus = upper(TXT2(4:984,1:2));
Switch = upper(TXT4(3:50,1:9));
for i=1:48
   SW1 = Switch(i,2);
   SW2 = Switch(i,3);
   B1 = Bus(:,1);

   r1 = strmatch(SW1,B1);
   r2 = strmatch(SW2,B1);

   if(isempty(r1)==1)
         r1 = 1;
   end
   if(isempty(r2)==1)
         r2 = 1;
   end

   Switch(i,5)=cellstr(Bus(r1,2));
   Switch(i,6)=cellstr(Bus(r2,2));

end
```

A.4. Matlab Script Created to Prepare DGS Formatted File

```
%*************************************************************************
%   This script imports Excel files and searches for
%   unique row IDs for each circuit elements in a feeder
%   and creates connection references in "Sta_Cubicle sheet"
%*************************************************************************
[NUM1,TXT1,RAW1]=xlsread('NEETRAC_Member_Feeder.xlsx','IntGrf');
[NUM2,TXT2,RAW2]=xlsread('NEETRAC_Member_Feeder.xlsx','IntGrfnet');
[NUM3,TXT3,RAW3]=xlsread('NEETRAC_Member_Feeder.xlsx','ElmTerm');
[NUM4,TXT4,RAW4]=xlsread('NEETRAC_Member_Feeder.xlsx ','ElmTr2');
[NUM5,TXT5,RAW5]=xlsread('NEETRAC_Member_Feeder.xlsx','StaCubic');
[NUM6,TXT6,RAW6]=xlsread('NEETRAC_Member_Feeder.xlsx','ElmLne');
[NUM7,TXT7,RAW7]=xlsread('NEETRAC_Member_Feeder.xlsx','ElmLod');
[NUM8,TXT8,RAW8]=xlsread('NEETRAC_Member_Feeder.xlsx','ElmCoup');

buses = TXT1(2:3782,2:8);
nodes = TXT2(3:end,2);
Elm_term = TXT3(2:end,2);
Elm_Tr2 = TXT4(2:end,1:2);
Sta_Cubic = TXT5(2:end,2);
Elm_Lne = TXT6(974:end,1:2);
Elm_Lod = TXT7(2:end,1:2);
Lines = TXT6(2:973,1:2);
Elm_Coup = TXT8(2:end,1:2);
 %*******************************************************
```

```
% get bus to switch connections
%*****************************************************
for i=1:length(Elm_Coup)
   SW = Elm_Coup(i,2);
   SW = char(SW);
   SW_fm = SW(4:8);
   SW_to = SW(13:end);

   r1 = strcat(SW_fm,'_Cub_Fm');
   r2 = strcat(SW_to,'_Cub_To');
   r3 = strmatch(r1,Sta_Cubic(:,1),'exact');
   r4 = strmatch(r2,Sta_Cubic(:,1),'exact');

   Sta_Cubic(r3,2) = cellstr(Elm_Coup(i,1));
   Sta_Cubic(r4,2) = cellstr(Elm_Coup(i,1));

end
 %*****************************************************
% get bus to bus connections
%*****************************************************
for i=1:length(Lines)
   Ln = Lines(i,2);
   Ln = char(Ln);
   Ln_fm = Ln(4:8);
   Ln_to = Ln(13:end);

   r1 = strcat(Ln_fm,'_Cub_Fm');
   r2 = strcat(Ln_to,'_Cub_To');
   r3 = strmatch(r1,Sta_Cubic(:,1),'exact');
   r4 = strmatch(r2,Sta_Cubic(:,1),'exact');

   Sta_Cubic(r3,2) = cellstr(Lines(i,1));
   Sta_Cubic(r4,2) = cellstr(Lines(i,1));

end
%*****************************************************
% get node to bus connections
%*****************************************************
for i=1:length(Lines)
   Ln = Lines(i,2);
   Ln = char(Ln);
   Ln_fm = Ln(4:8);
   Ln_to = Ln(13:end);

   r1 = strcat(Ln_fm,'_node_Cub_Fm');
   r2 = strcat(Ln_to,'_node_Cub_To');
   r3 = strmatch(r1,Sta_Cubic(:,1),'exact');
   r4 = strmatch(r2,Sta_Cubic(:,1),'exact');

   Sta_Cubic(r3,2) = cellstr(Lines(i,1));
   Sta_Cubic(r4,2) = cellstr(Lines(i,1));
```

```
 end
 %*****************************************************
% get inside node to bus connections
%*****************************************************
for i=1:length(Lines)
    Ln = Lines(i,2);
    Ln = char(Ln);
    Ln_fm = Ln(4:8);
    Ln_to = Ln(13:end);

    r1 = strcat(Ln_fm,'_Cub_up2');
    r2 = strcat(Ln_to,'_Cub_up1');
    r3 = strmatch(r1,Sta_Cubic(:,1),'exact');
    r4 = strmatch(r2,Sta_Cubic(:,1),'exact');

    Sta_Cubic(r3,2) = cellstr(Lines(i,1));
    Sta_Cubic(r4,2) = cellstr(Lines(i,1));

end
 %*****************************************************
% get buses dwn (conn to transformers)
%*****************************************************
for i=1:length(Elm_Tr2)
    tr = Elm_Tr2(i,2);
    tr = char(tr);
    tr_bus = tr(1:5);
    tr_phase = tr(10);

    r1 = strcat(tr_bus,'_Cub_dwn');
    r2 = strcat(r1,tr_phase);
    r3 = strmatch(r2,Sta_Cubic(:,1),'exact');
    Sta_Cubic(r3,2) = cellstr(Elm_Tr2(i,1));

end
for i=2:length(Elm_Tr2)
    tr = Elm_Tr2(i,2);
    tr = char(tr);
    tr_bus = tr(1:5);
    tr_phase = tr(10);

    r1 = strcat(tr_bus,'_Cub_dwn');
    r2 = strcat(r1,tr_phase);
    r3 = strmatch(r2,Sta_Cubic(:,1),'exact');
    Sta_Cubic(r3,2) = cellstr(Elm_Tr2(i,1));

end
for i=3:length(Elm_Tr2)
    tr = Elm_Tr2(i,2);
    tr = char(tr);
    tr_bus = tr(1:5);
    tr_phase = tr(10);
```

```
    r1 = strcat(tr_bus,'_Cub_dwn');
    r2 = strcat(r1,tr_phase);
    r3 = strmatch(r2,Sta_Cubic(:,1),'exact');
    Sta_Cubic(r3,2) = cellstr(Elm_Tr2(i,1));

end
%*****************************************************
% getg _X buses
%*****************************************************
for i=1:length(Elm_Tr2)
    tr = Elm_Tr2(i,2);
    tr = char(tr);
    tr_bus = tr(1:5);
    tr_phase = tr(10);

    r1 = strcat(tr_bus,'_X_A_Cub_Up_');
    r2 = strcat(r1,tr_phase);
    r3 = strmatch(r2,Sta_Cubic(:,1),'exact');
    Sta_Cubic(r3,2) = cellstr(Elm_Tr2(i,1));

end
for i=2:length(Elm_Tr2)
    tr = Elm_Tr2(i,2);
    tr = char(tr);
    tr_bus = tr(1:5);
    tr_phase = tr(10);

    r1 = strcat(tr_bus,'_X_B_Cub_Up_');
    r2 = strcat(r1,tr_phase);
    r3 = strmatch(r2,Sta_Cubic(:,1),'exact');
    Sta_Cubic(r3,2) = cellstr(Elm_Tr2(i,1));

end
for i=3:length(Elm_Tr2)
    tr = Elm_Tr2(i,2);
    tr = char(tr);
    tr_bus = tr(1:5);
    tr_phase = tr(10);

    r1 = strcat(tr_bus,'_X_C_Cub_Up_');
    r2 = strcat(r1,tr_phase);
    r3 = strmatch(r2,Sta_Cubic(:,1),'exact');
    Sta_Cubic(r3,2) = cellstr(Elm_Tr2(i,1));

end
%*****************************************************
% get _X down buses
%*****************************************************
 for i=1:length(Elm_Lne)
    L = Elm_Lne(i,2);
```

```
    L = char(L);
    L_bus = L(1:5);
    L_phase = L(13);

    r1 = strcat(L_bus,'_X_A_Cub_Dwn_');
    r2 = strcat(r1,L_phase);
    r3 = strmatch(r2,Sta_Cubic(:,1),'exact');
    Sta_Cubic(r3,2) = cellstr(Elm_Lne(i,1));

end
for i=2:length(Elm_Lne)
    L = Elm_Lne(i,2);
    L = char(L);
    L_bus = L(1:5);
    L_phase = L(13);

    r1 = strcat(L_bus,'_X_B_Cub_Dwn_');
    r2 = strcat(r1,L_phase);
    r3 = strmatch(r2,Sta_Cubic(:,1),'exact');
    Sta_Cubic(r3,2) = cellstr(Elm_Lne(i,1));

end
for i=3:length(Elm_Lne)
    L = Elm_Lne(i,2);
    L = char(L);
    L_bus = L(1:5);
    L_phase = L(13);

    r1 = strcat(L_bus,'_X_C_Cub_Dwn_');
    r2 = strcat(r1,L_phase);
    r3 = strmatch(r2,Sta_Cubic(:,1),'exact');
    Sta_Cubic(r3,2) = cellstr(Elm_Lne(i,1));

end
%*****************************************************
% get _S ups buses
%*****************************************************
 for i=1:length(Elm_Lne)
    L = Elm_Lne(i,2);
    L = char(L);
    L_bus = L(1:5);
    L_phase = L(13);

    r1 = strcat(L_bus,'_S_A_Cub_Up_');
    r2 = strcat(r1,L_phase);
    r3 = strmatch(r2,Sta_Cubic(:,1),'exact');
    Sta_Cubic(r3,2) = cellstr(Elm_Lne(i,1));

end
for i=2:length(Elm_Lne)
    L = Elm_Lne(i,2);
```

```
    L = char(L);
    L_bus = L(1:5);
    L_phase = L(13);

    r1 = strcat(L_bus,'_S_B_Cub_Up_');
    r2 = strcat(r1,L_phase);
    r3 = strmatch(r2,Sta_Cubic(:,1),'exact');
    Sta_Cubic(r3,2) = cellstr(Elm_Lne(i,1));

end
for i=3:length(Elm_Lne)
    L = Elm_Lne(i,2);
    L = char(L);
    L_bus = L(1:5);
    L_phase = L(13);

    r1 = strcat(L_bus,'_S_C_Cub_Up_');
    r2 = strcat(r1,L_phase);
    r3 = strmatch(r2,Sta_Cubic(:,1),'exact');
    Sta_Cubic(r3,2) = cellstr(Elm_Lne(i,1));

end
%*****************************************************
% get _S dwns buses(i.e. conn to loads)
%*****************************************************
 for i=1:length(Elm_Lod)
    L = Elm_Lod(i,2);
    L = char(L);
    L_bus = L(1:5);
    L_phase = L(10);

    r1 = strcat(L_bus,'_S_A_Cub_Dwn_');
    r2 = strcat(r1,L_phase);
    r3 = strmatch(r2,Sta_Cubic(:,1),'exact');
    Sta_Cubic(r3,2) = cellstr(Elm_Lod(i,1));

end
for i=2:length(Elm_Lod)
    L = Elm_Lod(i,2);
    L = char(L);
    L_bus = L(1:5);
    L_phase = L(10);

    r1 = strcat(L_bus,'_S_B_Cub_Dwn_');
    r2 = strcat(r1,L_phase);
    r3 = strmatch(r2,Sta_Cubic(:,1),'exact');
    Sta_Cubic(r3,2) = cellstr(Elm_Lod(i,1));

end
for i=3:length(Elm_Lod)
    L = Elm_Lod(i,2);
```

```
    L = char(L);
    L_bus = L(1:5);
    L_phase = L(10);

    r1 = strcat(L_bus,'_S_C_Cub_Dwn_');
    r2 = strcat(r1,L_phase);
    r3 = strmatch(r2,Sta_Cubic(:,1),'exact');
    Sta_Cubic(r3,2) = cellstr(Elm_Lod(i,1));

end
```

APPENDIX B: MATLAB SCRIPT USED IN "VOLTAGE DEVIATION CALCULATOR" BLOCK

```
function [UV1,UV2,UV3,OV1,OV2] = fcn(Vab,Vbc,Vca)
%##############################################
% This function computes voltage deviation per
% IEEE 1547 grid interconnection requirements
%##############################################

if((Vab<0.45)||(Vbc<0.45)||(Vca<0.45))
   UV1 = 1;%if(V<0.45, set UV1=1)
   UV2 = 0;
   UV3 = 0;
   OV1 = 0;
   OV2 = 0;
elseif(((0.45<=Vab)&&(Vab<0.6))||((0.45<=Vbc)&&(Vbc<0.6))||((0.45<=Vca)&&(Vca<0.6)))
   UV1 = 0;
   UV2 = 1;%if(0.45<=V<0.6, set UV2=1)
   UV3 = 0;
   OV1 = 0;
   OV2 = 0;
elseif(((0.6<=Vab)&&(Vab<0.88))||((0.6<=Vbc)&&(Vbc<0.88))||((0.6<=Vca)&&(Vca<0.88)))
   UV1 = 0;
   UV2 = 0;
   UV3 = 1;%if(0.6<=V<0.88, set UV3=1)
   OV1 = 0;
   OV2 = 0;
elseif(((0.88<=Vab)&&(Vab<=1.1))||((0.88<=Vbc)&&(Vbc<=1.1))||((0.88<=Vca)&&(Vca<=1.1
)))
   UV1 = 0;
   UV2 = 0;
   UV3 = 0;%if(0.88<=V<=1.1, no violation)
   OV1 = 0;
   OV2 = 0;
elseif(((1.1<Vab)&&(Vab<1.2))||((1.1<Vbc)&&(Vbc<1.2))||((1.1<Vca)&&(Vca<1.2)))
   UV1 = 0;
   UV2 = 0;
   UV3 = 0;
   OV1 = 1;%if(1.1<V<1.2, set OV1=1)
   OV2 = 0;
else
   UV1 = 0;
   UV2 = 0;
   UV3 = 0;
   OV1 = 0;
   OV2 = 1;%if(1.2<=V, set OV2=1)
end
```

APPENDIX C: MATLAB SCRIPT USED IN "FREQUENCY DEVIATION CALCULATOR" BLOCK

```
function [UF1,UF2,OF1,OF2] = fcn(f)
%##############################################
% This function computes frequency deviation per
% IEEE 1547 grid interconnection requirements
%##############################################

if(f<57)
   UF1  = 1;% if(f<57, set UF1=1)
   UF2  = 0;
   OF1  = 0;
   OF2  = 0;
elseif((57<=f) && (f<59.5))
   UF1  = 0;
   UF2  = 1;% if(57<=f<59.5, set UF2=1)
   OF1  = 0;
   OF2  = 0;
elseif((59.5<=f) && (f<=60.5))
   UF1  = 0;
   UF2  = 0;% if(59.5<=f<=60.5, no violation)
   OF1  = 0;
   OF2  = 0;
elseif((60.5<f) && (f<=62.5))
   UF1  = 0;
   UF2  = 0;
   OF1  = 1;% if(60.5<f<=62.5, set OF1=1)
   OF2  = 0;
else
   UF1  = 0;
   UF2  = 0;
   OF1  = 0;
   OF2  = 1;% if(62.5<f, set OF2=1)
end
```

APPENDIX D: MATLAB SCRIPT USED IN INCREMENTAL CONDUCTANCE AND PERTURB AND OBSERVE SUBSYSTEMS

A. Incremental Conductance Algorithm

```
function D_InCond = fcn(MPPT_init,Vpv,Ipv)
%*************************************************************
% This function implements Incremental Conductance MPPT algorithm.
% Created by Raeey Regassa
%*************************************************************

% Parameter inputs
Vdc_init_InCond = MPPT_init(1);    % Initial VDC
D_init_InCond   = MPPT_init(3);    % Initial duty cycle
Idc_init_InCond = MPPT_init(4);    % Initial DC current


% Define internal values for Voltage and Power as persistent
% variables
persistent Dprev_InCond Vprev_InCond Iprev_InCond;

% For first pass, initialize internal values
if isempty(Dprev_InCond)
   Dprev_InCond = D_init_InCond;
   Vprev_InCond = Vdc_init_InCond;
   Iprev_InCond = Idc_init_InCond;
end

% Initialize algorithm parameters
deltaD_InCond = 1e-5;

% Calculate measured array power
del_V = Vpv-Vprev_InCond;
del_I = Ipv-Iprev_InCond;
del_IoverV = del_I/del_V;

% Increase or decrease duty cycle based on previous condition
if(del_V)~=0
   if(Ipv+Vpv*del_IoverV)~=0
      if(Ipv+Vpv*del_IoverV)>0
         D_InCond = Dprev_InCond-deltaD_InCond;
      else
         D_InCond = Dprev_InCond+deltaD_InCond;
      end
   else
      D_InCond = Dprev_InCond;
   end
else
   if(del_I)~=0
```

```
      if(del_I)>0
         D_InCond = Dprev_InCond+deltaD_InCond;
      else
        D_InCond = Dprev_InCond-deltaD_InCond;
      end
   else
      D_InCond = Dprev_InCond;
   end
end

% Update internal values for the next iteration
Dprev_InCond = D_InCond;
Vprev_InCond = Vpv;
Iprev_InCond = Ipv;
```

B. Perturb and Observe Algorithm

```
function D_PandO = fcn(MPPT_init,Vpv,Ipv)
%*****************************************************************
% This function implements Perturb and observe MPPT algorithm.
% Created by Raeey Regassa
%*****************************************************************

% Parameter inputs
Vdc_init_PandO = MPPT_init(1);    % Initial VDC
Pdc_init_PandO = MPPT_init(2);    % Initial DC power
D_init_PandO   = MPPT_init(3);     % Initial duty cycle

% Define internal values for Voltage and Power as persistent
% variables
persistent Dprev_PandO Vprev_PandO Pprev_PandO;

% For first pass, initialize internal values
if isempty(Dprev_PandO)
   Dprev_PandO = D_init_PandO;
   Vprev_PandO = Vdc_init_PandO;
   Pprev_PandO = Pdc_init_PandO;
end

% Initialize algorithm parameters
deltaD_PandO = 1e-6;

% Calculate measured array power
Ppv = Vpv*Ipv;

% Increase or decrease duty cycle based on previous condition
if(Ppv-Pprev_PandO)~=0
   if(Ppv-Pprev_PandO)>0
      if(Vpv-Vprev_PandO)>0
```

```
            D_PandO = Dprev_PandO-deltaD_PandO;
        else
            D_PandO = Dprev_PandO+deltaD_PandO;
        end
    else
        if(Vpv-Vprev_PandO)>0
            D_PandO = Dprev_PandO+deltaD_PandO;
        else
            D_PandO = Dprev_PandO-deltaD_PandO;
        end
    end
else
    D_PandO = Dprev_PandO;
end

% Update internal values for the next iteration
Dprev_PandO = D_PandO;
Vprev_PandO = Vpv;
Pprev_PandO = Ppv;
```

APPENDIX E: SYNCHRONOUS GENERATOR CONTROLLER PARAMETERS USED

Figure E.1 and E.2 show the parameters used for the Hydraulic Turbine Governor and the Excitation System respectively.

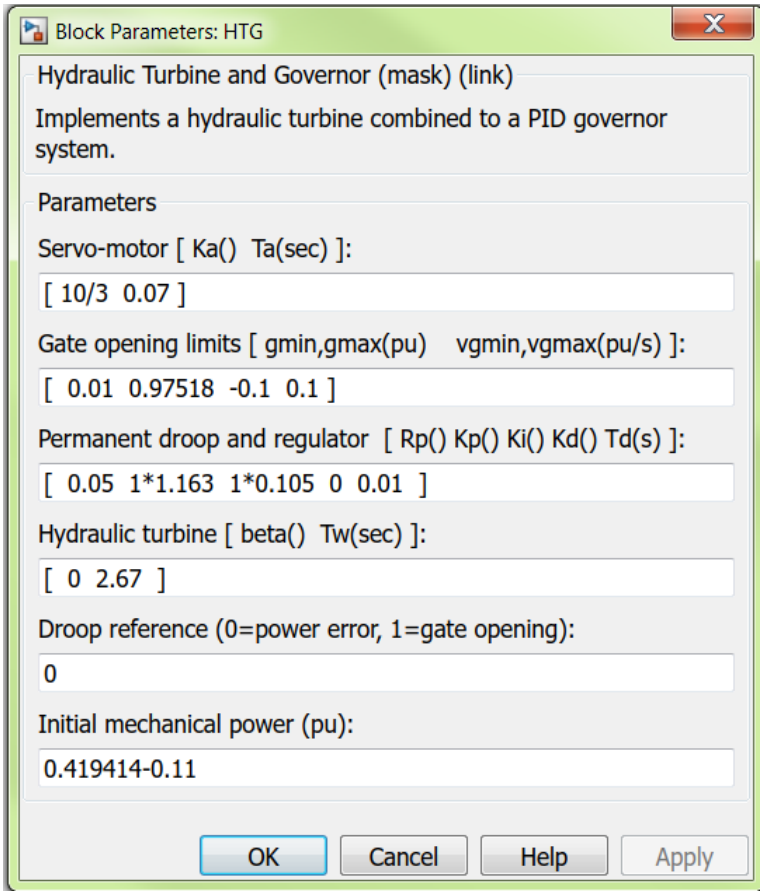

Figure E.1: Parameters used in the Hydro Turbine and Governor block

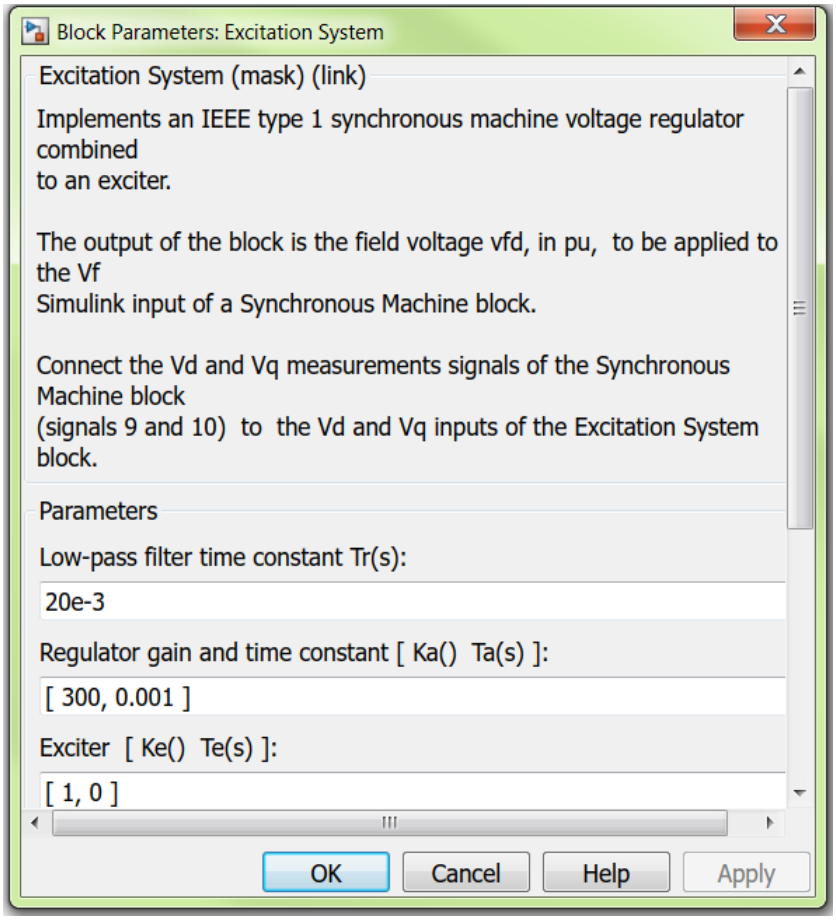

Figure E.2: Parameters used in the Excitation System block

REFERENCES

[1] *OpenDSS Manual*, EPRI, Palo Alto, CA, 2016.

[2] *User Manual*, DIgSILENT GmbH, Gomaringen, Germany, 2013.

[3] DIgSILENT GmbH, Gomaringen, Germany,"DIgSILENT Support," Available:http://www.digsilent.de/index.php/support.html. Accessed: December 2015.

[4] Bialek, T., "Renewable Impact on Electric Planning", Presented at High Penetration Solar Forum 2013, San Diego, CA, Feb 13-14, 2013.

[5] Sylvia, M., "RPS Solar Carve-Out II. Final Policy Design", Massachusetts Department of Energy Resources, Boston, MA, Dec 13, 2013.

[6] Impact of High-Penetration PV on Distribution System Performance. EPRI, Palo Alto, CA: 2011.1021982.

[7] Integration of Photovoltaic Generation into Distribution Systems. EPRI, Palo Alto, CA: 2010.1020870.

[8] Modeling High-Penetration PV for Distribution Interconnection Studies. EPRI, Palo Alto, CA: 2011.1021980.

[9] Planning Methodology to Determine Practical Circuit Limits for Distributed Generation: Emphasis on Solar PV and Other Renewable Generation. EPRI, Palo Alto, CA: 2010.1020157.

[10] Stochastic Analysis to Determine Feeder Hosting Capacity for Distributed Solar PV. EPRI, Palo Alto, CA: 2012.1026640.

[11] Commom Functions for Smart Inverters, Version 2. EPRI, Palo Alto, CA: 2012.1026809.

[12] Modeling High-Penetration PV for Distributed Analysis: Solar PV Systems and Relevant Grid-Related Responses. EPRI, Palo Alto, CA: 2011.1021980.

[13] Smart Inverter Functionality Survey: A State-of-the-Industry Assessment. EPRI, Palo Alto, CA: 2010.1022239.

[14] W. Sunderman, M Rylander, J. Smith, "FirstEnergy Distributed PV(DPV) Feeder Impact Study: Poplar Circuit 57305-C," unpublished.

[15] W. Sunderman, M Rylander, J. Smith, "FirstEnergy Distributed PV(DPV) Feeder Impact Study: Spotswood Circuit 47375-C," unpublished.

[16] Utility-Scale Photovoltaic Inverters: Specifications, Standards, and Product Options. EPRI, Palo Alto, CA: 2011.1021990.

[17] Integration of Distributed Resources in Electric Untility Distribuion Systems: Distribution System Behavior Analysis for Suburban Feeder. EPRI, Palo Alto, CA, and Ontario Hydro Tecnologies, Toronto, Ontario,Canada:1998. TR-111490.

[18] Modeling High-Penetration PV for Distributed Interconnection Studies: Smart Inverter Function Modeling in OpenDSS, Rev 2. EPRI, Palo Alto, CA: 2013.3002002271.

[19] Advanced Voltage Control Strategies for High Penetration of Distributed Generation: Emphasis on Solar PV and Other Inverter-Connected Generation. EPRI, Palo Alto, CA: 2010.1020155.

[20] M. Rylander, J. Smith, "Comprehensive Approach for Determining Distribution Network Hosting Capacity for Solar PV," 2nd International Workshop on Integration of Solar Power Into Power Systems, Lisbon, Portugal, Nov 2012.

[21] M. Rylander, J. Smith, "Stochastic Approach for Distributed Planning with Distributed Energy Resources," CIGRE 2012 Grid of the Future Symposium, Kansas City, MO, 2012.

[22] U.S. Department of Energy. (2013, August 16). *Solar Photovoltaic Cell Basics* [Online]. Available: https://energy.gov/eere/energybasics/articles/solar-photovoltaic-cell-basics

[23] BIPV - Building Integrated Photovoltaic. (2017, January 29). *Photovoltaic (PV) Cell* [Online]. Available: https://sites.google.com/site/reeetech/home/photovoltaic

[24] B. K. Dey, I. Khan, N. Mandal, and A. Bhattacharjee "Mathematical Modeling and Characteristic Analysis of Solar PV Cell," in *2016 IEEE 7th Annual Information Technology, Electronics and Mobile Communication Conference (IEMCON).*, Vancouver., BC, 2016, 1-5.

[25] A. N. R. Ahmed, K. Norwaz, J. Tasnim, and N. Afroze "A Complete Modeling and Analysis of Solar System (Cell/Module/Array) Based on MATLAB," in *2015 International Conference on Electrical & Electronic Engineering (ICEEE).*, Rajshahi., Bangladesh, 2015, 149-152.

[26] V. Tamrakar, S. C. Gupta, and Y. Sawle "Study of Characteristics of Single and Double Diode Electrical Equivalent Circuit Models of Solar PV Module," in *2015 International Conference on Energy Systems and Applications.*, Pune., India, 2015, 312-317.

[27] N. M. A. Shannan, N. Z. Yahaya, and B. Singh "Single-Diode Model and Two-Diode Model of PV Modules: A Comparison," in *2013 IEEE International*

Conference on Control System, Computing and Engineering., Penang., Malaysia, 2013, 210-214.

[28] D. S. H. Chan, and J. C. H. Phang, "Analytical Methods for the Extraction of Solar-Cell Single-and Double-Diode Model Parameters from I-V Characteristics," *IEEE Transactions on Electron Devices,* vol. 34, pp. 286-293, 1987.

[29] M. Suthar, G. K. Singh, and R. P. Saini "Comparison of Mathematical Models of Photo-Voltaic (PV) Module and Effect of Various Parameters on its Performance," in *2013 International Conference on Energy Efficient Technologies for Sustainability(ICEETS).*, Nagercoil., India, 2013, 1354-1359.

[30] D. Rekioua and E. Matagne, *"Modeling of Solar Irrandiance and Cells,"* in *Optimization of Photovoltaic Power Systems Modelization, Simulation and Control*, 1st ed. London, England: Springer, 2012, ch. 3, pp. 31-87.

[31] *Measurement of Photovoltaic Current-Voltage Characteristics*, IEC 60904-1, 2009.

[32] Energetic Macroscopic Representation. (2011, July 6). *Simulation of a PV System* [Online]. Available: http://www.emrwebsite.org/photovoltaic-system-using-emr-and-simuliktm.html

[33] W. Rahman, C. Bathina, V. Karthikeyan, and R. Prasanth "Comparative Analysis of Developed Incremental Conductance (IC) and Perturb & Observe (P&O) Algorithm for Photovoltaic Applications," in *2016 10th International Conference on Intelligent Systems and Control (ISCO).*, Coimbatore., India, 2013, 1-6.

[34] F. Mohamood, "*Improving the Photovoltaic Model in PowerFactory*," Msc. thesis, Dept. Elect. Eng., KTH Royal Institute of Technology in Stockholm., Stockholm, Sweden, 2012.

[35] A. S. Ahmed, C. B. A. Abdullah, and W. G. A. Abdelaal "MPPT Algorithms: Performance and Evaluation," in *2016 11th International Conference on Computer Engineering & Systems(ICCES).*, Cairo., Egypt, 2016, 461-467.

[36] T. Esram and P. L. Chapman, "Comparison of Photovoltaic Array Maximum Power Point Tracking Techniques," *IEEE Transactions on Energy Conversion,* vol. 22, pp. 439-449, 2007.

[37] L. Abderezak, B. Aissa, and S. Hamza "Comparative Study of Three MPPT Algorithms for a Photovoltaic System Control," in *2015 World Congress on Information Technology and Computer Applications (WCITCA).*, Hammamet., Tunisia, 2015, 1-5.

[38] M. A. Gomes, L. Galotto, L. P. Sampaio, G. Melo, and C. A. Canesin, "Evaluation of the Main MPPT Techniques for Photovoltaic Applications," *IEEE Transactions on Industrial Electronics,* vol. 60, pp. 1156-1167, 2013.

[39] M. Saeedifard, *"ECE 6331-A: Power Electronic Circuits"*, Georgia Institute of Technology, 2015.

[40] S. R. Wenham, M.A. Green, M. E. Watt and R. Corkish, *"Modeling of Solar Irrandiance and Cells,"* in *Applied Photovoltaics*, 2nd ed. Padstow, England: TJ International Ltd, 2007, ch. 5, pp. 75-95.

[41] D. K. Chaturvedi, and S. Sharma "An Experimental Study and Verification of the Facts Related to Factors Affecting the Performance of Solar PV Systems," in *2015 5th International Conference on Communication Systems and Network Technologies.*, Gwalior., India, 2015, 1185-1188.

[42] A. Fezzani, I. H. Mahammed, and S. Said "MATLAB-Based Modeling of Shading Effects in Photovoltaic arrays," in *2014 15th International Conference on Sciences and Techniques of Automatic Control & Computer Enginerring.*, Hammamet., Tunisia, 2014, 781-787.

[43] P. Samantaray, and S. Sasmita "Performance of Solar Photovoltaic Module Under Partial Shading Conditions," in *2016 10th International Conference on Intelligent Systems and Control(ISCO).*, Coimbatore., India, 2016, 1-4.

[44] P. Santos, E. M. Vicente, and E. R. Ribeiro "Relationship Between the Shading Position and the Output Power of a Photovoltaic Panel," in *2011 XI Brazilian Power Electronics Conference.*, Natal., Brazil, 2011, 676-681.

[45] M. Abdulazeez, and I. Iskender "Simulation and Experimental Study of Shading Effect on Series and Parallel Connected Photovoltaic PV Modules," in *2011 7th International Conference on Electrical and Electronics Engineering (ELECO).*, Bursa., Turkey, 2011, I-28 - I-32.

[46] D. Amorndechaphon "High-Efficiency DC-AC Inverter for Small PV Power Generation System," in *2016 International Conference on Cogeneration, Small Power Plants and District Energy (ICUE).*, Bangkok., Thailand, 2016, 1-6.

[47] A. Sandali, F. A. Alouahabi, K. Ayache, and A. Cheriti "Modeling and Design of a Three-Phase Grid Connected PV System Based on PWM Current Source Inverter and P-I Curve Slope MPPT Technique," in *2015 6th International Symposium on Power Electronics for Distributed Generation Systems (PEDG).*, Aachen., Germany, 2015, 1-7.

[48] V. Agarwal, and A. Vishwakarma "A Comparative Study of PWM Schemes for Grid Connected PV Cell," in *2007 7th International Conference on Power Electronics and Drive Systems.*, Bangkok., Thailand, 2007, 1769-1775.

[49] S. K. Show, and P. Parthiban "Analysis of Current Controlled Voltage Source Inverter with Space Vector PWM and Sinusoidal PWM Techniques," in *2015 International Conference on Innovations in Information, Embedded and Communication Systems (ICIIECS).*, Coimbatore., India, 2015, 1-6.

[50] D. G. Holmes, and T. A. Lipo, *Pulse Width Modulation For Power Converters Principles and Practice*. Piscataway, NJ: IEEE Press, 2003.

[51] R. Teodorescu, M. Liserre, and P. Rodeiguez, "*Photovoltaic Inverter Structures*," in *Grid Converters for Photovoltaic and Wind Systems*, 1st ed. Chichester, England: Wiley, 2011, ch. 2, pp. 5-29.

[52] E. Reiter, K. Ardani, R. Margolis, and R. Edge, "Industry Perspectives on Advanced Inverters for U.S. Solar Photovoltaic Systems: Grid Benefits, Deployment Challenges, and Emerging Solutions," NREL., Denver., CO, NREL/TP-7A40-65063, 2015.

[53] Smart Inverter Working Group (SIWG), "Recommendations for Updating the Technical Requirements for Inverters in Distributed Energy Resouces," CPUC., Sacramento., CA, 2014.

[54] IEEE Std 1547-2003, *Standard for Interconnecting Distributed Resources with Electric Power Systems*, IEEE, June 2003. ISBN 0-7381-3720-0 SH95144.

[55] IEEE Std 1547-2014, *Standard for Interconnecting Distributed Resources with Electric Power Systems Amendment 1*, IEEE, May 2014. ISBN 978-0-7381-9132-4 STD98667.

[56] IEC 61727 Ed. 2, *Photovoltaic (PV) Systems - Characteristics of the Untility Interface*, December 2004.

[57] IEC 62116 CDV Ed. 1, *Test Procedure of Islanding Prevention Measure for Utility-Interconnected Photovoltaic Inverters*, IEC 82/402/CD, 2005.

[58] M. Yagami, N. Kimura, M. Tsuchimoto, and J. Tamura "Power System Transient Stability Analysis in the Case of High-Penetration of Photovoltaics," in *2013 IEEE Grenoble Conference.*, Grenoble., France, 2013, 1-6.

[59] M. Yagami, N. Kimura, M. Tsuchimoto, and J. Tamura "Power System Transient Stability Analysis in the Case of High-Penetration of Photovoltaics (Part 2)," in *2015 IEEE Eindhoven PowerTech.*, Eindhoven., Netherlands, 2015, 1-6.

[60] U. Tamrakar, D. Galipeau, R. Tonkoski, and I. Tamrakar "Improving Transient Stability of Photovoltaic-Hydro Mircogrids Using Virtual Synchronous Machines," in *2015 IEEE Eindhoven PowerTech.*, Eindhoven., Netherlands, 2015, 1-6.

[61] M. Yagami, S. Ishikawa, Y. Ichinohe, K. Misawa and J. Tamura "Transient Stability Anaysis of Power System with Photovoltaic Systems Installed," in *3rd Renewable Power Generation Conference (RPG 2014).*, Naples., Italy, 2014, 1-6.

[62] S. Eftekharnejad, V. Vittal, G. T. Heydt, B. Keel, and J. Loehr, "Impact of Increased Penetration of Photovoltaic Generation on Power Systems," *IEEE Transactions on Power Systems*, vol. 28, pp. 893-901, 2013.

[63] A. M. Azmy, and I. Erlich "Impact of Distributed Generation on the Stability of Electrical Power System," in 2005 *IEEE Power Engineering Society General Meeting.*, San Francisco., CA, 2005, 1056-1063.

[64] J. G. Slootwed, and W. L. Kling "Impacts of Distributed Generation on Power System Transient Stability," in 2002 *IEEE Power Engineering Society Summer Meeting.*, Chicago., IL, 2002, 862-867.

[65] D. Paradis, F. Katiraei, and B. Mather "Comparative Analysis of Time-Series Studies and Transient Simulations for Impact Assessment of PV Integration on Reduced IEEE 8500 Node Feeder," in 2013 *IEEE Power and Energy Society General Meeting.*, Vancouver., Canada, 2013, 1-5.

[66] *Template Description Photovoltaic System (PhotovoltaicSystem_0.4kV_0.5MVA)*, DIgSILENT GmbH, Gomaringen, Germany, 2011.

[67] *PSCAD/EMTDC User Manual*. Version 4.7, Manitoba HVDC Research Centre.

[68] A. Yazdani, and R. Iravani, *Voltage-Sourced Converters in Power Systems*, NJ: Wiley, 2010.

[69] M. Bhardwaj, and B. Subharmanya, "PV Inverter Design Using Solar Explorer Kit" Texas Instruments. Application Report. SPRABR4A, 2013.

[70] TI Designs, "Voltage Source Inverter Design Guideline" Texas Instruments. Application Report. TIDUAY6A, 2015.

[71] IEEE PES, ″13-Bus Feeder," Available: https://ewh.ieee.org/soc/pes/dsacom/testfeeders/. Accessed: February 2017.

[72] *power_13NodeTestFeeder*. MATLAB R2016b, MathWorks.

[73] *W. H. Kersting, "Regulation of Voltages," in Distribution System Modeling and Analysis, 1st ed. Boca Raton, Florida: CRC, 2002, ch. 7, pp. 145-194.*

[74] *D. W. Hart, "DC-DC Converters," in Power Electonics, 1st ed. New York, NY: McGraw-Hill, 2011, ch. 6, pp. 196-264.*